Fifth European Conference on Controlled Fusion and Plasma Physics

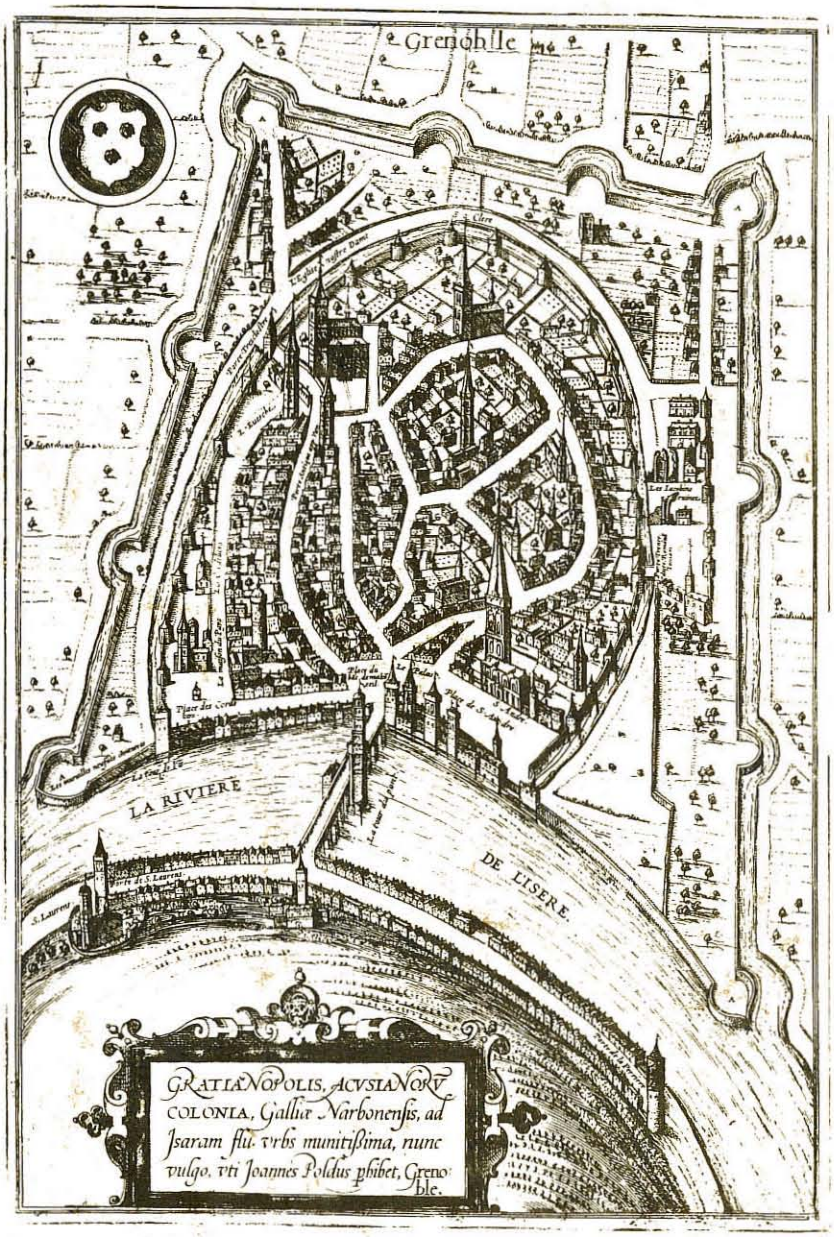

Vol-II

Grenoble 21-25 August 1972

commissariat à l'énergie atomique

DV

The map of Grenoble on the front cover is taken from : URBIUM PRAECIPUARUM TOTIUS MUNDI, LIBER TERTIUS, AUCTORIBUS GEORGIUS BRAUN, SIMONE NOVELLANO ET FRANCISCO HOGENBERGIO, COLONIAE AGRIPPINAE (*Cologne*), 1581.

Translation of the Cartouche : Gratianopolis, previously Colony of Ancona, fortified town of the Gaule Narbonnaise on the Isere river, now popularly called Grenoble according to Joannes Poldus.

FIFTH EUROPEAN CONFERENCE ON CONTROLLED FUSION AND PLASMA PHYSICS

GRENOBLE FRANCE AUGUST 21-25 1972

VOL II

INVITED PAPERS

and

SUPPLEMENTARY PAPERS

The Conference Proceedings (Vol. 1 : Contributed Papers, and Vol. 2 : Invited Papers and Supplementary Papers) are distributed free of charge to each registered participant. They will also be sold at the price of 50 FF. after the Conference. Orders must be given to the Service d'Ionique Générale, Association EURATOM-CEA, Centre d'Etudes Nucléaires de Grenoble, BP 85, 38041 - GRENOBLE Cedex, France.

CONTENTS

Preface Page *i*

Honorary Council *ii*

Committees and Supporting Organizations *iii*

INVITED PAPERS

EXPERIMENTS ON THE ST TOKAMAK DEVICE 1

(W. Stodieck)

ADVANCE IN THE TOKAMAK PROGRAMME 13

(V.S. Strelkov)

MEASUREMENT OF NEOCLASSICAL DIFFUSION IN THE DC OCTOPOLE 25

(T. Ohkawa et al)

SURVEY OF SCYLLAC EXPERIMENTS 35

(F.C. Jahoda et al)

THE HIGH BETA TOROIDAL EXPERIMENT 47

(D.C. Robinson et al)

TOROIDAL CONFINEMENT IN SCREW PINCHES WITH NON-CIRCULAR PLASMA CROSS-SECTION 59

(H. Zwicker et al)

CONFINEMENT STUDIES IN 2XII 71

(F.H. Coensgen et al)

PLASMA DIFFUSION IN TWO AND THREE DIMENSIONS 83

(J.B. Taylor)

RECENT DEVELOPMENTS IN COMPUTER SIMULATION OF PLASMAS 93

(D. Biskamp et al)

ANOMALOUS RESISTIVITY IN PLASMA 105

(R.Z. Sagdeev)

PROPERTIES OF SOME TYPES OF PLASMA SHOCK WAVES 119

(E. Hintz)

CONTAINMENT AND RF HEATING STUDIES IN THE PROTO-CLEO STELLARATOR 135
(D.J. LEES, W.MILLAR et al)

CERTAIN RESULTS OF STELLARATOR EXPERIMENTS IN THE USSR 147
(L.M. Kovrizhnikh)

NUMERICAL MODELS FOR PLASMA EVOLUTION IN TOKOMAK DEVICES 157
(C. Mercier et al)

LASER CREATED PLASMAS AND CONTROLLED THERMONUCLEAR FUSION 171
(J.L. Bobín)

RECENT PROGRESS IN RESEARCH ON PLASMA FOCUS 183
(Ch. Maisonnier et al)

THE EUROPEAN COMMUNITY ACTIVITIES IN THE FIELD OF CONTROLLED THERMONUCLEAR FUSION 195
(D. Palumbo)

RESEARCH AND PROSPECTS ON CONTROLLED THERMONUCLEAR FUSION IN THE USA 213
(R.W. Gould)

RESEARCH AND PROSPECTS ON CONTROLLED THERMONUCLEAR FUSION IN USSR 221
(L.A. Artsimovich)

SUPPLEMENTARY PAPERS 231

Author Index 247

PREFACE

This volume contains the texts of the invited papers and the supplementary papers presented to the Fifth European Conference on Controlled Fusion and Plasma Physics.

The invited papers were selected by the Paper Selecting and Programme Committee and by the Organizing Committee from a list suggested by the Responsibles of leading plasma research groups through the world.

From the list of presented subjects,it is apparent that they deal with a large part of the world effort in Plasma Physics as related to Research on Controlled Fusion.

These papers are printed in the same order as they were presented to the Conference,except for Dr. Kovrizhnikh's paper which was not presented orally. The invited lecture by L.A.ARTSIMOVICH was presented by B.B.KADOMTSEV.

Last minute arrangements during the Conference permitted the presentation of the following two additional invited lectures :

. M.N. Rosenbluth : Problems in physics of Laser-Plasma interaction.

. E. Velikhov : Comments on pulsed thermonuclear systems.

The Organizing Committee would like to thank warmly Professor Rosenbluth and Dr. Velikhov for accepting the heavy task of giving these important contributions within a very short dead line.

Some minor editorial work was carried out. Reproduction by photographic processes means that the authors must bear responsability for their texts.

We wish to thank authors for carrying out the relatively rigourous instructions necessary for this type of publication.

The Organizing Committee,

C O M I T E d' H O N N E U R

Honorary Council

Monsieur P. AIGRAIN,	*Délégué Général à la Recherche Scientifique et Technique.*
Monsieur B. BRUNELLI,	*Président du Comité d'Organisation de la IV^{e} Conférence Européenne sur la Fusion Contrôlée et la Physique du Plasma.*
Monsieur J. L. DELCROIX,	*Directeur du Laboratoire de Physique des Milieux Ionisés de la Faculté des Sciences d'Orsay.*
Monsieur B. LEHNERT,	*Président de la Division Plasma de la Société Européenne de Physique.*
Madame H.MATHIEU-FARAGGI,	*Président de la Société Française de Physique.*
Monsieur A. MESSIAH,	*Directeur de la Division de la Physique du Commissariat à l'Energie Atomique.*
Monsieur R.L. MÖSSBAUER,	*Prix Nobel de Physique, Directeur de l'Institut Max von Laue - Paul Langevin , Grenoble.*
Monsieur L. NEEL,	*Prix Nobel de Physique, Délégué du Haut-Commissaire auprès du Centre d'Etudes Nucléaires de Grenoble.*
Monsieur D. PALUMBO,	*Directeur du Programme Fusion de la Commission des Communautés Européennes.*
Monsieur M. PASCAL,	*Directeur du Centre d'Etudes Nucléaires de Grenoble.*
Monsieur M. SOUTIF,	*Président de l'Université Scientifique et Médicale de Grenoble.*
Monsieur J. YVON,	*Haut-Commissaire, Commissariat à l'Energie Atomique.*

ORGANIZING COMMITTEE

T. CONSOLI, *Chairman.*

E. CANOBBIO, *Scientific Secretary*
O. DE BARBIERI
C. GORMEZANO
P.P. LALLIA

Miss J. VERCIER, *Manager*
Mrs S. VASSALLO
B. BARRY
J.J. CAPITAIN

Mrs A.M. DUPAS, Mr. G. ICHTCHENKO and Mr. J. LUTY
Technical Assistants.

Association EURATOM-CEA
Département de Physique du Plasma et de la Fusion Contrôlée
Service d'Ionique Générale, Centre d'Etudes Nucléaires de
GRENOBLE, 38041 FRANCE

PAPER SELECTION AND PROGRAMME COMMITTEE

G. LAVAL, Ecole Polytechnique, Paris, France.
B. LEHNERT, Royal Institute of Technology, Stockholm, Sweden.
D.R. SWEETMAN, UKAEA, Culham Laboratory, Abingdon, United Kingdom.
H. ZWICKER, Max-Planck-Institut für Plasmaphysik, Garching, Federal Republic of Germany.

FINANCIAL SUPPORT

The Organizations listed below have contributed financially to the Conference.
Their support is gratefully acknowledged :

COMMISSARIAT A L'ENERGIE ATOMIQUE, PARIS
COMMISSION DES COMMUNAUTES EUROPEENNES, BRUSSELS.

INVITED PAPERS

Experiments on the ST Tokamak Device

W. Stodiek
Plasma Physics Laboratory, Princeton University
Princeton, New Jersey 08540, USA

Abstract: Experiments in the different operating regimes of ST tokamak are discussed. The optimum regime is limited at low density by electron runaway and at high density by radial shrinkage of the current channel, resulting in macroscopic instability.

At the last European conference we reported that quasistationary discharges had been produced in the ST tokamak.[1] Long confinement times and long time stability for these discharges for a given plasma current could be obtained for q values at the limiter of about 3 or larger and for the density regime from 2×10^{12} to 5×10^{13} cm^{-3}.

The operating regimes of the ST tokamak, depending on density and limiter q value are summarized in Fig. 1. For currents of about 50 kA and large enough q values, discharges at densities around 1×10^{13} cm^{-3} show the best longtime stability, this continues to lower densities, but here the electron velocity distribution has the tendency to develop into a runaway electron distribution. At densities around 1×10^{12} cm^{-3} most discharges terminate by current inhibition, and for gas pressures corresponding to electron densities lower than 1×10^{12} cm^{-3}, it is difficult to initiate a discharge at all. At high density the current channel has apparently the tendency to shrink, with the result of low central q values. Kink-type oscillations are observed, which frequently develop into the so-called disruptive instability. The density regime for these processes is very dependent on the conditions of the discharge tube. At higher density, but with good preionization to reduce the initial high voltage, a low temperature discharge develops. Without sufficient preionization apparently most of the current is carried by very high-energy electrons in a relatively cold main plasma.

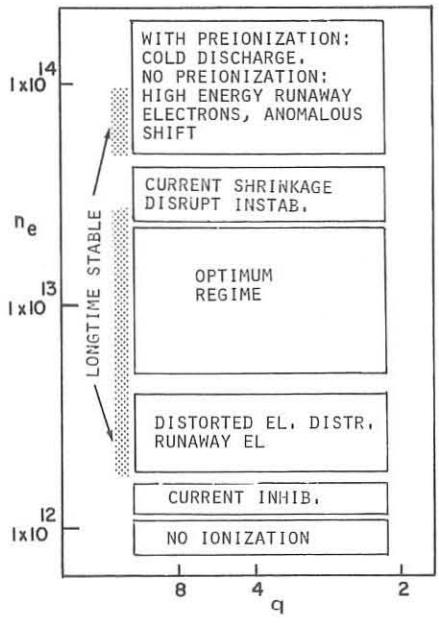

Fig. 1. Operating regimes of ST tokamak for about 50 kA plasma current.

The work on ST has been concentrated on detailed investigation of the plasma properties and development of diagnostic techniques. This survey will report on three main efforts. In the optimum density regime, the known characteristics of the discharge and the still open problems, especially in respect to the scaling of confinement with plasma parameters are discussed.[2] In the regime of larger density or low q values the problems of macroscopic stability are of interest. Thirdly the electron velocity distribution has been determined in all operating regimes, but especially in the low-density regime, where a non-Maxwellian distribution is found. The accurate determination of the relevant discharge parameters is very involved; this can best be demonstrated by describing a particular discharge and its time dependence. Figure 2 shows the current and voltage traces of a discharge in the optimum density regime,[3] which was produced in a toroidal field of 37 kΓ within an aperture of 13 cm radius, limited by a tungsten rail limiter. The working gas was hydrogen at pressure of 6×10^{12} cm^{-3}. The ramping time-shape of the current from 5 - 35 msec was designed to minimize the expenditure of volt-seconds of the transformer core by avoiding too large currents at early times, where the temperature and conductivity are low.

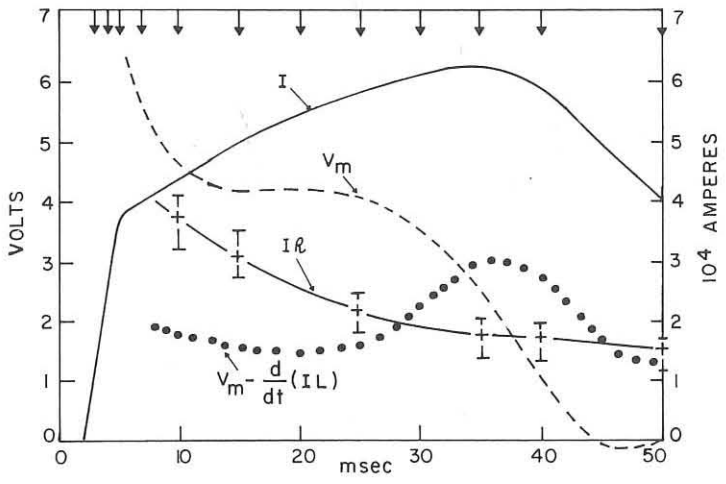

Fig. 2. Measured Ohmic heating current I and the loop voltage V_m. The curve IR is the voltage corresponding to a resistance R, determined from the Spitzer resistivity with a toroidal correction. The dotted curve is the resistive voltage calculated from the electron temperature profiles assuming negligible skin effects. The arrows indicate the time at which radial profiles of $T_e(r)$ and $n_e(r)$ were measured.

The dashed curve labeled V_m gives the loop voltage, which consists of a resistive voltage IR and an inductive part determined by the leakage inductance between plasma and vacuum vessel. The IR is the computed voltage corresponding to the Spitzer resistivity with toroidal correction. The dotted curve is the resistive voltage, as calculated with the help of the electron temperature profiles assuming negligible skin effect. The arrows at the top indicate the times at which the radial temperature profiles, which are shown in Fig. 3, were determined from Thomson scattering. The very initial phase (which is not shown) develops,

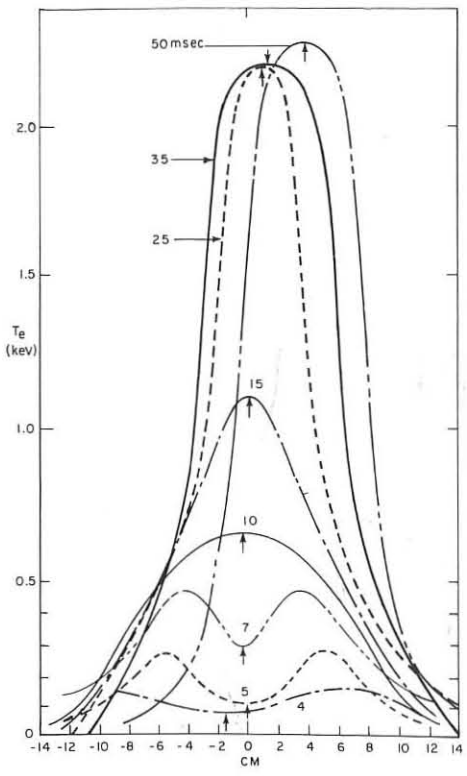

Fig. 3. Radial temperature profiles, at indicated times, on the horizontal midplane of the torus. Major radius increases to the right. The profiles are symmetrized about the short vertical arrows attached to each curve.

apparently due to the current skin effect, into a cylindrical shell with maximum temperatures nearly three times the central temperature. In the slowly varying part of the current rise the current penetrates to the center and the temperature distribution becomes monotonic. At 25 msec a peak temperature of 2.2 keV is reached. While the current grows further, the profile gradually widens. The density profiles are roughly parabolic; that is, distinctly wider than the temperature profiles. In these discharges, the total rate of H_α and impurity line emission and the Doppler width of H_α and of various impurity lines has been measured. From this we deduce (a) the total ionization rate and hence the particle confinement time, τ_p, (b) the effective charge of the ions for momentum transfer $\bar{Z} = (\Sigma Z_1^2 n_i)/(\Sigma Z_1 n_i)$, (c) the total power loss by radiation, (d) the ion and neutral atom energies at various locations. The impurity concentration was found here to be rather high, 12 - 14% oxygen; the other impurities are negligible compared with the error in the oxygen concentration. The probable radial distribtuion of $\bar{Z}$ was computed.

Two points are of particular interest: the resistivity and power input and the energy balance and particle confinement. We conclude from the previous figure that after 15 msec there is no skin effect and therefore the knowledge of the resistivity and of the <u>total</u> current allows the determination of the radial distribution of the current density and power input. We assume that the local resistivity is the Spitzer resistivity corresponding to the temperature and $\bar{Z}$ profiles, and taking into account the effect of trapped electrons.

Figure 4 shows the profiles of these quantities at 35 msec. The lower curve shows the electron conductivity $[\eta(r)]^{-1}$ multiplied by r/R. The area under this curve is the total conductance. Also shown are the electron temperature profile, the density profile, the profile of the average $\bar{Z}$, the ion

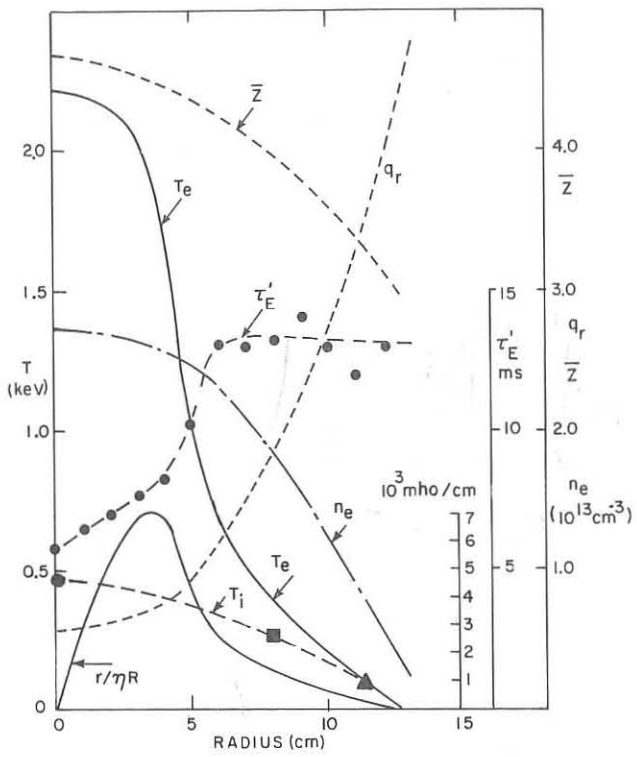

Fig. 4. At 35 msec the (symmetrized radial profiles of electron density, electron and ion temperature [O from charge exchange, [], Δ from Doppler broadening of the λ1623 OVII and λ1548 CIV lines, respectively], the mean ion charge $\bar{z}$, the inverse rotational transform q_r, the energy confinement parameter τ_E, and the electrical conductance per cm shell thickness.

temperature, (at the center from charge exchange and further outside from Doppler broadening of oxygen and carbon), the q value and the energy confinement parameter τ_E' defined as the local energy content divided by the local power input by Ohmic heating.

The low q-value implies that the current at the hot central part exceeds the Kruskal-Shafranov limit. It seems quite likely (and we have other data which confirms this idea) that the flattening of the $T_e(r)$ and its failure to grow after 20 msec is directly related to the $q < 1$ condition.

The <u>total</u> power input in these discharges is probably fairly well determined by I^2R. This quantity is shown in Fig. 5 as P_{in}. The total electron kinetic energy is W_e. The difference $P_{in} - \dot{W}_e$ (the dashed curve) represents the total power loss from the plasma electrons. The lowest curve gives the power loss by radiation (mostly from OVI and OV) emerging largely from the periphery of the plasma. The electron power loss to the ions by Coulomb collision is given by P_{ei}. The remainder of the power loss is expressed as an energy confinement time[2] $\tau_E = W_e/(P_{in} - \dot{W}_e - P_{ei} - P_{rad})$, which in this case is nearly equal to the particle confinement time, which is also shown.

Half of the ionization rate in this discharge is due to oxygen. The hydrogen ionization rate is deduced from the total H_α intensity measured at various locations around the torus. The basic difficulty with the determination of confinement times, is that the source function of particles and power input as a function of radius is not well known. The impurity atoms enter only at the periphery of the discharge and move inward as ions. Most

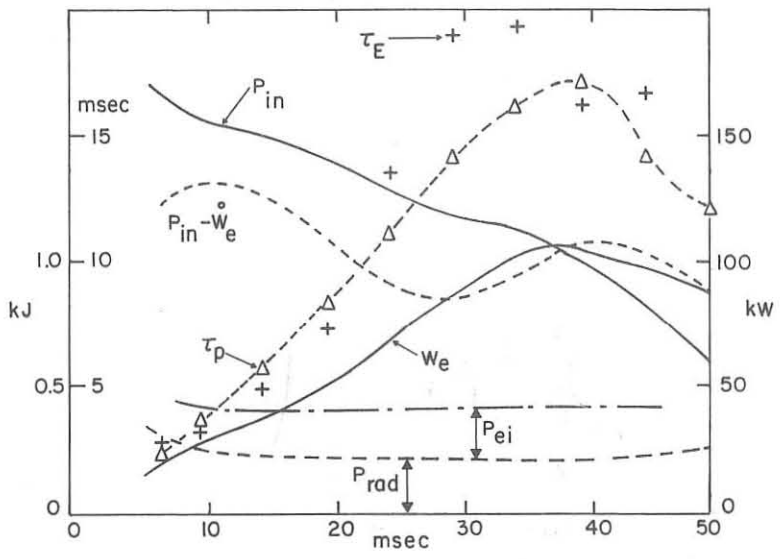

Fig. 5. The total electron energy, W_e, and average particle energy confinement times, τ_p(Δ0) and τ_E(+), with total power input, P_{in}, total power loss rate by electrons, $P_{in} - W_e$, the power loss by radiation, P_{rad}, and by Coulomb collisions with ions, P_{ei}.

neutral atoms of hydrogen or helium found near the periphery, far from the limiter, have an energy of 2 - 3 eV; but atoms with 25 to 30 eV are found to be injected near the limiter. A very rough estimate of the radial and circumferential neutral distribution of hydrogen is as follows[4]: At the port opposite to the limiter the central density is found to be about 3×10^8 cm^{-3} from optical measurements, and about 4×10^8 cm^{-3} from charge exchange neutrals; at the edge the density is about 1×10^{10} cm^{-3}. Within about 20 cm of the limiter the central density from H_α flux and Doppler energy measurements is 3×10^{10} cm^{-3} at atom energies 25 - 30 eV; the edge density is about 1×10^{11} cm^{-3}. The average around the whole torus is then: central density, 1×10^9 cm^{-3}, edge density 2×10^{10} cm^{-3}.

The main conclusions drawn from a number of ST tokamak discharges in the "optimum density regime," as described above, are the following: The resistivity measured in discharges in the optimum regime in H_2, He and Ne indicates no anomalous resistance factor when compared with the Spitzer resistivity. Here the current profile is inferred from the temperature profile, and the measured impurity content is taken into account.[5] The impurity effect is due mainly to oxygen (often ~5%) and high-Z material from the limiter (0.1-0.3% for molybdenum). In neon discharges[6] where impurities are less important because of the high Z of the neon itself, very good agreement has been found between the computed and measured resistivity values. Unfortunately, a direct measurement of the current distribution is still not available; we can, therefore, prove only internal consistency with the assumption of classical resistivity. The result may not be too surprising because the ratio of the electron drift to thermal velocity in these discharges is about 5%, and the ions are too hot for ion sound wave excitation. The plasma energy content was

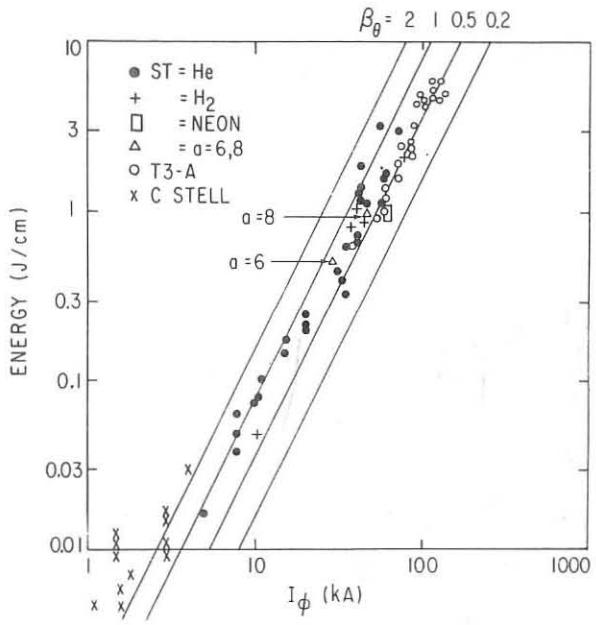

Fig. 6. The total plasma energy (electron + ion) per cm axial length, as a function of the Ohmic-heating current for a variety of conditions. Open circles are T3-A data [Culham Lab. Report R107 (1970)]. Aperture radii from 4 to 12 are included; two specific values of a are shown by Δ. The straight lines indicate the values of $\beta_\theta = 8\pi nkT/B_\theta^2(a)$ for the tokamak cases (poloidal field due to toroidal plasma current only).

scaling reported for T-3. ST values average about 0.75 instead of 0.5 (points at higher currents). Particle and energy confinement times were determined in discharges in hydrogen and helium at aperture limiter settings from 4 - 13 cm and plasma currents from 1.7 - 74 kA.[8] The average particle confinement time is plotted in Fig. 7 against average electron temperature. In the temperature regime above about 150 eV the ST tokamak confinement time increases with temperature about as $T_e^{3/2}$. In the regime determined from diamagnetics and also from laser scattering for the electrons, and charge exchange and Doppler broadening for the ions. The total plasma energy content per unit length is shown in Fig. 6 as a function of the toroidal current.[7] The results cover a wide range of minor radii (6 - 14 cm), different gases (H_2, He, Ne) and different toroidal fields. β_θ is about constant (although this is not strictly true for fixed current and varying density); this confirms the

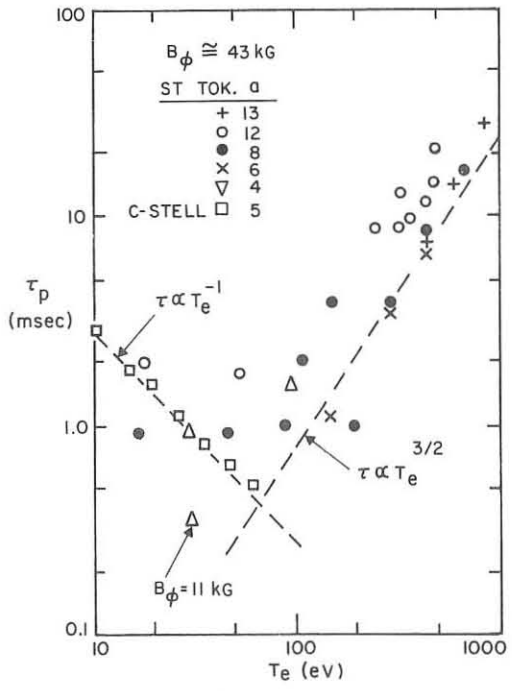

Fig. 7. Particle confinement time and temperature in the ST Tokamak and the C stellarator, for various values of aperture-limiter setting and plasma current. The $T_e^{3/2}$ line is drawn approximately through the upper points. The T_e^{-1} line is the Bohm-loss line for $B_\phi = 43$ and a = 5 cm (the C stellarator aperture).

below about 100 eV the stellarator results show $\tau_p \sim T_e^{-1}$. The confinement time τ_p also obeys roughly the $T_e^{3/2}$ relation during the temperature increase in the process of the discharge, and is inversely related to $\bar{Z}$. In Fig. 8 the observed overall particle confinement time is plotted versus the computed pseudoclassical time[9] with $c^2 = 1$. The points to the left represent discharges of low current and low temperature. At temperatures above 150 eV the points seem to follow roughly the 45° line. These points represent discharges of quite different plasma radii currents and densities.

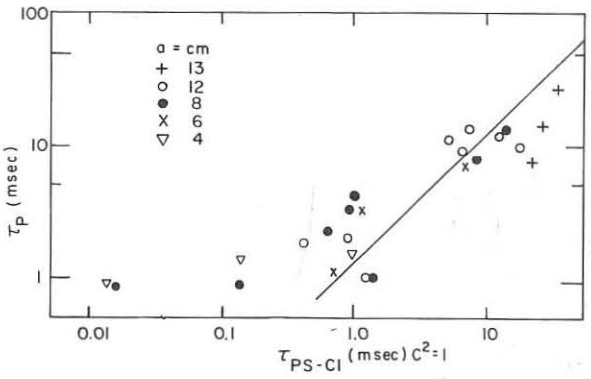

Fig. 8. The observed particle confinement time plotted against the computed Pseudoclassical time for $c^2 = 1$. The points at the right represent high current and high temperature. The temperature at 1 msec is about 150 eV, and the points to the left are lower in temperature. Observe that the points belong to very different limiter radii.

We tentatively conclude from our data that above a certain temperature the energy and particle confinement increase with temperature and poloidal field strength. The absolute values of the confinement times are more than an order of magnitude shorter than the neoclassical ones and (considering the shapes of the profiles for density and temperature) they can also not be fitted to the Bohm coefficient.[10] Heat conduction in addition to particle transport may be necessary to describe the observed profiles.

The treatment in terms of overall particle and energy confinement times is probably too rough an approximation of the problem, and it seems necessary to take the radial dependences more seriously into account than has been done so far. For instance, in Fig. 4 the electron temperature gradient is largest inside the quite flat part of the density profile. The energy input occurs mostly near the center; thermal conduction may be important for transport of heat to the outside layer; from there it can be taken to the limiter by particle transport, heat conduction, radiation and charge exchange. The outside layer acts then only as a virtual limiter. The particle replacement time referring only to the region near the center can be much longer than the energy replacement time. A detailed computer model has been employed to study the discharge behavior as a function of radius.[11]

Macroscopic instabilities are observed in the ST tokamak for high-density discharges where shrinkage of the current channel to low q values occurs, or

simply for low initial q values.[12] They are low frequency oscillatory modes with slow growth rates, often followed by the so-called disruptive instability. The low frequency oscillations are magnetic field and density perturbations detected with the ion-beam-probe or with magnetic pickup probes. Their mode structure is $(m\theta - n\phi)$, with $m = 6$ to 2 for $n = 1$. m/n is always less than q at the limiter, so that the point $q(r) = m$ is found at a radius r smaller than the limiter radius a. It is concluded that these instabilities could be tearing modes, that is, resistive MHD kink instabilities.[13] These modes have also been initiated by forced shrinking of the current channel by pulsed injection of hydrogen gas at the periphery during the discharge, causing m to decrease. These oscillations lead for $m = 2$ to the violently growing "disruptive" instability,[14] which is accompanied by a current channel expansion, a negative voltage spike, and the loss of a large fraction of the plasma energy. This is shown in Fig. 9. The instability mechanism acting here is still unknown. It may be related to magnetic surface breakup. Although the modes at higher m have little effect on the plasma confinement, it was observed that runaway electrons are lost from the discharge volume during this process. The occurrence of these instabilities is a severe restriction on the maximum density at which a long-time stable discharge could be produced, and the lowest q which can be obtained without additional stabilizing features. The detailed mechanism of the current shrinkage is not certain.

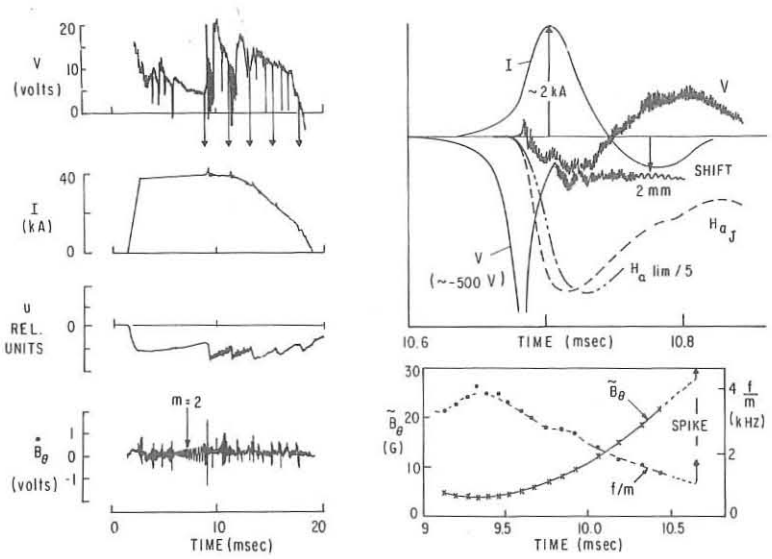

Fig. 9. Effect of the disruptive instability on the discharge voltage and current, and on $u = B_{\theta out} - B_{\theta in}$ (major radius shift outward is positive). Conditions are $B_\phi = -15.5$ kG. The short-time effects are shown expanded in time in the top right figure. H_α intensities are for locations A (limiter) and J (~opposite). The frequency and amplitude of the $m = 2$ oscillation leading into the instability are displayed in the bottom right figure.

The electron velocity distribution in the vicinity of the average energy can be obtained roughly from laser scattering. Above this energy, Bremsstrahlung spectra have been used to study the velocity distribtuion from about 2 keV

to the MeV range.[15] The distribution varies markedly with density. A typical spectrum is shown in Fig. 10. It consists of a Bremsstrahlung continuum with lines of the most prominent impurities superimposed. For simplicity of discussion, the continuum spectrum is characterized by sections of straight lines whose slopes determine equivalent temperatures. The low-energy continuum corresponds well to the Thomson scattering temperature. There is also an enhanced tail above 10 keV energy, indicating that the distribution is not Maxwellian. The limiter material, for instance molybdenum, gives rise to K_α and K_β lines. A rough indication of the degree of ionization of the M-shell can be obtained from the K_α:K_β ratio. In this case, Z is about 25 - 30. The absolute intensity of these lines gives the Mo concentration, estimated to be about 1×10^{10} cm^{-3}. Spectroscopic measurements[16] (Mo XIII and Mo XIV lines) give somewhat higher concentrations, but this discrepany could be explained by radial differences, the K lines originating from the hot center of the plasma and the Mo UV lines from nearer the outside. The character of the velocity distribution depends to a large extent on the filling pressure. This is seen in Fig. 11. Only the straight line approximation is shown, and the spectra are normalized to 1 at zero energy. The velocity distribtuion for condition b) represents a discharge in the optimum regime; with a gas pressure of 3×10^{-4} cm^{-3}, it was just below the high pressure instability region. The spectrum was Maxwellian over may orders of magnitude and shows a temperature of 800 eV. Condition c) is at somewhat higher pressure, and here negative voltage spikes occur. The spectrum has not been followed over as large a range of energy as the previous one but it appears again Maxwellian, with 800 eV temperature and without hard x-rays. As

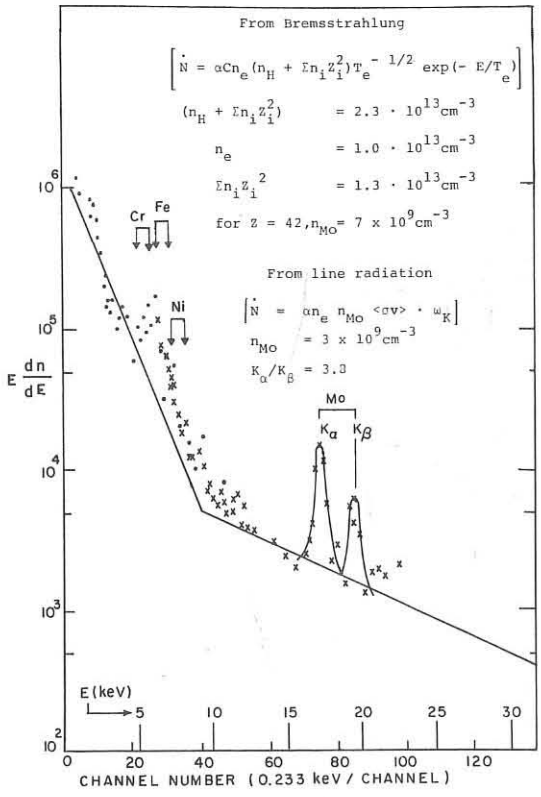

Fig. 10. Representative x-ray spectrum for an intermediate-pressure hydrogen discharge. Electron temperature derived from the low-energy end checks well with Thomson scattering of a laser beam. The high-energy end shows an appreciable runaway component in the electron-velocity distribution. The K_α and K_β lines of molybdenum are from impurity atoms originating from the aperture limiter.

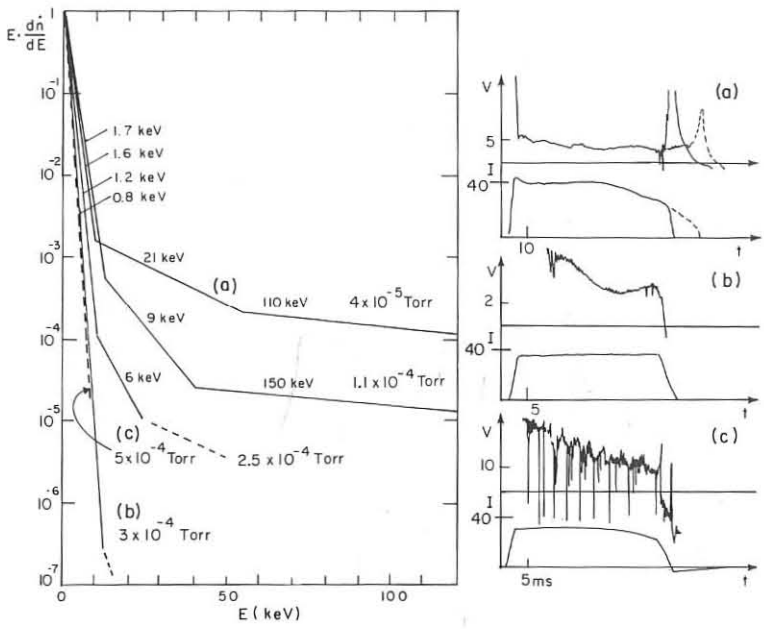

Fig. 11. Electron-velocity distribution functions determined from x-ray spectra; various gas-filling pressures. Typical current and voltage traces [subfigs. (a), (b), (c)] belong to the correspondingly marked curves.

the pressure is reduced, a continuous increase in the number of high-energy electrons is observed. The distribution bends slowly in the region of 10 keV and shows here large tails with temperature of 10 to 20 keV, followed by a less intense high-energy group with a slope of 100 to 200 keV. For curve a) taken at a pressure of 4×10^{-5} Torr, the number density of the runaways was estimated at 3×10^{11} cm^{-3} for the 21 keV group, and 3×10^{10} cm^{-3} for the 110 keV group. The angular distribution of the x-ray flux shows that the fast electrons are accelerated in the toroidal electric field.[17] The number density seems large enough to make a significant contribution to the value of $\beta_{||}$; a large part of the plasma current could be carried by this beam of electrons. The runaway electrons originate predominantly at the hot center of the discharge, where the value of E/E_{cr} is largest.

At very large pressures with insufficient preionization, the discharges are dominated by very high energy runaway electrons. These discharges exhibit the anomalous shift observed in TM-3 and T-3. It seems plausible that the runaway electrons in this case make dominant contributions to the current and $\beta_{||}$, but a quantitative answer to this question is not available yet. Discharges at very low density often show current and voltage characteristics similar to those of the current inhibition cases observed in stellarators at low density, where the current dies off prematurely.

The ST experiments have suffered from three main problems: the unknown current distribtuion, the coupling of heating and confinement, and the relatively low plasma current.

To determine the current distribution, three methods are being developed to measure the poloidal field as a function of the radius. The thallium ion beam method[18] uses deflection of the beam in the poloidal field. The space potential and the electron density in the interior of the plasma column can also be determined and the time response is so fast that also fluctuations of these quantities can be measure.[19] Preliminary results show that a reliable current distribution measurement seems possible but has not been obtained yet. The space potential on the other hand has been measured in a low confining field discharge at low density and current. It is shown in Fig. 12. Local fluctuations of density which occur in the presence of $m = 2$ oscillations are in perfect synchronism with the signals of magnetic B_θ probes.[20] The two other methods for obtaining the current distribution determine the direction of the field lines from radiation polarized with respect to the magnetic field vector. Microwave exitation of the extraordinary wave in the plasma is used in the microwave regime[21], and collisional excitation of Zeeman lines of neutral atoms of a cold beam is used in the optical regime.[22]

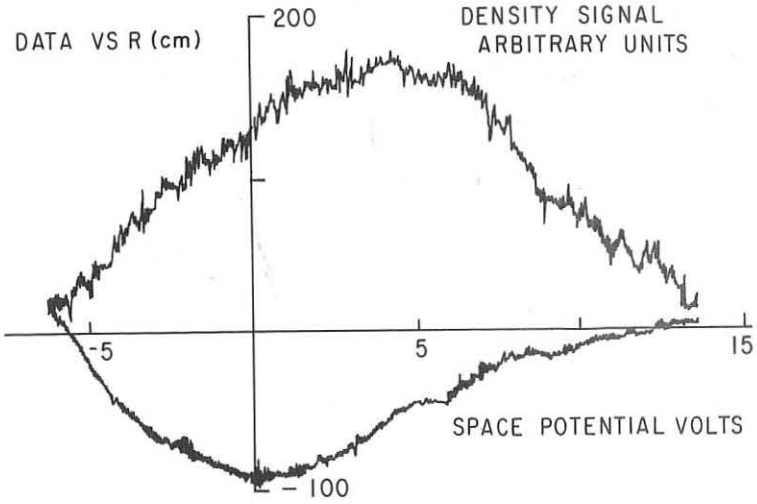

Fig. 12. Computer display of density (I_{Tl2+}) and space potential (V_{pl}) versus radius on the detector line for a 21 kA hydrogen discharge. These are the raw signals. The density profile appears skewed due to attenuation of the primary beam.

Ion cyclotron heating has been developed to work in the curved tokamak geometry for additional heating and to study confinement separate from heating. The very encouraging results with low power equipment are reported elsewhere at this meeting.[23]

In the near future the ST device will operate at the full capability of the iron core, increasing the current to somewhat above 100 kA for 70 msec duration.

We should like to thank Professor M. B. Gottlieb for his support and encouragement. We gratefully acknowledge many fruitful discussions with Professor H. P. Furth and members of the ST Group.

This work was supported by U. S. Atomic Energy Commission Contract AT(11-1)-3073.

References:

[1] D. J. GROVE et al., Princeton Plasma Physics Laboratory MATT-813 (1970).
[2] D. DIMOCK et al., Princeton Plasma Physics Laboratory MATT-852 (1971); in Plasma Physics & Controlled Nuclear Fusion Research (IAEA, Vienna, 1971), I, p. 457.
[3] D. DIMOCK et al., Princeton Plasma Physics Laboratory MATT-906 (1972).
[4] E. HINNOV, Private Communication.
[5] E. HINNOV, Princeton Plasma Physics Laboratory MATT-Q29 (1972), p. 23; Ref. 2.
[6] E. HINNOV et al., Princeton Plasma Physics Laboratory MATT-875 (1971); Bull. Am. Phy.-Soc. 16 (1971), 1231.
[7] E. MESERVEY, Princeton Plasma Physics Laboratory MATT-Q29 (1972), p. 14; Ref. 2.
[8] E. MESERVEY, Princeton Plasma Physics Laboratory MATT-Q29 (1972), p. 15; Ref. 2.
[9] S. YOSHIKAWA, Phys. Rev. Letters 25 (1970), 353.
[10] P. H. RUTHERFORD, Private Communication.
[11] D. F. DÜCHS et al., Princeton Plasma Physics Laboratory MATT-Q29 (1972); in Plasma Physics & Controlled Nuclear Fusion Research (IAEA, Vienna, 1971), I, p. 369; Proceedings Fifth European Conference (1972).
[12] J. C. HOSEA, Princeton Plasma Physics Laboratory MATT-Q29 (1972), p. 26; Bull. Am. Phy.-Soc. 16 (1971), 1232.
[13] H. P. FURTH et al., Princeton Plasma Physics Laboratory MATT-897 (1972); Princeton Plasma Physics Laboratory MATT-872 (1971).
[14] J. C. HOSEA et al., Ref. 12.
[15] S. VON GOELER et al., Princeton Plasma Physics Laboratory MATT-Q29 (1972), p. 21; Bull. Am. Phy.-Soc. 16 (1971), 1231.
[16] E. HINNOV, Private Communication.
[17] S. VON GOELER et al., Proceedings Fifth European Conference (1972).
[18] R. L. HICKOK et al., Bull. Am. Phy.-Soc. 16 (1971), 1231; Mobil Research Development Report AFOSR TR-72-0018 (1972); Princeton Plasma Physics Laboratory MATT-Q29 (1972), p. 34; Nuclear Fusion 10 (1970), 195.
[19] F. C. JOBES et al., Bull. Am. Phy.-Soc. 16 (1971), 1231.
[20] J. C. HOSEA et al., Bull. Am. Phy.-Soc. 16 (1971), 1232.
[21] R. CANO et al., Phys. Rev. Letters 27 (1971), 783.
[22] S. VON GOELER et al., Private Communication.
[23] W. HOOKE et al., Proceedings Fifth European Conference (1972).
[24] Princeton Plasma Physics Laboratory MATT-Q29 (1972), p. 40.

ADVANCE IN THE TOKAMAK PROGRAMME

V.S. STRELKOV
Kurchatov Institute Moscow

The Tokamak devices are intended for the production and investigation of a hot plasma. The current flowing through the plasma column in these devices is known to heat the plasma and to play the main role in its insulation. MHD instabilities are supressed by the strong longitudinal magnetic field.

The plasma macroscopic equilibrium and stability conditions, the energy and particles losses and the heating mechanisms were investigated in the early experiments. The measured energy confinement time was shown to be considerably longer than that of Bohm and Bohm-type scaling did not describe these discharges. Such a result showed the toroidal systems were of interest from the fusion point of view.

The appearance of the so called neoclassical theory based upon the works of A.A. Galeev and R.Z. Sagdeev cast a new light on transport problems in a toroidal system. On the other hand there is marked progress in the plasma temperature reached in experiments. Fig. 1 shows the dependence of the electron and ion temperature on time over the last fifteen years. In our largest machine T-4 we have reached electron temperatures of some keV, a deuteron temperature of more than six hundred eV, an energy confinement time of order of 10^{-2} sec and a particle confinement time of order of 10^{-1} sec.

Table 1 shows the principal characteristics of the Soviet tokamaks. One can see the main lines of research are: instability investigations, the dependence of transport processes on plasma parameters and plasma heating. The last problem is of a great importance because the calculations show /1/ that an Ohmically heated tokamak will allow as to reach fusion temperatures only at very large fields and currents. The value $\beta = 16nkT/H_z^2$ then appears to be small and the reactor to be unprofitable. The next problem of the reactor of such a type is the cyclotron radiation and the bremsstrahlung radiation due to impurity ions but the losses due to the former mechanism can be reduced by the multiple reflections at the walls. Tokamak of non-circular cross-section seems to be more preferable than the circular

one from this point of view because of the better MHD stability at lower magnetic fields /2/.

TABLE 1

Name	Major radius, R_o(cm)	Limiter radius, a(cm)	Copper shell radius, b(cm)	Magnetic field, H(kOe)	Peak current, J(kA)	The main lines of research
T-4	90	I7	23	45	200	Ohmic heating, dependence of transport coefficients on plasma parameters
TM-3	40	8	I2,5	45	40	The same as T-4 plus electron-cyclotron heating
T-6	70	I5÷25	25	I5	70	Conducting shell effect on plasma stability
TO-1	60	I4	I8	I5	30	Feedback stabilization, the magneto-acoustic waves heating (MAWH)
TM-1-HF	40	8	I2,5	I5	I5	MAWH
FT -1	62,5	I7	25	7	30	Hybrid resonance heating

Now let us look at the progress made in solving the three above mentioned problems.

From the theoretical point of view it is possible to have a stable plasma column at stability factor $q \simeq 1$ at the edge of the plasma. However the instability appeared at $q \simeq 3$ in early experiments. It was the so called disruptive instability which is characterized by negative spikes in the voltage and by singularities in other traces. The hard X-ray radiation, hydrogen and impurity radiation appear at this moment simultaneously with non-thermal atoms. The experiments carried out in the T=3a device showed that the regimes with $2 < q < 3$ could be obtained by specially programming the form of the plasma current pulse. /3/ /4/.

A similar result was obtained in the T-6 device by varying the proximity of the plasma edge to the conducting wall. In Fig. 2 the current amplitude is plotted against the stability factor for different limiter radii. When the stability factor is large enough, the plasma is stable and the current generator produces a pulse of fixed amplitude. When a gross instability appears the column resistance increases and the current decreases. This occurs at $q \simeq 2$ if the limiter radius a is equal to 15 cm ($a/b = 3/5$). If the limiter radius is 25 cm ($a/b=1$) the current amplitude does not change till q has decreased approximately to one. Thus the experiment on T-6 shows the possibility of improving the plasma column stability by approaching the conducting shell.

The plasma column at $q \simeq 2$ does not contain energy as long as in the regimes with large q. In future experiments the transport processes in such a plasma are to be investigated..

The disruptive instability is also observed if either one increases gas pressure to the high density limit, or if the impurity level increases due to operating the machine under less clean conditions, or due to the injection of neutral hydrogen.

The correlation analysis of magnetic probe signals and streak photography of the plasma column give evidence for the existence of a kink structure which changes at the instant of the spikes. The absence of correlation at this instant seems to be the result of small-scale perturbations /6/ . This fact as well as the stability improvement due to approaching the conducting shell appears to point to the MHD nature of this instability. T-4 experiments show that a shrinking of the channel seems to be a possible

explanation of the plasma column outward shift observed before a spike. Such a constriction may be caused by the relative conductivity increasing in in the centre of the plasma column. Slow constriction of the current channel is observed also in the stable discharges. On the other hand a similar outward shift observed in the TM-3 device at low currents /8/.cannot be explained in some cases by only the current channel shrinking. It is most likely to result from a runaway electron current /9/.

Generally speaking the stable discharge region in TM-3 lies between two lines in the diagram plotting the plasma current against electron density (Fig. 3). The disruptive instability takes place to the right of the line 1. The anomalous outward shift is observed to the left of this line and near to it. When the density decreases the plasma becomes stable up to line 2. An instability similar to the disruptive one can be produced by lowering the density to a critical value.

This instability is characterized in particular by regular diamagnetic spikes in the diamagnetic loop traces. These spikes can be attributed to the increase of transverse energy of the electrons because of the absorption of a runaway electron beam.

A new type of instability was observed and investigated in the Tokamak T-6 installation in the Kurchatov Institute /10/. The distinguishing feature of these discharges are positive spikes in the voltage in contrast to the negative spikes of the usual disruptive instability. An analogous instability was observed also in the Ormak device in Oak Ridge Nationa Laboratory and in the Tokamak FT-1 in the Ioffe Institute. Attention must be called to the fact that these installations are characterized by the very good homogenity of the main magnetic field. Experiments on T-6 show that the unstable discharge becomes of the usual type if an inhomogenity of 2-3% is produced on the axis of the column. The phenomena observed seem to be connected with the existence of a very energetic electron beam carrying almost all the current.

The energy balance investigations show that energy losses due to electrons are at least three to five times greater than neoclassical even in the macroscopically stable discharges while the ion temperature seems to be in accordance with this theory. Neoclassical ion energy balance in the plateau region suggest the dependence of the ion temperature on plasma parameters $T_i \sim (nH_zJ)^{1/3}$ provided that ion heating is due to the ion heat conductivity /11/ . L.A. Artsimovich has called attention to the fact that in

the collisionless region the ion temperature is proportional to J^2. The collisionless regimes in the T-4 device should be produced at plasma currents of more than 100 kA provided that impurities do not increase the collision frequency. The dependence of the ion temperature on the current in the T-4 device calculated by Yu. N. Dnestrovskii is shown in Fig. 4. One can see the transition between the two region becomes much smoother if one takes into account the radial distributions of the plasma parameters. The dashed curves correspond to Artsimovich's formula for the plateau. Preliminary experiments carried out on T-4 at a current of about 150 kA do not permit us to choose between the two mentioned dependences.

Experiments on the additional heating by high-frequency (HF) and radio-frequency (RF) techniques have begun in the TM-3, TO-1 and TM-1-HF devices in the Kurchatov Institute and in the FT-1 device in the Ioffe Institute. Additional heating was observed also in the experiments on plasma stabilization by RF in the toroidal installations in the Efremov and Sukhumi Institutes.

In the TM-3 device electron-cyclotron was identified by the increase of the plasma column diamagnetism together with a change of other quantities /12/.

In the TO-1 and TM-1-HF devices the excitation of fast magneto-acoustic waves was used for ion heating. In booth experiments the heating was identified using the diamagnetic method and Doppler broadening of impurity lines.

To summarize the preliminary results we can say that HF energy is absorbed by the plasma and confined for at least the usual energy confinement time. Nowaday one of the problems is to estimate whether thse methods of heating perturb the initial distribution functions of the plasma species. Such a perturbation can lead to instability which can be dangerous in future large devices.

It is great interest to make use of the additional heating for investigate the dependence of the plasma confinement on the plasma temperature. Using Ohmic heating alone one cannot estimate such a dependence because the electron density, temperature and plasma current in tokamak are connected by a definite relation. The additional heating allows us to vary them in an independant fashion. Such a possibility was realized in the TM-3 device /13/. Fig. 5 shows the dependance of the energy confinement time on the electron temperature. The latter was changed by the variation of the microwave

generator power. The improvement in insulation seen in the graph does not contradict the neoclassical theory but eh experimental transport coefficients are much larger than the theoretical ones.

The conclusions to which these main lines of tokamak.research lead so far are :

1. The disruptive instability sets limits for stable regimes in tokamak as well as an instability which seems to be connected with runaway electrons.

2. The approach of the conducting shell to the edge of the plasma promotes the MHD stability of the plasma column and there is no evidence of disruptive instabilities when the q is decreased to 1.

3. Phenomena are observed which are possibly connected with the electrons carrying almost all the current in the machines with good homogenity of the main magnetic field. The instability in such discharges is characterized by a positive spike in contrast to the negative spike of the usual disruptive instability. It is possible that we have a beam-plasma instability in this case. An additional inhomogenity of 2-3% of the main magnetic field produces the usual tokamak discharges.

4. The experiments carried out so far do not contradict the neoclassical mechanism of ion energy losses provided that the collision frequency corresponds to the plateau region and the electron-ion energy exchange is classical.

5. Using additional heating of the electrons we have obtained the dependence of the energy confinement time τ_E on the electron temperature. τ_E is found to increase when the lectron temperature increases at low density.

6. The first optimistic results on additional heating of the plasma by HF have been obtained in some small tokamaks.

Fig. 1 The dependence of the electron and ion temperature on time over the last fifteen years.

Fig. 2 The current amplitude as a function of stability factor q .

Fig. 3 Boundaries between stable and unstable discharges on the TM-3.

Fig. 4 The calculated dependence of ion temperature on the current in the T-4.

Fig. 5 The dependence of the energy confinement time on the electron temperature.

REFERENCES

1. G.N. POPKOV and V.S. STRELKOV. Report on the IV International Working Sessions at technology of fusion reactors. Oak Ridge U.S.A. (1971).
2. L.A. ARTSIMOVICH and V.D. SCHAFRANOV. J.E.T.P. Letters. V. 15 p. 72 - 76.
3. S.V. MIRNOV and I.B. SEMENOV. Atomnaya Energiya. V. 30, p. 20 - 27 (1971).
4. S.V. MIRNOV and I.B. SEMENOV. Nucl. Fus. Suppl. V. 2. p. 401 - 406. Vienna (1971).
5. N.D. VINOGRADOVA and K.A. RAZUMOVA. Nucl. Fus. Suppl. V. 2. Vienna (1965).
6. S.V. MIRNOV and I.B. SEMENOV. J.E.T.P. V. 60 p. 2105 (1972).
7. L.A. ARTSIMOVICH and the others. Nucl. Fus. Suppl. V.2. p. 595 Vienna (1965).
8. L.A. ARTSIMOVICH and the others. Nucl. Fus. Suppl. p. 157 Vienna (1969).
9. V.S. MUCHOVATOV and V.D. SCHAFRANOV. Nucl. Fus. V. II. p. 605 - 634 (1971).
10. N.D. VINOGRADOVA and the others. Nucl. Fus. Suppl. V. 2. p. 441 (1971).
11. L.A. ARTSIMOVICH and the others. J.E.T.P. Letters. V. 11. p. 449 - 452 (1970).
12. V.V. ALIKAEV and the others. J.E.T.P. Letters. V. 15. p. 41 -44 (1972).
13. V.V. ALIKAEV and the others. Report on this conference.

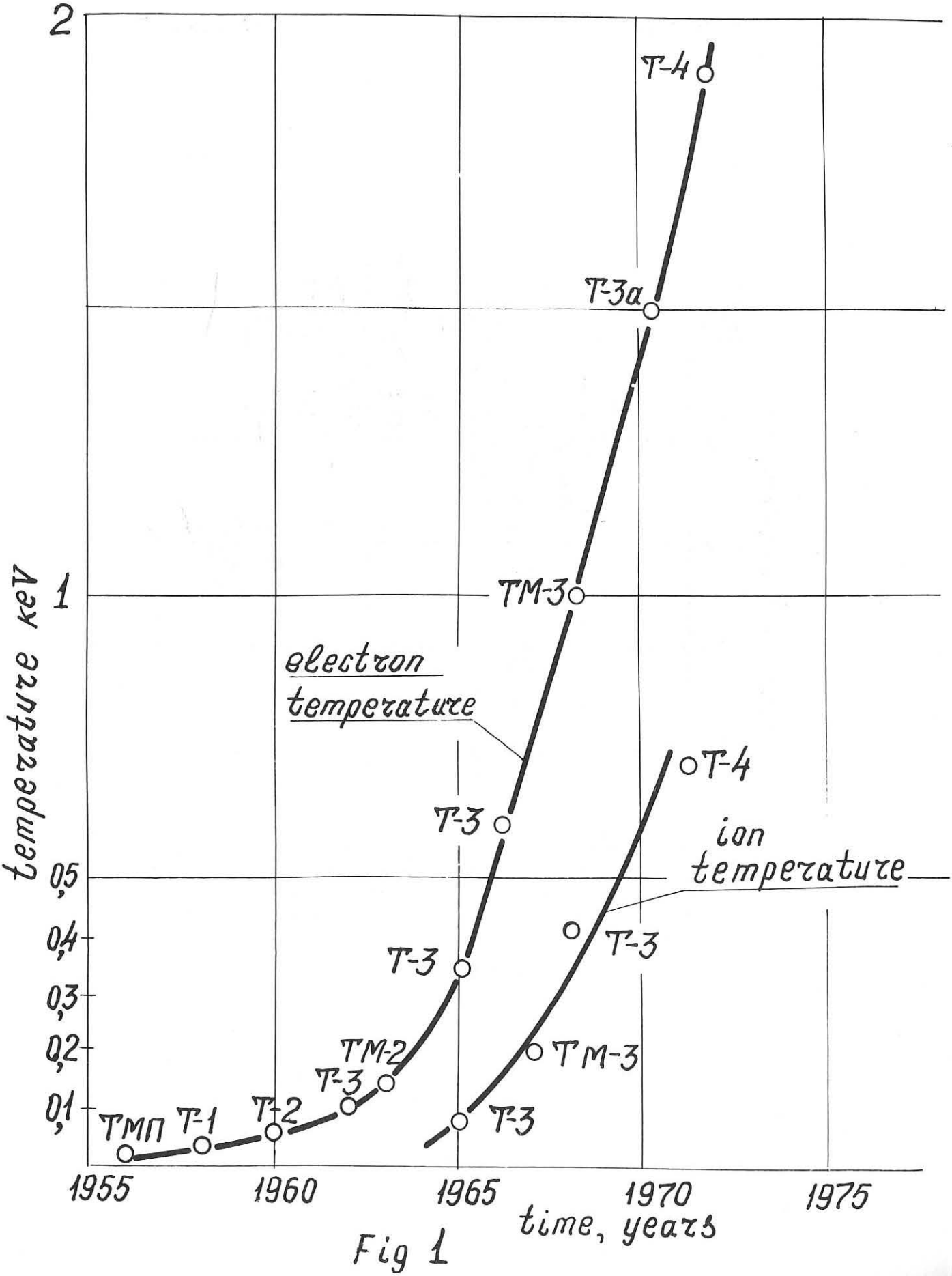
2
1
0,5
0,4
0,3
0,2
0,1
temperature keV
T-4
T-3a
TM-3
electron
temperature
T-3
T-3
TM-2
T-3
TMП
T-1
T-2
T-4
ion
temperature
T-3
TM-3
T-3
1955
1960
1965
1970
1975
time, years

Fig 1

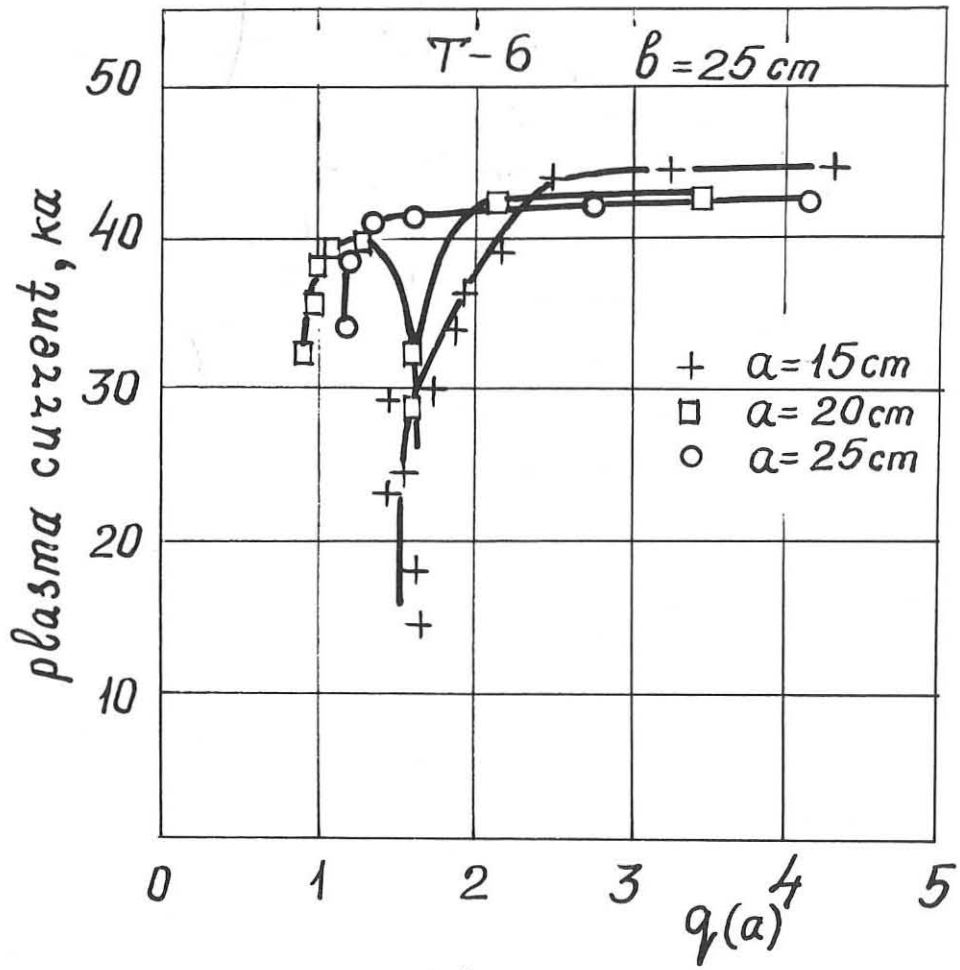
T-6
b=25cm
plasma current, ka
50
40
30
20
10
0
1
2
3
4
5
q(a)
a=15cm
a=20cm
a=25cm

Fig 2

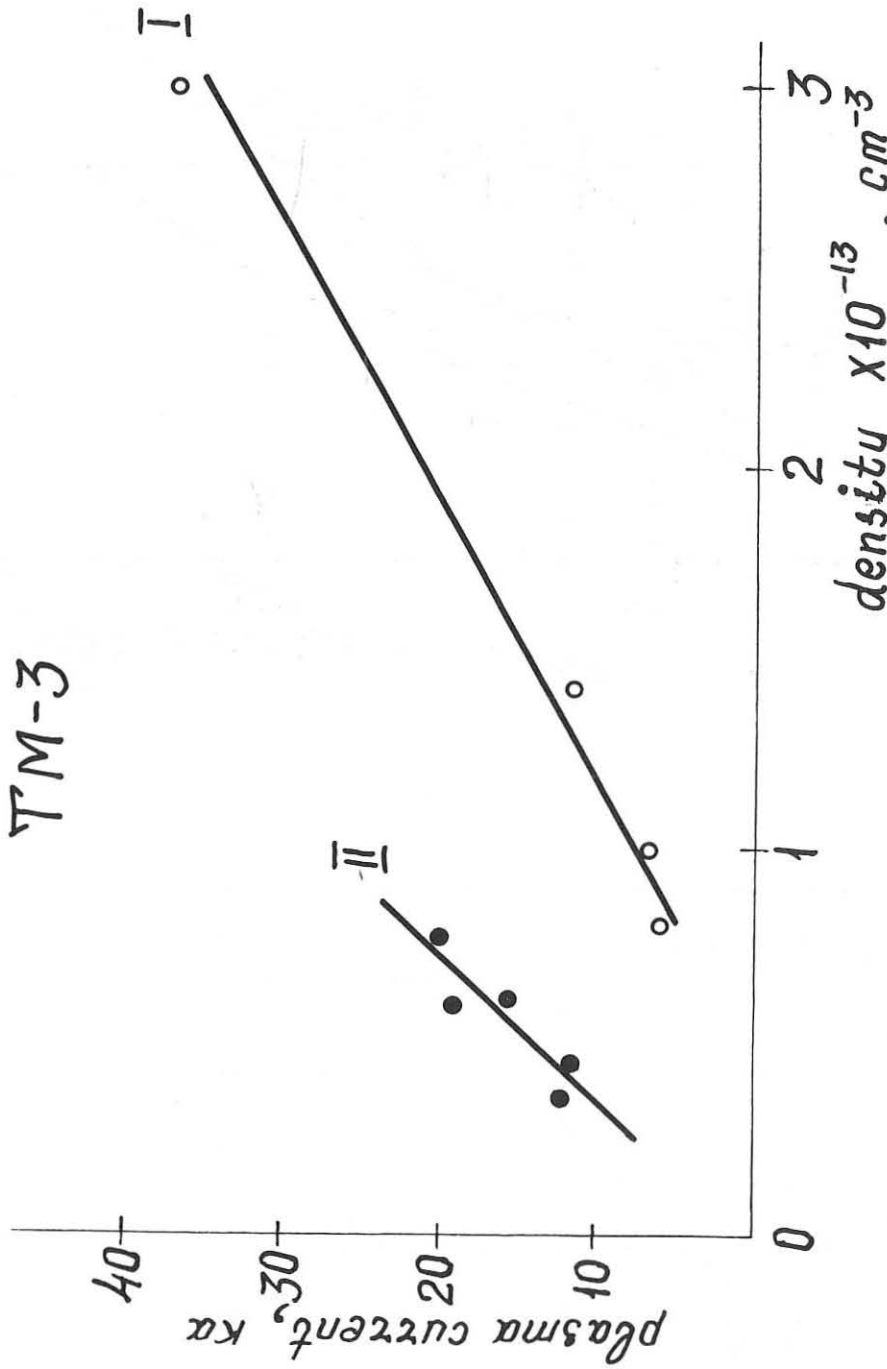

Fig. 3

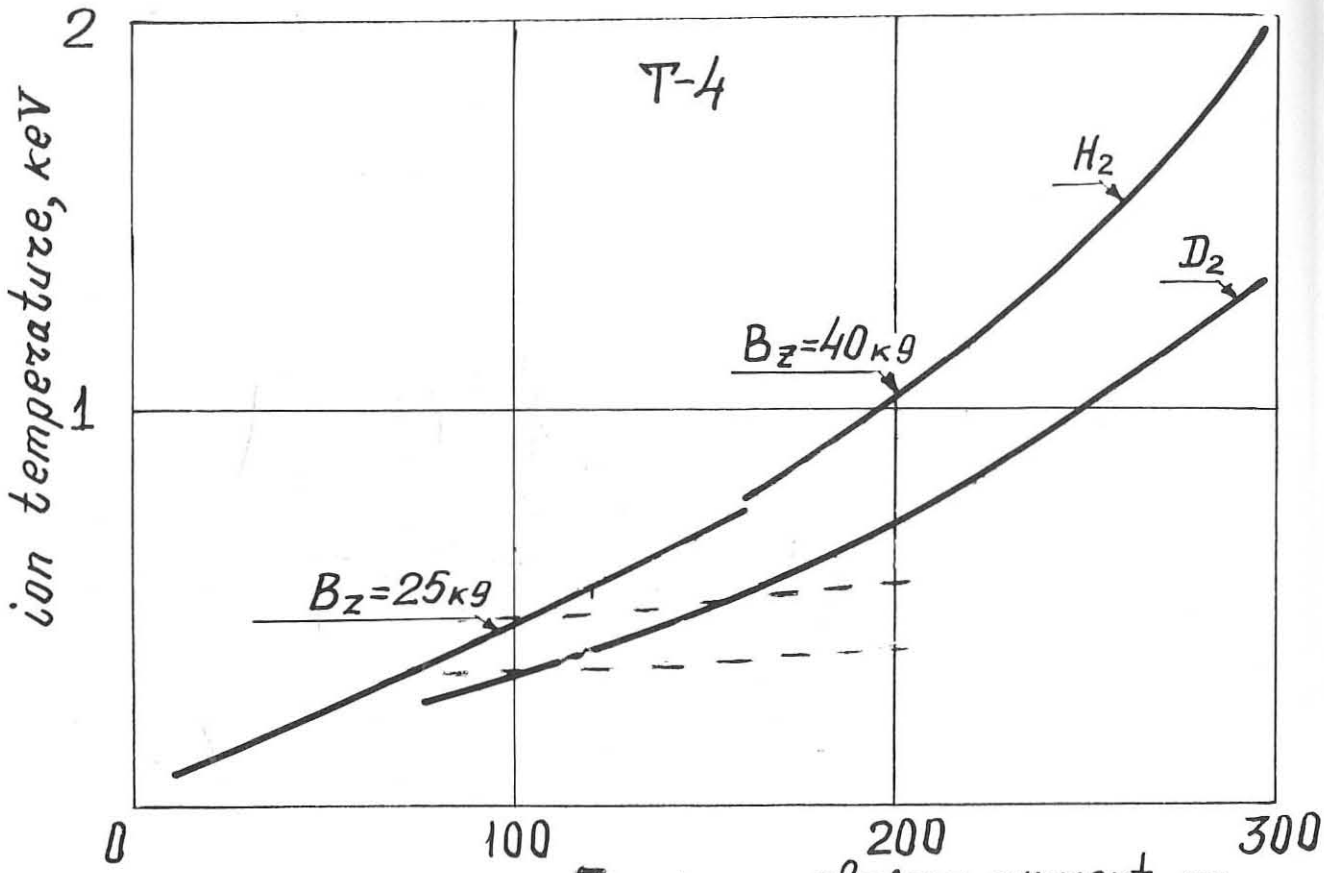
T-4
H_2
D_2
B_z=40кэ
B_z=25кэ
ion temperature, keV
2
1
0
100
200
300
plasma current, ка.

Fig 4

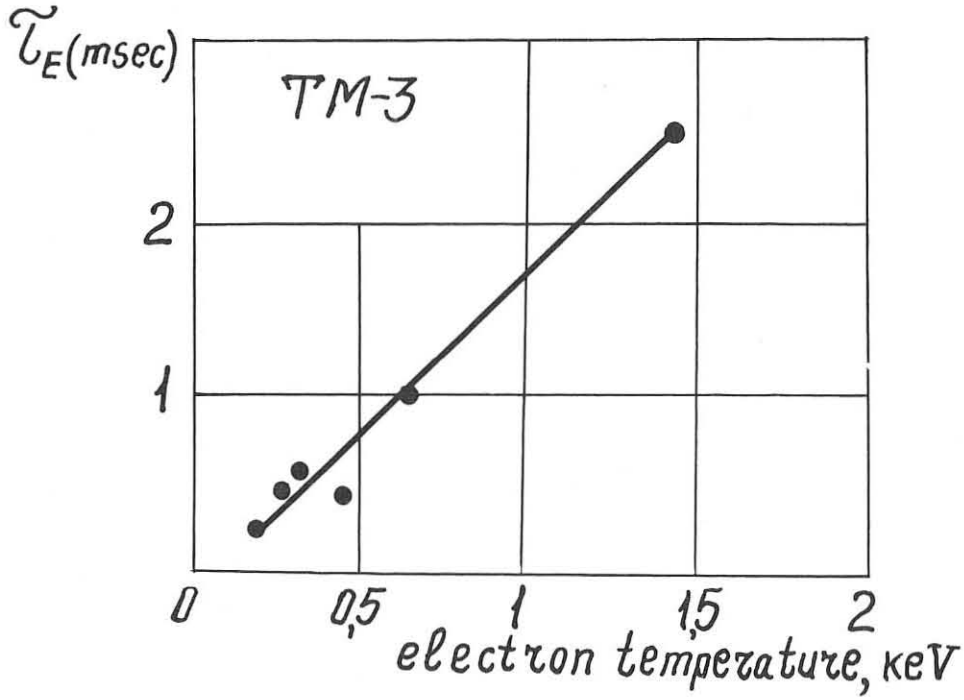
τ_E(msec)
TM-3
2
1
0
0,5
1
1,5
2
electron temperature, keV

Fig 5

MEASUREMENT OF NEOCLASSICAL DIFFUSION IN THE d.c. OCTOPOLE

by

Tihiro Ohkawa, Teruo Tamano, and Ronald Prater

Gulf General Atomic Company
San Diego, California 92112

Abstract: The plasma transport rates in the dc Octopole device are measured for various values of collision frequency. The diffusion rates are proportional to the inverse square of the magnetic field strength independent of collision frequency. For short mean-free path regimes, the experimental results agree with the Pfirsch-Schlüter theory in magnitude of the coefficient and dependence on temperature and density. For the long mean-free path regime, the results agree with the neoclassical theory. The value of the mean-free path where the transition from the classical to neoclassical diffusion, agrees with the theory for a wide range of temperature and density.

Introduction

Plasma transport processes have been studied in the dc Octopole device. Many types of plasma loss have been observed.[1-3] They may be classified into two types that depend strongly on the magnetic field strength and that are insensitive to the magnetic field strength. The latter include the loss to the ring support, the loss due to the atomic processes, the loss due to magnetic field imperfections, and the diffusion due to thermally excited convection cells[4] (Okuda-Dawson diffusion). Each process may be studied separately by choosing the machine and the plasma parameters so that the particular process is enhanced.

This paper describes the processes dependent on the magnetic field strength. It was found that the diffusion rate depends not only on the magnetic field strength but on the collision mean-free path. It will be shown that the dependence on these parameters and the magnitude of diffusion rate agree with the classical-neoclassical[5] diffusion theory. Namely, the diffusion rate in the collisional regime is given by the Pfirsch-Schlüter formula and is given by the neoclassical formula in the long mean-free path regime.

Section I gives a brief description of the device and the experimental procedure. Section II describes the diffusion in the absence of the toroidal magnetic field. Sections III, IV, and V deal with the diffusion with the toroidal magnetic field.

1. Description of the Octopole and Experimental Procedure

The octopole field is produced by the six current rings, four of which are internal to the plasma and are each held by three mechanical supports. The outer two rings carry the return current. The field configuration is shown in Fig. 1. The current to each ring is supplied by a bank of batteries through a coaxial electrical feed. The total area of the supports is about 100 cm^2. The maximum average magnetic field on the stability limit line is $\bar{B}_\chi \equiv \oint d\ell/(\oint d\ell/B_\chi) = 520$ G, where B_χ is the octopole field (poloidal field). This corresponds to 36 gyroradii from the separatrix to the stability limit line for 1 eV protons.

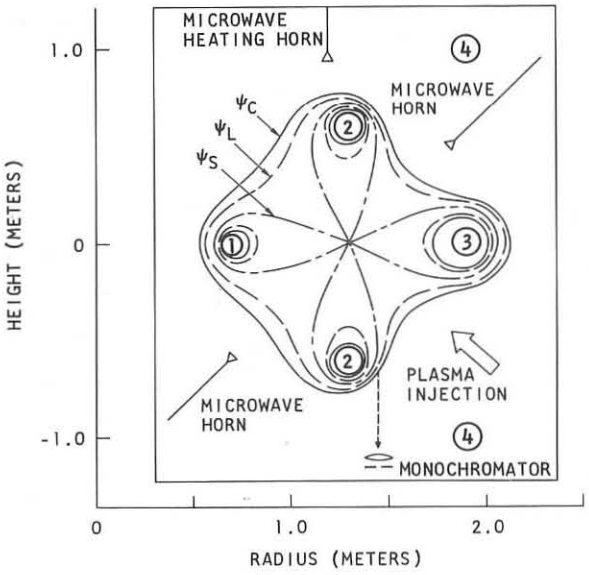

Fig. 1--Octopole magnetic flux configuration

The diameter of the rings is from 1.4 to 4.0 m and the effective plasma volume is 1×10^7 cm^3. All the rings are installed inside an aluminum vacuum tank, 8 ft high and 16 ft in diameter. The volume of the tank is 4×10^7 cm^3 which is evacuated below 10^{-7} Torr by four 10-inch diffusion pumps with liquid nitrogen traps and by a titanium pump.

The toroidal field is produced by a 36-turn toroidal coil wound outside the vacuum tank. This coil is also energized by a bank of batteries, and generates a field on the octopole axis of up to 450 G, which is comparable to the octopole field. Nonuniformity of the magnetic field in the toroidal direction is an order of one part in a thousand.

The plasma (hydrogen, or helium) is produced by a coaxial gun and is injected as shown in Fig. 1. Initial plasma density is up to $10^{12}/cm^3$. After the injection of plasma, the influx of neutral gas from the gun increases the pressure to about 3×10^{-5} Torr in 0.1 sec.

Microwave interferometers (10 cm, 3 cm, and 8 mm) measure the plasma density integrated over the path shown in Fig. 1. Langmuir probes are employed to make localized measurements of the plasma density and plasma temperature. Optical monochromators measure the emitted light intensity of the plasma from which the electron temperature is determined.[6,7] A 10-cm microwave source provides up to 1 kW for nonresonant electron heating.

2. Classical Diffusion in the Pure Octopole Field Configuration

The test of the scaling of the diffusion coefficient is made in pure octopole fields of the order of 10^{-2} Wb/m^2 in the same way as reported in the previous paper.[1,2] In the large collision frequency regime the reciprocal of the density is a linear function of time at every point on the profile. Namely, the $n\tau$ profile is constant, or $\partial(n\tau)/\partial t = 0$, where $\tau^{-1} \equiv (1/n)(\partial n/\partial t)$.

The diffusion equation in the flux function coordinates is given by

$$\frac{\partial n}{\partial t} \oint \frac{dX}{B_X^2} - \frac{\partial}{\partial \Psi}\left(\oint DR^2 dX \frac{\partial n}{\partial \Psi} \right) = 0 \quad , \tag{1}$$

where Ψ is the flux function, X is the magnetic potential, n is the plasma density, D is the diffusion coefficient, and R is the major radius. By use of the fact that $\partial(n\tau)/\partial t = 0$, we obtain

$$\frac{\oint \left(\frac{DR^2}{2n} \right) dX}{\oint \left(\frac{R^2}{B_X^2} \right) dX} = \frac{\int_{\Psi}^{\Psi_S} \left\{ (n\tau) \oint \frac{dX}{B_X^2} \right\} d\Psi}{\frac{\partial (n\tau)^2}{\partial \Psi} \oint \left(\frac{R^2}{B_X^2} \right) dX} \quad , \tag{2}$$

where Ψ_S is the value of the flux function at the separatrix. The right-hand side is computed from the experimental data. If the diffusion is classical, the left-hand side becomes

$$\frac{\oint \left(\frac{DR^2}{2n} \right) dX}{\oint \left(\frac{R^2}{B_X^2} \right) dX} = \frac{\eta (T_e + T_i)}{2} \quad , \tag{3}$$

where η is the perpendicular electric resistivity and T_e and T_i are electron and ion temperatures, respectively.

The right-hand side of Eq. (2) is computed from the measured $n\tau$ curve and from the magnetic geometry and the result is shown in Fig. 2 as a function of Ψ. The quantity $\oint (DR^2/2n) dX / \oint (R^2/B_X^2) dX$ is almost a constant in Ψ-space, which demonstrates the B^{-2}-dependence of the diffusion coefficient since the magnetic field is quite non-uniform in space.

The magnitude $\oint(DR^2/2n)dX/\oint(R^2/B_X^2)dX$ is about 50% greater than the theoretical classical value $\eta(T_e+T_i)/2$ for the plasma temperature of 0.1 eV ($T_e=T_i$).

The dependence of the diffusion coefficient upon the magnetic field strength is also tested by changing the magnitude of the octopole field. The result shows that the $n\tau$ value is inversely proportional to B_X^2 for a wide range of magnetic fields. Since the shape of the density profile does not change for various magnetic fields, it can be concluded that the diffusion coefficient goes as the inverse square of the magnetic field strength.

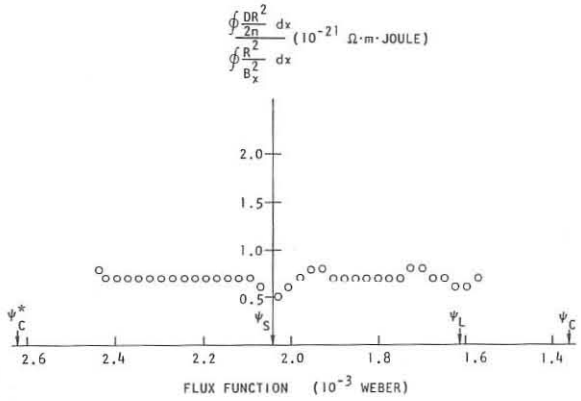

Fig. 2--Diffusion coefficient as a function of flux function

Temperature dependence of the diffusion coefficient is checked with a helium plasma. The plasma temperature is varied by use of the 10 cm microwave heating system. The electron temperature is measured by the optical method. The quantity $\oint(DR^2/2n)dX/\oint(R^2/B_X^2)dX$ is evaluated from the $n\tau$ profile in the same way as for the test of the B-dependence. The quantity is a decreasing function of temperature and the experimental values are in agreement within a factor of two with the classical theory ($T^{-\frac{1}{2}}$-dependence).

Thus, both the magnetic field and temperature dependence of the measured diffusion coefficient in the low pure octopole field indicate that the diffusion is classical in the octopole field.

3. Characteristics of the Density Decay with Toroidal Field

The experimental plasma decay rate with and without the toroidal field is shown in Fig. 3. Here the instantaneous density decay rate ($1/\tau$) is plotted as a function of R_o/Λ, where R_o is the major radius of the axis of the octopole field and Λ is the electron mean-free path for electron-ion momentum transfer. Each curve of Fig. 3 is based upon the decay of the Langmuir probe current during a single plasma shot. Low magnetic fields of the order of 10^{-2} Wb/m^2 are employed so that diffusion processes are dominant and other losses, such as support losses and recombination, are insignificant in comparison.

The decay is characterized by three regimes, In the high collision frequency regime ($R_o/\Lambda > 5$) the reciprocal of the density is a linear function of time. When the mean-free path becomes comparable to the machine dimensions ($R_o/\Lambda \sim 3$), the decay becomes approximately exponential. For a longer mean-free

path ($R_o/\Lambda < 1$), that is, in a lower collision frequency regime, the reciprocal of the density again becomes a linear function of time.

The dependence of the decay rate upon the magnetic field strength is shown in Fig. 4. Here the ratio of the octopole ring currents to the toroidal coil current is held constant and the reciprocals of plasma density are plotted as a function of t/B^2, where B is the total magnetic field. With this normalized time axis, almost exactly the same curves are observed several different magnetic field strengths, although only two cases are shown in Fig. 5. This feature indicates an inverse square dependence of the plasma decay upon the magnetic field strength in all the regimes.

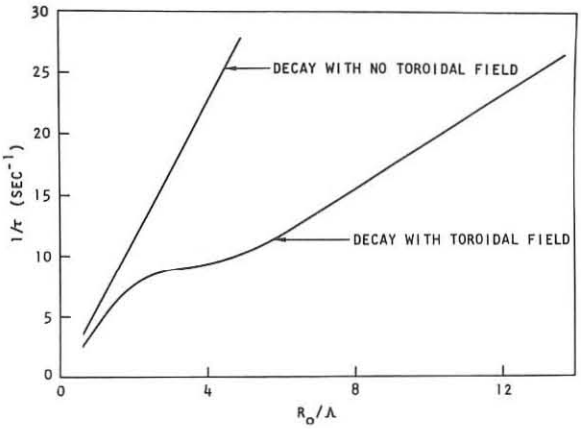

Fig. 3--The observed instantaneous decay rate as a function of R_o/Λ

4. Diffusion in the High Collision Frequency Regime - Pfirsch-Schlüter Diffusion

In the high collision frequency regime the curves 1/n vs t at various points of the density profile are all straight lines originating from one point on the time axis as shown in Fig. 5. This indicates that the decay process is collisional and the shape of the density profile is constant in time, i.e., $\partial(n\tau)/\partial t = 0$. Thus, local diffusion coefficients can be evaluated from the measured $n\tau$ profile for various magnetic field configurations in a way similar to that described in Sec. 1. One may rewrite the diffusion Eq. (1) as

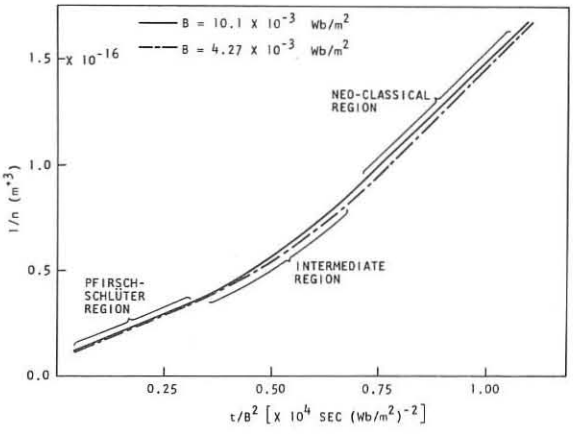

Fig. 4--The reciprocal of plasma density as a function of t/B^2

$$\frac{\oint\left(\frac{DR^2}{2n}\right)d\chi}{\oint\left(\frac{R^2}{B^2}\right)d\chi} = \frac{\int_{\Psi}^{\Psi_S}\left\{(n\tau)\oint\frac{d\chi}{B_\chi^2}\right\}d\Psi}{\frac{\partial(n\tau)^2}{\partial\Psi}\oint\left(\frac{R^2}{B^2}\right)d\chi} \quad . \tag{4}$$

If the diffusion is Pfirsch-Schlüter diffusion as the theory has predicted, then the left-hand side of Eq. (4) is

$$\frac{\oint\left(\frac{DR^2}{2n}\right)dX}{\oint\left(\frac{R^2}{B^2}\right)dX} = \eta\,\frac{(T_e + T_i)}{2}\cdot F \quad , \qquad (5)$$

where F is the Pfirsch-Schlüter enhancement factor. The general formula for the geometric factor F is given by J. L. Johnson and S. von Goeler[8] as

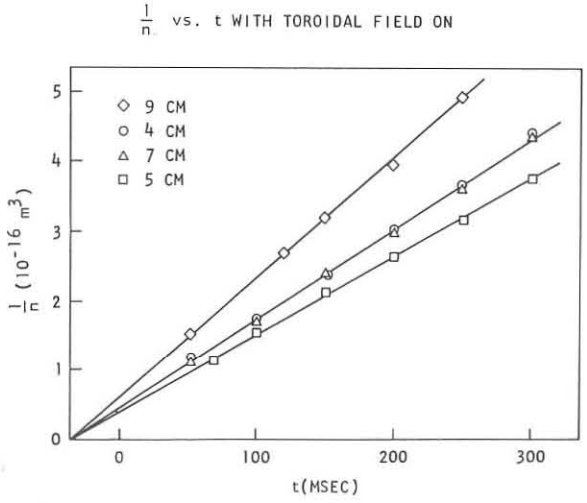

Fig. 5--The reciprocal of local plasma density versus time

$$F \equiv \frac{D}{D_{classical}} = 1 + \left[\oint \frac{dX}{R^2 B_X^2} - \frac{\left(\oint \frac{dX}{B_X^2}\right)^2}{\oint\left(\frac{B^2}{B_X^2}\right)dX}\right]\left(\oint \frac{dX}{B^2 B_\varphi^2}\right)^{-1} \quad , \qquad (6)$$

where B_ϕ is the toroidal field. Here we have neglected the difference between perpendicular and parallel resistivities.

The quantity $\oint(DR^2/2n)dX/[\oint(R^2/B^2)dX\cdot F]$ is evaluated from the measured $n\tau$ profile by use of the right-hand side of Eq. (4) and Eq. (6) and the result is shown in Fig. 6. The values are found to be constant for the greater portion of Ψ-space. Since both the magnetic field strength B and the rotational transform ι vary with Ψ, this result confirms that the measured diffusion coefficient has the B-dependence and ι-dependence predicted by Pfirsch-Schlüter diffusion theory.

The ι-dependence of the diffusion coefficient can be further tested by varying the ratio of poloidal to toroidal coil current. The ratio of the measured diffusion coefficient to

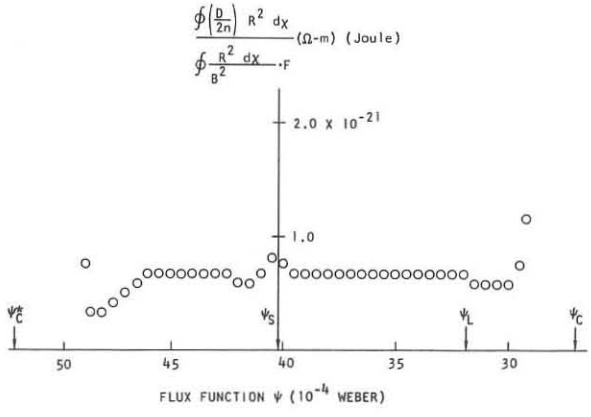

Fig. 6--Diffusion coefficient with toroidal field as a function of flux function

the classical diffusion coefficient is plotted as a function of $(2\pi/\iota)^2$ in Fig. 7. The experimental values are indicated by the points and are in good agreement with the theoretical curve, which is the Pfirsch-Schlüter enhancement factor calculated from the Johnson and von Goeler formula [Eq. (6)] for the magnetic field geometry of the octopole.

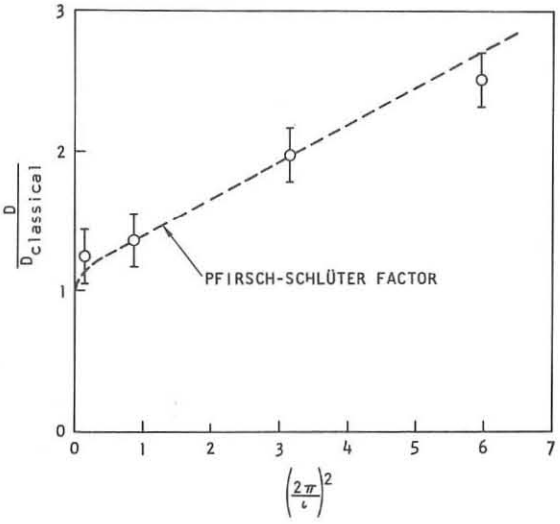

Fig. 7--Pfirsch-Schlüter factor as a function of $(2\pi/\iota)^2$

The theoretical value for the diffusion coefficient may be calculated by use of Spitzer's formula for the resistivity η with the assumption that $T_e = T_i$. The absolute value of the measured diffusion coefficient is about 50% greater than the theoretical value for a temperature of 0.1 eV. Inaccuracy of the electron temperature measurement for hydrogen plasma may be the main source of error. Also the difference between perpendicular and parallel resistivities has been neglected and it may introduce an error of less than 30% for the magnetic field configurations.

Temperature dependence of the diffusion coefficient is studied by use of a helium plasma. The 10 cm microwave system is used to increase the plasma temperature up to about 1.5 eV by nonresonant heating. In this range of plasma temperature the ionization rate is much smaller than the diffusion rate. This is also inferred from the fact that the reciprocal of the plasma density is a linear function of time. The diffusion coefficient temperature dependence is shown in Fig. 8. Circle points indicate the experimental values and the solid line show the theoretical curve for Pfirsch-Schlüter diffusion. The experimental points clearly indicate that the quantity $\oint(DR^2/2n)dX/[\oint(R^2/B^2)dX \cdot F]$ is a decreasing function of temperature, and all the data points fall within a factor of two of the theoretical curve which has $T^{-\frac{1}{2}}$ dependence. The ion temperature is possibly lower than

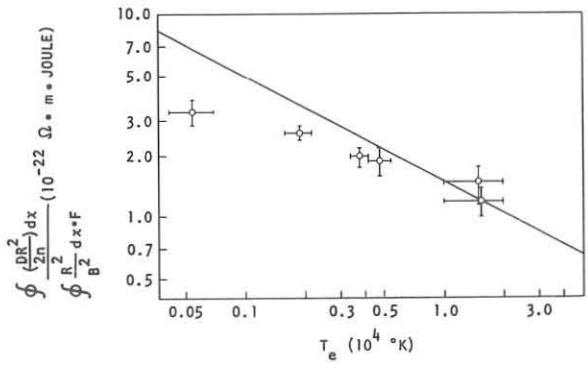

Fig. 8--Diffusion coefficient as a function of electron temperature

the electron temperature so that the experimental quantities may be larger at most by a factor of two.

In summary in the high collision frequency regime the B-dependence, ι-dependence, and T-dependence of the diffusion coefficient all agree with the dependence predicted by the Pfirsch-Schlüter theory. The magnitude of diffusion coefficients are in agreement with the theoretical values within a factor of two.

5. Diffusion in the Low-Collision Frequency Regime - Neoclassical and Intermediate Diffusion

In the low collision frequency regime the plot of $1/\tau$ versus R_o/Λ is approximately a straight line through the origin. (See Fig. 3.) The slope of the straight line in the low collision frequency regime in Fig. 3 is 2.2 times greater than the slope of the straight line observed in the high collision frequency regime. In Fig. 3 we have also plotted the decay rate observed with no toroidal field. The poloidal field is the same in both cases. For the large mean-free path regime the decay rate with the toroidal field is enhanced beyond the Pfirsch-Schlüter factor, and comparison of the two curves indicates that the presence of the toroidal field hardly affects the diffusion rates. This feature strongly suggests neoclassical diffusion due to trapped particles.

Diffusion coefficients for the neoclassical diffusion is computed for the octopole geometry by use of Rutherford's formula[9] given by

$$\frac{D_{neoclassical}}{D_{classical}} = 1 + \left[\oint \frac{d\chi}{B^2 B_\chi^2} - \frac{3}{4} \left(\oint \frac{d\chi}{B_\chi^2} \right)^2 \int_0^{B_{max}^{-1}} \frac{\lambda d\lambda}{\oint d\chi (1 - \lambda B)^{1/2} / B_\chi^2} \right] \left(\oint \frac{d\chi}{B^2 B_\phi^2} \right)^{-1} . \quad (7)$$

Figure 9 shows the ratio of the neoclassical to classical diffusion coefficient as a function of $|\Psi - \Psi_S|$ evaluated by Eqs. (6) and (7) for the particular magnetic field configuration used in the experiment. Here, the separatrix and the stability limit line (or the flux line at the ring limiter) are indicated by Ψ_S and Ψ_C, respectively. The method for calculation of diffusion coefficient described in the previous sections can not be used for this case. The plasma is in a different regime depending on the local plasma density. When the plasma is collisionless at the wings of the density

profile, the plasma may still be collisional at the density peak. This makes $n\tau$ profile time dependent. However, the diffusion coefficients do not vary much as a function of $|\Psi-\Psi_S|$ where the density gradient is large as shown in Fig. 9. Therefore the observed $n\tau$ value may be used to estimate the diffusion coefficient evaluated at the flux line where the density gradient is maximum. The observed ratio of the slopes of the short and long mean-free path regimes in Fig. 3 is 2.2 which agrees with the theoretical value 2.5 within experimental error.

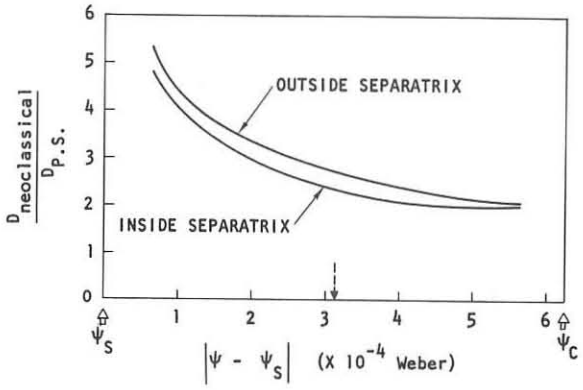

Fig. 9--The theoretical ratio of neoclassical to Pfirsch-Schluter coefficient

The transition value of R_o/Λ from Pfirsch-Schlüter to the plateau regime has not been calculated accurately for the octopole configuration. However, a rough estimate may be obtained by equating the collision frequency to the transit time between the trapped regions. The calculated value is five for the case shown in Fig. 3 and agrees with the experimental value. The transition values are further examined experimentally by varying the plasma temperature. Application of the nonresonant microwave heating gives a temperature range of 0.1 eV to 2 eV. The results are shown in Fig. 10. The decay rates are measured at the same density with various temperatures. The diffusion coefficient increases with longer mean-free path. The region $R_o/\Lambda > 5$ represents the Pfirsch-Schlüter regime and $R_o/\Lambda < 1$ the neoclassical regime. These values agree with the prediction by the neoclassical theory for the configuration.

Similar results were obtained at the higher temperature and higher density regime. Shortly after injection the electron temperature is 8 eV and the density is 2×10^{11} cm^{-3}. The mean-free path is long and $R_o/\Lambda < 1$. The temperature cools rapidly because of the interaction with the neutral gas. The mean-free

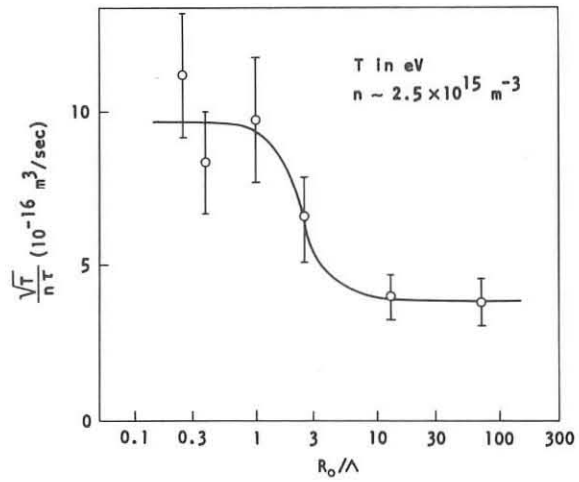

Fig. 10--The decay rates as a function of the mean-free path

path becomes shorter and $R_o/\Lambda > 5$. The measurement of instantaneous decay rate shows the results similar to the one shown in Fig. 10.

When the plasma density decays to a low value ($R_o/\Lambda < 0.25$), the decay becomes exponential with time. The electron-ion collision frequency becomes smaller than the electron-neutral collision frequency at these densities. The decay rate is proportional to the inverse square of the magnetic field strength. From these characteristics this regime may be explained by the neoclassical diffusion due to electron-neutral collision.

The reduction of the neutral gas pressure eliminates the above diffusion. Instead, a new diffusion process that is tentatively interpreted as the Okuda-Dawson diffusion dominates. This subject will be discussed in a separate paper.

In conclusion, enhanced diffusion due to trapped particles (neoclassical and intermediate diffusion) is observed. The type of diffusion experienced by the plasma is determined by the mean-free path, which is a function of plasma density and temperature. The experimental results are consistent with the predictions of neoclassical theory.

Work supported by the U.S. Atomic Energy Commission, Contract No. AT(04-3)-167, Project Agreement No. 38.

REFERENCES

1. T. Ohkawa, et al., Phys. Rev. Letters 24, 95 (1970).
2. T. Ohkawa, et al., Phys. Rev. Letters 27, 1179 (1971).
3. T. Ohkawa, J. R. Gilleland, and T. Tamano, Phys. Rev. Letters 28, 1107 (1972).
4. H. Okuda and J. M. Dawson, Phys. Rev. Letters 28, 1625 (1972).
5. A. A. Galeev and R. Z. Sagdeev, Zh. Eksp. Teor. Fiz 53, 348 (1967) [Sov. Phys. - JETP 26, 233 (1968)].
6. L. C. Johnson, private communication.
7. L. C. Johnson and E. Hinnov, Phys. Fluids 12, 1947 (1969).
8. J. L. Johnson and S. von Goeler, Phys. Fluids 12, 255 (1969).
9. R. H. Rutherford, Phys. Fluids 13, 482 (1970).

SURVEY OF SCYLLAC EXPERIMENTS *

by

S.C. Burnett, W.R. Ellis, R.F. Gribble, C.F. Hammer, C.R. Harder, H.W.Harris, F.C. Jahoda, W.E. Quinn, F.L. Ribe, G.A. Sawyer, R. E. Siemon and K.S. Thomas

Los Alamos Scientific Laboratory, University of California, Los Alamos, New Mexico, U. S. A.

ABSTRACT:

"Scyllac" research is currently divided among three major experimental efforts: a) the 5-meter 120° toroidal sector [1] b) a 5-meter linear theta-pinch with strong end mirrors [2] and c) a feedback stabilization experiment on Scylla IV-3 [3].

In the sector the toroidal force and outward plasma drift are compensated by a combination of $\ell = 1$ helical fields and $\ell = 0$ bumpy fields. A period of equilibrium on the toroidal axis is followed by sideward motion of the plasma column, predominantly in the plane of the torus, that could either be an imbalance between the $\ell = 1,0$ and toroidal forces or a long wavelength $m = 1$ instability. Containment times up to 11 μsec, comparable to times for plasma end loss, have been observed.

Without mirrors the linear device produces a 2-3 keV plasma that shows a "wobble" of up to 1.5 cm amplitude but otherwise remains centered more than 35 μsec (~ 3 e-folding times for end loss). With simultaneously applied mirror fields of 2.5 mirror ratio the plasma column shows evidence of an $m = 1$ instability that carries it to the wall at some point along its length early in time. However, the column re-forms and the neutron yield is larger than without mirrors for the entire plasma lifetime.

In the feedback experiment, $\ell = 0$ windings are driven by a power amplifier from a signal generated by plasma displacement as determined by an

optical sensor. Initial results confirm feasibility of the feedback concept.

A. TOROIDAL SECTOR

The Scyllac toroidal sector, 5 meters of an eventual 15-meter circumference torus, came into operation prior to the Madison IAEA meeting in June, 1971. At that time [4] it was shown that the toroidal drift force $F_R = \beta B_o^2 a^2/4R$, which in a smooth-bore coil drives the ~ 1 keV plasma to the outside wall in approximately 2.5 μsec, was balanced for about 4 μsec by the $F_{1,0}$ force [5, 6] produced by a combination of an $\ell = 1$ helical field (33-cm period) provided by capacitor-driven coils, and an $\ell = 0$ field formed by rectangular grooves of equal period cut into the compression coil wall.

The Madison data were obtained from "land" regions of the $\ell = 0$ field; i.e. those regions where the coil is not cut away and the main field is undiminished. Subsequently it was determined that the plasma was hitting the wall in every groove region, a type of local "ballooning" very different from the expected long wavelength m = 1, k ≈ 0 instability. This unfavorable situation resulted from the large groove depth (1.8 cm) which caused a large Z dependence (34%) of the $\ell = 1$ fields on account of the varying image current strength with coil to wall distance. Also this groove depth gives a δ_o (relative plasma bumpiness) considerably larger, relative to the presumably more stable δ_1 helical plasma displacement, than is desirable according to existing theory. [7]

Experiments were subsequently conducted with a shallower groove depth (0.9 cm) both with and without stainless steel "stuffer" inserts to delay the onset of the $\ell = 0$ bumpiness until after the shock implosion phase,

and also at effective groove depths of 0.75 cm and 0.60 cm without stuffers, but with thin copper shells over the grooves to provide an effectively uniform wall for the $\ell = 1$ image currents. The $\ell = 1$ field strength and timing were varied until the plasma containment time, observed with image convertor streak cameras, was optimized.

A significant result is that in each of these cases the plasma behavior in lands and grooves is now approximately the same, i.e. long wavelength effects predominate. Also it is a characteristic of all the streak pictures (e.g. Fig. 1) that the plasma takes up a helically displaced equilibrium position that persists for a number of μsecs before the entire column moves to the wall with an effective growth rate of ~ 1 MHz. The motion is predominantly in the toroidal plane, and consistently changes from outward to inward with only a slight increase in $\ell = 1$ current. This suggests a loss of equilibrium, which may be due to changing β, changing plasma radius, poor tracking of the main field by the $\ell = 1$ field, or incipient end effects, although a late onset of the m = 1 instability cannot presently be ruled out.

The longest plasma containment times (~ 11 μsec) were obtained in the 0.75-cm groove-with-shell configuration ($\ell = 1$ current of 62 kA and 0.3-μsec onset delay). The improvement is presumably the result of better uniformity in the $\ell = 1$ field or the reduction in groove depth or a combination of these. Also the 0.9-cm "unstuffed" grooves give longer containment than the 0.9-cm "stuffed" grooves, presumably because of a more effective initial δ_o loading of the plasma. The "unstuffed" geometries, however, show a more precipitous drop in neutron production at times near peak field. (Fig. 1). This is believed to be due to an energy transfer from land to groove regions that lowers the effective ion temperature. Support for this interpretation

is given by the detailed measurements of plasma properties derived from: a) a coupled-cavity gas laser interferometer measurement of electron density integrated along a chord of the plasma cross-section b) a loop and probe arrangement that measures the amount of magnetic flux excluded from the plasma and c) a 10-channel side-on luminosity profile that is unfolded to give radial density distributions as a function of time. In the groove regions the value of plasma β on axis increases, and the inflection point radius of a best fit Gaussian distribution decreases, for about 4 μsecs. [1]

Values of δ_o and δ_1 for the optimized containment times are derived, respectively, directly from the luminosity profiles in land and groove regions and from the measured β through the sharp-boundary-model relation $\delta_1 = B_{\ell=1}/(B_o ha(1-\beta/2))$. [2] The product $\delta_1\delta_o$ is in good agreement with sharp-boundary theory, although the density distribution is distinctly Gaussian.

In the most recent experimental configuration a doubly grooved coil, in which both the ℓ = 1 and ℓ = 0 configurations are cut into the interior wall of the main compression coil,has been used. (Fig. 3). The groove depths on this first composite bore coil were intentionally underdesigned by 25% from the optimum value predicted by the ℓ = 1 current-driven coil with unstuffed groove results, and additional ℓ = 1 windings are energized to provide a fine adjustment on confinement. Subject only to the smaller field corrections of these ℓ = 1 trimmer windings, the ℓ = 1 field now tracks the main field more closely, and the ℓ = 1 image current effect is greatly reduced. In this configuration the reproducibility between discharges is significantly better and the streak pictures are suggestive of an m = 1 instability preferentially triggered in a nearly vertical plane at about 6 μsec and striking the wall at about

8 μsec. Computer fits to the observed motion favor a parabola (constant force) rather than exponential growth, although an instability would be expected on the best available theory. Furthermore, instability growth need not appear exponential once the column moves away from the equilibrium position.

Both feedback stabilization (see below) and conversion to a full torus are planned in the near future.

B. LINEAR SCYLLAC

The 5-meter linear Scyllac has as its primary objectives the investigation of end-loss scaling for collisionless plasma (by comparison with the 1-meter Scylla IV results) and the effects of strong end mirrors on MHD stability and containment of high β plasma.

Initial operation without end mirrors at 10 mTorr and 45 keV gave a reasonably well behaved plasma of $n \sim 2.5 \times 10^{16}$ cm^{-3}, $T_i \approx 2$ keV, $\tau \simeq 20$ μsec, B = 60 kG, $\beta \approx 0.5$ and approximately 5×10^6 neutrons/cm. Streak pictures often showed a "wobble" [8] of up to 2 or 3 plasma diameters starting 3 to 5 μsec after initiation of the discharge, but saturating at a low level far from the walls. End-on holographic interferograms showed a turbulent structure beginning near the walls that progressively obscured the field of view and terminated the usefulness of this diagnostic at early times. The explanation is now known to be an end effect due to high energy plasma flow along magnetic lines that bombarded the quartz tube outside the coil. The discharge tube material that "boiled off" contaminated nearby wall areas for subsequent discharges. At the same time that mirror coils were initially installed, enlarged quartz sections (20 cm diameter, 45 cm length) were added to the shortened discharge tube just outside the mirror coils to lessen the effects of wall bombardment. Figure 3 shows that with the mirror coils energized there was almost no wall debris on the interferograms as late as 10 μsec. Even without the mirror coils energized, when some flux

lines still connect plasma to the narrow discharge tube ends, considerable improvement is noted compared to the case without the enlarged end sections (in which case, by 10 μsec, the plasma column was completely obscured). Nonetheless, for the no-mirror case, the wall material at the ends makes it difficult to get a good particle inventory (loss rate) from the interferograms. An e-folding time of 15 μsec is approximated from the streak pictures.

The mirror coils used are of high strength steel, 16-cm long and driven by capacitor banks identical to the banks which independently drive each 1-meter section of the main coil. There is a 5-cm gap between the main and mirror coils. At 45 keV bank voltage the mirror coil field rises to 150 kG in 7.5 μsec. When the main and mirror fields are applied simultaneously the plasma column, as indicated by streak pictures at two locations, side-on luminosity at a third location, and end-on interferograms, always shows motion off the discharge tube axis. For times up to 8 μsec this typically has the form of a m = 1, long wavelength instability of ~ 2 μsec e-folding time. Generally the column touches the discharge tube wall, probably at only one axial position, and then recovers with a "wobble" that on average has bigger amplitude than in the no-mirror case, but does not restrike the wall. The neutron yield in the mirror case is enhanced over the non-mirror case for the entire period of observation, particularly in the two end meters [2], indicating no drastic cooling over any substantial length even when the column grazes the wall. Streak pictures with and without mirrors are shown in Fig. 4. The streak pictures labeled R-7 are stereo views 1.5 m from one end, while R-10 are single-plane views 0.5 m from the other end of the main coil. The interferogram with mirrors at 10 μsec shown in Fig. 3 clearly indicates a displaced column, which at least at some point along the integrated length is connected to (presumably cold) plasma that touches the wall.

If the present indication of mirror-driven MHD instability persists through subsequent parameter changes (e.g. time of mirror field application, tube clean-up) it would contradict previous more hopeful indications from the Scylla IV 1-meter device, but be in accord with recent diffuse profile 2-dimensional MHD stability calculations of Freidberg and Marder.[9]

C. FEEDBACK STABILIZATION

An $\ell = 0$ MHD feedback experiment, designed to control the m = 1 mode induced by $\ell = 1$ helical fields, is being implemented on the three meter linear Scylla IV-3, prior to installation on the toroidal Scyllac sector.

The feedback force is the same $F_{1,0}$ uniform transverse body force that provides the toroidal equilibrium in the curved geometry and has been previously shown to exert the predicted push on a deliberately induced $\ell = 1$ instability in the linear Scylla IV-3 geometry [4, 10]. Its magnitude per unit length is given by sharp-boundary theory as

$$F_{1,0} = [\beta\ (3 - 2\ \beta)/8]\ B_o^2 h^2 a^3 \delta_1 \delta_o$$

where a is plasma radius, and δ_1 and δ_o are the normalized helical displacement and plasma bumpiness, respectively, and h is the common wavenumber of the applied $\ell = 1$, $\ell = 0$ fields. The destabilizing force per unit length due to the $\ell = 1$ fields is

$$F_1 = \pi a^2 \rho \gamma_1^2\ \xi$$

where ρ is the maximum plasma mass density on axis, ξ is the displacement from equilibrium, and γ_1 is the e-folding growth rate of the instability. The latter has been measured [10] to be $\gamma_1 = 0.54 \pm 0.09 \times 10^6$. Equating these two forces for the given amount of feedback current (and thus the programmed δ_o) available in the present experiment sets an upper limit of $\xi_{max} = 1.3$ cm on the maximum displacement that can be stabilized. Computer modeling indicates the additional

constraint that the electrical system delay τ be less than $1/\gamma_1 \approx 2$ μsec.

In Scylla IV-3 both the $\ell = 1$ field as well as the $\ell = 0$ feedback fields are generated by coils, whose configuration relative to the main compression coil is illustrated in Fig. 5. The system [3] consists of the following three basic components: 1) Plasma position detectors, bi-cell silicon diodes capable of detecting plasma motion of < 1 mm to > 1 cm away from equilibrium position. 2) Signal processing units which act as intermediate amplifiers while adding damping and filtering to the signal, gate the position detectors off during the first 2 μsec when the plasma forms, and electronically select the plasma position at the time when the gates open as the null position for feedback. 3) Power Amplifier Modular units, each of which consists of 3 separate stages of amplification ending in push-pull operation of two ML-8618 power vacuum tubes operating at 35-kV plate voltage. The output is an 8:1 step-down transformer that drives up to 6.8 kA for times up to 20 μsec in the $\ell = 0$ feedback coils. Initial current response to a plasma displacement signal occurs at about 0.2 μsec and risetime to 90% peak current is 1.3 μsec.

In the present Scylla IV-3 configuration a single position detector monitors the plasma motion in the plane in which, due to some assymetry, the $\ell = 1$ instability is invariably initiated [10], and the outputs of 10 power modules drive 20 $\ell = 0$ coils extending over 10 periods of 30-cm wavelength each. Because of the very large system power gain [3] extremely good noise shielding is essential to avoid self oscillation. The power tubes are pulse operated well above their nominal ratings after extensive conditioning.

Some degree of stabilization has been observed in preliminary experiments. At the time of writing however, there have not been sufficient full bank discharges with feedback followed by control discharges without feedback to document the apparently promising results sufficiently well for publication. Figure 6 summarizes the important parameters of the experiment.

REFERENCES

1. W. R. Ellis, et al. Paper A-1, 2nd Topical Conference on Pulsed High-Beta Plasmas, Garching, W. Germany, July 3-6, 1972.

2. K. S. Thomas, et al. Paper C-3, 2nd Topical Conference on Pulsed High-Beta Plasmas, Garching, W. Germany, July 3-6, 1972.

3. R. F. Gribble, et al. Paper G-1, 2nd Topical Conference on Pulsed High-Beta Plasmas, Garching, W. Germany, July 3-6, 1972.

4. S. C. Burnett, et al. Plasma Physics and Controlled Nuclear Fusion Research, (IAEA, Vienna, 1971), 3, 201.

5. F. L. Ribe and M. N. Rosenbluth, Phys. Fluids 12, 726 (1969).

6. R. L. Morse, W. B. Riesenfeld and J. L. Johnson, Plasma Physics 10, 543 (1968).

7. J. P. Freidberg, Plasma Physics & Controlled Nuclear Fusion Research, (IAEA, Vienna, 1971), 3, 215.

8. H. A. Bodin et al., Plasma Physics & Controlled Nuclear Fusion Research (IAEA, Vienna, 1965), 1, 193.

9. J. P. Freidberg and B. M. Marder, submitted to Phys. Fluids.

10. C. R. Harder, et al., Phys. Rev. Letters 27, 386, (1971).

FIGURE CAPTIONS

Fig. 1. Streak photographs of the toroidal sector plasma showing horizontal (top and bottom) and vertical (center) motions at two filling pressures for 0.75-cm-unstuffed-grooves-with-shells. Main compression field and neutron-scintillator signal for same case (lower left) and 0.9 cm stuffed grooves (lower right).

Fig. 2. Sector coil with both $\ell = 1$ and $\ell = 0$ grooves.

Fig. 3. Holographic interferograms of Linear Scyllac plasma without and with mirrors activated.

Fig. 4. Streak photographs of Linear Scyllac without and with mirrors activated. R-7 is 1.5 meters from one end, R-10 is 0.5 meters from other end.

Fig. 5. Coil arrangement for $\ell = 1$ and $\ell = 0$ on Scylla IV-3 feedback stabilization experiment.

Fig. 6. Pertinent parameters for Scylla IV feedback experiments. All symbols as defined in text.

*Work performed under the auspices of the Atomic Energy Commission.

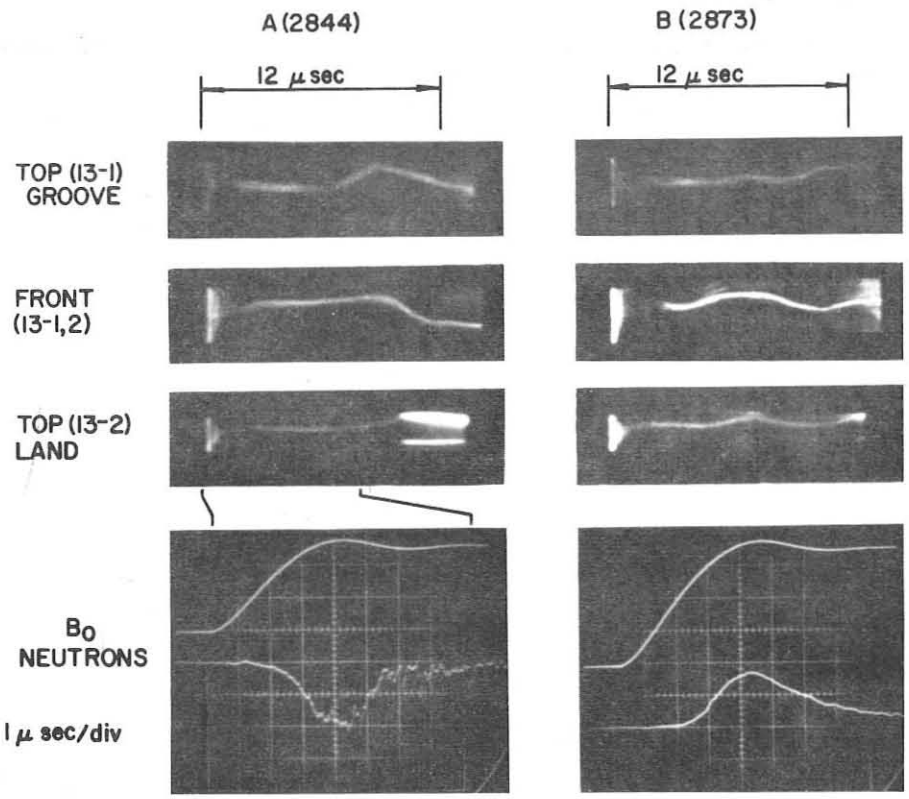

P_{D_2} =	15 mTorr	10 mTorr
V_{PB} =	50 kV	50 kV
$I_{\ell=1}$ =	60 kA	62 kA

FIG. 1

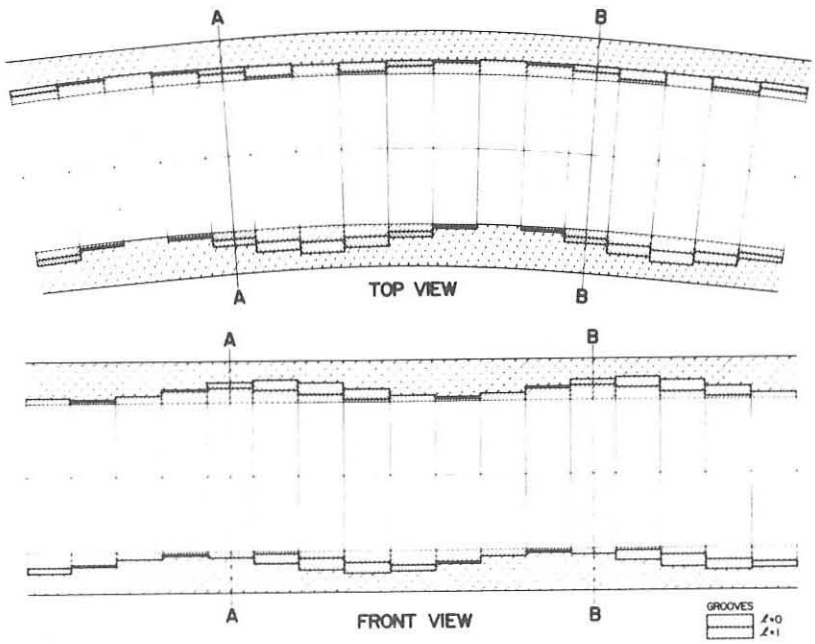

FIG. 2

WITHOUT MIRRORS

WITH MIRRORS

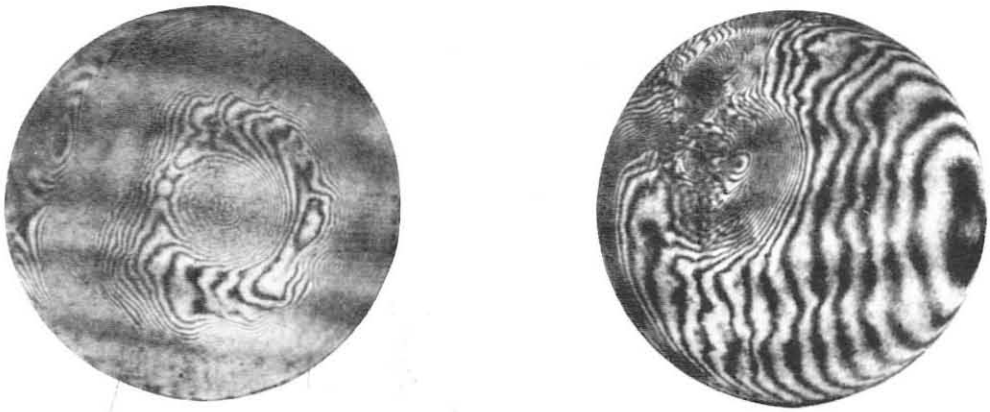

FIG. 3

t = 10 μ sec

t = 10 μ sec

R-7

R-10

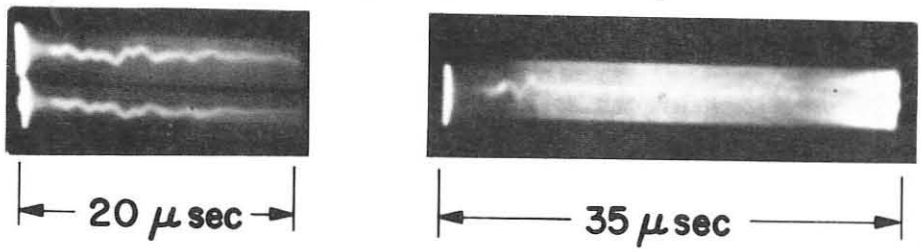

WITHOUT MIRRORS

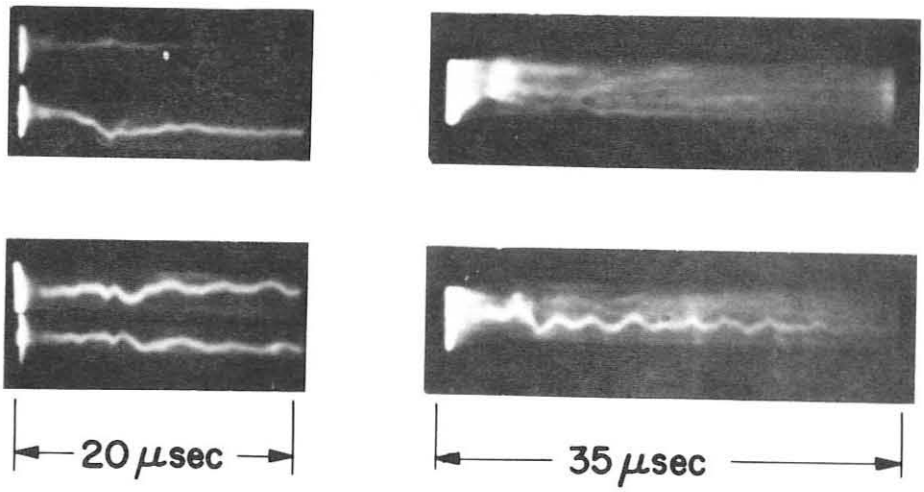

FIG. 4

WITH MIRRORS

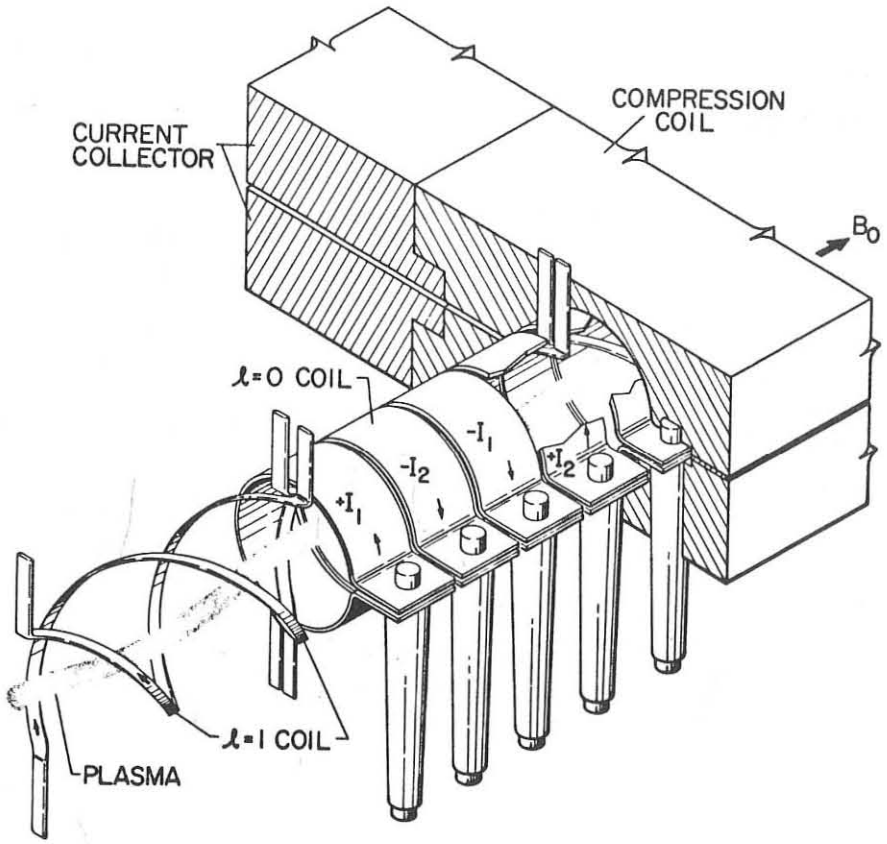

FIG. 5

FEEDBACK STABILIZATION

$$r = a[1 + \delta_\ell \cos(\ell\theta - hz)]$$

$$F_1 = \pi a^2 \rho \gamma_1^2 \xi$$

$$F_{1,0} = \frac{\beta(3-2\beta)}{8} B_o^2 h^2 a^3 \delta_1 \delta_o$$

SCYLLA IV-3 PARAMETERS

$B_o = 42$ kG, $n = 2.7 \times 10^{16}$

$a = 0.7$ cm, $\beta = 0.88$

$\delta_1 = 0.7$, $\gamma_1 = 0.54 \times 10^6$

$$\delta_o = \frac{4\delta B_o}{B_o} = \frac{0.14\ I_{\ell=0}}{B_o}$$

$$\xi_{max} = \frac{F_{1,0\ max}}{\pi a^2 \rho \gamma^2} = 1.3 \text{ cm}$$

$$\gamma_1 \tau = 0.8$$

FIG. 6

THE HIGH BETA TOROIDAL EXPERIMENT

D.C. Robinson, J.E. Crow, C.W. Gowers*, G.F. Nalesso+,
A.A. Newton, A.J.L. Verhage, H.A.B. Bodin
U.K.A.E.A., Culham Laboratory, Abingdon, Berks., England

ABSTRACT: The setting up and MHD stability of diffusing pinch configurations has been studied. For a reverse field pinch the axial flux should not change sign and decay for the maximum stable time. Conditions for setting up such a stable distribution are discussed and experiments described in which configurations are generated without instability. The plasmas have $\beta_\theta \sim 0.6$ and provided the axial flux is positive, the lifetime can be 30-40 μsec which corresponds to the computed classical resistive decay time of the fields. The configuration is not perfectly MHD stable but the localised modes predicted are not observed and may be stabilized by finite larmor radius effects.

INTRODUCTION: Toroidal diffuse pinches are devices in which the longitudinal magnetic field B_z is comparable to the azimuthal magnetic field B_θ, generated by the current. In contrast to Tokamaks where $B_z >> B_\theta$ and average magnetic well stabilization is effective with the current below the Kruskal-Shafranov limiting value, the diffuse pinch relies on shear and wall stabilization. From the works on infinite conductivity MHD stability theory for such devices it was apparent that appropriate field configurations could confine stable plasmas with high values of β. A number of experimental devices were designed to set up such configurations, in particular Ohkawa et al[1] presented results from a toroidal pinch in which the external fields could be varied in times of a few μsecs. Of particular interest also was the large toroidal pinch device Zeta[2] in which the fields varied much more slowly and in this case a stable field distribution was set up after a period of instability and wall contact. In both devices the most favourable field configuration had the longitudinal magnetic and electric fields reversed at the outer edge of the plasma.

This review will be devoted to results obtained with reverse field configurations on the HBTX at Culham[3], though screw pinches, high-β Tokamak like plasmas and stabilized z-pinches have also been studied in some detail. This device has a major radius of 1M, radius of the quartz vessel 6 cm and the conducting shell 7.5 cm. The I_z current has been varied between 30 and 100 kA together with fast and slow B_z fields of 2-6 kG. The fields and currents are established on a timescale of 2-4 μsec. Deuterium at a filling pressure of 30-40 mtorr has been used. Plasma parameters are determined from laser light scattering, field configurations from magnetic probes (envelope sizes 9.5 and 4 mm) with a variety of B_θ, B_z, B_r coils of diameter $\leq$ 2.8 mm. The growth and wavelength of instabilities are studied using external B_r, B_θ coils, helical sine/cosine Rogowski coils[4] and stereoscopic streak photographs taken through 8 mm diameter holes in the shell using small lenses and fibre guides.

STABILITY AND DIFFUSION: The necessity of a reversed field for the stability of diffuse pinch configurations to m = 1 current driven instabilities has been established both theoretically[2,5] and experimentally[1,2,3]. This arises from the fact that a plasma confined with an outer vacuum region would possess a minimum in the pitch $P = rB_z/B_\theta$ if the field were not reversed and this leads to a kink instability. Such a stable field configuration has to satisfy other requirements (see Table I) notably that $\beta_\theta = 4\pi\frac{\int prdr}{I^2} < 1$ which for an optimum field configuration gives β values approaching 30% and that the axial flux $\Phi = \int_0^{r_w} rB_z\, dr > 0$ to ensure wall stabilization. The pressure profile must remain hollow or flat near the magnetic axis, if flat $p_2 = \left(\frac{1}{2r}\frac{dp}{dr}\right)_{r\to 0} \to 0$, a critical shear $\alpha = \frac{P}{2}\frac{d^2P}{dr^2}\Big|_{r\to 0} < -\frac{4}{9}$ is required if $\frac{P}{R} \ll 1$. If the pressure profile is hollow a lower value of β is required for stability. The reversed electric field observed experimentally[1,2] is associated with a reversed current which creates more shear and automatically satisfies the Suydam criterion in that region.

Due to dissipative processes within the plasma the field configuration will evolve in time, thus we must consider the compatibility of stability and diffusion. For example, if the outer reversed field decays rapidly then stability will be lost or if the central region of such a pinch is such that $p_2 = 0$ then we require $\frac{dp_2}{dt} \geq 0$ for stability in time[6].

Consider first the central regions of such a pinch. If we expand the two fluid equations of motion in the neighbourhood of the magnetic axis, we obtain an equation for $\frac{dp_z}{dt}$ of the form

$$\frac{dp_2}{dt} = - \frac{B_z^2 \, b_1^4}{4\pi^2 \, \sigma_{||}} \left\{ (3 + 4\alpha)(\gamma - 1) + \gamma\beta \frac{v_3}{b_1^3} + K \right\} \qquad \ldots (1)$$

for $p_2 = 0$. γ is the ratio of specific heats, $b_1 = \left(\frac{B_\theta}{rB_z} \right)_{r \to 0}$, $v_3 = \frac{B_z(o) \, v}{E_z(o) \, r^3} - v$ being the radial velocity. K is a term related to the thermal conductivity and temperature gradient. As $\beta \to 0$, the last two terms in (1) vanish and therefore $\alpha < - \frac{3}{4}$ for stability in time. The stability criterion for $p_2 = 0$ is $\alpha < - \frac{4}{9}$, consequently diffusion demands more shear than MHD stability theory. The behaviour of p_2 in time is demonstrated in Fig.1 where $\alpha_1 = - \frac{(3 + \beta_2/b_1^2)}{4}$ is the generalization of the critical shear to cases where $p_2 \neq 0$ and $\beta_2 = 8\pi p_2 / B_z^2$. The curve marked 'Zeta' depicts the temporal behaviour of p_2 up to the time of improved stability observed in that device where $p_2 \to 0$[2]. The most desirable case of $\alpha < \alpha_1$ is hard to attain in practice as current diffusion tends to limit $\alpha > - 1$. As the value of β increases the imposed electric fields controlling v play an important role. Axial flux conservation within this region reduces the necessary critical value of the shear whereas an axial field maintained at the outer edge increases the value. For classical cross field thermal conductivity ($3.3 \, \beta \frac{nk}{\sigma_{||}}$), K becomes

$$- 20.8 \frac{\beta^2}{b_1^4} \left(\frac{2T_4}{T_o} - \frac{T_2}{T_o} \left(b_1^2 + \frac{5T_2}{2T_o} \right) \right)$$

where the temperature profile is given by $T = T_o - T_2 \, r^2 + T_4 \, r^4 + \ldots$. This term imposes a limitation on β compatible with full current diffusion

stability and $\frac{dp_2}{dt} \geq 0$, of 13%.

Let us now consider the overall behaviour of a reverse field configuration and how it evolves in time. If such a configuration were to be maintained in a stationary state in cylindrical geometry then curl $\underline{E} = -\frac{\partial \underline{B}}{\partial t} = 0$ implies $E_\theta = 0$ and E_z = constant, but even a generalised ohms law resolved in the θ direction gives $j_\theta = 0$ at the point where $B_z = 0$ for any velocity field. Consequently there is no j_θ to maintain the reverse field and therefore such a field configuration is a non-stationary state. For example, a projected device with the initial reverse field configuration shown in Fig.2 with the B_z, B_θ fields maintained at the outer boundary and $T_e(r) = 640(1-(r/18)^4)$eV held constant, diffuses inwards towards the stationary state possessing no reversal. Thus the computed field evolution leads to instability in a small fraction of a field diffusion time, as Φ becomes negative and wall stabilization is ineffective. If the axial flux is conserved and positive the diffusion is favourable for stability as shown in Fig.3, until the field reversal disappears. For appreciable positive values of the axial flux, giving a better margin of stability, the reverse field disappears quite quickly (see Fig.13), however this can be improved by allowing the axial flux to decay at the same rate as the current.

Table I compares the stability and diffusion requirements and it seems that diffusion necessitates a higher shear and lower β than MHD stability. The resistive tearing mode also imposes a stronger limitation on the axial flux to maintain wall stabilization.

INITIAL STAGES: It is not an easy task to set up a reverse field configuration without instability for the pinch has to evolve through a period in time where sufficient positive axial flux is created without field reversal and this can lead to a strong current driven instability. In the case of a stabilized z-pinch with no applied reverse field[7] with B_z and B_θ at the wall of 2 kG and the plasma away from the wall, thereby creating a pitch minimum, a current driven instability partially localised within the minimum of the pitch

variation is both predicted by solving the eigenvalue problem for the growth rate and observed. The agreement between theory and experiment is within the experimental errors giving a growth time of 1.2 μsec and a wavelength of 33 cm corresponding to pitch length close to the minimum in the pitch. The measured eigenfunction is also closely in agreement with that predicted numerically.

As B_z at the wall becomes less than B_θ at the wall corresponding to the initial application of a fast B_z field which will ultimately reverse the B_z, so the growth time increases as the pitch length at the minimum becomes much shorter than the wall radius. Unfortunately the real situation is not quite as favourable as this might suggest because the value of β_θ in such discharges is about 0.6 and the pressure distribution is annular in form which leads to pressure driven instabilities whose growth time is only a little longer than the worst current driven instability.

These experimental and theoretical studies show that we have 1-2 μsec in which to effect field reversal at the fields and densities used in the above studies.

In addition to generating a quasi-stationary reverse field distribution without instability we must minimise the time for which the Poynting vector, $E_\theta B_z - E_z B_\theta$ is directed outwards during the formation of such a pinch. Fig.4 shows oscillograms of the B_z and I_z variation where such minimisation has been achieved.

The strength of the $\underline{E} \wedge \underline{B}$ driving force must not be such as to give rise to too high an inward radial velocity which will lead to overcompression of the plasma and violation of wall stabilization. This control is effected by crowbarring B_θ and B_z at the appropriate instants in time (E_θ, $E_z \rightarrow 0$) to give a plasma of the desired size.

Diffusion of the magnetic fields during the formation phase must not be so rapid that current diffusion near the axis leads to a negative pressure gradient there or that a large fraction of the trapped axial flux is lost making it difficult to satisfy the condition $\Phi > 0$. This has been

STABILITY REQUIREMENTS	DIFFUSION REQUIREMENTS
B_z (wall) < 0	(no steady state)
β < 30%	β < 13% ($\Omega\tau$ >> 1)
$\int_0^{r_w} r\, B_z\, dr > 0$	$\int_0^{r_w} r\, B_z\, dr > 0$
$\left(\frac{P\,P''}{2}\right)_{r\to 0} < -\frac{4}{9}$	$\left(\frac{P\,P''}{2}\right)_{r\to 0} < -\frac{3}{4}$

Table I

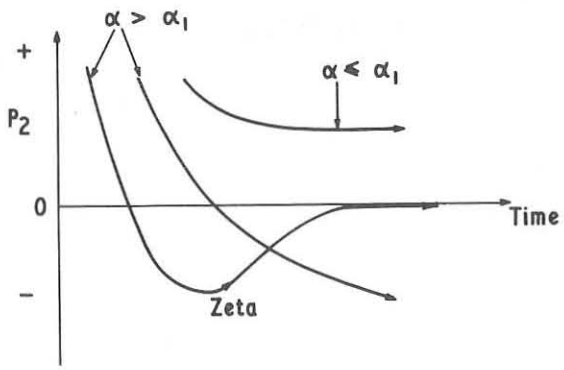

Fig.1 Evolution of P_2

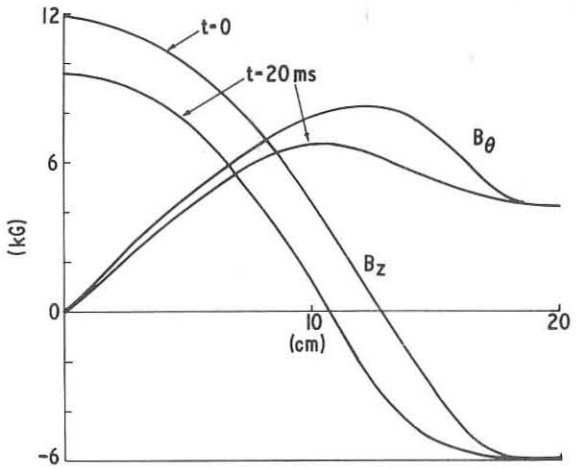

Fig.2 Field diffusion Φ < 0

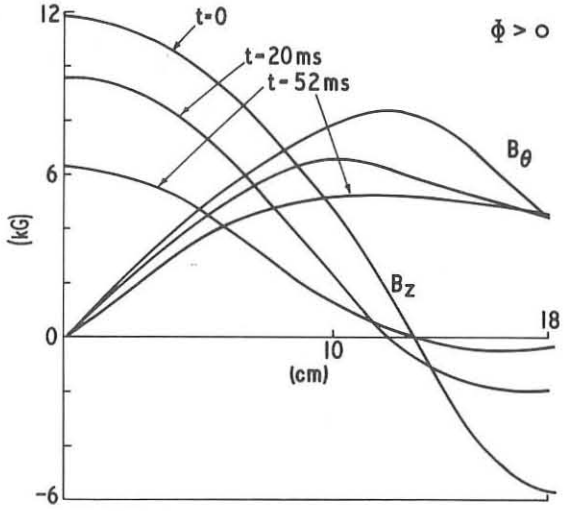

Fig.3 Field diffusion Φ > 0

INITIAL STAGES OF A REVERSE FIELD PINCH

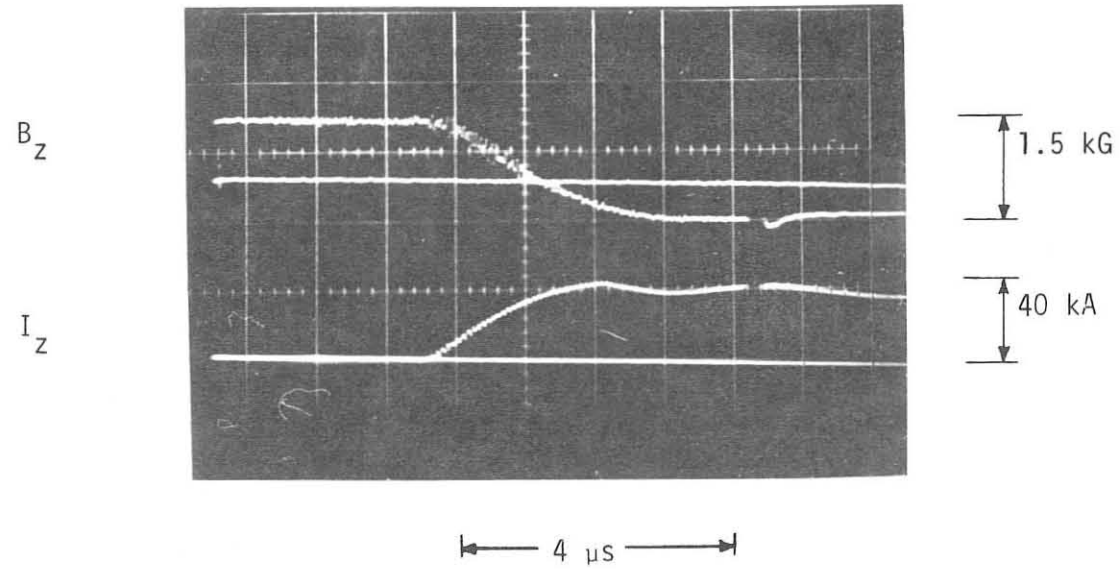

Fig.4

achieved by not using preionization and operating at filling pressures greater than 30 mtorr, when a plasma sheath or skin current is readily obtained. By taking account of these four considerations reverse field configurations have been set up stably for currents up to 100 kA at present.

PLASMA PARAMETERS: Using Thomson scattering of ruby laser light we have studied the temperature and density distributions of stabilized pinch and reverse field pinch discharges, Both exhibit hollow density and temperature profiles though in the case of the stabilized pinch the density profile fills in just before instability. Fig.5 shows the temperature and density distributions at about the time of crowbar for a current of 45 kA. Assuming that $T_i = T_e$ this gives a β_θ value of 0.6, a value 50% higher than that usually observed in stabilized pinches, presumably due to the extra heating caused by the additional j_θ current associated with the reversal of B_z. The variation of the mean temperature as a function of gas current at 30 mtorr for a stabilized pinch and 40 mtorr for a reversed field pinch is shown in Fig.6 indicating a relation of the form $\beta_\theta I^2 = 2\ NkT$ with $\beta_\theta = 0.4$ and 0.6 respectively.

We have studied also the variation of β_θ using magnetic probes. With a probe envelope size of 9.5 mm the observed motion of the plasma is modified leading to inconsistencies in deriving the electric field configuration and 'long'-lived plasmas are perturbed by the presence of such an envelope. A consistent picture has been obtained using a 4 mm diameter envelope. The evolution of β_θ is shown in Fig.7 for an uncrowbarred discharge, the normal crowbar time is about 3-3.5 μsec when $\beta_\theta \sim 0.6$ (a value which is too large for absolute stability for an annular form of pressure profile). The measured field configuration at 3.4 μsec is shown in Fig.8, after corrections have been applied to B_θ and B_z for the aperture in the metal wall through which the probe is admitted to the system. Note the narrow pressure distribution and current sheath formed in this case ($\sim$ 7mm). As this field

configuration exhibits no detectable instability - and in its quasi-stationary form is observed to last for many growth times, it is of interest to examine its stability properties in detail.

The plasma radius and axial flux are such that wall stabilization should be quite effective, but pressure driven modes are to be expected, associated with too large a value for β_θ. We have computed the growth rate, wavelength and eigenfunctions associated with this field configuration. All possible unstable modes arise from a region 4.4 → 5.2 cm where the Suydam criterion is not satisfied. The shortest growth time is 2.3 μsec for a mode whose eigenfunction is localised about the point where Suydam failure occurs and whose extent, 4 mm, is about an ion larmor radius. This field configuration lasts for much longer than 2 μsec, though modified by diffusion of course, and no instability is observed electrically or optically. In this case we believe that finite larmor raius effects are stabilizing the localised Suydam mode and we have used some results due to Stringer[8] to estimate the modified Suydam criterion in the region of failure. The pressure gradient can be up to three times larger than that obtained from the usual criterion and this is adequate to stabilize the modes in this region.

The diffusion of such a field configuration is controlled by both $\sigma_{\parallel}$ and $\sigma_{\perp}$ and during the formation of the pinch we have studied both these quantities. The electric field configuration derived from the changing magnetic one (Fig.8) and using the measured volts per turn is shown in Fig.9. The internal negative E_θ is due to compression of the trapped axial flux rather than paramagnetism in this case. From these fields we then obtain the $\sigma_{\parallel}$ variation shown in Fig.10 - again note the thin sheath and the close agreement with the Thomson scattering results for the temperature (Fig.5). Almost no anomaly in the conductivity is indicated; the ratio of the drift speed to sound speed is less than unity everywhere in this case.

The behaviour of the transverse conductivity $\sigma_{\perp}$ or the ratio of $\sigma_{\perp}/\sigma_{\parallel}$ is of direct interest as a small value of this ratio can lead to rapid

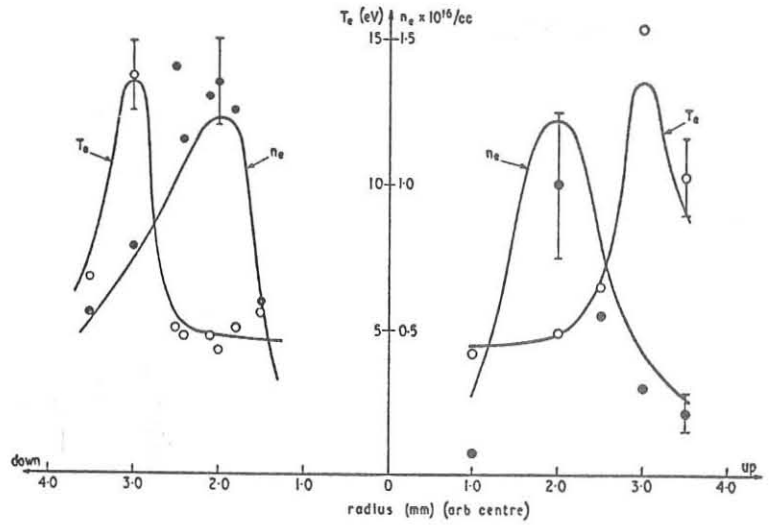

Fig.5
Temperature and density distribution in the reverse field pinch

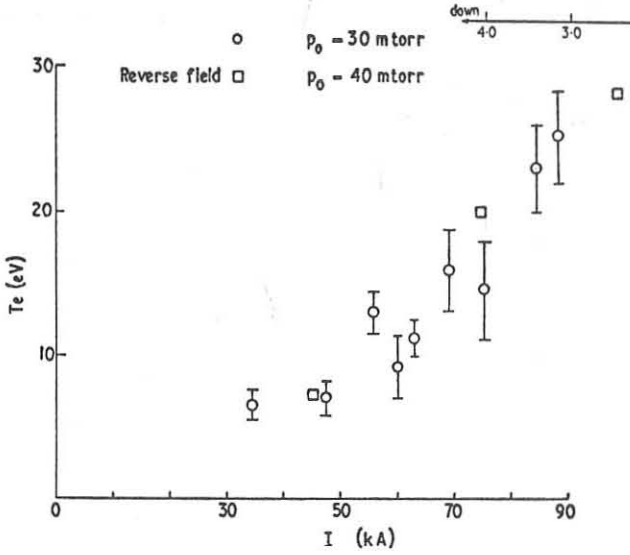

Fig.6 Variation of T_e with I

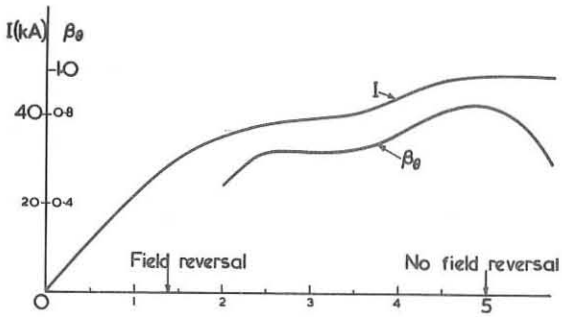

Fig.7 β_θ as a function of time

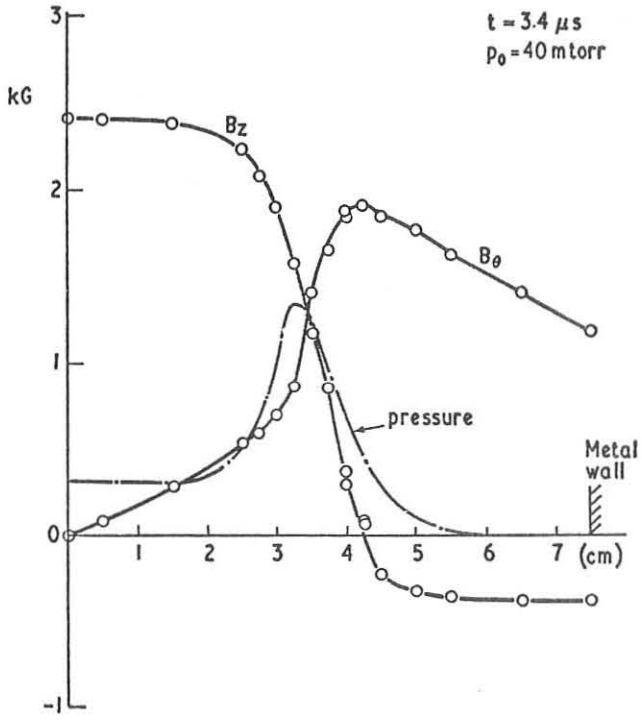

Fig.8 Magnetic field configuration

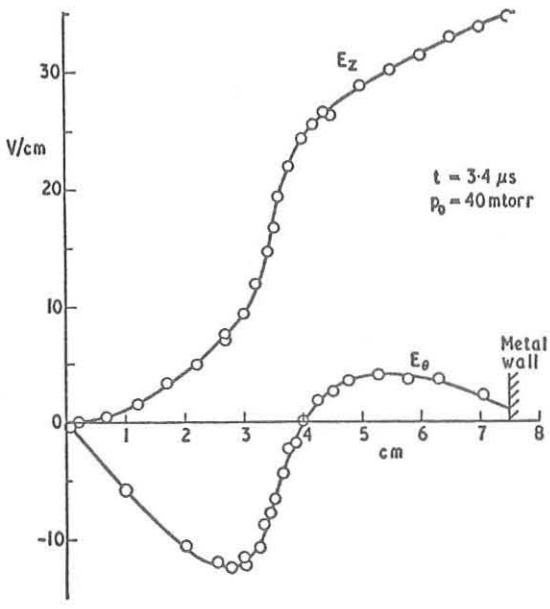

Fig.9 Electric field configuration

erosion of the trapped flux and a collapse of the plasma column, similar to that observed in some early reversed field experiments. Resolving Ohm's law in the transverse direction gives a radial velocity with corrections due to cross field diffusion as shown in Fig.11. Independent measurements of v_r from the density profile obtained from continuum measurements and also from the evolution of the pressure profile support the conclusion that $\sigma_\perp$ cannot be very different from $\sigma_{||}$.

PLASMA LIFETIME: Stereoscopic streak pictures taken of the plasma with the crowbar, Fig.12, show plasma lifetimes extending to 30 or 40 μsec though a gross but weak m = 1 instability is sometimes seen at about 20-25 μsec. The most reproducible discharges are obtained when $\Phi \gtrsim 0$ and the current is crowbarred sufficiently early for wall stabilization to be effective. For the same total current the e-folding decay time of the current can vary from 25-37 μsec depending on the size and therefore the inductance of the plasma.

As Thomson scattering data show little change in the temperature or density for the first 16 μsec we have studied the decay of the field configuration using a one-dimensional diffusion code with the temperature held constant, as an apparent balance between heating and losses is set up. Starting with the field configuration at 3.4 μsec and the measured conductivity the predicted decay of the fields at the wall is shown in Fig.13, and compared with that measured experimentally. The agreement is sufficiently good to indicate that the field diffusion is described by purely classical effects. At later times field reversal disappears and the pressure becomes peaked on axis which will lead to instability, though at these later times the current has decayed sufficiently to make the growth times rather long ($\gtrsim$ 5 μsec).

On the basis of the I and B_z decay times we can evaluate the energy confinement time assuming that the velocity is sufficiently low that any adiabatic heating or cooling effects are negligible, obtaining 12-16 μsec, for this particular case. This is close to the rate expected for classical losses.

CONCLUSIONS : MHD stability criteria impose strict limitations on the setting up of pinch discharges. More severe restrictions are encountered if stability is to be maintained in the presence of magnetic field diffusion. Reverse field configurations with $\beta_\theta \sim 0.6$ have been set up experimentally without wall contact or instability. Good agreement between theory and experiment for the growth and character of gross instabilities has been obtained but in the case of the reverse field pinch finite larmor radius effects appear to allow a somewhat higher β than predicted on MHD stability theory. Their lifetime, provided the diffusion condition that the axial flux be positive is satisfied, can be 30-40 μsec corresponding to the classical resistive decay time of the fields. The behaviour is comparable to that observed on Zeta where the larger radius (48 cm) permitted lifetimes of 3 msec but in that case the field configuration was not set up in a controlled way. Of the configurations studied on the high-β toroidal experiment the lifetime of the reverse field discharge exceeds that of other configurations.

REFERENCES:

(1) T. Ohkawa et al. Phys. Fluids 66 (1963) 846.

(2) D.C. Robinson, R.E. King, 3rd Int. Conf. on Plasma Phys and Nucl. Fus. Novosibirsk, vol 1, p.263 (1968).

(3) H.A.B. Bodin et al., 4th Int. Conf. on Plasma Phys. and Nucl. Fus. Madison, vol.1, p.225 (1971).

(4) R.E. King et al. Culham Report CLM-P 302 (1972).

(5) D.C. Robinson, Plasma Physics 13, 429 (1971).

(6) M.G. Rusbridge, Culham Report CLM-R 41 (1964).

(7) J.E. Crow, D.C. Robinson, 2nd Topical Conf. Pulsed High-β Systems, Garching, Paper C1, 1972.

(8) T.E. Stringer, Princeton University Report MATT 289 (1964).

* A.W.R.E., Aldermaston, Berks. + University of Padua, Italy.

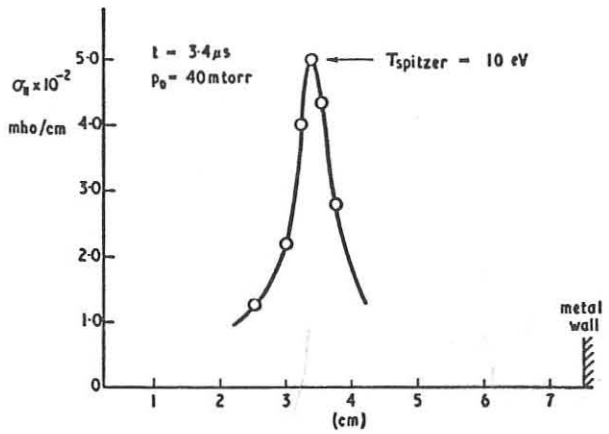

Fig.10 Conductivity distribution

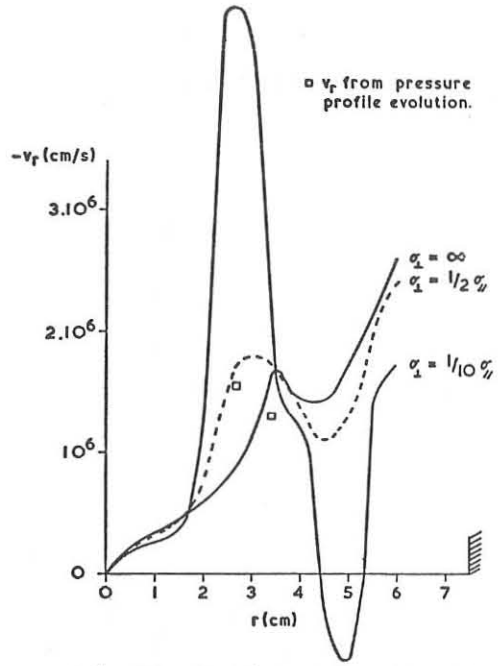

Fig.11 Radial distribution of velocity

Stereo views 26 cms apart

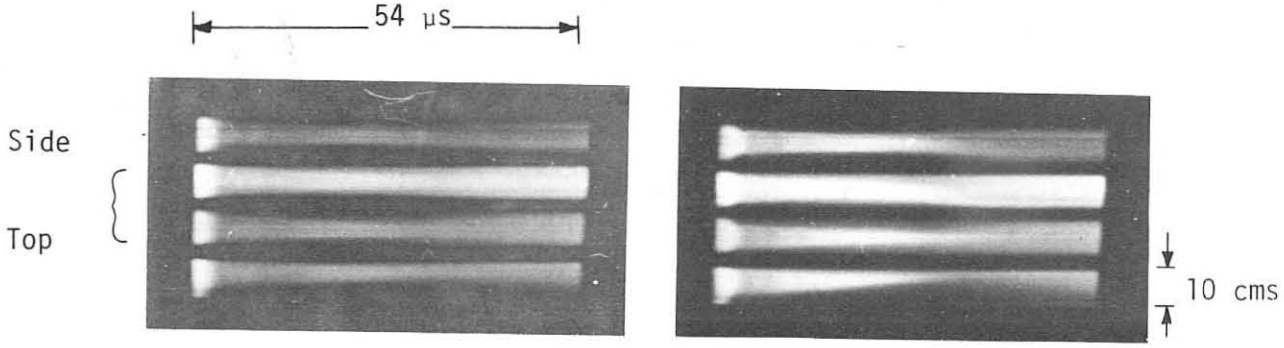

I = 38 kA, p_0 = 40 mtorr

Fig.12 Crowbarred reverse field pinch

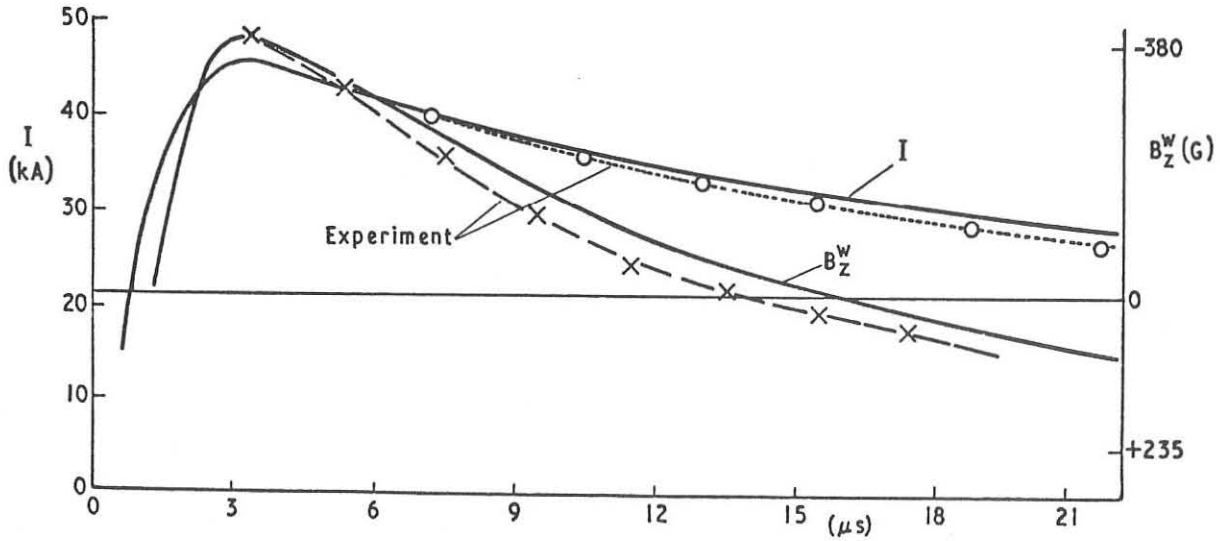

Fig.13 Field diffusion, computation and experiment

Toroidal Confinement in Screw Pinches with Non-circular Plasma Cross-Section

H.Zwicker and R.Wilhelm

Max-Planck-Institut für Plasmaphysik, Euratom Association

Garching bei München, Germany

Abstract: Toroidal Screw Pinches with elliptical or bar shaped plasma cross-section can be operated below the Kurskal-Shafranov limit also at high-β values. In this case piston heating can be used. Experimental results are given. They show a belt-pinch plasma which is grossly stable for about 100 μsec. The life-time is obviously limited by diffusion.

The most simple toroidal confinement systems are of the axisymmetric type with a toroidal plasma current. Besides simplicity a further advantage is here that usually the toroidal equilibrium is automatically obtained by compression of the poloidal flux towards the conducting wall. Typical representatives of this class are of the Tokamak and of the Screw Pinch type.

A Tokamak by definition operates below the Kruskal-Shafranov limit and is therefore m = 1 stable. This implies, however, very small β-values and a compression ratio near one. Consequently the temperatures can be obtained up to now only by Ohmic heating with all its problems or, perhaps, by some other methods which, however, are just now being tested really in experiments.

The toroidal Screw Pinch on the other hand operates at high β-values and at higher compression ratios. It can be heated therefore rather effectively by piston or fast magnetic compression heating. However, at high β-values, necessary for these heating mechanism, the screw pinch is basically m = 1 unstable.

With respect to high-β-confinement therefore the question arises how to change the high-β Screw Pinch into a stable equilibrium. One possible way is here to stay above the Kruskal-Shafranov limit and to get stability by an additional dynamic

stabilization. This principle seems to work experimentally but technically it is rather complicated.

A second way is to go below the Kruskal-Shafranov limit even at high-β-values in the Screw Pinch by changing the plasma cross-section from a circular to a strongly elongated one. Then one might obtain something like a high-β Tokamak which operates without any limiter and which could be heated by piston or fast magnetic compression heating.

The basic principle for this transition to other cross-sections is very simple. In a simplified sharp boundary model one needs for the toroidal equilibrium a certain ratio of the toroidal field B_z to the poloidal field B_φ at the plasma surface which is roughly given by

$$\left.\frac{B_z}{B_\varphi}\right|_{r_p} \approx \left(\frac{2A\delta}{\beta}\right)^{1/2} \qquad (1)$$

A is the coil aspect ratio and δ the relative shift of the equilibrium position.

For stability with respect to the Kruskal-Shafranov modes the pitch length of the helical field at the plasma surface has to exceed the major circumference of the torus. This requires a second condition for the field ratio which can be written as

$$\left.\frac{B_z}{B_\varphi}\right|_{r_p} = q \cdot \frac{2\pi R}{u_p} \quad ; \quad q \geq \frac{2}{2-\beta}. \qquad (2)$$

Here R is the major radius of the torus and u_p is the minor circumference of the plasma cross-section. For a circular cross-section with plasma radius r_p the stability condition is then in the usual form

$$\left.\frac{B_z}{B_\varphi}\right|_{r_p} = q \cdot \frac{R}{r_p} \,. \qquad (3)$$

For an elongated cross-section of height h, we have practically $u_p \approx 2\,h$ and the Kruskal-Shafranov condition becomes

$$\left.\frac{B_z}{B_\varphi}\right|_{r_p} = q \cdot \frac{\pi R}{h} \,. \qquad (4)$$

Compared to the circular cross-section one can fulfill here, at fixed B_z, the stability condition (4) for much higher poloidal fields B_φ because h can be chosen independently of R. Consequently stability and equilibrium can be obtained simultaneously also for high-β-values in contrast to the circular case. In this way the critical β for an m = 1 stable equilibrium can be increased considerably.

The equilibrium considered in equ. (1) is necessarily connected to a radial plasma shift which by flux compression produces the restoring force compensating for the drift force.

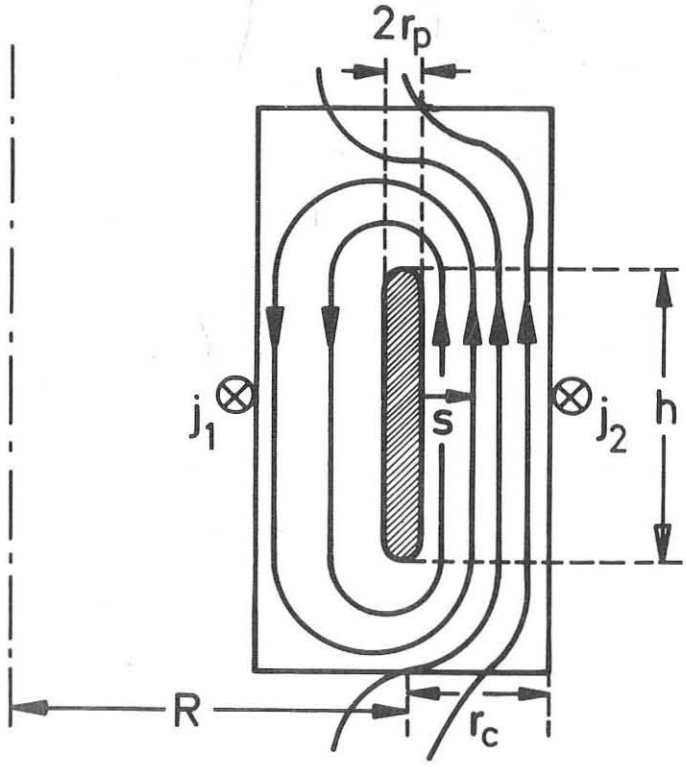

Fig.1: Scetch of currents and poloidal field in the compression coil.

One can obtain, however, also an equilibrium with the help of an additional transverse magnetic field the j x B force of which just compensates for the drift force without any radial shift of the plasma. Experimentally this transverse field can be produced easily by an additional toroidal current j_2 which flows in the outer wall of the compression coil which now has a rectangular cross-section as it is shown in fig.1. The current j_1 at the inner wall is the primary for the induction of the toroidal current in the plasma.

The current j_2 results now in a separatrix for the poloidal field. One has a last closed flux surface while the more outer ones do not close within the compression coil.

Let us denote the distance of the separatrix from the plasma by s and the other dimensions of the coil and the plasma as indicated in fig.1. Then we define the following quanti-

ties:

$$\sigma = \frac{s}{r_c} \; ; \; \epsilon = \frac{r_c}{r_p} \; ; \; A = \frac{R}{r_c} \quad .$$

Simple model calculations in a sharp boundary model indicate then, that also for the system of fig.1 a high-β equilibrium below the Kruskal-Shafranov limit should be possible if

$$\frac{h}{2R} \gtrsim 4\pi \sqrt{\frac{\beta}{A \cdot \epsilon}} \cdot F(\sigma) \qquad (5)$$

where $F(\sigma)$ is a certain function of σ.

For example with $A = 3$; $\epsilon = 6$; $\sigma = 0{,}5$ and $\beta \approx 1$ it follows from (5) $h/_{2R} \gtrsim 1{,}1$.

In a Screw Pinch with a rectangular cross-section of the compression coil the plasma after the first implosion is usually not in axial equilibrium. It starts with height h, and is subject to an axial contraction to the final height h. The degree of this axial contraction h_o/h can be estimated only very roughly in the simple model under certain assumptions. It turns out that h_o/h should be in the order of 2 for the parameters mentioned above. Initially one should fulfill then $h_o \gtrsim 4$ R for these parameters.

This is only a very rough model which indicates some essential features of a configuration with very elongated plasma cross-section. More detailed theories have been done by a number of authors [1,2,3,4,5]. Here are considered, however, mainly special cross-sections of elliptical and triangular shape. With respect to fast compression heating in a Screw Pinch one would like, however, plasma cross sections with nearly flat sides as in the belt pinch. For ohmically heated Tokamaks also special elliptic cross sections may be advantageous because they allow higher plasma currents and therefore higher ohmic heating rates as it has been pointed out by Artsimovich and Shafranov /6/. Besides stability with respect to Kruskal-Shafranov modes it is necessary to consider also localized and ballooning modes. For special ellipsis like cross-sections some authors give positive results also for these modes [1,4]. For non elliptical shapes Herrnegger [7] has investigated a special analytical solution of the toroidal equilibrium with a nearly bar-shaped cross-section. Similar calculations are reported al-

so by Luc et al.[8]. It turned out that also for this special belt pinch like configuration the generalized Mercier criterion [9] is satisfied. Of course this is only a necessary condition but these calculations give some indication that also bar shaped cross-sections could be stable for localized modes. But nevertheless in this situation the stability behaviour of Screw Pinches with non-circular cross-sections has to be investigated experimentally.

At Jülich one is essentially concerned with elliptical and triangular cross-sections of moderate excentricity and with the influence of the shape on stability. Experiments are carried out so far on the TESI installation. This is a special hard core θ-pinch which produces the closed configuration [10]. As an example fig.2 shows the magnetic surfaces 2 μsec after ignition as they follow from very precise probe measurements. They agree relatively good with calculations. The plasma behaves grossly stable and disappears after about 25 - 30 μsec mainly because of the decay of the currents.

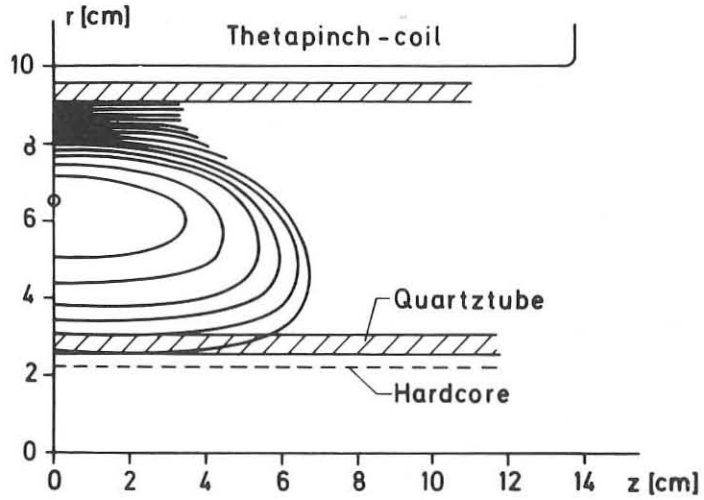

Fig.2: Magnetic surfaces, measured 2 μsec after ignition in the Jülich RESI experiment.

At Garching we are interested in very elongated cross-sections with nearly flat sides. These belt pinch experiments are carried out so far on the 110kJ device ISAR IV [11,12]. The toroidal screw pinch coil has a rectangular cross-section, a height of 110 cm which is somewhat more than 4 times the major radius of 23 cm, according to the simple model mentioned above. The toroidal and the θ-pinch currents are produced simultaneously by one bank in a screwed arrangement of copper layers which form the compression coil as it is shown in fig.3. Horizontally there are 30 copper loops in parallel which can be short-circuited by spark gaps. This allows an adjustment of the outer toroidal current j_2 for a proper equilibrium position and

for momentum compensation. The bank is crowbared with a time constant of 600 μsec. The total field is about 7 kG. Filling pressure is from 20 to 50 mTorr deuterium.

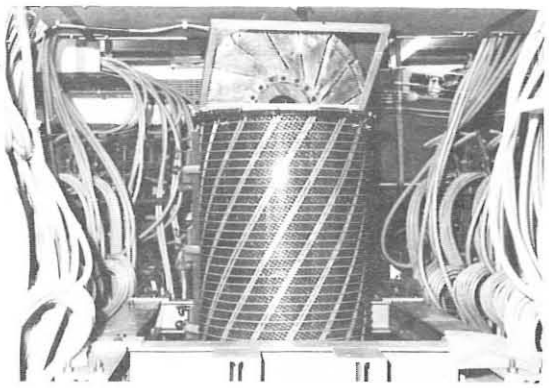

Fig.3: Coil-system of ISAR IV belt pinch.

The influence of the j_2 variation by crowbaring the copper loops on the equilibrium is shown in fig.4. These are streak pictures taken end-on from the top of the torus through a radial slit. The top picture is with open loops. j_2 is too large, the plasma is pushed inwards and then reflected. The second picture is with short-circuited loops. j_2 is smaller but the initial outward momentum is not fully compensated. A change of the crowbar time of the loops gives the third case where the plasma remains more or less in the midplane. The discharges are very reproducible and fig.5 gives a streak picture at 50mTorr which is obtained from five subsequent shots. The clear fast implosion, a slow oscillation and then a grossly stable behaviour during the observation time of 50 μsec is to be seen. The sharp boundaries in the pictures indicate a very straight plasma belt but these pictures give only local information. With respect to the gross stability behaviour there are three further problems: the degree of axial contraction, the behaviour of the edges with their unfavourable curvature and the deformations in toroidal direction.

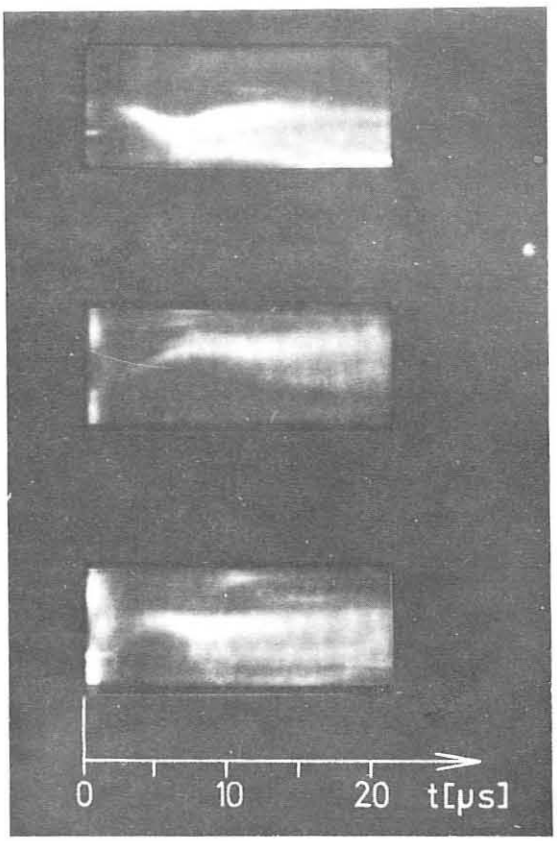

Fig.4: End-on streak picture. p_o = 50 mTorr D_2

For this reason there were taken framing pictures side-on of the whole plasma belt through the perforated coil and end-on of one half of the toroidal circumference.

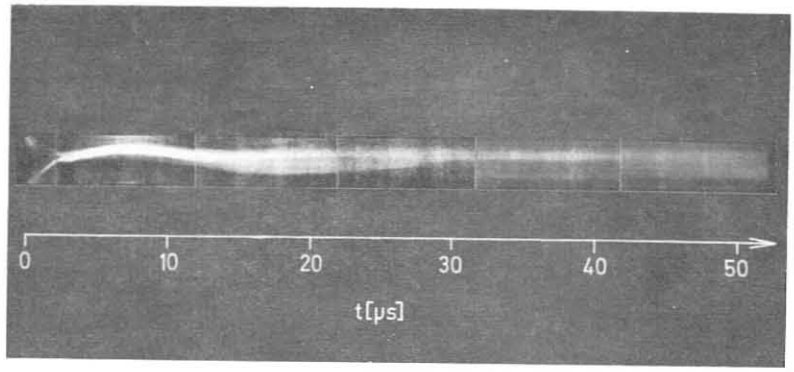

Fig.5: End-on streak picture. p_o= 50mTorr D_2

A typical result is shown in fig.6 giving three framings of one shot again at 50 mTorr.
5 μsec after ignition the formation of a well defined sharp belt.
15 μsec later the axial contraction without any deformation at the ends.
After 25 μsec the final state. The ends behave more or less stable and no serious deformation is to be seen.

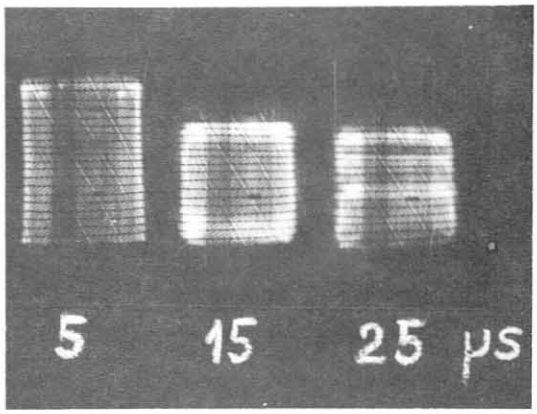

Fig.6: Side-on framing pictures. p_o = 50 mTorr D_2

The bright region in the midplain could be two colliding waves as a result of the axial contraction. Note, that here we have a ratio of h/2R of about 1 and an axial contraction factor around 2, which is not inconsistent with the simple model mentioned earlier.

The toroidal behaviour can be seen in

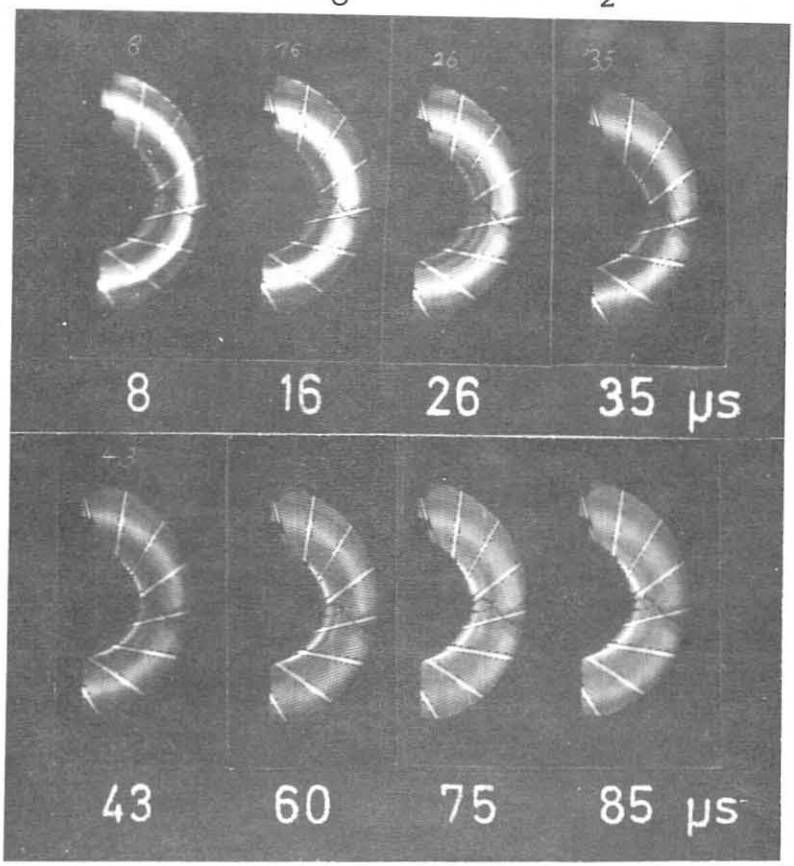

Fig.7: End-on framing pictures.
p_o= 50mTorr D_2

fig.7. It gives a series of end-on framings at various stages of the discharge. For technical reasons we cover only 1/2 of the circumference. First implosion, axial contraction and then a stable stage with no essential deformations except a small deviation from a circle. But also this slight asymmetry does not destroy the plasma belt. Its width is increased somewhat but it can be clearly seen still after 85 µsec.

In order to obtain information on the long time behaviour of the ends and on possible motion in axial direction one can take side-on streak pictures with the streak slit all over the height of the tube at the equilibrium position. A typical example of these observations is shown in fig.8. One recognizes the axial contraction and then the plasma stays essentially symmetrical for at least 100 µsec. Note, that also in this time scale at the upper and lower edges there appear no serious instabilities. There are some structures with respect to the height for which so far we have no explanation.

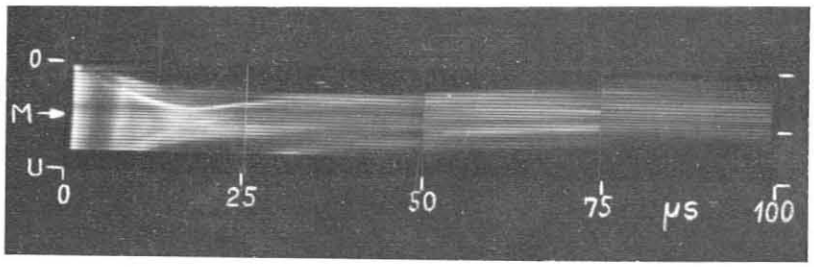

Fig.8: Side-on steak picture. p_o=50 mTorr D_2

Besides these optical observations there were performed probe measurements of the magnetic field. A typical radial distribution of the fields after the first implosion is shown in fig.9. For technical reasons it is only around the plasma centre in the toroidal midplane. Note, that the point of symmetry of $B_\varphi(r)$ is shifted by about 0.5 cm outwards with respect to the plasma centre. The B_z-measurements give at this stage a β of about 85 % at the axis.

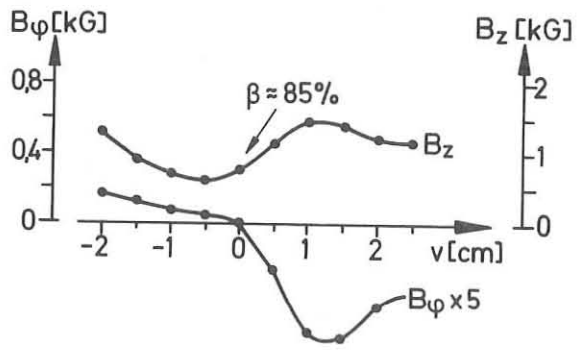

Fig.9: Measured radial field distributions after the first implosion. Torus midplane. p_o = 20 mTorr D_2.

A second set of measurements concerned the axial component B_y, of the poloidal field at the inner and outer wall of the tube as a function of the distance from the midplane: B_y (y,t).

Fig.10 gives the measured distribution along the inner surface for various times. After initial stages the axial component decreases towards the end because of the field curvature. Then the distribution contracts towards the midplane because of the axial contraction. In certain regions, B_y changes its sign. This indicates field lines which leave the coil so that there could be situated the separatrix.

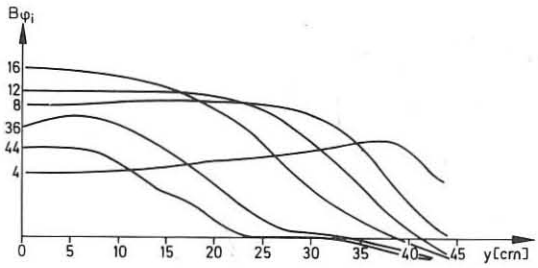

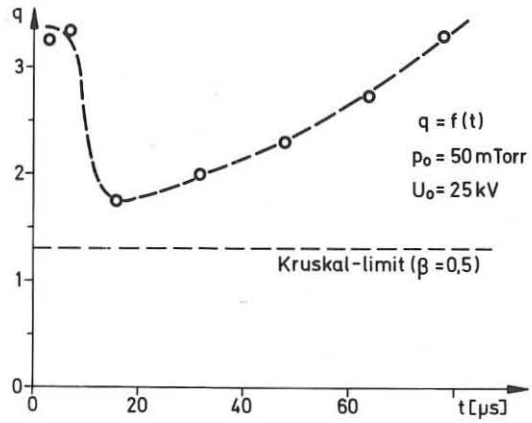

Fig.10: Axial field component $B_y(y)$ at various times after ignition.

Fig.11: q(t) as evaluated from optical and magnetic field measurements. p_o = 50 mTorr.

The optical and the probe measurements allow also a first evaluation of the development of the q-value in the configuration. The rough result is shown in fig.11. The first drop of q down to about 1.8 is due to the axial contraction while the further increase is the result of the different decay times for the poloidal and the toroidal field. But all over the time q is well above the value for the Kruskal-Shafranov condition at reasonable β-values.

A further point of interest is the time behaviour of the toroidal plasma current I_z. Field measurements indicate an exponential decay with a time constant τ_z of about 60 - 80 μsec. Assuming classical resistivity in a simple model this would correspond to electron temperatures of about 25 eV which on the other hand is in agreement with pressure balance for a mean electron density of about $n_e \approx 5.10^{15} cm^{-3}$ as it follows from the compression ratio.

For the belt pinch geometry it turns out that there are two different time scales for the decay of the toroidal and the poloidal plasma currents in the sense that the poloidal θ-pinch current decays faster than the current I_z because of the different L/R ratios. In other words, the containment changes at our low electron temperatures from a θ- pinch after about 30 μsec to a stabilized z-pinch and the decay time τ_z then limits the plasma life-time to about 80 - 100 μsec as is observed experimentally. For higher temperatures both time constants and therefore also the containment should be increased drastically provided that classical diffusion can be assumed and that energy losses at higher temperatures do not become dominant. Radiation losses can be overcome by fast compression heating. At long time scales, however, charge exchange and heat conduction have to be taken into account. These losses should be compensated by corresponding ohmic heating rates, and, it might be, due to estimates by Bateman [13], that this limits the energy confinement time. But this depends strongly on the situation out of the plasma belt and about this at present we know very little, so that precise predictions cannot be made at this time.

A second question of interest is the long time MHD stability behaviour of the configuration. Here we are still at the beginning. W.Grossmann has performed an ideal MHD analysis of a simplified belt pinch model [14]. He has shown that higher m-modes with respect to the torus axis should grow faster than the observed stable behaviour of about 100 μsec at ISAR IV. Finite Larmor radius effects yield, however, plausibility arguments that these modes should grow serveral orders of magnitude slower than predicted by ideal MHD theory. Also wall stabilization has been shown to be a strong effect in the belt pinch geometry. But even here precise theoretical predictions cannot be made and lots of work has to be done especially in the Vlasov regime when one approaches the collision free situation.

Therefore experimentally the further steps are in 3 directions. In the present experiment we are going to measure temperature and density distributions by laser-scattering and holography. I intended to give you the first results here but

the technique of high voltage insulation was against us and we had some trouble which delayed the measurements. Secondly we use a new coil system which will allow to go also to smaller q-values in order to find the stability limit of the belt-pinch.

The decisive question is, however, whether or not the plasma life time can be drastically increased at higher temperatures. In other words the question for stability and diffusion processes in the keV temperature regime.

For this reason as a third branch we are building a new device of 1 MJ with a discharge tube of 1.5 m diameter and 2.5 m hight. The experiment will operate at 40 kV charging voltage. However, during the initial piston heating stage it is planned to add a 120 kV pulse with the help of a small high voltage bank which then is decoupled by a saturated transformer [15]. The main bank is crowbared with a measured time constant of 2.6 msec at a field of about 8 kG.

In this arrangement ion temperatures up to 1.8 keV should be obtained at densities around $10^{15} cm^{-3}$. Part of the installation has just been tested successfully. Of course, we are aware of the possible difficulties we may meet. But I think, it is worth to do such an experiment now in order to find out whether or not the belt pinch can be a useful configuration for a long time confinement of high-β-plasmas.

References

[1] Solovev,L.S., V.D.Shafranov, E.J.Yurchenko, Vienna 1969 IAEA Conf., 1,175 (1969)

[2] Laval,G., E.K.Maschke, R.Pellat, M.N.Rosenbluth,IC/70-35, Trieste Report (1970)

[3] Janike,L., Jül.-700-PP (1970)

[4] Laval,G., H.Luc, E.K.Maschke, C.Mercier, R.Pellat,Madison 1971, IAEA Conf., Vol.II, 507 (1971)

[5] Küppers,G., H.Tasso, Z. Naturforschung, 27a, 23 (1972)

[6] Artsimovich,L.A., V.D.Shafranov,JETP Lett.,13,51 (1972)

[7] Herrnegger,F., Paper 26 these proceedings

[8] Luc,H., E.K.Maschke, J.Touche, Paper 23 these proceedings

[9] Mercier,C., Nucl. Fusion, 4. 213 (1964)

[10] Belitz et al., Madison 1971, IAEA Conf.,Vol.III,179(1971)

[11] Wilhelm,R., H.Zwicker, Madison 1971,IAEA Conf.,Vol.I, 159 (1971)

[12] Krause,H., R.Wilhelm, H.Zwicker, W.Grossmann, Proc. 2nd Topical Conf. on Pulsed High-β-Plasmas, Garching 1972,195,

[13] Bateman,R.G., IPP-Report; to be printed /F 1

[14] Grossmann,W., Proc. 2nd Topical Conf.on Pulsed High-β-Plasmas,Garching 1972,221,F 8.

[15] Wilhelm,R., IPP-Report in preparation.

CONFINEMENT STUDIES IN 2XII*

by

F. H. Coensgen, W. F. Cummins, A. W. Molvik, W. E. Nexsen, T. C. Simonen

Lawrence Livermore Laboratory, University of California

Livermore, California U.S.A.

Abstract: The containment of deuterium plasmas in a magnetic mirror well has been investigated for mean plasma ion energies in the range from 1 to 10 keV. Evidence indicates that detectable plasma turbulence in this experiment arises primarily from instabilities driven by the presence of two or more maxima in the ion velocity function. Plasmas with no detectable turbulence have been formed with mean energies in the range from 1.2 to 2.7 keV. The ion velocity functions of all quiescent plasmas have a single maxima. For these plasmas neither the magnitude nor the density dependence of the loss rate was noticably different for runs which were theoretically stable for the Dory-Guest-Harris mode and those that were unstable. In both cases $n\tau$ at high densities was below that calculated for collisional losses by a factor of two to three and decreased as the density fell. Although losses induced by other instabilities (e.g., drift-cyclotron, loss-cone mode) cannot be ruled out, the high density data from quiescent decays appear to be in agreement with the Baldwin-Callen[1] theory of "collective scattering".

EXPERIMENT - The 2XII experiment at the Lawrence Livermore Laboratory was constructed to further investigation of plasma containment in magnetic minimum-B wells. As in the earlier 2X experiments, an energetic plasma is formed in the well by trapping and subsequently compressing a portion of a plasma burst which is injected along a uniform steady magnetic field. Trapping is achieved through the use of an appropriately programmed set of pulsed magnets. These pulsed magnets are short circuited at time of peak discharge current and plasma behavior is followed during the exponential

decline of the magnetic field. As the lifetime of the plasma is much less than that of the magnetic field the contribution of the field decay to plasma loss is assumed to be limited to the density change calculated for adiabatic plasma expansion. Characteristic field and plasma parameters of the initial 2XII experiments are compared in Table I with those of the previously reported[2][3] 2X experiments.

TABLE I

Magnetic Field and Plasma Parameters for 2XII and 2X

Parameter	2XII Initial Operation	2X Ref. 3	2X Ref. 2
Maximum dc guide field (kG)	2	2	2
Maximum central magnetic field (kG)	6.5	13.2	16.3
Longitudinal mirror ratio	2	1.33	1.33
Radial well depth measured at wall (%)	21	2.5	2.5
Plasma to wall distance along magnetic field lines (cm)	300	20	20
Pulsed magnetic field rise time (μsec)	400	160	160
Magnetic field decay time (msec)	8	8	8
Distance between mirror points (cm)	100	160	160
Plasma diameter (FWHM cm)	12	6	6
Maximum plasma density	6×10^{13}	5×10^{13}	3×10^{13}
Maximum mean ion energy (keV)	1 - 10	8	6
Electron temperature (eV)	80 - 250	200	200
$\omega_{ci}(sec^{-1})$	3.1×10^{7}	6.4×10^{7}	7.9×10^{7}
$(\omega_{pi}/\omega_{ci})^2$ at $n_i = 10^{12}$ cm^{-3}	900	210	130

All field lines which thread the 2XII plasma exit into the 1.5 meter diameter end chambers where adequate pumping is provided for non-trapped injected plasma and for plasma lost through the mirrors. As predicted, this feature has reduced the influence of the central chamber walls on plasma

containment. The field lines are convex toward the center at all points between the magnetic mirrors, so there is absolute hydromagnetic stability rather than "$\int d\ell/B$ stability". Adiabaticity is assessed by calculating particle orbits[4] through 50 or more mirror reflections. Deuterium ions up to 100 keV are found to behave adiabatically for the 6.5 kG central magnetic field level. Stability against interchange instabilities in the fully developed magnetic well is predicted for all values of β by the Cordey-Watson criterion[5].

Seven 2-inch washer-type plasma guns are located 340 cm from the center of the containment chamber. When driven by a low inductance 30 μf capacitor bank, each injector provides an energetic deuterium plasma of approximately 2.5 keV mean ion energy. The output of a single injector is proportional to the square of the capacitor bank potential and at 10 kV, is approximately 5×10^{17} ions/pulse. The equivalent total injected ion current exceeds 10^5A. When used intermittently (as in operation thus far) the injector electrodes tend to load with hydrogen from the residual background gases. Consequently the concentration of hydrogen ions in the energetic plasma is in the range from 30 to 50%. Although the velocity ranges of the hydrogen and deuterium ions are nearly the same, the velocity distribution of the hydrogen component is not necessarily the same as that of the deuterium component. The mean energy of the trapped and compressed plasma can be varied in the range from approximately 1 to 10 keV. Limited control of the plasma ion velocity distribution is achieved by firing groups of the plasma gun array at different times.

Base pressures are in the range of 2×10^{-9} to 10^{-8} torr. To insure clean, "active-pumping-surfaces", titanium is deposited on all interior surfaces just before each plasma containment run.

MEASUREMENTS - The central electron density is measured with a 70 GHz stabilized wave interferometer and a second 4 mm interferometer is occasionally

used to determine the density 5.7 cm off axis. The ratio of these two agrees with the radial distribution estimated by assuming that the radial distribution of the trapped plasma ions was the same as that measured for the injected plasma burst and that the motion of the trapped ions is adiabatic during magnetic compression. Longitudinal density scans are made with a moveable 35 GHz μwave interfeormeter. Two 10 GHz μwave interferometers are used to monitor plasma densities external to the magnetic mirrors.

The magnitude and frequency spectra of the fluctuating electric fields during periods of plasma turbulence are determined from forward angle scattering of 4 mm μwaves.

The intensity and radial distribution of line radiation from heavy ions is monitored through the use of a dual-channel, grazing-incidence, vacuum ultra-violet monochrometer. Time dependent intensities of radiation in the visible range and the H_α line are also recorded.

For the operation discussed here we have no direct measurement of electron temperature. A Thomson scattering measurement is now installed and evidence from initial operation indicates that it is possible to determine T_e at least early in the decay.

Time dependent energy spectra of the transverse fast atom current at the center of the plasma containment chamber are determined by allowing neutral particles to pass through a nitrogen gas cell ($n\ell \simeq 2 \times 10^{14}$ atoms cm^{-2}) then through an 11-channel tandem mass analyzer. Particles which are ionized in the gas cell are deflected in the magnetic field of the analyzer and those in the proper momentum ranges enter one of the eleven separate electrostatic energy analyzers. An automatic data system comprised of an analog disc, a mini-computer, a digital tape and a high-speed printer is used to store and process the data.

Plasma ion energy spectra are derived from the neutral analyzer signals assuming that plasma ions charge exchange with thermal neutral methane (i.e.

the residual gas) flowing into the plasma volume. Both atomic and molecular hydrogen may be formed through neutralization of part of the injected plasma and contribute to a transient increase of neutral density external to the trapped plasma. Atomic hydrogen would not appreciably alter the derived spectra but the relative charge exchange cross-sections fall off at low energies for molecular hydrogen so if it forms an appreciable component of the background gas the relative magnitude of low energies in the spectra have been underestimated.

We estimate that less than one-third of the fast atom current is formed in the plasma interior by charge exchange with the flux of relatively energetic neutrals (Franck-Condon neutrals) resulting from dissociation of the thermal molecules in the plasma boundary. Since the mean free path for ionization of thermal particles is $\leq n_i^{-1} \times 10^{12}$ cm, fast atom energy spectra are dominated by conditions in a shallow low density boundary where interaction with the cold background gas is greatest. Plasma potentials derived from the low energy cutoff of the energy distributions are characteristic of the plasma boundary.

Except for low densities late in time the diameters of 2XII plasmas are greater than the mean free path for the ionization of Franck-Condon neutrals. Consequently the fast atom current is proportional to the neutral density external to plasma rather than the plasma density. Based on absolute calibration of the neutral analyzer the charge exchange rate is found to be a factor of 10 to 100 too low to account for the lowest observed plasma loss rates. J. R. Hiskes[6] in an independent evaluation of the data has also concluded that charge exchange is not a significant loss in 2XII.

OBSERVATIONS AND DISCUSSION - As judged from the density histories and the energetic deuterium content of the fast atom flux the period of detectable deuterium plasma densities in 2XII is frequently longer than 3.5 msec and exceeds by about 1.5 ms that of the best 2X operation.

In contrast with 2X data, short periods of very rapid plasma loss are observed for some modes of operation. Typical examples of these "plasma dumps" are shown in Fig. 1 at t = 1300 μsec in the run B density history and 630 μsec in run C. However, such obvious plasma catastrophies before 2 msec are the exception and the density decay of the trapped plasma is usually similar to that of run A in Fig. 1.

From inspection of the data we see that the plasma dumps are always accompanied by increases in all of the following: a) scattered μwave power, b) the relative number of high energy atoms in the charge exchange current, c) total light, and d) H_α radiation. The H_α signal is very similar to the total light signal and is not included in Fig. 2 where data from run C are reproduced to illustrate the time correlations of these data. In addition to temporal correlations the magnitudes of the logarithmic decay rate and the scattered μwave power are found to be directly related. A similar correlation is found between the logarithmic decay rate and the normalized 17.5 keV neutral analyzer signal (normalized by dividing by the total

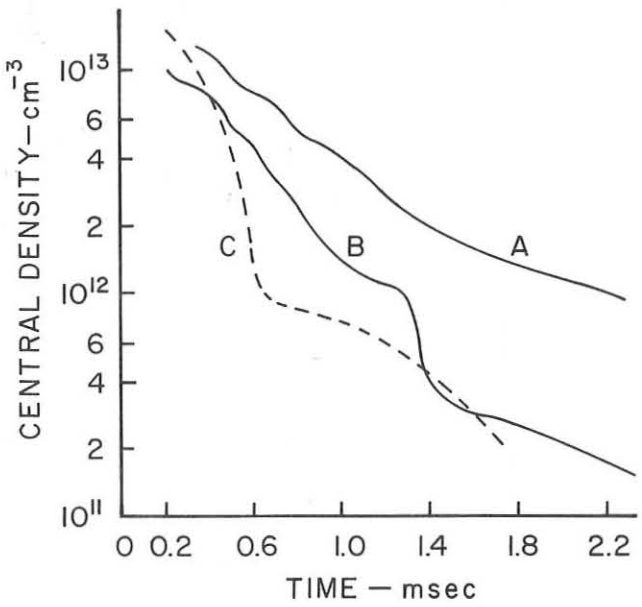

FIG. I DENSITY HISTORIES

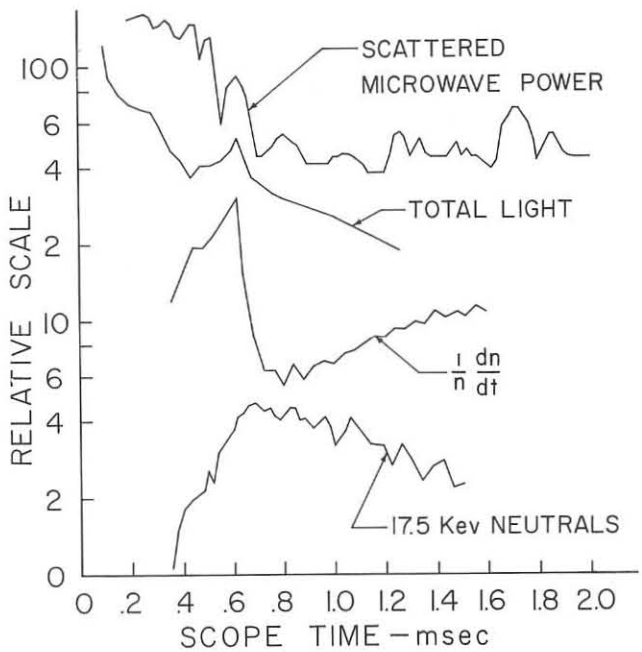

FIG. II RUN (C) DATA

charge exchange current). In fact, broadening of the energy distribution as indicated by relative increase of energetic particles in the charge exchange current has been found to be our most sensitive indicator of plasma turbulence.

No correlation has yet been established between the plasma decay rate or the occurrence of plasma dumps and the magnitude or time dependence of plasma external to the magnetic mirrors.

If the sequence of operation is timed to trap low energy plasma the trapped ion energy spectra usually have a single maximum lying near the low energy cutoff similar to that in the 420 μsec run A spectrum shown in Fig. III. As predicted shorter delays between injection and trapping increases the relative number of high energy ions but a lower energy group is also formed resulting in two and even three maxima in the trapped ion velocity functions; e.g., the 420 μsec run C spectrum shown in Fig. III.

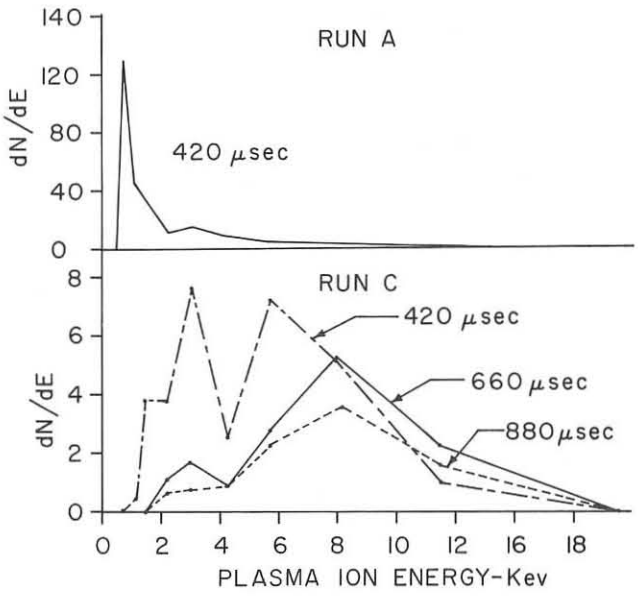

FIG. III ENERGY SPECTRA

Frequently, as in run C, during periods of rapid plasma loss the low energy maximum disappears and evidence of plasma turbulence is no longer detectable. This transition is accompanied by an abrupt decrease of the loss rate (see Fig. II).

In run B the charge exchange current rises before evidence of plasma turbulence (at t = 1300 μsec) suggesting that this particular plasma dump is triggered by the influx of cold gas. Run B energy spectra have two or more maxima and the evidence from this run as well as that from run C suggests

plasma losses resulting from double-humped[7] instability.

The correlation of detectable plasma turbulence with double-humped velocity functions is not restricted to the case of obvious plasma dumps, but rather such evidence is found in all runs where the velocity function has more than one maximum. In weakly turbulent runs where only a single maximum is evident, a second peak could escape detection due to the large separation between analyzer channels or because the observed spectra are representative of the plasma boundary rather than its interior.

The mechanisms leading to the formation of the lower energy maxima have not been identified. However, intense r. f. fluctuations occur in every run during trapping and into the magnetic compression. Thus when the cycle is adjusted to trap high energy ions lower energy ions streaming along the field lines will be trapped in the magnetic well if they can acquire sufficient rotational energy in one transit time. The fluctuating electric field $\tilde{E}$ necessary to provide one keV rotational energy to a one keV deuterium ion which is moving directly along a field line may be estimated by $\sqrt{V^2_{final}} = (e/M)\,\tilde{E}\sqrt{t\tau}$ where t is the transit time ($\sim$ 3 μsec) and τ is the electric field correlation time which we take to be one cyclotron period ($\sim$ 0.2 μsec). The required field, $\tilde{E} \gtrsim$ 90V/cm, is much less than the values deduced from the intensity of the μwave scattering during plasma trapping. Fluctuations at this level, which may escape detection, provide a mechanism for accumulating low energy ions. Since the ionization mean free paths are much less than the plasma radius this mechanism could lead to double-humped instability losses localized in the plasma boundary. This mechanism may account for the observed variation of loss rates in runs in which the energy spectra are quite similar.

Infinite medium $k_{||} = 0$ stability analysis[8] of the 420 μsec run C energy spectrum shows unstable frequencies around $1.1\omega_{ci}$ for the densities above 6×10^{11} cm^{-3}. As suggested by the appearance of the spectrum the

instability results from the presence of two maxima in the velocity function. Following the plasma dump when there is no detectable μwave scattering or energy spreading, unstable frequencies were found in analysis of run C spectra due to the limited spread of ion velocities; i.e. Dory-Guest-Harris mode[9].

With the exceptions of the occasional appearance of a component in the frequency band about $\omega_{ci}/2$ the scattered μwave frequency spectra associated with these plasma dumps are consistent with the double-humped instability. The lower frequency component may indicate a secondary effect due to an influx of cold heavy ions which drive a lower frequency double-humped instability.

On the basis of limited analysis of data from runs with double-humped energy distributions we observe that the $n\tau$ values at 425 μsec decrease with increasing relative depth of depression between the two maxima. From instability analysis the bandwidth of unstable frequencies and wavelengths are found to increase with increasing slope of velocity function between the maxima. We conjecture that marginally unstable cases would be stabilized after flute averaging the dispersion relation and including stabilizing electromagnetic corrections. These results may also contribute to the observed variation of $n\tau$ from a value less than 10^8 during plasma dumps to 5×10^9 cm^{-3} sec in weakly turbulent runs.

Quiescent plasmas such as that of run A have been generated with mean ion energies in the range from 1.2 to 2.7 keV. The velocity functions of these plasmas are all single peaked. Observed $n\tau$ values in the turbulence-free plasmas at the end of magnetic compression are only a factor of two to three less than the $n\tau$ values calculated (through the use of Fokker-Planck codes) for coulomb collisions. However the plasma decay in these "best" cases is in obvious disagreement with collisional losses as $n\tau$ decreases by about a factor of ten during the density decay from 2×10^{13} to 2×10^{12} cm^{-3}.

In an earlier discussion[1] of plasma containment similar to that of run A we advanced arguments that the anomalous loss rate resulted from either the Dory-Guest-Harris[9] or the drift-cyclotron loss-cone instability mode[8]. Infinite medium $k_{||} = 0$ stability analysis of run A spectra shows instability for the zero frequency DGH mode. Inclusion of the hydrogen term in the dispersion relation shifts the predicted threshold density to higher values in this example and in other cases leads to predicted absolute stability for the DGH mode. Deuterium velocity functions in two turbulence-free runs were found to be DGH stable. Thus, in the absence of recent theory of "collective scattering" for loss-cone particle distributions we would have been inclined to attribute the anomalous losses to the drift-cone mode. However, as shown in paper 91[10] of this Conference, it appears necessary to add to the classical ion-ion scattering loss rate a correction. Such a correction has the right functional form to fit the observed dependence of $n\tau$ with density and indeed the initial comparison of experimental data[10] with theory suggests that the anomalous loss rate could arise solely from this process.

In comparison of 2XII data with theory it is convenient to rewrite Eq. (2) of Ref. 10 in the form

$$\frac{1}{n^2}\frac{dn}{dt} = \left(\frac{1}{n^2}\frac{dn}{dt}\right)_{\text{classical}} + \frac{A}{[1 + \omega_{pe}^2/\omega_{ce}^2]^2} \exp \int d\alpha \left(\frac{\omega_{pe}^2/\omega_{ce}^2}{1 + \omega_{pe}^2/\omega_{ce}^2}\right)^{1/2}$$

where dependence upon the ion velocity function is included in the factor α and A is inversely proportional to the 3/2 power of electron temperature. If the density is expressed in units of 10^{13} and magnetic field in units of 10^4 gauss then $\omega_{pe}^2/\omega_{ce}^2 \simeq \frac{n}{B^2}$. For large values of $(\omega_{pe}^2/\omega_{ce}^2)$ where the exponential is independent of density (provided that the velocity function is time invariant) the curve n^{-2} dn/dt vs $(1 + n/B^2)^{-2}$ should be a straight line which intercepts the axis at the classical value of $(n\tau)^{-1}$. High density data from low energy (1 to 2.7 keV) plasmas lie close to straight lines

and $n\tau$ values derived from the intercepts show an $E^{3/2}$ dependence within the accuracy of experimental uncertainties. In runs with higher energy plasmas the velocity functions are found to change with time so that the comparison with theory is more difficult and has not been completed.

CONCLUSIONS

- Turbulence in 2XII appears to arise primarily from double-humped instabilities.
- Plasma loss rate resulting from the double-humped instability appears to increase with increasing relative depth between maxima in the velocity function.
- Plasma losses from quiescent plasmas are greater than predicted for coulomb scattering and do not have an n^2 dependence.
- Charge exchange effects are negligible.
- It is unlikely that Dory-Guest-Harris instability mode contributes to the anomalous loss rate.
- Theoretically 2XII is unstable to the drift-cyclotron loss-cone mode but other than the anomalous loss rate there is no direct evidence suggesting its existence.
- The data from low energy quiescent plasma decays is consistent with the Baldwin-Callen theory of collective scattering.

ACKNOWLEDGEMENTS: We wish to thank R. F. Post and W. M. Tang for the numerical procedures utilized in the 2XII stability analysis. D. E. Baldwin has participated in the comparison of the experimental results with collective scattering theory.

REFERENCES

[1] Baldwin, D. E., Callen, J. D., Phys. Rev. Lett. 28 1683 (1972).

[2] Coensgen, F. H., Cummins, W. F., Nexsen, W. E. Jr., Finlayson, V. A., and Simonen, T. C., "Proc. 4th International Conference on Plasma Physics and Controlled Fusion" Vol. II IAEA, Vienna 721 (1971).

[3] Coensgen, F. H., Cummins, W. F., Ellis, R. E., Nexsen, W. E. Jr., Proc. 3rd International Conference on Plasma Phys. and Controlled Nuc. Fusion Res. Vol. II, IAEA 225 (1969).

[4] Foote, J. H., Plasma Physics 14 543 (1972).

[5] Cordey, J. G., and Watson, C. J. F., Nuclear Fusion Reactors Conference Culham Laboratory, Culham, England 122 (Sept. 1969).

[6] Hiskes, J. R., Private Communication UCRL-51247

[7] Hall, L. S., Heckrotte, W., Kammash, T., Phys. Rev. 139 A117 (1965).

[8] Post, R. F. and Rosenbluth, M. N., Phys. of Fluids 9 739 (1966).

[9] Dory, R. A., Guest, G. E., Harris, E. G., Phys. Rev. Lett. 14 (1965).

[10] Baldwin, D. E., Paper 91 of this Conference.

*Work performed under the auspices of the U.S. Atomic Energy Commission

PLASMA DIFFUSION IN TWO AND THREE DIMENSIONS

by

J.B. Taylor

Culham Laboratory, Abingdon, Berks., England.

Abstract: Investigation of diffusion in two dimensional plasmas has shown that at high magnetic fields it is always proportional to $1/B$. When this investigation is extended to three-dimensions a 2D-like contribution to diffusion is found which dominates the classical, $(1/B^2)$ diffusion at high fields. This 2-D like contribution diminishes slowly with the size of the system and is susceptible to shear. Its importance in experimental plasmas is discussed.

1. INTRODUCTION

One of the cornerstones of plasma confinement theory is the calculation of diffusion across a strong uniform magnetic field. It is generally believed that for stable plasmas this is proportional to $1/B^2$ and in thermal equilibrium is given by[1]

$$D_c \simeq (18\pi^3)^{-\frac{1}{2}} \rho_e^2 \omega_{pe} \frac{1}{n\lambda^3} \log (n\lambda^3) \qquad (1)$$

where ρ_e^2 is the mean square electron larmor radius, ω_{pe} the plasma frequency and $n\lambda^3$, ($\gg 1$) the number of particles per debye cube. Equation (1) gives the mass diffusion (Flux/Density gradient) or the electron 'test-particle' diffusion; the ion 'test-particle' diffusion is $(M/m)^{\frac{1}{2}}$ times greater. There has often been discussion of a larger, anomalous, diffusion proportional to $1/B$ for which Bohm originally proposed the expression

$$D = \frac{1}{16} \frac{c\kappa T}{eB} \qquad (2)$$

but it has always been assumed that such anomalous diffusion is due to <u>non-thermal</u> fluctuating electric fields.

Some time ago the author[2] investigated diffusion in a two-dimensional guiding-centre plasma. This can be envisaged as an assembly of charged rods, aligned with a strong magnetic field, which move under the influence of their mutual electric fields with the guiding centre drift velocity. The results of this investigation were somewhat surprising; it was found that in this two dimensional guiding centre system the diffusion coefficient <u>always</u> has the $1/B$ variation with magnetic field - <u>even in thermal equilibrium</u>. Far from being anomalous, therefore, a Bohm-like diffusion is the classical one for this system.

This surprising result led to several further investigations, both of the two dimensional system itself and of the role played by this two-dimensional phenomena in real, three-dimensional, plasmas. In this paper I shall try to review the original results and some of the extensions, endeavouring to keep clear what is in some sense exact, what is approximate, and what is speculative.

2. THE TWO DIMENSIONAL MODEL

In this model the plasma is represented by rods with a charge e_i/ℓ per unit length ($e_i = \pm e$), aligned with a uniform magnetic field B. The guiding centre equation of motion for these rods is*

$$\dot{R}_i = c(B \times \nabla\varphi)/B^2 \tag{3a}$$

and the potential φ is determined by

$$\nabla^2\varphi = 4\pi \sum \frac{e_i}{\ell}\,\delta(r-R_i) \tag{3b}$$

where the sum is over all particles. Together with an initial probability distribution these two equations completely determine all the plasma properties. In thermal equilibrium the appropriate distribution would be

$$W\{R_i\} \sim \exp\left(-\sum_{i\neq j} \frac{e_i e_j}{\ell\kappa T} \log |R_i - R_j|\right)$$

These equations can be reduced to a universal form by the scale transformations, $\varphi = 4\pi e\psi$ and $t = (B\ell/4\pi ec)\tau$ and in the scale variables the problem involves only N, the total number of particles, and $\eta \equiv \kappa T\ell/4\pi e^2$ the number of particles per square debye length ($\lambda^2 = \kappa T\ell/4\pi ne^2$). It is apparent then that all plasma properties can be expressed in the scale variables as functions of N and η alone.

To make use of this result in determining the diffusion coefficient we write it in terms of the velocity correlation as

$$D = \int_0^\infty \langle v_i(0) v_i(t) \rangle dt = \frac{c\kappa T}{eB} \int_0^\infty \langle \dot{X}_i(0)\, \dot{X}_i(\tau) \rangle d\tau \tag{4}$$

which, in accordance with the remarks above, must take the universal form

$$D = \frac{c\kappa T}{eB} f(\eta, N) \tag{5}$$

We see therefore that, if a diffusion coefficient exists, then even in thermal equilibrium it can only be proportional to 1/B. Furthermore this result is an exact consequence of the guiding centre two dimensional model.

To determine the function $f(\eta,N)$ we again use (4), writing

$$D = \frac{c^2}{B^2} \int_0^\infty < E_\perp(0,0)\, E_\perp(r,t) > dt \qquad (6)$$

where $r(t)$ is the orbit of a test particle. Using fourier transforms the electric field may be written as the sum of contributions from each field particle,

$$\underset{\sim}{E}(x,t) = \sum_k \sum_j \frac{4\pi e_j}{\ell} \frac{\underset{\sim}{k}}{k^2} \exp\,(ik\cdot[R_j(t)-x]) \qquad (7)$$

so that

$$< \underset{\sim}{E}(0,0)\underset{\sim}{E}(r,t) > = \sum_{ij} \frac{16\pi^2 e_i e_j}{\ell^2} \sum_k \frac{\underset{\sim}{k}\,\underset{\sim}{k}}{k^4} H_k(R_i,R_j,r) \qquad (8)$$

where

$$H_k = < \exp(i\ k\cdot[R_i(0) - R_j(t)])\exp(i\ k\cdot[r(0) - r(t)]) > \qquad (9)$$

It is at this point that an approximate procedure must be invoked. Originally Taylor and McNamara concentrated on the correlation function at a fixed point $< \underset{\sim}{E}(0,0)\underset{\sim}{E}(0,t) >$, which they calculated self-consistently using the hypothesis that, for the calculation of particle velocities, the time history of $\underset{\sim}{E}(t)$ could be adequately represented by a single, jointly normal, distribution[2]. The diffusion coefficient was then calculated as if the test particle were at rest.

Within the same approximation the test particle motion may be retained and H_k written as

$$H_k = \langle \exp i\ k\cdot[R_i(0)-R_j(0)] \rangle \langle \exp i\ k\cdot[R_j(0)-R_j(t)] \rangle \langle \exp i\ k\cdot[r(0)-r(t)] \rangle \qquad (10)$$

Since they obey the same equation of motion, the averages involving test and field particles are both of the form

$$\exp(i\ c\ \underset{\sim}{k}\cdot \int dt\ \underset{\sim}{E} \times \underset{\sim}{B}/B^2) \qquad (11)$$

and the result of including the motion of the test particle is only to change[3] the final calculated diffusion coefficient by a factor $2^{\frac{1}{2}}$. Using the hypothesis that the field fluctuations are normally distributed, the average (11) becomes[2]

$$\langle \exp(ick\cdot\int dt\ \frac{E \times B}{B^2}) \rangle = \exp\left(- \frac{c^2 k_\perp^2}{4B^2} \int_0^t d\tau_1 \int_0^t d\tau_2\ \langle E(\tau_1)\cdot E(\tau_2) \rangle \right) \qquad (12)$$

Then introducing

$$R(t) = \frac{c^2}{2B^2} \int_0^t \int_0^t \langle E(\tau_1)E(\tau_2) \rangle \, d\tau_1 \, d\tau_2 \qquad (13)$$

using equation (12) and the approximation (10), one obtains from (8) an equation for the field auto-correlation

$$\frac{d^2R}{dt^2} = \frac{c^2}{2B^2} \sum \langle E_k^2 \rangle \exp\left(-2k^2 R(t)\right) \qquad (14)$$

Integrating this equation, and observing that as $t \to \infty$, $R \to \infty$ and $dR/dt \to D/2$, the diffusion coefficient is finally given by[2]

$$D_o = \frac{c}{B} \left[\sum \frac{1}{k^2} \langle E_k^2 \rangle \right]^{\frac{1}{2}} \qquad (15)$$

Equation (15) is the fundamental expression for the diffusion of two-dimensional guiding-centre plasmas. In thermal equilibrium the two dimensional fluctuation spectrum is given by

$$\langle E_k^2 \rangle = \frac{4\pi\kappa T}{\ell} \cdot \frac{1}{(1+k^2\lambda^2)} \qquad (16)$$

and, after replacing the k summation by the usual integral approximation with a cut-off at $k = 2\pi/L$,

$$D_o = \frac{c\kappa T}{eB} \left[\frac{1}{2\pi n\lambda^2} \log \frac{L}{2\pi\lambda} \right]^{\frac{1}{2}} = \frac{c}{B} \left(\frac{2\kappa T}{\ell} \right)^{\frac{1}{2}} \left(\log \frac{L}{2\pi\lambda} \right)^{\frac{1}{2}} \qquad (17)$$

This expression shows the Bohm like $(1/B)$ dependence on field strength; it also shows a weak dependence on the size of the system. In terms of the preceding discussion the function $f(\eta,N)$ is

$$f(\eta,N) = \left(\frac{1}{2\pi\eta} \log N/\eta \right)^{\frac{1}{2}}$$

Before discussing the significance of this two dimensional diffusion, which Dawson[4] has aptly termed "Vortex diffusion", we shall describe some extensions of the theory. These are of two types, (a) extensions of the two dimensional model itself and (b) investigations of the importance of the two dimensional (or Vortex) diffusion in real three dimensional systems.

3. EXTENSIONS OF THE 2-D MODEL

The model used so far is one in which the inertia of the particles (rods) is completely neglected. This is valid in the limit $B \to \infty$ or, more specifically, when $(\omega_p/\omega_c)^2 \ll 1$. Dawson, Okuda and Carlile[4] have extended the calculation to finite ω_p/ω_c. The most important change is in the electric field fluctuation spectrum. Although the exact partition function, and therefore the spectrum E_k^2, is independent of B, that part of

E_k^2 associated with frequencies below the gyro frequency does depend on B. It may be calculated by observing that at low frequencies the energy associated with a mode is not $E_k^2/8\pi$ but

$$\left(1 + \frac{4\pi\rho c^2}{B^2}\right)\frac{E_k^2}{8\pi}$$

so that the low frequency fluctuation spectrum is given by

$$\langle E_k^2 \rangle = \frac{4\pi\kappa T}{\ell} \frac{1}{(1+4\pi\rho c^2/B^2)} \cdot \frac{1}{(1+k^2\lambda^2)} \qquad (18)$$

When this modification is incorporated into equation (15) the diffusion coefficient retains the 1/B variation at large $B^2/4\pi\rho c^2$ but at smaller magnetic fields it becomes independent of field strength and takes the value[4]

$$D = (\kappa T/2\pi\rho\ell)^{\frac{1}{2}} (\log L/2\pi\lambda)^{\frac{1}{2}} \qquad (19)$$

As the field is still further reduced the guiding centre model becomes invalid and there is presumably a transition to the classical $1/B^2$ variation.

4. THREE DIMENSIONAL SYSTEMS

We now consider the role of the two dimensional, or vortex, diffusion mechanism in a three dimensional situation. The model for this discussion is one in which particles move across the magnetic field solely by the E × B drift but are free to move parallel to the field. This motion parallel to B introduces a rapid decay of all fluctuations with $k_{\parallel} \neq 0$; however, the $k_{\parallel} = 0$ fluctuations continue to behave in an entirely 2-D fashion and contribute to the diffusion exactly as they would in two dimensions.

The self correlation of the electric field is again given by

$$\langle E(0,0)E(r,t)\rangle = \sum_{ij} 16\pi^2 e_i e_j \sum_{k} \frac{1}{k^2} H_k(R_i, R_j, r) \qquad (20)$$

and H by

$$H_k = \langle \exp i\, k\cdot[R_i(0)-R_j(0)]\rangle \langle\langle \exp i\, k\cdot[R_j(0)-R_j(t)]\rangle \langle \exp i\, k\cdot[r(0)-r(t)]\rangle \qquad (21)$$

the only change being that $\underset{\sim}{k}$ is now a three dimensional vector. If we consider, for the moment, only the $k_{\parallel} = 0$ terms in (20) the diffusion coefficient may be calculated exactly as in section (2), with a similar result

$$D_v = \frac{c\kappa T}{eB}\left[\frac{1}{2\pi n\lambda^3}\frac{\lambda}{L_{\parallel}} \log\frac{L_{\perp}}{2\pi\lambda}\right]^{\frac{1}{2}} = \frac{c}{B}\left(\frac{2\kappa T}{L_{\parallel}} \log\frac{L}{2\pi\lambda}\right)^{\frac{1}{2}} \qquad (22)$$

as given by Montgomery, Liu and Vahala[5].

This expression is again proportional to 1/B. It tends to zero as $L_{\parallel} \to \infty$ because in 3-D the fraction of the total energy carried by the $k_{\parallel} = 0$ fluctuation diminishes with the length of the system.

If we again introduce the modification to the spectrum induced by finite gyro frequency, as discussed by Dawson and Okuda[6], the vortex contribution to diffusion becomes

$$D_v = 2^{3/2} \frac{c}{B} \left[\frac{\kappa T \log (L/2\pi\lambda)}{(1+4\pi\rho c^2/B^2)L} \right]^{\frac{1}{2}} \tag{23}$$

At high magnetic fields this is again proportional to 1/B but when $(\omega_{ci}/\omega_{pi})^2 \ll 1$ it becomes independent of B, exactly as in 2-D. The ratio of 'vortex' diffusion to classical diffusion is

$$\frac{D_v}{D_c} = \frac{6\pi}{(1+\omega_{pi}^2/\omega_{ci}^2)^{\frac{1}{2}}} \frac{\omega_{ce}}{\omega_{pe}} \cdot \left(n\lambda^3 \cdot \frac{\lambda}{L} \right)^{\frac{1}{2}} \cdot \frac{(\log L/2\pi\lambda)^{\frac{1}{2}}}{\log(n\lambda^3)} \tag{24}$$

and it should be noted that while λ/L is typically small, the parameter $n\lambda^3$ is equally typically large, and the two factors tend to cancel each other.

To calculate 3-D diffusion in full we return to eqs. (20) and (21). Assuming free streaming along the magnetic field and E × B drift across it

$$k \cdot [R(t)-R(0)] = k_{\parallel} v_{\parallel} t + k_{\perp} \cdot \int c(E \times B)/B^2 \, d\tau \tag{25}$$

The averages indicated in (21) can be carried out, using a Maxwellian distribution for $v_{\parallel}$ and the "jointly normal" hypothesis for $E_{\perp}$. Then

$$\langle \exp i\, k \cdot [R_j(0)-R_j(t)] \rangle = \exp [- k_{\perp}^2 R(t)] \cdot \exp [- k_{\parallel}^2 v^2 t^2] \tag{26}$$

where R(t) has been defined earlier and $2v^2$ is the mean square thermal velocity. A similar expression is obtained for the average over the test particle motion r(t). Rather than attempt to calculate R(t) in detail, we use the approximation $2R(t) \simeq Dt$ then, after integrating equation (20), one obtains D directly in the form

$$D = \alpha^2/D + \beta \tag{27}$$

where

$$\alpha^2 \equiv \frac{c^2}{B^2} \sum_{k_{\parallel}=0} \frac{1}{k^2} \langle E^2(k) \rangle \simeq D_v^2$$

and

$$\beta \equiv \frac{c^2}{B^2} \sum_{k_{||} \neq 0} \langle E_{\perp}^2(k) \rangle \int_0^{\infty} \exp\left[-(k_{||}^2 v^2 t^2 + k_{\perp}^2 Dt)dt\right]$$

It is tempting to argue, as do Vahala[7] and other authors[5,6] that in evaluating the $k_{||} \neq 0$ term one may neglect $k_{\perp}$. However there is always a region of k space, $k_{||} < k_{\perp}^2 D/v$, where the influence of the transverse motion may be important. Accordingly we retain $k_{\perp}$ in evaluating β. After substituting the thermal spectrum for E_k^2 and replacing the sum by an integral

$$\beta = \frac{c^2 \kappa T}{B^2} \int dt \int d^3k \, \frac{k_{\perp}^2}{k^2} \frac{1}{(1+k^2\lambda^2)} \exp\left[-(k_{\perp}^2 Dt + k_{||}^2 v^2 t^2)\right].$$

An approximate evaluation of this integral, valid when $\lambda v/D > 1$, leads to

$$\beta \simeq D_c \frac{[\log(\lambda v/D)]^2}{\log(n\lambda^3)} \qquad (28)$$

which is proportional to $1/B^2$ and close to the classical value. Vahala[6] derived a somewhat similar expression but with a different logarithmic factor.

Thus equation (27) shows that 3-D diffusion consists of two distinct contributions. First there is a 2-D like term, proportional to $1/B$ at high fields and independent of B when $4\pi\rho c^2/B^2 \ll 1$. This contribution is given by equation (23) and is always dominant as $B \to \infty$ for fixed L but tends slowly to zero as $L \to \infty$ at fixed B. The second contribution is a classical-like term, proportional to $1/B^2$, which is independent of the size of the system. The relative importance of these two contributions is given by eq.(24).

5. EFFECT OF SHEAR

So far we have considered diffusion only in a uniform magnetic field. Rosenbluth and Liu[8] have recently investigated the effect of introducing 'shear' into the problem. This will have a significant effect on the 2-D like vortex contribution since, in the presence of shear, there are no longer any modes unaffected by the parallel motion of the particles. Rosenbluth and Liu's calculation is based on a W.K.B. solution for the fluctuating fields. Here we give an alternative derivation following more closely the methods used in the earlier sections of this paper.

We confine ourselves to the high field limit and consider a simple sheared magnetic field $\underset{\sim}{B} = B_0 (\hat{z} + \hat{y}x/L_s)$. We return to equations (8) and (9) but now set

$$(\underset{\sim}{R}_i(t) - \underset{\sim}{R}_i(0)) = \left(\hat{y}\, \frac{X_i}{L_s} + \hat{z} \right) V_i t$$

$$(\underset{\sim}{r}_i(t) - \underset{\sim}{r}_i(0)) = \hat{z} v t$$

and treat all the field particles as independent, then

$$\langle E_y(0)\, E_y(t) \rangle = 16\pi e^2 n \sum_i \sum_{k_y k_z} \sum_{k_x k'_x} \frac{k_y^2}{k^2 k'^2} \cdot$$

$$\langle \exp i[k_x - k'_x) X + (k_z + k_y X/L_s)\, Vt + k_z v t] \rangle$$

The k_x, k'_x integrations lead to a factor $\exp(-2\kappa|X|)$ where $\kappa^2 = (k_y^2 + k_z^2)$. The averages over maxwellian velocities V, v can be carried out when

$$\langle E_y \cdot E_y \rangle = 16\pi n e^2 \sum \frac{k_y^2}{\kappa^2} \int dX \exp(-2\kappa|X|) \exp -\left(\left[k_z + k_y \frac{X}{L_s} \right)^2 + k_z^2 \right] v^2 t^2 \Big) .$$

The corresponding diffusion coefficient is, with $(k_z + k_y X/L_s) = k_z \beta$,

$$D = \frac{8\pi^{\frac{1}{2}} n e^2 c^2 L_s}{B^2 v_{th}} \sum \frac{k_y^2}{\kappa^2} \int d\beta\, [\beta^2 + 1]^{-\frac{1}{2}} \exp\left(- 2 \frac{k_y}{\kappa} |k_{||}| |\beta - 1| L_s \right)$$

In this integral the major contributions are from $k_z \ll k_y$, so that $\kappa \sim k_y$. An approximate evaluation of the integral gives finally

$$D \simeq D_c \frac{\log(\lambda/\rho_e) \log(L_s/\lambda)}{\log(n\lambda^3)} \qquad (29)$$

as given by Rosenbluth and Liu[8] which is close to the classical value.

It should be noted that in deriving this result only electrons were considered. If ions had been included in this model diffusion would be increased by $(M/m)^{\frac{1}{2}}$. However, because of screening, the independent test particle model cannot be applied to the ions and (29) is probably a more accurate assessment. The important point is that, while the numerical coefficient may be in doubt, eq.(29) shows that a small shear can remove the vortex contribution to diffusion. Only in shear-free systems, therefore, can one expect an important 2-D like contribution to diffusion in thermal equilibrium.

6. CONCLUSIONS

The central theme of this work is the recognition that in two dimensions diffusion always exhibits a 1/B dependence at high magnetic fields rather than the classical $1/B^2$. There is nothing 'anomalous' about this - it is true in thermal equilibrium and is an exact consequence of the guiding centre model. The magnitude of this 2-D diffusion has been calculated in

thermal equilibrium using a normal functional distribution hypothesis for the fluctuating field and is given by equations (17) and (19).

Apart from its fundamental interest, this result is of importance for real plasmas in two respects. Firstly, (and here we depart temporarily from the discussion of thermal equilibrium) there are circumstances in which real plasma may behave like a 2-D system. This is because equilibrium is attained quickly along the lines of force but much more slowly perpendicular to them. Furthermore all charges on a given flux tube tend to remain together so the flux tubes and the particles on them retain their identity. If therefore a plasma acquires an imbalance of charge between various flux tubes, e.g. during its formation or as a result of an unstable phase, then these tubes behave exactly as the charged rods of our 2-D model.

Secondly, even if the plasma is in thermal equilibrium, there is still a two-dimensional-like vortex contribution to the cross field diffusion. This arises from the $k_{\parallel} = 0$ fluctuations which, as in the genuine 2-D system, have an exceptionally long lifetime. The magnitude of this vortex contribution may be calculated in the same way as the 2-D result and is given by eq. (23). This contribution is dominant as $B \to \infty$ but diminishes slowly with the length of the system.

The total diffusion in a 3-D system is thus made up of two parts; the vortex contribution and a classical, $1/B^2$, contribution. The ratio of these two contributions is given by equation (24). In multipole experiments such as CLIMAX[9] ($T \sim 50$ eV, $n \sim 10^{11}$/cc, $B \sim 2000$ g, $L \sim 100$ cm) or the G.G.A. Octopole[10] ($T \sim 0.5$ eV, $n \sim 3 \times 10^9$, $B \sim 150$ g, $L \sim 400$ cm) vortex diffusion would be comparable with the classical value and would become dominant at higher magnetic fields. However as a small amount of shear is sufficient to remove the vortex contribution it is only in shear free systems that one can expect it to be important for diffusion in thermal equilibrium.

It is clear that the present theory, in addition to throwing light on the ubiquitous Bohm diffusion, is closely connected with, and places on a much firmer footing, the phenomena previously described as 'convective cells'. As we have emphasised, such 2-D vortex like phenomena are to be expected both in non-equilibrium situations, due to charge imbalance on different flux tubes, and in thermal equilibrium. The fact that they are susceptible to shear should be borne in mind when interpreting the influence of shear on plasma confinement. This has hitherto been discussed solely in terms of instabilities but we now see that when vortex diffusion is important shear can influence plasma loss even if the plasma were entirely stable.

ACKNOWLEDGEMENTS

I am grateful to D. Montgomery, G. Vahala, J. Dawson and M. Rosenbluth for pre-prints of their papers referred to in the text and for several valuable comments and suggestions. The result (28) was obtained jointly by the author and M.N. Rosenbluth.

REFERENCES

1. C.L. Longmire & M.N. Rosenbluth, Phys. Rev. 103, 507 (1956).
2. J.B. Taylor & B. McNamara, Phys. Fluids 14, 1492 (1971).
3. I am indebted to D. Montgomery for pointing this out.
4. J.M. Dawson, H. Okuda & R.N. Carlile, Phys. Rev. Lett. 27, 491, 1971.
5. D. Montgomery, C.S. Liu & G. Vahala, Phys. Fluids 15, 815, 1972.
6. H. Okuda and J. Dawson, Princeton University Report PPL AP52.
7. G. Vahala, Phys. Rev. Letts. 29, 93, 1972.
8. M.N. Rosenbluth & G.S. Liu, Proceedings of this Conference (1972).
9. A. Dellis et al., Plasma Physics and Controlled Nuclear Fusion, IAEA Vienna (1971) Paper CN28/A-6.
10. T. Ohkawa et al., loc. cit. Paper CN28/A-2 and Phys. Rev.Letts. 24, 95 (1970)

* Vectors are to be understood. They are underlined $\underset{\sim}{E}$ only where necessary to avoid ambiguity.

Recent Developments in Computer Simulation of Plasmas

D. Biskamp and R. Chodura

Max- Planck-Institut für Plasmaphysik, Garching b.München

In recent years computer simulation has become a valuable tool of plasma physics research. This was essentially due to the development of powerful computers such as the CDC 6600, 7600 or the IBM 360-91, which combine sufficient storage capacity (internal or external) with high-speed execution. To begin with, let us briefly describe the general concept of plasma simulation. The basic idea is to follow numerically a large number of electrons and ions under the influence of their self-consistent fields, in contrast to solving the only approximately valid fluid equations. Now it is easy to see that if one intends to include the details of the microfields around each particle the number of particles, one can handle even on the largest machines, is ridiculously small. However, because of the long range of the Coulomb field, many particles interact with each other simultaneously, the effect of small angle scattering dominates that of close encounters. Thus the main contribution to the interaction is due to certain average fields produced by average charge and current densities.

The simplest model based on this concept of average fields, is the PIC (particle-in-cell) method[1)2)]. Here the fields are computed on a Eulerian grid whose meshsize Δx should be small compared with the wavelengths of the effects under consideration. For collective modes with $\lambda >> \lambda_D, \Delta x \sim \lambda_D$ is sufficiently fine. This method has the double advantage of reducing collisional effects, which allows simulation of collisionless processes with relatively small numbers of particles per Debye cell, and of being numerically very simple, which allows to use a large number of particles i.e. to treat (relatively) large systems. Combined with certain interpolation procedures (area weighting=finite particle size, and field interpolation) this method is the one now generally used in simulations of microscopic plasma processes (another name of this method is CIC=clouds-in-cell[1)]). Fig. 1 shows the Coulomb cross-section in 2D and 3D demon-

strating the smoothing properties of finite particle size or cell size Δx. Note the particularly strong dependence in 3D[3].

Let us briefly indicate what kinds of systems can presently be treated by computer simulation. 1D systems do not cause any troubles. Usually $N = 10^4$ particles are sufficient. Only if very large system size is required, or if very weak collective effects are investigated requiring a large number of simulation particles per cell, N must be larger. 2D computations are possible for a number of problems. Typical N's are several times 10^4 to several times 10^5. These numbers can usually only be handled by use of external storage, and 2D runs are in general rather expensive (a number of hours per run). 3D runs are just marginally possible in very special cases and this situation is likely not to change in the near future. Even if there are computers 10 times as powerful as the present ones, in 3D this means only an improvement of a factor of 2 in the linear dimensions. Hence real life simulation is practically not possible, and for a rather long time plasma simulation will have to use appropriate 1D and 2D models.

To characterize developments in plasma simulation of the last one or two years we would like to distinguish three main tendencies:

a) Inclusion of multiple length and time scales. Special topics are turbulent electrical resistance and collisionless magnetic shock waves.
b) Development of fully electromagnetic codes including radiation. First application: simulation of the Weibel instability.
   Main interest: Investigation of plasma interaction with laser light or relativistic electron beams.
c) Investigation of collisional effects, to study collisional transport phenomena such as cross-field diffusion.

This list is by far not complete, the different items given being just examples. There are of course multiple (time and length) scales in any two-species code, and in cases where electromagnetic and electrostatic effects are treated simultaneously. The emphasis in category a) is on computations where either these scales are largely different, for instance if a large mass ratio is required, or where a whole variety of different scales

appear explicitely.

If the meshsize Δx of the grid is made smaller than λ_D, discreteness effects appear in the particle model, and in 3D, PIC reliably describes physical binary collisions. This can be used to study collision dominated transport processes, which corresponds to solving the Boltzmann equation in a stable plasma. The most interesting results on cross-field plasma diffusion[4] were reported in the preceding talk by Dr.Taylor. So we will not touch the last topic c) here. We primarily discuss some results on turbulent heating and on magnetic collisionless shock waves, and then briefly survey progress in simulation of electromagnetic and radiation phenomena.

Electrostatic instabilities excited by an electric current in a plasma are well suitable for investigation by particle simulation. Since typical wavelenths are much shorter than any macroscopic plasma scale, these processes may be regarded as quasilocal and the assumption of a homogeneous system is a good approximation. First simulation results on turbulent heating were presented at the Madison conference a year ago. We think that the situation is somewhat clearer now. The present status of the simulation work on turbulent resistance is as follows:

1) No external magnetic field, $B_o = 0$:

   In 1D no substantial resistance exists in the ion-sound regime $v_d < v_{the}$ [5)6)7)].

   In 2D appreciable electrical resistance is found, which is caused by a broad cone of unstable ion-sound waves. The numerical value of the effective collision frequency ν_{eff}, however, is still too small to explain the resistance in turbulent heating experiments[7].

   In 3D computations are just marginally possible. It has been found here, that ν_{eff} is about 2-3 times larger than in 2 D, because of the more rapid thermalization of electrons in a 3-dimensional turbulent field[8]. This value comes closer to experimental observations.

   In all these cases the formation of an electron tail in the distribution fuction gradually reduces the resistance.

2) External field parallel to the current $B \parallel j$:

   This is the usual situation in turbulent heating experiments.

   Simulations in 2D show a resistance comparable to the one in unmagnetized

plasmas for $\Omega_{ce}/\omega_{pe} < 1$, and a much lower value when Ω_{ce} becomes greater than ω_{pe}. No appreciable level of electron cyclotron oscillations is observed that could isotropize the electron distribution and thus enhance resistance. Thus if strong anomalous resistance is found in experiments in the regime $\Omega_{ce}/\omega_{pe} > 1$, it cannot be simply interpreted in terms of ion-sound instability.

3) Magnetic field perpendicular to the current, $B \perp j$:

Electron runaway is prevented, when the current is flowing perpendicularly to B, which is the case in high -β configurations such as shock waves and magnetic sheaths. We want to treat this case somewhat more in detail. The discussion about the type of instability producing anomalous resistivity in collisionless shock waves was initiated by the experimental observations of Keilhacker and coworkers[9]. These experiments seem to indicate that the presence of anomalous resistance is not depending on a high temperature ratio T_e/T_i. Thus the usual ion-sound instability appeared to be a somewhat doubtful candidate. The electron cyclotron drift instability at first sight seems to solve the problem, since it predicts unstable wave growth quite independently of T_e/T_i. However, in a high density plasma, $\Omega_{ce} << \omega_{pe}$, this instability will saturate at very low fluctuation levels (Lampe et al.[10]) and hence cannot explain the anomalous resistivity observed.

On the other hand computer simulations show strong instability and efficient electron heating in a parameter range where the usual two-stream instability does not exist[11]. An intense discussion on this point came up. We believe that these points are clarified by now and we want to describe briefly the essential results of the $j \perp B$ instability for amplitudes greater than the saturation level of the electron cyclotron drift instability. The following features have been found in the 1D case:

i) The instability threshold is not much different from that of the usual two-stream instability, see Fig. 2, in contrast to the electron cyclotron drift instability. The numerical simulations of Forslund, Morse and Nielson[11] reported at the Madison Conference had parameters just between the two curves of Fig.2.

ii) Nevertheless, the basic nonlinear mechanism suggested by Forslund, Morse and Nielson is correct. In 1D electron heating occurs by a rather coherent process of trapped electron acceleration, and not by some

stochastic (quasilinear) electron scattering . This is seen directly in Fig.3. While the quantity $W/nT \simeq$ const, $W = \langle E^2\rangle/8\pi$, in the turbulent phase, the thermal velocity and hence the effective collision frequency increase linearily with time $v_{the} \propto \nu_{eff} \propto \Omega_{ce} t$ in contrast to the quasilinear prediction $\nu_{eff} \simeq W/nT \simeq$ const.

iii) The electron temperature finally saturates (Fig.2c), when the drift approaches a certain value v_{ds}. The theory of ion-sound instability predicts $v_{ds} \sim c_s$, while the electron cyclotron instability predicts $v_{ds} \sim v_{the}\, \Omega_e/\omega_{pe}$ (although the linear electron cyclotron instability does not play a role in these cases, the strong dependence of the collision frequency on Ω_e may suggest a dependence of the switch-off drift v_{ds} on the magnetic field in the sense of the electron cyclotron drift instability threshold). Running a number of computer experiments up to saturation of T_e, we find that $v_{ds} \simeq 2\, c_s$ and that there is only very weak dependence on B. If one assumes the thickness Δ of a magnetic sheath to be determined by anomalous resistivity in the way that resistive magnetic field penetration occurs until the current density approaches env_{ds}, we would obtain the usual $\Delta \sim c/\omega_{pi}$ (for $\beta_e \sim 1$), and not $\Delta \sim (c/\omega_{pe})(c/v_{the}) \sim c/\Omega_{ce}$ (for $\beta_e \sim 1$) as predicted previously on account the electron cyclotron drift instability[10].

In 2D the general behaviour is rather different from the 1D case. The main result is that the strong coherent electron heating observed in the 1D runs does not exist here, since a broad cone of modes leading to a short correlation length effectively prevents longtime electron trapping. Fig.3 shows some results of a run with $T_{eo}/T_{io}=50$ and $m_i/m_e = 1600$. One finds, that ν_{eff} reaches a maximum at about the same time as W/nT, and that afterwards $\nu_{eff}/(W/nT)$ becomes constant, indicating stochastic heating. The decay of ν_{eff} after the maximum is a common feature of all 2D runs. It is roughly consistent with the following scaling:

$$\nu_{eff}/\omega_{pe} \propto \frac{v_d - \alpha c_s}{v_{the}}, \quad \alpha \sim 2 .$$

Thus we find that the gross features of the development of the instability in 2D may be described as an ion-sound instability with electron runaway prevented by gyration. The strong trapped electron heating seems to be an artefact of the 1D system. Nevertheless 1D simulations are useful, since

they may give upper or lower bounds of certain quantities which cannot be studied in 2D because of computer limitations. Thus, for example, the fact that in 1D where magnetic effects are strongest, v_{ds} is found independent of B, suggest that this will also be the case in higher dimensions.

It seems that computer simulations have clarified the somewhat confused theoretical situation. However, they can not fully explain Keilhacker's experiments. It appears that to understand these high-β shock waves, additional measurements of the local drift velocity especially at the upstream edge, of possible magnetic oscillations, and of the full ion distribution are required.

After describing the simulation results on turbulent resistivity especially in collisionless shock waves, we briefly discuss some results about the global structure of magnetic shock waves in the high Mach number range. Here the mechanism of ion dissipation has been a major theoretical problem. The question is: are there strong (electrostatic) beam instabilities between the reflected ions and the upstream plasma or is ion thermalization due only to gyration effects. To investigate this point one first omits the magnetic force on the ions. In the case of shock waves propagating perpendicularly to the magnetic field one finds that there is no beam interaction[13], Fig.5a. In the case of a wave propagating obliquely with respect to B, the whistler precursor can trigger a nonlinear ion beam instability which leads to rapid ion thermalization Fig.5b. In addition electrostatic subshocks are formed giving rise to microturbulence which strongly enhances dissipation. These computations have been performed with a two-species code including all electrostatic and electromagnetic length and time scales[14].

Finally we briefly touch recent developments in simulation of electromagnetic properties of plasmas including radiation. An electromagnetic code has to deal with a specific noise problem which does not arise in electrostatic codes. Since in most cases of interest the radiation energy is much smaller than the thermal energy, the plasma is in strong non-equilibrium with the radiation field and collisions will tend to gradually build up radiation by bremsstrahlung. This means that the thermal noise excited by collisions is not constant but increases linearily with time. To reduce this noise production is an important problem. Examples of good electromagnetic codes were given by Morse and Nielson[15] and Boris[16]. Interesting results have been obtained

for instance by Morse and Nielson in the 2D simulation of the Weibel instability[15] and in describing the heating of the edge of a plasma pellet by laser radiation. In the latter case strong collisionless absorption was observed, leading to very high energy tails in the electron distribution, a somewhat undesirable feature in the present laser fusion concept.

In conclusion we would like to say that computer simulations have provided considerable insight into basic collective and collisional processes in plasmas. They have enriched theoretical understanding by proceeding into strongly nonlinear regimes where standard analytical methods are mostly inadequate. Topics not mentioned here, where computer simulations are and will be very useful are problems of r.f.heating of plasmas and microinstabilities in toroidal plasmas.

References

1) C.K.Birdsall and D.Fuss, J.Compt.Phys.3, 494 (1969)

2) R.L.Morse and C.W.Nielson,Phys.Fluids 12, 2418 (1969)

3) H.Okuda and C.K.Birdsall, Phys.Fluids 13, 2123 (1970)

4) H.Okuda and J.M.Dawson, Phys.Rev.Lett. 28, 1625(1972)

5) J.P.Boris,J.M.Dawson,J.H.Orens, and K.V.Roberts,Phys.Rev.Lett.25,706(1970)

6) R.L.Morse and C.W.Nielson Phys.Rev.Lett. 26, 3 (1971)

7) D.Biskamp and R.Chodura, Phys.Rev.Lett.27, 1553 (1971)

8) D.Biskamp, K.U.v.Hagenow, and H.Welter, Phys.Lett. 5A, 351 (1972)

9) M.Keilhacker and K.H.Steuer, Phys.Rev.Lett. 26, 694 (1971)

10) M.Lampe, W.M.Manheimer, J.B.McBride, J.H.Orens, K.Papadopoulos, R.Shanny, and R.N.Sudan, Phys.Fluids 15, 662 (1972)

11) D.W.Forslund, R.L.Morse, C.W.Nielson and J.Fu, Physics Fluids 15, 1303 (1972)

12) R.Z.Sagdeev, Proc.Symp.Appl.Math., N.Y. 1965

13) see e.g. D.Biskamp and H.Welter, Nucl.Fusion 12, Nr. 4

14) D.Biskamp and H.Welter, Phys.Rev.Lett. 28, 410 (1972)

15) R.L.Morse and C.W.Nielson, Phys.Fluids 14, 830 (1971)

16) J.P.Boris, Proc.fourth Conf.Num.Sim.Plasmas, Naval Research Inst. 1970

Figure Captions

Fig. 1 Coulomb cross section for finite size particles in 2D and 3D, taken from Ref.3

Fig. 2 Critical drift velocity for $j \perp B$ instability in 1D, as obtained from simulations. The critical velocity for two-stream instability is given for comparison.

Fig. 3 Computer run of the $j \perp B$ instability in 1D: $m_i/m_e=1600$, $v_d/v_{theo}=1$, $T_{eo}/T_{io} = 2$. The drift velocity v_d is kept constant during the computatuion. $W \equiv \langle \tilde{E}^2 \rangle / 8\pi$. $\Omega_{ce}/\omega_{pe} = 0.04$.

Fig. 4 Computer run of the $j \perp B$ instability in 2D: $m_i/m_e=1600$, $v_d/v_{theo}=1$, $T_{eo}/T_{io}=50$, $\Omega_{ce}/\omega_{pe} = 0.04$.

Fig. 5 Magnetic collisionless shock waves, propagating from right to left. The ions are not magnetized. Plots of ion phase space, total magnetic field and electric potential. a) Perpendicular propagation; b) oblique propagation $\theta = 45^{\circ}$.

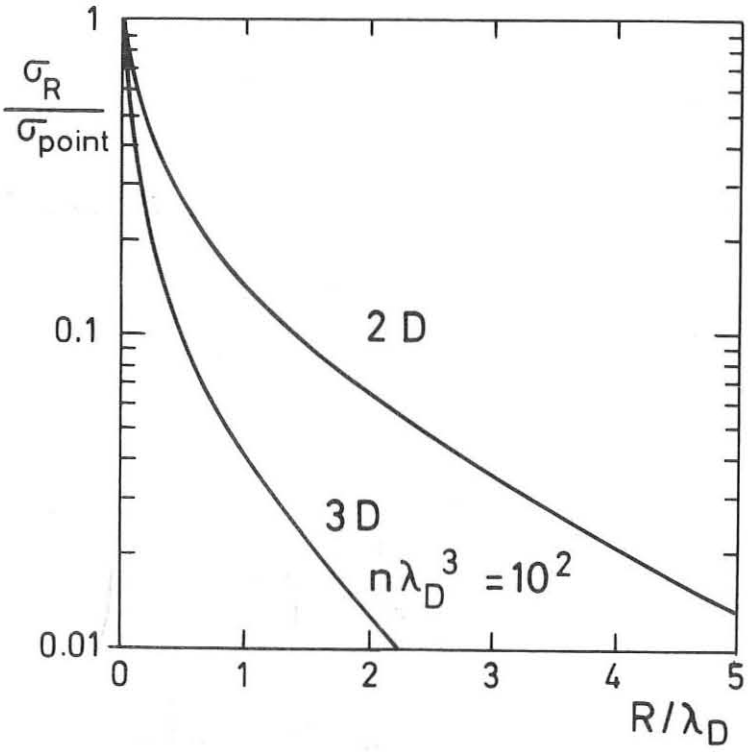

COULOMB CROSS SECTION FOR 2- AND 3-DIM. FINITE SIZE PARTICLES.

Fig.1

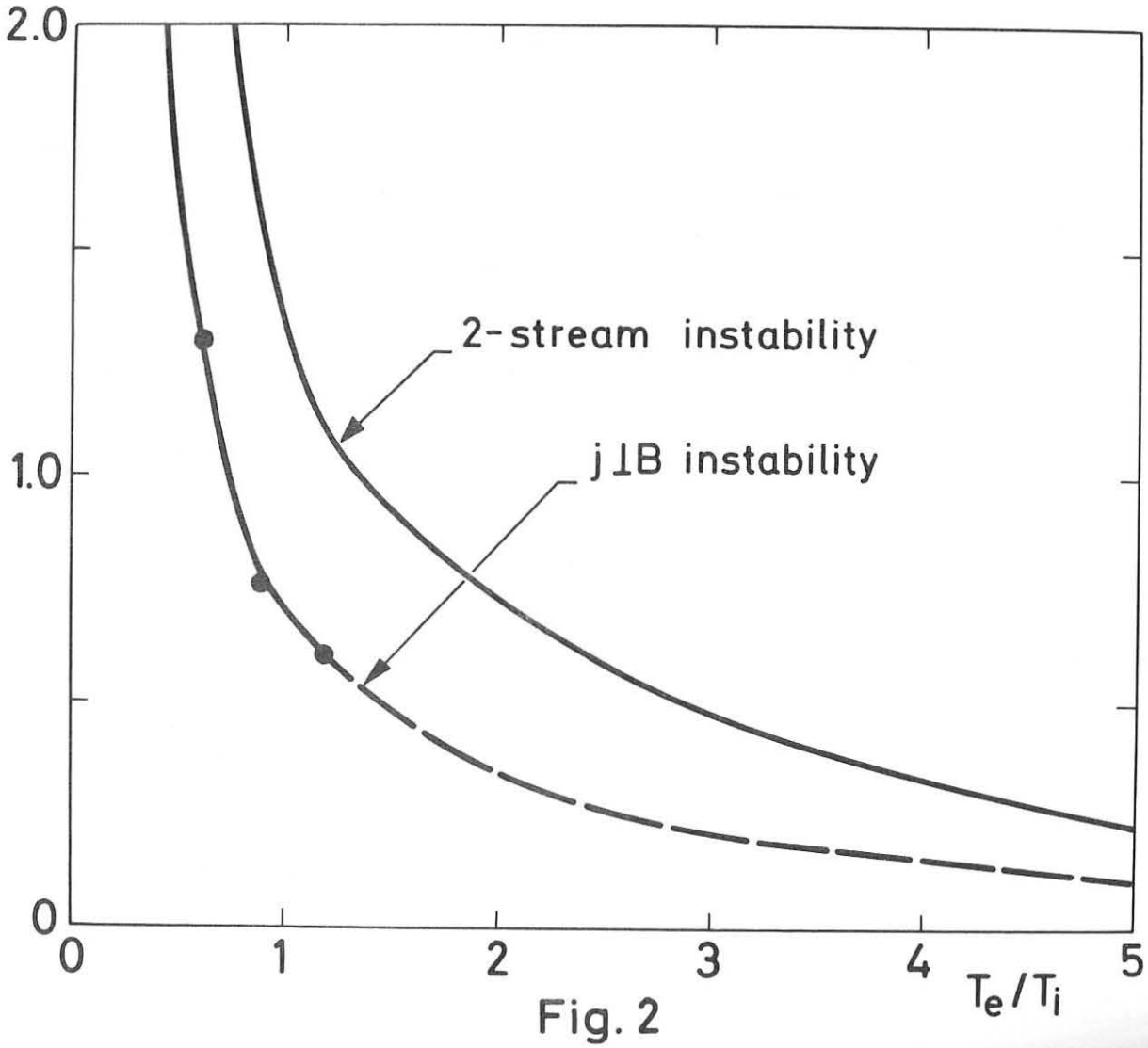

Fig. 2

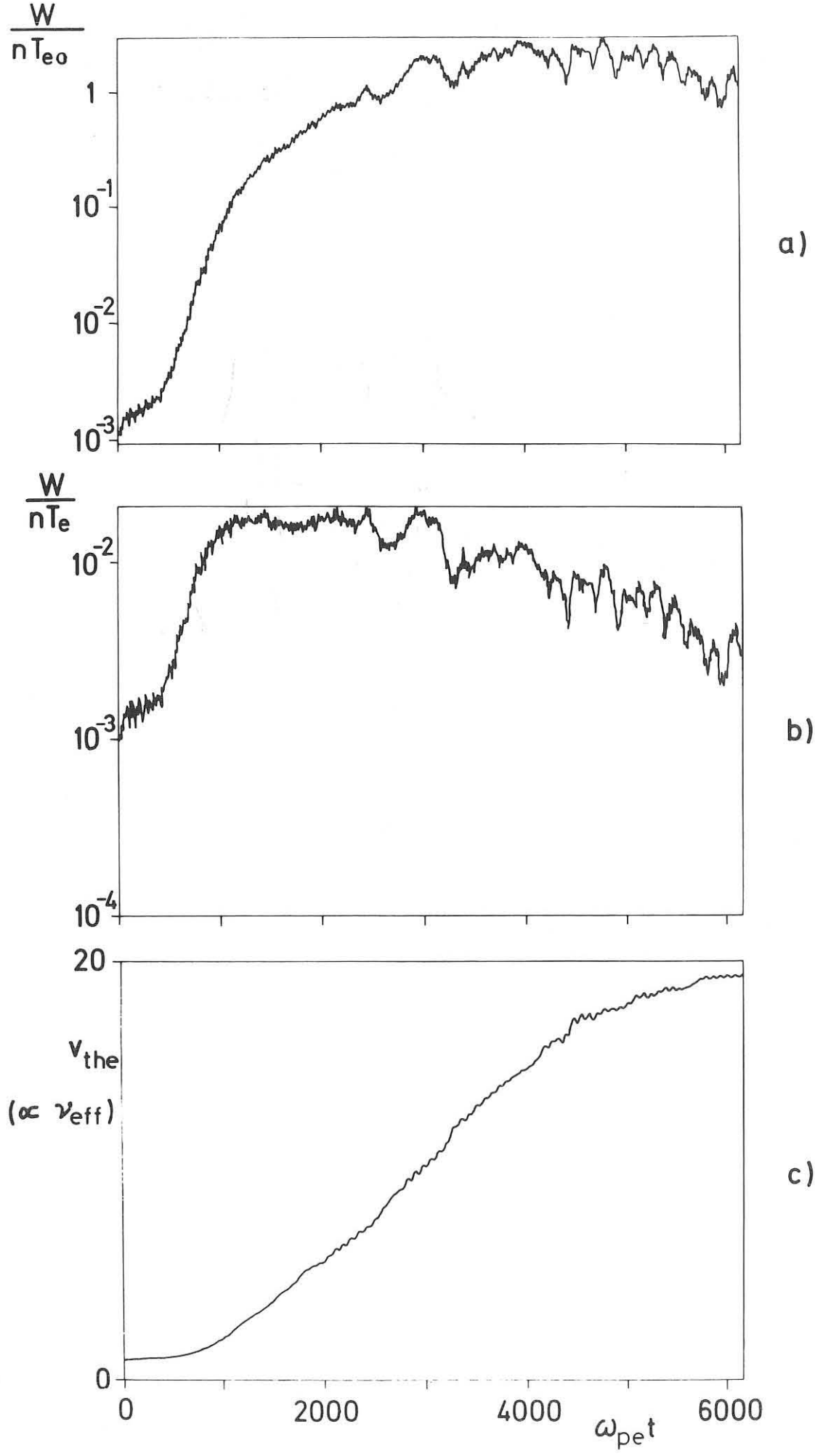
W / nTeo
1
10^-1
10^-2
10^-3
a)
W / nTe
10^-2
10^-3
10^-4
b)
20
vthe
(∝ νeff)
0
c)
0
2000
4000
6000
ωpet

Fig. 3

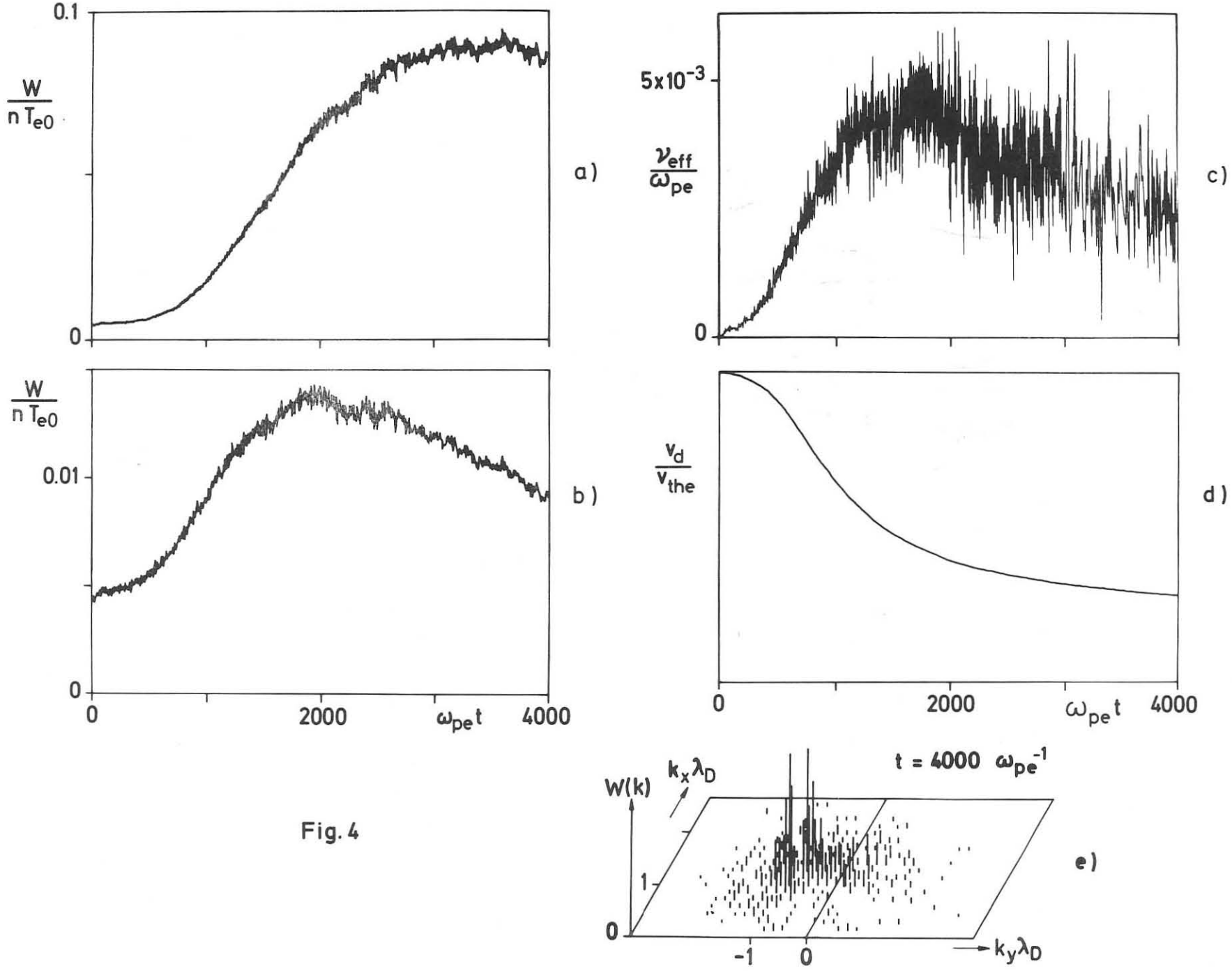
0.1
W / n T_e0
0
a)
W / n T_e0
0.01
0
0
2000
ω_pe t
4000
b)
5x10^-3
ν_eff / ω_pe
0
c)
v_d / v_the
0
2000
ω_pe t
4000
d)
t = 4000 ω_pe^-1
W(k)
k_x λ_D
1
0
-1
0
k_y λ_D
e)

Fig. 4

a) Perpendicular propagation

b) Oblique propagation $\Theta = 45°$

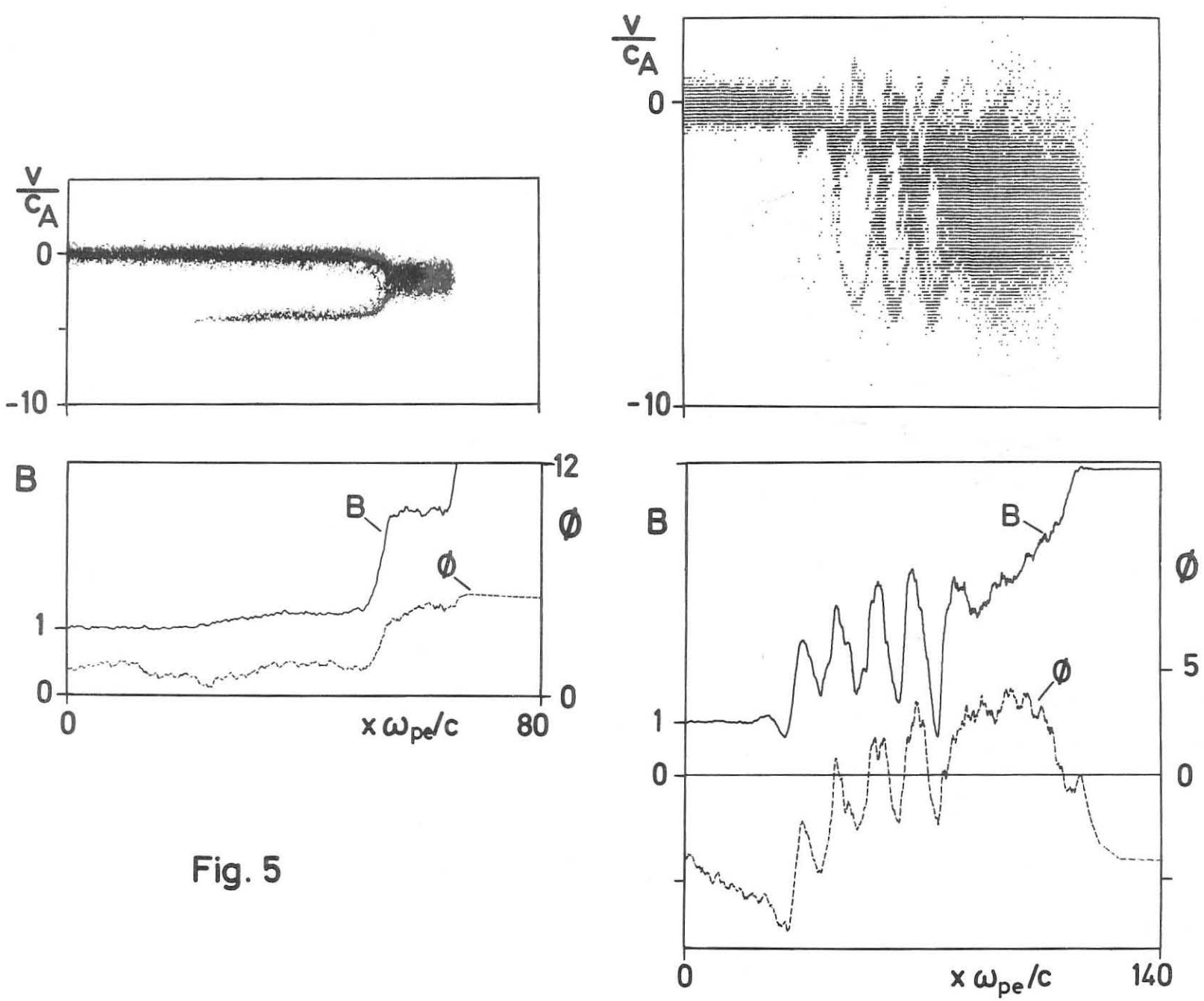

Fig. 5

ANOMALOUS RESISTIVITY IN PLASMA

R. Z. SAGDEEV*

Ecole d'Eté de Physique Spatiale
Lannion - 1972.
(Université de Rennes - Centre National d'Etudes Spatiales)

ABSTRACT

The critical discussion of present state understanding of anomalous resistivity problem is given. Different types of instabilities, invoked in the problem, and their non-linear saturation are considered.

* On leave from USSR Academy of Sciences, Moscow.

I - INTRODUCTION.

(List of essential instabilities - Conservation equations for particle-wave interaction).

An anomalcus resistivity appears, when the electric current in plasma exeeds some critical value : $j > j_c$. The rise of anomaly can be interpreted as a result of some of instabilities, leading to an additional loss of momenta by electrons due to the coherent radiation of appropriate waves(1).In the table I the list of different plasma instabilities is given, whose participation in anomalous resistivity is suspected. It is completely adequate to the problem to divide all possible cases into two groups :

I - D.C. currents

II - A.C. currents

As it is seen from the table I, D.C. currents instabilities also can be generated in A.C. situation, if characteristic time scale for an appropriate instability is much smaller, then A.C. period. But besides them in A.C. situation another instabilities should be considered.

You can see here all familiar instabilities. Buneman instability is essential only for very high relative drift of electrons through ions $\bar{V} \gtrsim v_{th}^{e}$, and is believed to evolve eventually into ion-acoustic one. This last one represents the object of the most intense and hard attack by experimentalists and theorists.

Magnetic field usually ($\omega_H < \omega_p$) does not change these modes significantly, but brings new modes. As an old example, the Drummond-Rosenbluth mode could be mentioned (2). It is comparitively slow growing mode and, probably, is easy saturated by simple quasilinear plateau effect. In contrast to this instability, inherent to the currents along $\vec{H}_o$, the so called modified Buneman instability is dr ven by perpendicular current (3).

This mode allows also generalisation to kinetic resonant type (4) and dissipative one. The latter is believed to play an important role in ionospheric phenomenas. These instabilities have very small growth rate, but also a low threshold $\underline{j}_c$.

As a last example of D.C. current instabilities we have to discuss current driven Bernstein modes. These modes are driven with very high growth rate by perpendicular currents. But the net result of it does not look very impressive, probably because of quite sensitive resonant features ($\omega \simeq n\omega_M$).

A.C. currents in addition to all already mentioned instabilities can generate specific modes, inherent to regular periodicity in driving current. These are so called "oscillating beam" instabilities with considerably high thresholds, and parametric instabilities with surprisingly low thresholds and therefore with more importance.

Most of these instabilities, though having different origin, lead to quite general formulas for their net effect on anomalous resistivity, based on momenta and energy exchanges between electrons and waves.

It is convenient to start with definition of electric conductivity :

$$\sigma = \frac{Ne^2}{m\nu}$$

where ν - collision frequency of electrons in respect to the loss of momenta. In unstable situation, when electrons generate the waves, an anomalous transfer of momenta is taking place (i.e. to collective modes, involving ions, from electrons). To get an impression of $\underline{\nu}_{eff}$ is sufficient to apply the conservation of net momenta of a system, containing electrons and waves (5,6). In the case of D C. current this momenta eventually goes to ions. So it is reasonable to leave the discussion of at least some A.C. situations for the last moment . The loss of momenta per unit time is :

$$m N \bar{V} \nu_{eff} = - F \qquad (1a)$$

where F - collective drag force due to waves. If waves with spectral energy density W_k are generated, F is proportional to :

$$F = \int \gamma_k^e W_k \frac{K_j}{\omega_k} \frac{d^3K}{(2\pi)^3} \qquad (1b)$$

here γ_k^e - the contribution of electrons to imaginary part of frequency, K_j - projection of wave vector on j (electric current). Thus we have (5,6) :

$$\nu_{eff} = \frac{1}{m N \bar{V}} \int \gamma_k^e W_k \frac{K_j}{\omega_k} \frac{d^3K}{(2\pi)^3} \qquad (2)$$

If we would have in mind that γ_k^e should be understood in quasilinear sense, the whole problem is reduced to the finding of waves spectra $\underline{\underline{W}}_k$. The formula (2) can be derived also from the quasilinear theory.

If plasma resistivity is anomalous, the Joule's heating of plasma is anomalous :

$$Q = \frac{j^2}{\sigma_{an}}$$

Such a heating (which often is called "turbulent") would heat the plasma species (ions and electrons) at different rate, generally speaking. As a rule, the electrons are heated faster then ions. We can see why, using following arguments. The power of friction force is an energy, dissipated in plasma per 1 sec.

$$Q = \bar{V} F = m N \bar{V}^2 \nu_{eff} =$$

$$= \int \frac{d^3K}{(2\pi)^3} \gamma_k^e W_k \frac{(\bar{K}.\vec{\bar{V}})}{\omega_k} \qquad (3)$$

In a steady state, which is reached when nonlinear effects saturate instability, the momenta of waves (and therefore their energy) must be absorbed by ions. Hence in a state of nonlinear saturation ions would absorb the energy of waves at the same rate as electrons would generate it :

$$\sim 2 \int \gamma_k^e W_k \frac{d^3K}{(2\pi)^3}$$

As a result the rate of ions heating is :

$$\frac{d\varepsilon_i}{dt} \sim \int \gamma_k^e W_k \frac{d^3K}{(2\pi)^3} \qquad (4)$$

Now from equations (3) and (4) we obtain :

$$\frac{d(\varepsilon_e+\varepsilon_i)}{d\varepsilon_i} \quad \frac{\int \gamma_k^e W_k \frac{(K.\bar{V})}{k} d^3K}{\int \gamma_k^e W_k d^3K} \qquad (5)$$

(there we used $Q = \frac{d(\varepsilon_e+\varepsilon_i)}{dt}$). For an estimation by the order of magnitude is sufficient to put :

$$\int \gamma_k^e W_k \quad \frac{(K.\bar{V})}{\omega_k} d^3K \sim \frac{<K>\cdot\bar{V}}{<\omega_k>} > \int \gamma_k^e W_k d^3K \qquad (6)$$

where $<K>$, $<\omega_k>$ - average wave number and frequency, representative of the spectra. Thus we have :

$$\frac{d\varepsilon_e}{d\varepsilon_i} \simeq \frac{\bar{V}.K}{\omega} - 1 \qquad (7)$$

This formula, as it written here, does not depend on specification of unstable mode, and therefore has universal character. For a majority of modes eq. (7) indeed leads to a predominant heating of electrons, since $\frac{\bar{V}}{\omega/_k}$ usually >> 1 (Buneman, or ion acoustic, for example).

For this latter examples time expression (2) can be reduced to a more conclusive form. The main contribution ot integral in (2) comes from wave numbers, corresponding to the highest growth rate, so $K \lesssim r_D^{-1}$.

Substituting $\gamma_k^e \simeq \omega_p \frac{\bar{V}}{V_T}$,

we obtain :

$$\nu_{eff} \simeq \omega_p \frac{\bar{W}}{NT_e} \qquad (8)$$

Similar estimate is often used, when quick answer is needed.

In conclusion of this chapter we can stress again, that the main problem is in finding $\underset{\sim}{W}$.

II - THE STATUS OF ION ACOUSTIC TURBULENT RESISTIVITY

Ion wave turbulence was especially promising, since it can be qualified as a weak turbulence. But after a decade we are still far from complete understanding. At the limit of sufficiently high electric fields instability can not be saturated by quasilinear effects and nonlinear mode-mode coupling should be taken into account. B. Kadomtsev in a wellknown work (1). considered induced scattering of ion waves on ions ($\omega_1 - \omega_2 \simeq |K_1 - K_2| . V_i$) as a dominant mechanism of nonlinear saturation. Kadomtsev's spectra

$$W \sim K^{-3} \ln K \qquad (9)$$

represents approximate solution for low wave numbers $Kr_D << 1$. Therefore we must confess, that an enthusiasm of some authors, who claim to confirm spectra (9) at $Kr_D \sim 0.5$, is too naive. The spectra (9) results in an often cited formula for anomalous resistivity

$$\nu_{eff} \quad 10^{-2} \Omega_p \frac{\bar{V}}{C_s} \frac{T_e}{T_i} \qquad (10)$$

But still it has to be confirmed by experiments, where $\frac{\bar{V}}{C_s}$ and $\frac{T_e}{T_i}$ dependences would be deciphered.

The full energy in spectra (9) $\int W_K \, d^3K$ is divergent as $\log \underset{\sim}{K}_{min}$ and needs in cut off at small $\underset{\sim}{K}$. However, momentum loss (equation (2) for ν_{eff}) is convergent. So we should'nt worry about this unprincipal divergence.

Induced scattering on ions, of course, goes with small factor $\sim \frac{T_i}{T_e}$, since it has to do with ions thermal motion. Therefore some investigators made an attempt to find a stronger nonlinear saturation effects.

Making routine weak turbulence expansion some authors have got a very strong nonlinear effect in electron contribution (essentially for the beats $\omega_1 + \omega_2 \simeq (K_1 + K_2)V_e$). Nonlinear saturation level for $\bar{W}$ due to this mechanism would be almost $\frac{m}{M}$ times smaller. But detailed analysis has shown that such electron resonances do not play a role because of nonlinear broadening (7).
So this question is completely settled now.

All mentioned above about ion sound relates to sufficiently high electric fields

$$E >> 10^{-2} \frac{(m M^3)^{1/4}}{e} \Omega_p C_s ,$$

when $\gamma_k^e >> \gamma_k^i$ (linear damping by ions).

If it is not so, electric field is not strong enough to drive electrons up to high $\bar{V}$, so that γ_k^i would be insignificant. Moreover we could expect an opposite situation with electrons $\bar{V}$ almost at the threshold of instability. Such a case was considered in a number of papers (8) . The most complicate question lies in the great sensitiveness of threshold $\bar{V}_c$ on the form of distribution function for resonant ions, so to speak, from the far tail of ion distribution. Even if it was given at t = 0 and was, for example, maxwellian, it would be completely distorted after a while, because only a small fraction (resonant ions) would interact with waves. So the main difficult point is to know the evolution of ions distribution. Two approaches were tried till now. One is by reporter and coauthors (8) . They used an intuitive idea, that long-time behaviour of plasma in a regime of anomalous conductivity would lead to an establishing of self-similarity, for example, in a shape of distribution function. $(\frac{m}{M})^{1/4}$ amount of ions in this case were always resonant getting thermal energy $\sim T_e$ and keeping threshold on $\bar{V} \sim C_s (\frac{M}{m})^{1/4}$. Data on resistive collisionless shock fine structure ⊥H are in preliminary agreement with this results. In numerical simulation works (14) the nonlinear trapping of ions by waves was reported to give a

a saturation for ion sound instability. I think it is essentially similar phenomena, besides the fact, that more harmonics are needed in numerical plasmas to get an overlapping of ions trapped by different waves.

Thus, more work is needed in interaction of ions with ions sound turbulence

One of the most crucial problems in anomalous resistivity is an electron interaction with ion sound waves. Velocity dependence $\sim \frac{1}{V^3}$ of electrons scattering on ion waves remind the situation with Lorenz gas, with the electrons eventually going to "runaway" . Would it lead to eventual increase of V ? Of course it is not related to the currents H. But for the currents to the very strong magnetic field it is certainly the big problem. Yet is was impossible to avoid runaway in a theoretical model without speculations about new modes of instabilities or "macroparticles" (bunches) . Of course in many real experimental situations, this runaway may not be reached because of finitness of time, or due to the predominant loss of runaway electrons.

III - MAGNETIC D.C. CURRENT MODES

Modified Buneman instability is described by dispersion equation :

$$1 + \frac{\omega_p^2}{\omega_n^2} - \frac{\Omega_p^2}{\omega^2} - \frac{\omega_p^2 K^2 / K^2}{(\omega - K.V)^2 - K^2 V_{T_e}^2} = 0 \qquad (11)$$

It gives the growth rate :

$$\gamma \sim (\omega_H \Omega_H)^{1/2} \qquad (12)$$

at $Kr_H \sim 1$, $K \sim K \frac{V}{V_{T_e}}$

The formula (7) has a meaning if $V >> V_{T_i}$. The opposite limit is often called "an electron sound". If $\omega_p >> \omega_H$ the corresponding to it growth rate is :

$$\gamma \sim \frac{\omega}{|K| V_{T_i}} (\omega - KV) \qquad (13)$$

Both limiting cases lead to a much smaller growth rate then ion sound instability. Therefore they may contribute to ν_{eff} , generally speaking, only if ion sound turbulence is absent. Instabilities (12) and (13) cannot be qualified as leading to weak turbulence. So it is difficult to expect to get more then rough estimation of corresponding ν_{eff} (strong turbulence type estimate). As usual we will put in nonlinear saturation regime typical linear and nonlinear terms in appropriate equations for the problem. Modified Buneman mode is described in fluid model. Therefore, let us compare $\frac{\partial V}{\partial t}$ and $(V\nabla)V$ in equation for electron fluid (6)

We obtain :

$$KV \sim \frac{KC}{H_o} \Sigma \phi$$

or

$$\sum_k \frac{N_e^2 |\phi_k|^2}{2T_e} \sim m N V^2 \quad (Kr_{H_e} \sim 1) \qquad (14)$$

But equation (14) gives the estimate for energy in turbulence, and with the use of equation (2) we are getting (6)

$$\nu_{eff} \sim \omega_H \frac{V}{v_T} \qquad (15)$$

From the expression (7) we can also obtain the ratio of electron to ion heating

$$\frac{T_e}{T_i} \sim \frac{\overline{V}}{V_{T_i}}$$

The last example of D.C current instabilities is current driven Bernstein mode instability.

High frequency electron oscillations $\omega \sim l\omega_H$ ($K \perp H_o$) are seen by ions as $\omega' = l\omega_H - KV \sim \Omega_p$ and hence represent mixed electron-ion modes.

Growth rate is quite high :

$$\gamma \sim \omega_H \frac{V}{V_{T_e}} \quad ,$$

but . small nonlinearity, developing as result of an instability is sufficient to smear out Bernstein resonances. So the net result is small (9)

$$\nu_{eff} \lesssim \omega_H \left(\frac{V}{V_{T_e}}\right)^3$$

I do not believe that such a resistivity was already observed.

IV - A.C. CURRENT INSTABILITIES

As it was mentioned any D.C. current mode could in principle be excited by A.C. current. Besides $V > V_c$ it is necessary to fullfill the condition :

$$\gamma >> \frac{1}{T} \qquad (16)$$

where γ - D.C. growth rate, T - A.C. period. In the right side of (16) in fact, enters a factor, accounting for initial fluctuation amplitude (noise). If there was thermal equilibria at $t = 0$, this factor may be the same order of magnitude as Coulomb Log.

Specific oscillatory instabilities are representing the eigenmodes for plasma with A.C. current. So they don't need such criterid . The most important class of such eigenmodes is parametric instabilities. Suppose in plasma there is A.C. electric field :

$$E_o \sin(\omega_o t - K_o r) \quad ,$$

which we would relate to so called "pump wave". Plasma as an any wave media can be considered as an ansamble of oscillators-waves.

Nonlinearity of plasma equations couples this waves to a "pump" in a parametric way. The situation is analogous to a parametrically coupled system of oscillatory in classical mechanics. This analogy leads to Mathieau-type zones in the frequency-amplitude (of pump wave) plane (6).

Condition of parametric instability is resonance (1st zone)

$$\omega_o = \omega_1 + \omega_2 \qquad (17)$$

$$K_o = K_1 + K_2 \qquad (18)$$

$$(|\omega_o| > |\omega_1|, |\omega_2|)$$

between "pump" wave and perturbation waves ω_1 and ω_2, is similar to kinematics of decay processes. This is why in original paper it was called "decay" instability (10). This width of the Mathieau zones

$$\Delta\omega = \omega_o - \omega_1 - \omega_2$$

(γ - growth rate of instability).

The first example of such an instability was a decay of "pump" wave with $\omega \gtrsim \omega_p$ into ω_1 - electron plasma wave + ω_2 - ion acoustic wave. Corresponding growth rate is (10, 1) :

$$\gamma \sim \Omega_p \left(\frac{\omega p}{KC_s}\right)^{1/2} \frac{V\sim}{V_{T_e}}$$

where $V\sim = \dfrac{eE_o}{m\omega_o}$

When E_o is becoming comparable or greater then $\sim$

$$\frac{m\,\omega_o\,V_{T_e}}{e}\left(\frac{m}{M}\right)^{1/4}$$

the width of the main Mathieau zone is becoming $> \omega_2$, so another approach is needed (11). The parametric instability has a threshold, if ω_1 and ω_2 have a damping. It is seen from expression for growth

rate (12)

$$\gamma = \frac{\nu_e}{2} \left(\frac{\omega_p \omega_s}{2\nu_e \nu_s} \frac{|E_o|^2}{4\pi N T_e} - 1 \right) \qquad (19)$$

(ν_e - damping in ω_1 , ν_s - in ω_2)

This formula from linear theory of instability could help with a quick answer to the question of ν_{eff} , which would be a result of instability on "pump wave". Namely, we could expect that in nonlinear saturation state ν_{eff} of electrons is elevated up to such a level, that

$$\gamma \sim \left(\frac{\omega_p \omega_s}{2\nu_{eff} \nu_s} \right) \frac{|E_o|^2}{4\pi N T_e} - 1 \Big) = 0$$

it gives :

$$\nu_{eff} \simeq \frac{\omega_p \omega_s}{2\nu_s} \frac{|E_o|^2}{4\pi N T_e} \qquad (13) \qquad (20)$$

This is not a bad approximation for an early age of nonlinear theory of parametric instabilities.

This paper could not pretend to give a comprehensive list of references, since it was prepared for an oral presentation. Moreover, a few referred articles contain most of necessary references.

In conclusion I would like to acknowledge the hospitality of Prof. F. CAMBOU, the Director of Lannion Summer School on Cosmic Physics, where this paper was written.

TABLE 1

-=-=-=-

List of plasma instabilities, involved in anomalous resistivity

I - D.C. CURRENT INSTABILITIES

Type of instability	Its threshold	Frequency range	Growth rate
Buneman instability	$\bar{V} > V_{Te}$	$\gtrsim \Omega_p$	$\gtrsim \Omega_p$
Ion acoustic	$\bar{V} > C_s$ $(T_e >> T_i)$	$\lesssim \Omega_p$	$\lesssim \Omega_p \frac{\bar{V}}{V_{Te}}$
Drummond- - Rosenbluth	$\bar{V} > C_s$	$\sim \Omega_H$	$\sim \Omega_H \frac{\bar{V}}{V_{Te}}$
Modified Buneman inst.	$\sim T_i$	$<< \omega_H$	$\sqrt{\omega_H \Omega_H}$
Bernstein modes	$\bar{V} > V_{Ti}$	$\ell\omega_H$	$\sim \omega_H \frac{\bar{V}}{V_{Te}}$

II - A.C. CURRENT INSTABILITIES

Any D.C. mode, if $\gamma >> \frac{1}{T}$			
Oscillating beam type	$\bar{V}_\sim > V_{Te}$		
Parametric instabilities	Depends on damping	$\omega_o \longrightarrow \omega_1 + \omega_2$	$\sim \lvert V \rvert$ V - matrix element for 3-wave coupling

REFERENCES

(1) B. KADOMTSEV - Plasma Turbulence - 1964.

(2) W. DRUMMOND, M. ROSENBLUTH - Phys. Fluids, 5, 1507 (1962).

(3) O. BUNEMAN - J. Nucl. Energy, c4, 111 (1962).

(4) V. SIZONENKO, K. STEPANOV - Nucl. Fusion, 7, 131 (1967).

(5) R. SAGDEEV - Proceed. of Symp. Appl. Math., vol 18, 281 (1967).

(6) R. SAGDEEV, A. GALEEV - TRIESTE LECTURES, PREPRINT, 1968.

(7) V. TZYTOVICH, L. RUDAKOV, Plasma Phys., 13, 213 (1971).

(8) G. VEKSTEIN, R. SAGDEEV, D. RYTOV - MADISON Paper, 1971.

(9) D. LOMINADZE - Gordon Conference on Plasma Physics, 1972.

(10) V. ORAEVSKY, R. SAGDEEV - JTP, 32, 1291 (1962).

(11) V. SILIN - JETP, 48, 1679 (1965).

(12) K. NISHIKAWA - J. Phys. Soc. Jap., 24, 916, 1152 (1968).

(13) J.E. VALEO, C. OBERMAN, F. PERKINS - Phys. Rev. Lett., 28, 340 (1972).

(14) D. BISCAMP - Invited Paper at this Conference.

PROPERTIES OF SOME TYPES OF PLASMA SHOCK WAVES

E. Hintz

Institut für Plasmaphysik der Kernforschungsanlage Jülich GmbH
Assoziation EURATOM-KFA, Jülich, Germany

Abstract:

Shock relations for strong mhd-shock waves are summarized. Generation of such shocks in the laboratory and their utilization for plasma heating is discussed. Some results of experimental studies on plasma heating by fast magnetic compression are reported. The present status of theory with regard to the steady state structure of plasma shock waves is described for two special cases: a) collision-dominated shocks in a magnetic-field-free plasma, b) shocks in a plasma with $\beta << 1$ and $\omega_{ce} \tau_{ei} >> 1$. Experimental results on shock structures are compared with theory. The significance of these studies for the understanding of dissipative processes in thermal and nonthermal plasmas is examined.

I. Introduction:

Plasma shock waves have been studied in order to improve our basic understanding of physics and because there are important practical applications. In this talk we shall direct our attention to both aspects but in particular to the latter one. Shock waves have been used to compress and to heat plasmas mainly in the various linear pinch experiments. Presently

several laboratories plan to use the existing knowledge and experience on shock waves for heating plasmas in high-ß-toroidal confinement experiments. What are the main questions?

Apart from the question what temperatures can be achieved, and how, one would like to know, in particular, what compression ratio, i.e. what ratio of final to initial density and what ß-value can be obtained; both the compression ratio and the ß-value are important for the equilibrium and the stability properties of the plasma. It is also of interest to know the development of these quantities as a function of time.

Knowing what in principle can be achieved by shock waves, the question arises under which conditions can the steady state shocks be realized, which are assumed to exist, when the shock relations are derived. For this to answer we need to know the shock structure, for example the width of the various shock layers out of which the shock transition consists and how the energy in the shocked gas is distributed among electrons and ions.

A study of the structure of plasma shocks is of great interest also from a basic physics point of view. It permits the investigation of dissipation and relaxation processes in plasmas which, depending on the shock strength, are removed from thermal equilibrium by a variable amount. At small shock strength, when shocks are laminar, we can examine the theory of transport coefficients; at larger shock strength when microturbulence may develop dissipation due to collective interaction, i.e. anomalous transport can be studied.

In this talk it is not possible to present a complete survey on the present state of knowledge on plasma shocks waves. Only three areas shall be discussed:

a) Heating and compression of low density, magnetic field free plasmas in Θ-pinches. This appears to be of great interest for high-ß-stellarators and for belt-pinches (low density means in this context that the mean free path of the imploding ions is of the order or larger than the radius). For these experiments it is probably not justified to assume that steady state shocks are formed. The free particle model seems to be better suited to describe plasma dynamics under these circumstances. We discuss these experiments under the topic of this talk since it has become customary to apply the term "shock heating".

b) Shocks in low-ß-plasma with $\omega_{ce} \cdot \tau_{ei} >> 1$ and the direction of propagation perpendicular to the magnetic field; for simplicity we call these shocks resistive shocks.

c) Collision-dominated shocks in magnetic-field free plasmas which we shall call viscous shocks. Viscous shocks might be of interest in dense plasmas, e.g. in plasma focus experiments and in laser induced plasmas.

II. Shock compression of plasmas in pinches

Let us first shortly review shock dynamics in pinches. In order to analyse the processes it is useful to make some simplifications. First of all, instead of assuming the standard circular geometry we consider an elongated rectangular or elliptical cross-section; this eliminates the cylindrical convergence problem. We can then approximate the temporal development of the plasma by a sequence of four steps, shown schematically in Fig. 1.

1. We start with a fully ionized plasma in thermal equilibrium.

2. By connecting a low inductance capacitor bank by means of switches to a cylindrical, single turn coil a magnetic field is switched on in the coil and an inward moving shock is generated. Pressure equilibrium exists between the pressure of the piston $B_p^2/8\pi$ and the pressure in the shocked plasma $n_2 kT_2 + B_2^2/8\pi$.

3. When the shock front arrives at the centre of the discharge tube, the shock is reflected; the reflected shock moves outwards bringing the plasma to rest, i.e. all flow energy is converted into thermal energy.

4. When the reflected shock encounters the piston, the plasma expands ($n_3\ kT_3 > B_p^2/8\pi$) until pressure equilibrium is reached again.

5. A phase of adiabatic compression usually follows, it shall not be discussed here.

For the following we assume the existence of steady state plane shocks; the driving magnetic field shall be constant in time. We consider only strong shocks, i.e. initial plasma pressure and magnetic field pressure are negligible compared to the pressure of the piston. One advantage of this approximation is that the existence of a magnetic field in the plasma is of no significance for the shock relations. Also - the shock relations get very simple.

The following symbols will be used:

n	=	particle density	β	=	$8\pi nK(T_e+T_i)/B^2$
B	=	magnetic field	T	=	temperature
u	=	flow velocity	K	=	Boltzmann constant
R	=	plasma radius	p	=	pressure
E	=	electric field	L	=	coil inductance
ω_{ce}	=	electron cyclotron frequency	J	=	electric current
ω_{pe}	=	electron plasma frequency	V	=	bank voltage

The subscripts e, i, p, 1, 2 ... 4 denote electrons, ions, the piston and the various states (1 ... 4) through which the plasma passes, respectively (see also Fig. 1). f is the number of translational degrees of freedom of the particles.

Shock relations:

1. Initial state:

   n_1, T_1, B_1

2. Inward moving shock:

$n_2/n_1 = u_1/u_2 = B_2/B_1 = f + 1; \qquad u_p = (f/f+1)u_1;$

$P_2 = (f/f+1)n_1 m_i \cdot u_1^2; \qquad m_i u_2^2 / 2 = (f/2)kT_2$

i.e. equipartition of energy takes place between flow energy and thermal energy ;

$\beta_2 = (2f/(f+1)^3) M_A^2; \quad (f = 3; \beta_2 = \frac{3}{32} M_A^2)$

3. Reflected shock:

$u_3/u_1 = 2/(f+1) \qquad n_3/n_2 = (f+2)/2$

$p_3/p_2 = f + 3 \qquad T_3/T_2 = 2(f+3)/(f+2)$

$\beta_3 = 4((f+3)/(f+2)^2)\beta_2$

$R_3/R_1 = 2/ (f+2) (f+1)$; this expression shows that at least collisional plasmas pass through a state of rather high compression.

4. Equilibrium phase after expansion:

Instead of assuming an adiabatic expansion, as sometimes is done, we let the plasma do mechanical work by displacing a constant magnetic field B.

From energy conservation:

$$n_3 R_3^2 (f/2) kT_3 = n_4 R_4^2 (f/2) kT_4 + (B^2/8\pi) (R_4^2-R_3^2)$$

$$\frac{T_4}{T_2} = \frac{2 \cdot f (f+1) (f+2) (f+3) + 8}{(f+1) (f+2)^3}$$

$$\frac{n_4}{n_1} = \frac{(f+1)^2 (f+2)^3}{2 \cdot f (f+1) (f+2) (f+3) + 8} \quad ; \quad (f = 3; \frac{n_4}{n_1} = 2.75)$$

The expressions for T_4/T_2 and n_4/n_1 become slightly modified if we assume that in state 3 or 4 the plasma always passes over into a two- or three-dimensional thermal equilibrium.

5. Adiabatic compression:

$$f = 2: \quad \frac{n_5}{n_4} = \frac{B_5}{B_p} ; \quad \frac{T_5}{T_4} = \frac{B_5}{B_p}$$

The following considerations refer only to theta pinches. For low inductance circuits it is appropriate to use an electrical circuit equation of the form $V = J \cdot dL/dt$; this can be transformed into $E_p = (1/c) \cdot u_p \cdot B_p$. Together with

$p_2 = B_p^2/8\pi = (f+1/f)\, n_1 m_i u_p^2$ one obtains:

$$u_p = (c\, E_p)^{1/2} \left((f+1)/f\right)^{-1/4} (8\pi n_1 m_i)^{-1/4}$$

Putting $f = \infty$ and $f = 1$ we obtain the well known snow plough and free particle model results, respectively.

III. Experimental studies of plasma heating in fast theta pinches

We shall now turn our attention to the results of some experimental investigations of the dynamic phase in low density, magnetic field free theta-pinches /1/, /2/, /3/. We are mainly interested in how the quantities T_i, $\gamma = \frac{n_2}{n_1}$, ß and T_e depend on the initial density n_1 and the applied azimuthal electric field E_p. The studies reported here were performed on a theta-pinch with a coil of 80 cm length and 40 cm diameter at initial electron densities between 10^{12} cm^{-3} and 10^{13} cm^{-3} and electric fields between 400 V/cm and 900 V/cm. The mean ion energy and the compression ratio were measured as function of n_1 and E_p at the instant of maximum compression, i.e. when $R = R_3$. Fig. 2 and Fig. 3 show results /2/. The measured ion energy W_i' - scales as expected with n_1 and E_p and agrees in magnitude with the values calculated by means of the free particle model, i.e.

f = 1. The compression ratio has a value $\eta \approx 10$, as expected. The ion energy was also measured at the time of maximum current when pressure equilibrium exists /3/. In this case a scaling $W_i \sim n^{-3/4}$ was observed, (Fig. 4), as one expects if the shock compression is followed by an adiabatic compression with f = 2.

Measurements indicated that the electron temperature is large in the current carrying sheath ($\simeq 1$ keV), while on the axis it is negligible compared to that of the ions ($\leq$ 50 eV); after a transit phase T_e seems to adjust itself in such a way that energy transfer from the hot ions is balanced by thermal conduction losses to the ends.

Under the given circumstances $\tilde{\beta}^+$ on the axis should be close to one if magnetic field diffusion would be normal. This is not the case. The high electron temperatures observed in the current sheath do already indicate that the electrical conductivity is anomalously low, probably as a result of current driven instabilities. Current understanding of turbulent resistivity suggests that the electron drift velocity must not exceed the ion sound velocity for the sheath to become stable, i.e. the width of the sheath should be of the order c/ω_{pi}. This was also confirmed by experiments. The condition for achieving high $\tilde{\beta}$-values is then $R_p > c/\omega_{pi}$, or

$$\left(\frac{c^2}{\omega_{pi}^2}\right) \cdot \pi \cdot n_{e1} \approx 3 \cdot 10^{15} \text{ cm}^{-1} = N_c < N = R^2 \pi n_{e1}.$$ Fig. 5

shows $\tilde{\beta}$ on the axis as a function of the line density N; one sees that $\tilde{\beta}$ decreases drastically as N drops below N_c.

IV. Shock structures

a) Resistive shocks

For small shock strength $\mathcal{E} = (u_1 - u_2)/2u_s$ a rather complete theory of the shock structure does exist /4/. An important result is that the plasma in general behaves as a single fluid; there is just one shock layer. Just as for a gas-

$^+\tilde{\beta}$ is defined using the external B-field

dynamic shock the profile is given by: $p - (p_2 + p_1)/2 = (p_2 - p_1)/2 \tanh(\xi \cdot x/L)$. In general L is a complicated function of plasma parameters $\omega_{ce}\,\tau_{ei}$, ß etc. However, in certain regions of parameter space just one dissipation mechanism prevails. For the parameter range discussed here $ß \ll 1$; $\omega_{ce}\,\tau_{ei} \gg 1$; the shock structure is determined by resistivity and $L \approx c^2/4\pi\sigma\, u_1 = (c^2/\omega_{pe}^2) \cdot \nu_{ei}/u_1$ where c is the velocity of light, σ the electrical conductivity and $\nu_{ei} = 1/\tau_{ei}$ the electron-ion-collision frequency. In Fig. 6 we show an observed magnetic field profile for a resistive shock with $\xi \approx 0.2$ and for comparison the tanh-profile; the agreement is quite good. In fig. 7 we have plotted the measured width $\Delta = L/\xi$ against $1/\xi$. One observes a linear dependence, as expected, and the slope of the straight line is in agreement with theory /5/ within the experimental errors (20 % in Δ, L; 15 % in $1/\xi$).

The physical processes occurring in resistive shocks are roughly as follows. The electron cyclotron radius is small compared to the shock width. As an electron enters the shock front the flow vector is turned around; the new direction of electron flow is approximately that of the current; i.e. perpendicular to the direction of the shock and that of the magnetic field. The ion cyclotron radius, at least for not too small ξ, is large compared to Δ; the ion trajectories are little influenced by the jump in B. As a result electrons and ions are separated; a space charge field builds up which decelerates the ions. If the plasma is cold ($ß \ll 1$) the only relative motion between particles which permits dissipation of flow energy is that between electrons and ions; the rate at which energy is dissipated accordingly is j^2/σ. Above a critical Alfven-Mach-number $M_{A,C} \approx 3$ /6/, resistive dissipation is no larger sufficient to provide the dissipation for the shock to exist and viscous dissipation is required.

With increasing $\mathcal{E}$ the drift velocity v_d increases ($v_d/v_{e,th} \approx \omega_{ce}\,\tau_{ei} \cdot \beta^{-1/2} \cdot \mathcal{E}^2$). Depending on the ß-value and the ratio of T_e/T_i and ω_{ce}/ω_{pe} one expects that the plasma state becomes unstable against one of the current-driven electrostatic instabilities. As a result of the instability, microturbulence develops. The amplitudes of the electrostatic fluctuations can become much larger than in thermal equilibrium and accordingly the effective electron-ion collision frequency may be strongly enhanced.

Writing the expression for ν_{ei} as follows:

$$\nu_{ei} \approx (n \cdot \lambda_D^3)^{-1} \cdot \omega_{pe} \cdot \ln(\text{const.} \cdot n \cdot \lambda_D^3)$$

we obtain with $\langle \tilde{E}^2 \rangle / 4\pi\, nkT_e = W$ and $W_{th} \sim 1/(n \cdot \lambda_D^3)$ for thermal plasmas:

$$\nu_{ei} \sim W_{th} \cdot \omega_{pe} \cdot \ln\left(\frac{\text{const}}{W_{th}}\right)$$

In case of ion sound turbulence one expects $\nu_{eff} \approx W \cdot \omega_{pe}$; this leads to the relation $\nu_{eff}/\nu_{ei} \sim W/W_{th}$.

Let us now consider some of the experimental results /1/. Fig. 8 shows density and magnetic field profiles and T_e ahead of and behind the shock front for a shock wave in deuterium at $M_A = 2.4$. T_e and n_e were determined by means of laser light scattering. In fig. 9 we present the measured intensity distributions of the scattered laser line ahead of and behind the shock, which are identical with the electron velocity distributions and from which the initial and the final temperature were derived.

For the given conditions the energy balance equation for the electrons can be written as

$$3/2\; n_1 u_1 k\; dT_e/dx = -nkT_e\; du/dx + j^2/\sigma$$

Assuming a linear increase of the electron temperature in the shock the measured B- and n_e-profiles suffice to calculate the data we need in order to evaluate δ from the above equation.

In the following table we have summarized some of the data characterizing the investigated shock front:

$\tau_s \cdot (\nu_{ei})_1$	ν_{eff}/ν_{ei}	$\omega_{ce}\tau_{eff}$	v_d/v_e	T_e/T_i	$n\lambda_D^3$
2	10^3	15	0.17	22	$5\cdot10^4$

Here τ_s is the rise time of the shock, v_d is the electron drift, v_e the electron thermal velocity, λ_D is the Debye-length.

From this data we can conclude: the shock is "collision-free"; the plasma is magnetized although the turbulent resistivity is three orders of magnitude larger than in a thermal plasma. The data are consistent with the assumption that the enhanced resistivity is the result of an ion sound turbulence. The observation that the measured T_e agrees with the value calculated from the shock relations indicates that only electrons are heated.

Further results on resistive shocks at different $\omega_{ce}\tau_{ei}$- and ß-values are presented in /7/. In these experiments ν_{eff}/ν_{ei} is varied by almost three orders of magnitude. We have compared the measured ν_{eff} with the predictions by Sagdeev /8/ ($\nu_S \approx 10^{-2} \left(\frac{T_e}{T_i}\right) \cdot \left(\frac{v_d}{v_e}\right) \cdot \omega_{pe}$) and Krall and Liewer /9/ ($\nu_{KL} \leq \frac{1}{2}\left(\frac{v_d}{v_e}\right) \frac{1}{\sqrt{2}} \left(\frac{\omega_{ce}}{\omega_{pe}}\right) \omega_{pe}$). The comparison is visualized in fig.10. Concerning the proposal by Sagdeev we find good agreement with respect to the scaling of ν_{eff}; this is confirmed by measurements reported by J. Paul (the data point marked with "Culham") /10/. There exists a discrepancy of about a factor of 10 with regard to the absolute magnitude of ν_{eff}. In contrast, the theoretical predictions by Krall and Liewer agree quite well with the measurements concerning

the magnitude of ν_{eff}, concerning the scaling the agreement is not as good.

Working at rather low electron densities it was not possible at Jülich with existing light sources to do cooperative scattering measurements and measure amplitude and spectrum of the enhanced density fluctuations. This was, however, done at Culham /11/ for low-ß, resistive shocks at higher electron densities.

Some important results shall be summarized here. The fluctuations are more than two orders of magnitude above the thermal level. The turbulence is strongly anisotropic: waves are observed only in directions lying within an angle of 50 degrees with the direction of the electric current. The k-spectrum has been measured within a certain range of k-values and does agree with the form of the spectrum calculated by Kadomtsev for ion sound turbulence. For a given k_o a scattered line is observed with a frequency shift ω_o such that the pair of values ω_o, k_o fits the ion wave dispersion relation. The measured effective collision frequency agrees quite well with that calculated by means of a stochastic theory using the measured fluctuation spectrum.

Although most of the existing evidence suggests that the observed turbulence is the result of ion-sound instabilities some observations cannot be explained by this proposition and it cannot be excluded that other types of instabilities /9/, /12/ are responsible for the observed enhanced resistivity.

b) Viscous shocks

We shall now discuss shocks in a collision-dominated plasma, containing no magnetic field and with the ion-ion mean free path large compared to the Debye length, but small compared to the spatial extension of the shock. The fluid consisting of two gases with strongly different masses which are closely coupled by the Coulomb forces, three transport processes are of interest for which the following characteristic length scales exist:

/1o/ J.W.M. Paul, C.C. Daughney, L.S. Holmes;
Collision-Free Shocks in the Laboratory and in Space,
Proc. Study Group, ESRIN, Frascati, Italy (1969),
ESRO Report SP 51, p. 2o7.

/11/ J.W.M. Paul, C.C. Daughney, L.S. Holmes, P.T. Rumsby,
A.D. Craig, E.L. Murray, D.D.R. Summers, J. Beaulieu;
Plasma Physics and Controlled Nuclear Fusion Research,
Proc. Conf. Madison 1971, paper CN-28/J-9, Vienna, IAEA 1971.

/12/ D. Forslund, R. Morse, C. Nielson;
Plasma Physics and Controlled Nuclear Fusion Research,
Proc. Conf. Madison 1971, paper CN-28/J-12, Vienna, IAEA 1971

/13/ M.Y. Jaffrin, F.R. Probstein;
Phys. Fluids 7, 1658 (1964).

/14/ Ya. B. Zel`dovich, Y.P. Raizer;
Physics of Shock Waves and High Temperature Hydrodynamic
Phenomena, Academic Press, New York 1967.

/15/ P. Bogen, K.H. Dippel, E. Hintz, F. Siemsen;
Proc. Xth Conf. on Phenomena in Ionized Gases, Oxford 1971.

/16/ P. Bogen, F. Siemsen;
private communication, to be published.

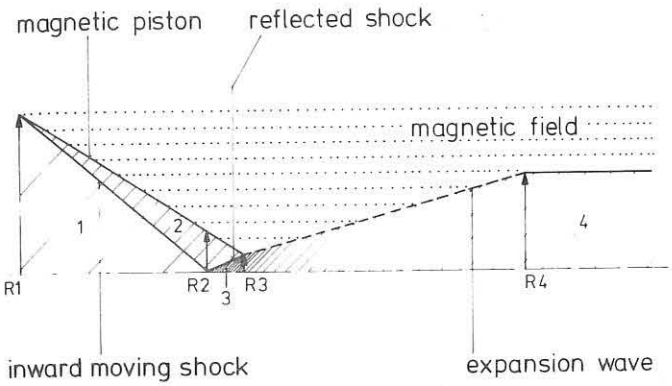

Fig. 1: Shock compression in pinches, schematic (for f=3)

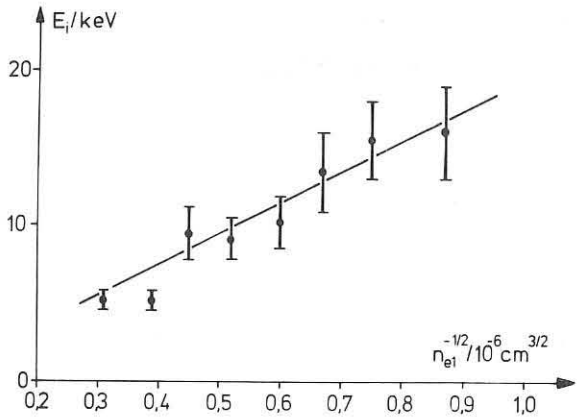

Fig. 2: Mean ion energy as function of initial density, U=8o kV, at the time of max. compression

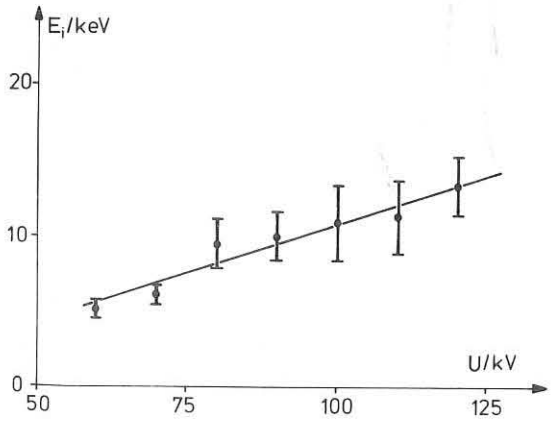

Fig. 3: Mean ion energy as function of voltage, $n_e=5\cdot10^{12}cm^{-3}$, at the time of max. compression

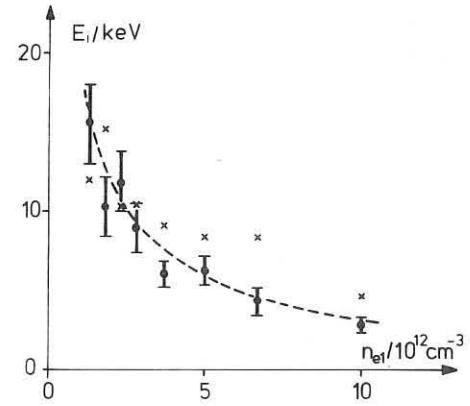

Fig. 4: Ion energy as function of initial density at the time of current maximum (• neutron measurements, x pressure equilibrium; U = 8o kV)

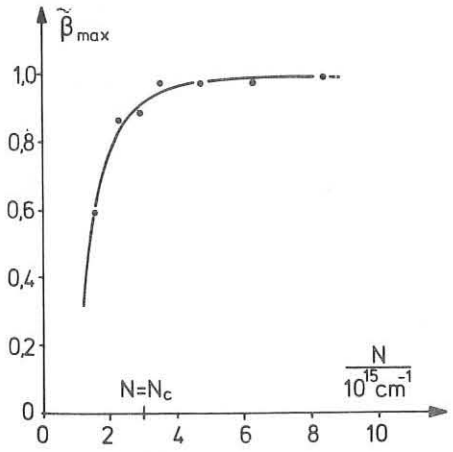

Fig. 5: $\tilde{\beta}_{max}$ as a function of the line density

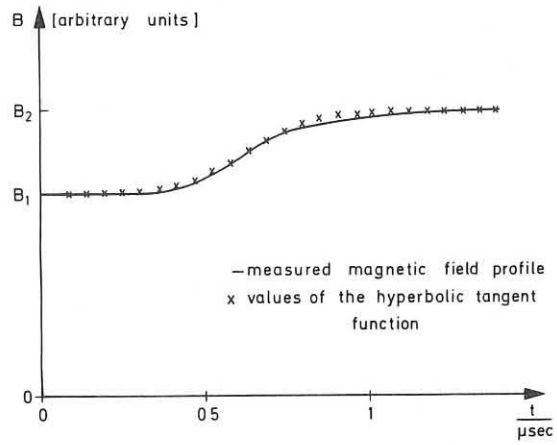

Fig. 6: Comparison of experimental B-profile with tanh-function

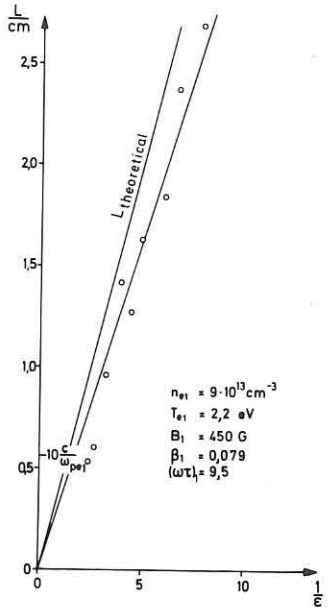

Fig. 7: Measured and calculated shock widths as function of the reciprocal shock strength 1/ε

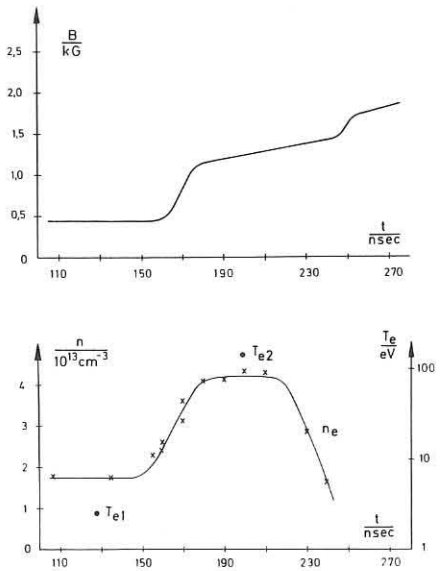

Fig. 8: Measured profiles of B and n_e; T_e ahead of and behind the shockfront ($\beta_1 = 1{,}7\cdot10^{-2}$, $\omega_{ce}\tau_{ei} \approx 90$)

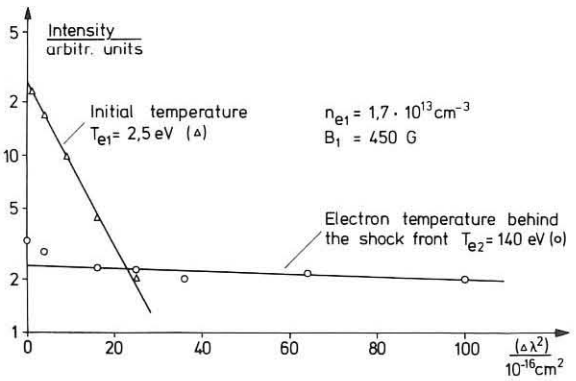

Fig. 9: Intensity distribution of the scattered laser light ahead of and behind the shock front (conditions as in Fig. 8)

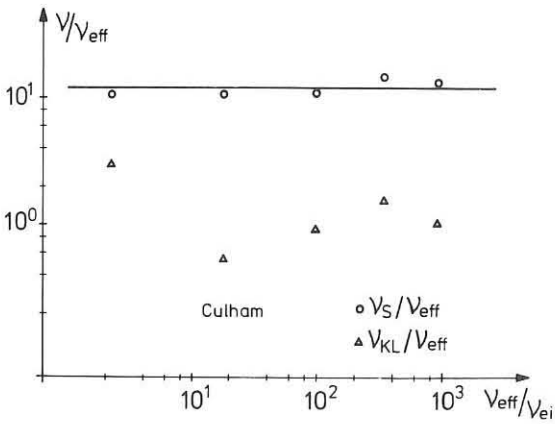

Fig. 1o: Comparison of measured effective collision frequencies ν_{eff} with theoretical predictions /8//9/.

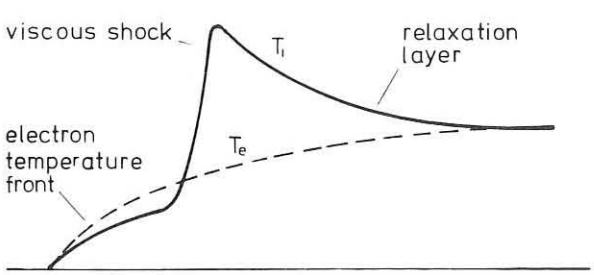

Fig. 11: Viscous shock profile, schematic

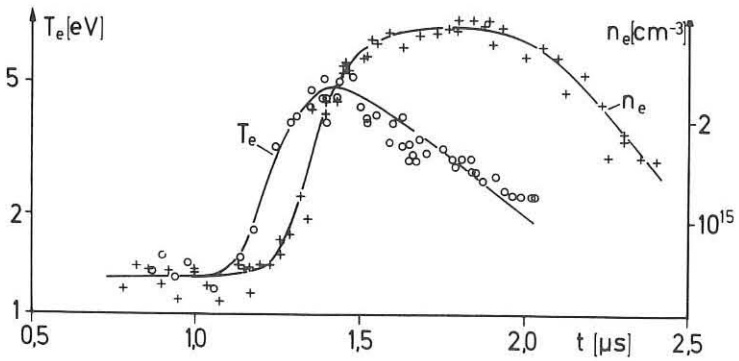

Fig. 12: Measured profiles of T_e and n_e for a collision-dominated viscous shock at M ≈ 3.8.

CONTAINMENT AND R F HEATING STUDIES IN THE PROTO-CLEO STELLARATOR

by

D.J. Lees, W. Millar, R.A.E. Bolton, G. Cattanei* & P.L. Plinate*
(UKAEA Research Group, Culham Laboratory, Abingdon, Berks., U.K.)

Abstract: Experiments are described, using the $\ell = 2$ and $\ell = 3$ helical windings, in which the containment of plasma injected into the two systems is compared, both with each other and with the predictions of neo-classical theory. Transit time magnetic pumping (TTMP) has been attempted on the $\ell = 2$ system. The chief effect is a large reduction in confinement time, although some heating is observed. Experimental results concerning the increased plasma loss rate are given.

I. Apparatus and Diagnostics

The $\ell = 3$ helical winding[1] used for these comparison measurements has 7 field periods, a major radius of 40 cm and a minor radius of 9 cm. The $\ell = 2$ winding has 6 field periods with the same major radius but a minor radius of 9.3 cm. The current in the windings is adjusted to give approximately the same plasma radius namely approximately 5 cm. For the purpose of magnetic pumping, 14 circular coils are disposed around the torus, each of radius 22 cm and having three turns of 6.5 mm copper tubing. The coils are in vertical planes, with their centres on the minor axis of the torus, and lie outside the helical windings but inside the vacuum vessel. The copper tubing was covered with Kaptan insulation to give some protection against possible flash-over. The coils are energised from a 60-180 kHz oscillator, in such a way as to add to the quasi-steady φ field, of amplitude B_o, a small field given on the minor axis by $bB_o \sin \omega t \sin k\varphi R$ in the same direction, where the modulation factor b is variable from 0 to 5%.

The frequency and wave-number were chosen for optimum heating, i.e. wave velocity $\sim$ ion thermal velocity, with a hydrogen ion temperature of 10 eV, although the resonance is very broad.

The expected e-folding time for T_i increase[2], in the absence of competing mechanisms, is approximately 1 msec for $b = 5\%$, and varies as b^{-2}. The critical density, below which heating becomes less effective, is about $2 \times 10^{11} cm^{-3}$ for $b = 5\%$, and varies as $b^{\frac{3}{2}}$.

Plasma density is measured by a 20 GHz microwave interferometer[1] and also with a double probe[1]. Electron temperature is measured by a time-swept double probe[1] and for $\ell = 3$ by a conductivity method[3]. Ion temperature is measured with a multi-gridded analyser[4] situated just outside the separatrix Measurements of neutral background show that since $T_e \sim 4$ eV the error in containment time due to recycling is considerably less than 10%.

II. Scaling Laws for Containment

Fig.1 shows graphs in which the particle containment time τ, normalized to that for a collisional toroidal plasma τ_{ps}, is plotted as a function of the ratio of connection length to electron-ion mean free path. The full line on the figure is the prediction of neo-classical theory for a similar axi-symmetric system taking into account the fact that the condition $\rho i\theta / r_n \ll 1$ is not fulfilled [$\rho i\theta$ is the gyro radius in the poloidal field and r_n is the density gradient scale length]. The experimental

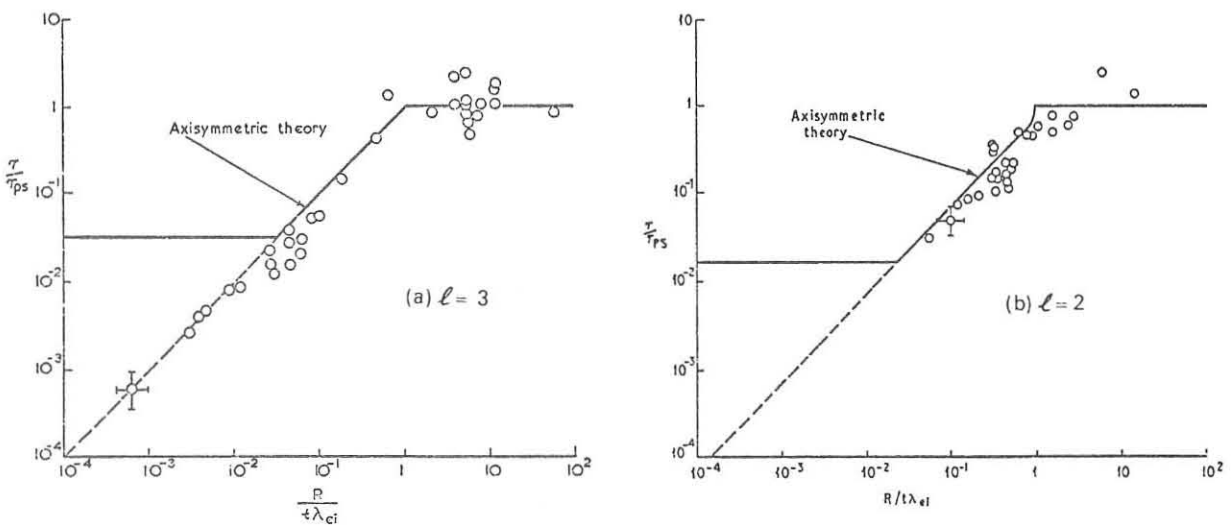

Fig. 1 Normalized particle containment time as a function of the ratio of connection length to electron-ion mean free path for (a) $\ell = 3$ and (b) $\ell = 2$ experiments.

points shown on the curve take account of the measured τ, T_e, T_i and n. It is seen that for both $\ell = 2$ and $\ell = 3$ there is reasonable agreement with neo-classical theory within the experimental error, except at lower densities in $\ell = 3$ where localized particle effects could be important. There are no results for $\ell = 2$ in a comparable region of density.

III. Fluctuation Measurements

Correlated values of $\tilde{n}$, $\tilde{E}_\theta$, $\tilde{E}_\varphi$ and $\tilde{V}_f$ have been measured as a function of radius in the minor cross section. The results are shown in Fig.2. It is seen that for both $\ell = 2$ and $\ell = 3$ there is a peak of $\tilde{E}_\theta$ and $\tilde{n}$ in the region of decreasing density at the edge of the plasma (note that the hole in the centre of n(r) is possibly a probe effect). Measurements of the instantaneous cross correlation $\langle \tilde{E}_\theta(\tau)\, \tilde{n}(\tau) \rangle$ averaged over time have been made in each case. The results are as follows for the radii at which fluctuation is a maximum:-

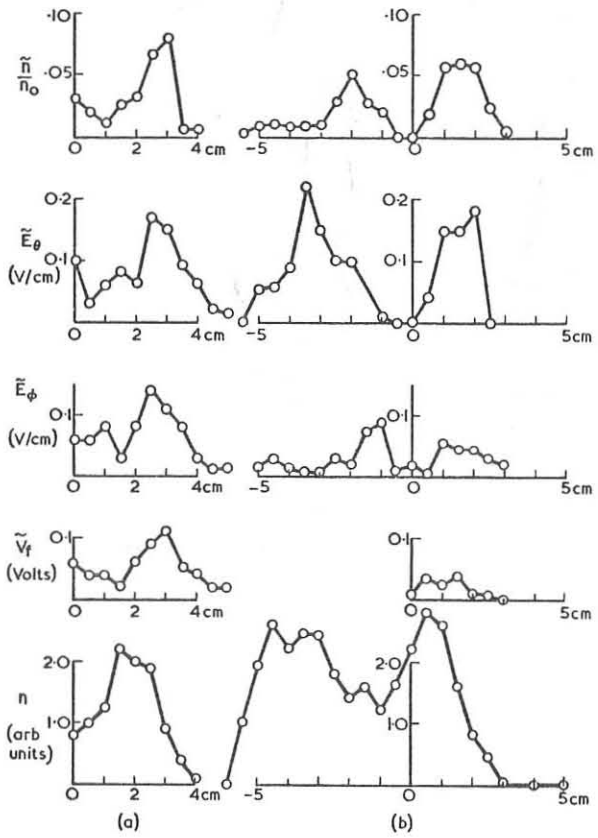

Fig.2 Radial profiles of fluctuation measured in (a) $\ell = 3$ and (b) $\ell = 2$ experiments.

$\ell = 3$ $\quad \tilde{E}_\theta = 0.10$ V/cm

$r = 3.0$ cm $\quad \tilde{n}/n_o = 0.036$

(Note r is distance from centre of minor cross section)

$\ell = 2$ $\qquad$ coefficient $\alpha = 0.05$

$r = +1.5$ cm	$\tilde{E}_\theta = 0.069$ V/cm	$r = -4.5$	$E_\theta = 0.024$ V/cm
	$\tilde{n}/n_o = 0.048$		$\tilde{n}/n_o = 0.016$
	$\alpha = 0.154$		$\alpha = 0.15$

(Note: There is a large shot-shot variation of fluctuation level.) From these can be evaluated a radial flux $\langle \tilde{E}_\theta \tilde{n} \rangle B_\varphi^{-1}$

and assuming that these measurements average around a magnetic surface a containment time. The times so calculated are 0.4 sec ($\ell = 3$) and 0.15 sec ($\ell = 2$) (compared with a measured ~ 5 msec) i.e. too long to explain the observed loss.

IV. Density and Potential Contours

In order to assess the importance of convection as a mechanism for plasma loss it is necessary to measure the surfaces of constant density and potential[5]. It is known that no strong temperature variation exists and thus contours of floating potential are expected to be equivalent to plasma potential surfaces. For both cases it is found that in the outer regions of the plasma the n and V_f surfaces are nearly coincident with no evidence of displacement. In the inner regions there are some non-symmetric effects which may be due to the probe or to the filling mechanism. For $\ell = 3$ these regions have little effect on diffusion since here i is small and thus $D_\perp$ large anyway. Fig.3 indicates typical contours of n and V_f compared with a computed magnetic surface for both $\ell = 2$ and $\ell = 3$ experiments, with the errors of the experiment indicated. Assuming that the V_f contour is orthogonal to the electric field direction a diffusion flux can in principle be calculated. The errors inherent in the measurement are so large that the results are not meaningful (in particular the fact that V_f is measured and not V_p) and thus it is only possible to state qualitatively that because of the good agreement between the contours of n, V_f and the magnetic surfaces, that we believe convection not to play

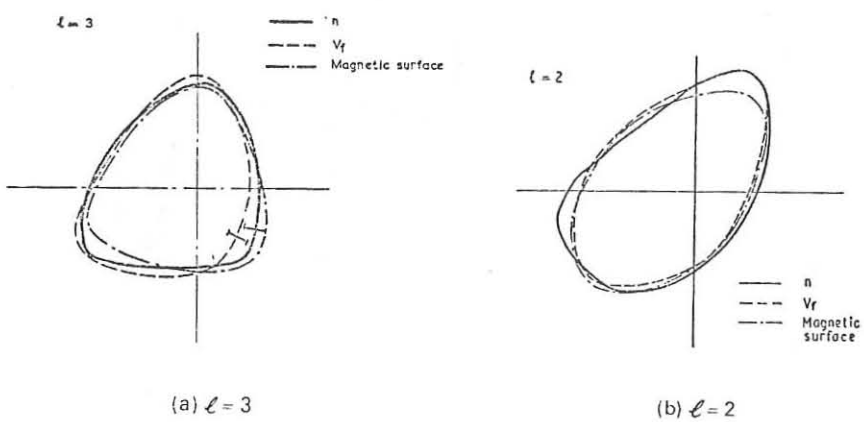

Fig. 3 Contours of density and floating potential superposed on a magnetic surface for (a) $\ell = 3$ and (b) $\ell = 2$ experiments.

an important part in plasma loss. It should be noted in particular that the errors are too large to resolve the small charge separation potentials given by neo-classical theory for the plateau region.

V. Discussion of Containment Results

The results so far obtained from $\ell = 2$ show that the plasma behaves similarly to $\ell = 3$. It should be noted that in the absence of a limiter there is considerable shear at the separatrix for $\ell = 2$, comparable with that for $\ell = 3$. This may account for the absence of any broad resonances found in other experiments[6,7] at integral values of t.

In both cases there are fluctuations of n and E centred mainly on the region of steep density gradient. If wave-numbers $k_\perp$ and $k_\parallel$ are inferred from $\tilde{V}_f$ and $\tilde{E}$ then we see that $k_\perp \sim k_\parallel \sim 1\ \mathrm{cm}^{-1}$. This is not in accord with an interpretation of the fluctuations as drift waves, in which the fastest growing mode has $k_\perp a_i = 1$ and $k_\parallel \ll k_\perp$. It is seen that the inferred fluctuation flux if averaged around a magnetic surface is too small to account for the observed plasma loss.

There appears for both $\ell = 3$ and $\ell = 2$ to be good agreement both in magnitude and scaling of particle containment time with neo-classical theory. In the presence of such good agreement it is appropriate to seek some definitive experiment as independent confirmation that plasma is in fact being lost solely by collisions. One such experiment is to determine the existence of the diffusion-driven current. The magnitude of this current has been given in the plateau regime for an axisymmetric system by Galeev[8] and it is now believed that the current should actually exist in stellerator geometry[9]. A search has been made for this current using the $\ell = 3$ system by two methods, (1) Rogowsky coil, (2) using the helical winding as the secondary of an air cored transformer with the current carrying plasma as the primary. The limit of measurement is about 50 times less than the current expected theoretically, but no signal can be detected

which is attributable to the diffusion-driven current. It is thought this may be due to the fact that the diffusion is an equilibrium phenomenon and since τ_{ii} is approximately equal to the containment time, equilibrium may not be established on the time scale of the experiment. In the absence of any cogent reason for the lack of diffusion-driven current, there must remain a few doubts that collisional diffusion is the sole source of plasma loss in this experiment.

In this respect it has been suggested recently that for a toroidal system the outward plasma flux due to fluctuations is given by $\langle \tilde{E}_\varphi \tilde{n} \rangle B_\theta^{-1}$ rather than $\langle \tilde{E}_\theta \tilde{n} \rangle B_\varphi^{-1}$. Since $B_\theta \ll B_\varphi$ and $\tilde{E}_\varphi \sim \tilde{E}_\theta$ this greatly increases the importance of fluctuation in our experiments. More detailed correlation measurements are necessary to resolve this point.

VI. The Effect of Applying TTMP

When the TTMP coils are energised, the dominant effect is a serious reduction in confinement time. Some plasma heating is observed, but it is not very significant in view of the large decrease in density. The reason for the increased loss rate is not clear at present, but the experimental results to be described may help in finding an explanation. In this series of experiments a number of different plasma guns were used, giving a range of initial densities and a variation in the number of neutral particles produced, which in turn affect T_i and T_e and the natural cooling rate. Thus although conditions were approximately the same within each experiment, it should not be assumed that they were so throughout the series. The toroidal confining field B_φ was 3 kG in all cases.

Figure 4 shows typical density decay curves, with and without the heating pulse of 1.3% modulation. Each curve is the interferometer trace of a single shot. The initial density was 5×10^{11} cm^{-3}. The enhanced plasma loss is clearly seen. Fig.5 shows the time variation of electron temperature, with and without the RF pulse. These results were put together from many

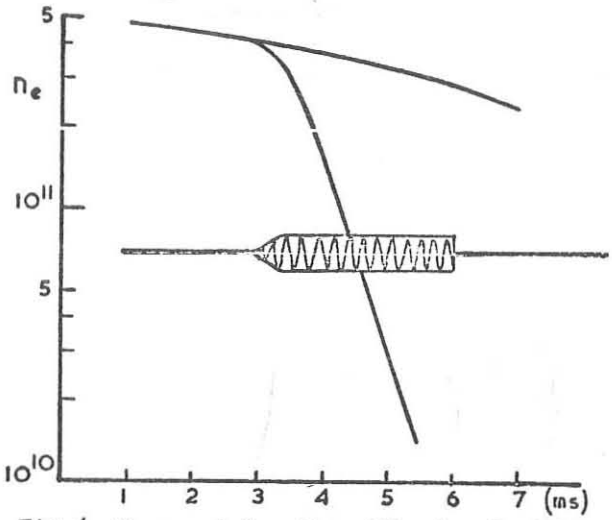

Fig.4 Decay of density without and with magnetic field modulation of 1.3%. The RF envelope is shown.

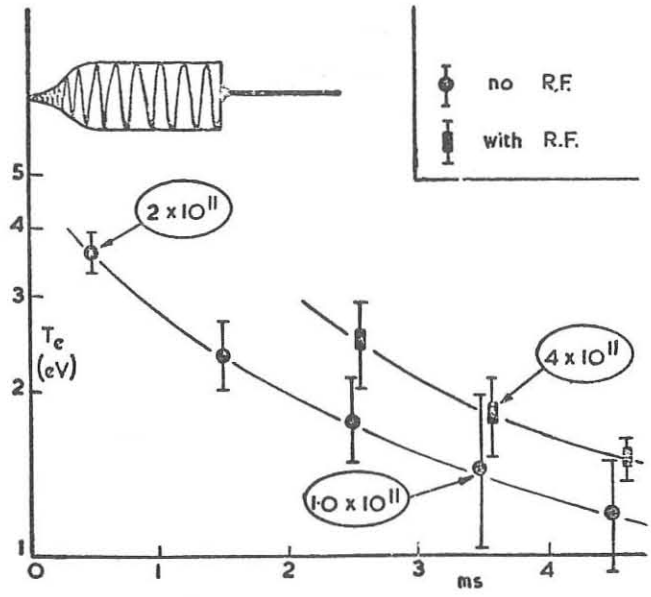

Fig.5 Electron temperature without and with 1.5% modulation. Ringed numbers are density. The RF envelope is shown

shots, and the error bars show the effect of shot-to-shot variations. Note that here the duration of the RF pulse is the same in each case, and that measurements are made at various times after the end of, but not during, the RF pulse. Approximate electron density values are marked at three points on the figure.

VII. The Enhanced Decay Rate

The following parameters were varied in order to study the effect on plasma loss rate: initial density, modulation amplitude and frequency, plasma gun loading gas (H_2 or D_2), phase of RF coil current. The enhancement of decay rate was found to be almost independent of initial density, over the range 5×10^9 to 5×10^{11} cm^{-3}.

The affects of varying most of the other parameters is shown in Fig.6. Here the loss rate $1/\tau$, where τ is the time for the density to decay by a factor $1/e$, is plotted against the RF coil voltage, which is proportional to the vacuum electric field at all frequencies. We notice the following properties of these results:

(a) The decay rate varies linearly with the modulation amplitude over at least one decade.

(b) The decay rate with H_2 in the gun is not very different from that with D_2. A mass spectrometer was used to show that the plasma from the gun was predominantly D_2 in the latter case.

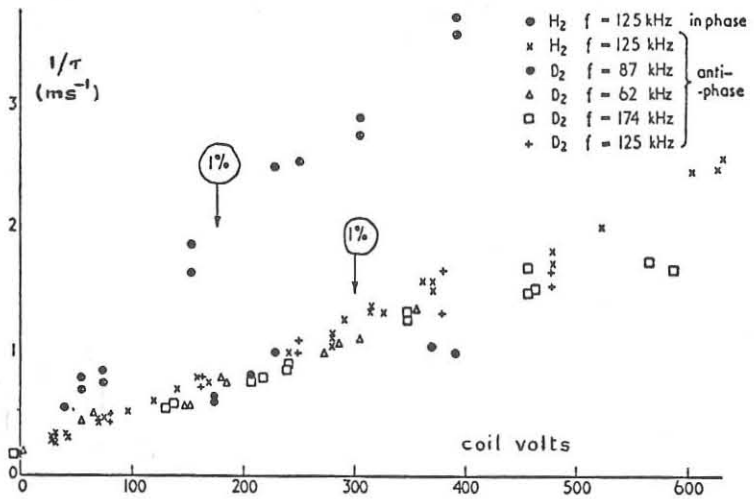

Fig.6 Inverse of density confinement time, as a function of RF voltage. The modulation factors (ringed) are for a frequency of 122 kHz, and vary as 1/frequency. The voltage shown is peak value, from either side of the balanced 3-turn coil to the vacuum vessel

(c) The decay, over the range of frequencies and amplitudes used, is proportional to coil voltage and hence to plasma electric field, if the latter is assumed to have the same geometrical form in each case.

(d) Whatever the loss enhancement mechanism may be, it does not seem to require the modulation to have a spatial variation. Indeed we cannot say that we have found any effects strongly dependent on the phase of the RF coil currents. It should be pointed out however that wave-like effects may still be present, because of the spatial variation in the confining stellarator field.

The effect of varying the helical winding current, and hence the rotational transform, is shown in Fig.7. The loss rate is increased by RF roughly in the same ratio for all values of the helical current, including zero. But we must explain the long confinement with zero helical current and zero RF, before we can draw conclusions about whether the RF pump-out is an effect specific to stellarators.

In order to test whether the TTMP field might be affecting the magnetic surfaces, a quasi-steady modulation of 2.5% was applied; no change in confinement time was observed whether the coils were connected in the same or in alternate directions. This result is in accordance with computer predictions, where such perturbations were found to have negligible effect on the magnetic surfaces.

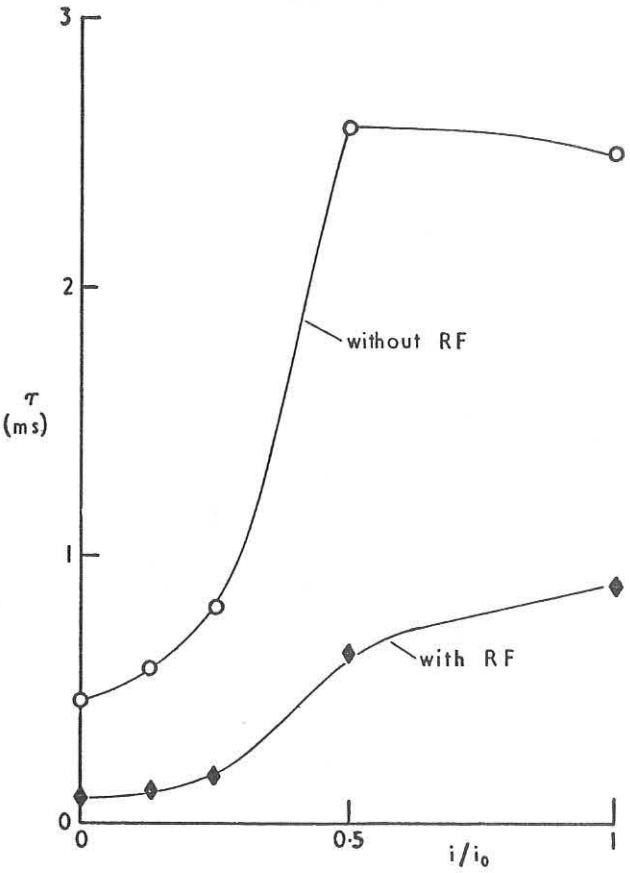

Fig.7 Confinement time as function of helical winding current. i_0 is the optimum current used in the other experiments. In this case there was a probe placed in the plasma, so the confinement was not as good as usual.

A double Langmuir probe was used to examine the electron density profile as a function of plasma radius. It was found that the application of TTMP did not appreciably alter the shape of the profile; that is, the density decayed at almost the same rate everywhere. One interesting result that was found with the probe was the existence during the TTMP pulse of a substantial non-oscillatory local electric field in the φ direction. The field was roughly proportional to b, and with a modulation factor of 0.6% (coils in phase) it amounted to about 10 V/cm at 2.5 cm from the mirror axis, and was zero on it. It was found that the field reversed in direction on changing the polarites of the mean potential of the helical winding with respect to the vacuum vessel.

When the coils were open-circuit and an RF voltage, equal to that which would be used between each end of the

balanced coil and earth for 5% field modulation, was applied between the coils and the vacuum vessel, a pump-out effect was produced. The decay time fell from 4.7 msec without RF to 1.7 msec with RF. Although this is a substantial effect which calls for explanation, it is an order of magnitude down on the field modulation effect.

VIII. Measurements of Ion Temperature

Using the ion energy analyser, we have measured ion energies shortly before and shortly after the RF pulse. The analyser yields a current-voltage characteristic which has an exponential tail over a decade or so, and we define 'temperature' from the voltage change required for an e-fold decrease in current. Although by RF we have never produced a final temperature higher than the initial one, we have always found that the final ion temperature is higher than it is after the same lapse of time in shots under the same plasma conditions but without RF. We have found this over a wide range of plasma conditions, and with alternate coils connected either in phase or in anti-phase. For example with 1.5% modulation, and a pulse width of 1 msec, we find T_i initial 12 eV, T_i final 4 eV with RF and 3 eV without, Although the amount of effective plasma heating which this represents is not inconsistent with TTMP theory (except perhaps in the in-phase case), we do not attach much importance to the result because of the large decrease in density over the time of the pulse.

We have also attempted to measure T_i during the RF pulse. The resultant signal always contains a long RF component of a certain waveform, which is not instrumental in origin. The shape of the waveform is consistent with the assumption that there is an RF electron field between the plasma and the analyser. If we so interpret the analyser signal, then we can define a temperature from the exponential curve which can be drawn through the minima of the signal waveform. When this is done we obtain surprisingly large values, greatly in excess of

the measured T_i taken shortly after the pulse when there is no RF component in the analyser signal. Some results of this kind are shown in Fig.8. We deduce that during the RF pulse the analyser is receiving mainly ions which are not representatives of the whole plasma. If however this way of interpreting the signal is correct, the fact that such energetic ions are produced may well be associated with the pump-out mechanism.

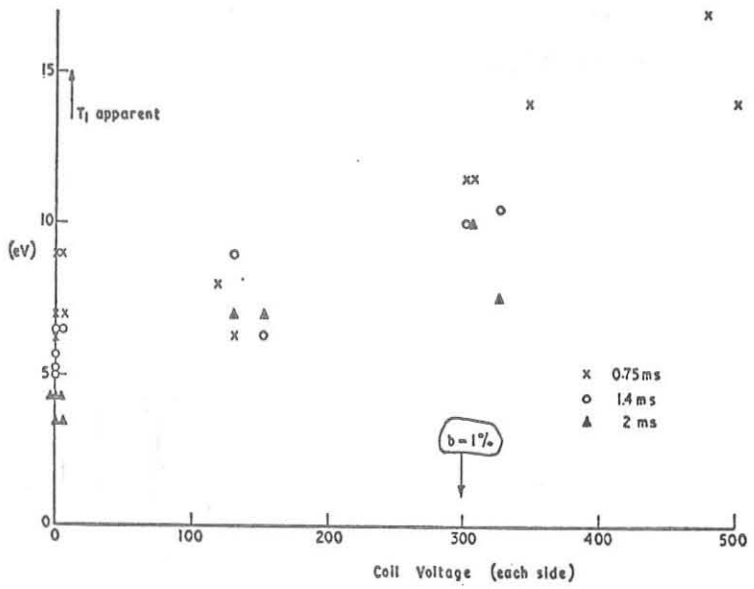

Fig.8 Apparent ion temperatures at various times during the RF probe, as a function of coil voltage. Loading is H_2, f = 122 kHz, coils in anti-phase

Conclusions

(1) We have compared the containment properties of similar $\ell = 2$ and $\ell = 3$ stellarators and concluded that, from the evidence we have, they are the same. From the practical point of view, therefore, $\ell = 2$ shows a distinct advantage, since for the same plasma size and B_φ field the current in the helical conductors is lower than in $\ell = 3$.

(2) In both cases fluctuations and convection are inadequate to explain the observed loss and the magnitude of this is comparable with that expected by neo-classical theory.

(3) No detectable diffusion-driven current exists in the $\ell = 3$ system.

(4) TTMP produces an unacceptable plasma loss, at least in $\ell = 2$ stellarators.

(5) An explanation is required for the loss mechanism. It is associated with RF electric fields but not with break-up of the magnetic surfaces.

Acknowledgements

The authors gratefully acknowledge the experimental and technical help given by Messrs J.E. Allen, P.A. Shatford, R.J. Storey and B.J. Parham: we are also grateful to Mr T.E. Stringer for many helpful discussions. Finally we thank Dr R.J. Bickerton for his suggestions and encouragement.

References

* On attachment from Euratom.

/ On attachment from C E A, Fontenay-aux-Roses, France.

[1] R.A.E. Bolton et al., Phys. Fluids, 14, 1566 (1971).

[2] J.M. Dawson and M.F. Uman, Nucl. Fusion, 5, 242 (1965).

[3] D.J. Grove et al., in 'Plasma Physics and Controlled Thermonuclear Research' [IAEA Vienna, 1969] vol.1, p.479.

[4] S.S. Medley and D.R.A. Webb, J. Phys. D., 4, 658 (1971).

[5] K. Miyamoto et al, Phys. Fluids, 14, 2748 (1971).

[6] E. Berk et al., Novosibirsk, IAEA, vol.I, p.513 (1969).

[7] M.S. Berezhetsky et al., Novosibirsk IAEA, vol.I, p.529 (1969).

[8] A.A. Galeev, Zh. Eksp. Teor. Phys., 59, 1378 (1970).

[9] J.W. Connor, R.J. Hastie and J.B. Taylor, (this conference).

CERTAIN RESULTS OF STELLARATOR EXPERIMENTS IN THE USSR

L.M.Kovrizhnikh
P.N.Lebedev Physical Institute, Moscow, USSR

Abstract: The report presents a survey of stellarator experiments which have been carried out in the Soviet Union after the Madison Conference /I97I/. The data on the particle confinement are briefly analyzed.

This report presents a brief survey of experiments which were carried out on stellarators at Lebedev Physical Institute /Moscow/ and Physical Technical Institute /Kharkov/ after the Madison Conference/I97I/.

The Soviet stellarator program consists of two parts one of which is devoted to creation and heating of plasmas. The second one includes investigations of plasma confinement and its dependence on magnetic trap parameters /such as confining magnetic field B_o , angle of rotational transform ι , shear and aspect ratio r/R / and on macroscopic plasma parameters /density N, temperatures T_e , T_i , their gradients, proper electric fields, plasma oscillations etc/.

As has been already reported the laser injection in the TOR-I stellarator /Lebedev Institute/ was performed, these experiments were carried out on the $\ell = 2$ stellarator of major and minor radii 60 cm and 5 cm respectively, the angle of rotational transform $\iota = \iota/2\pi = 0{,}25$, the magnetic field being varied from 3 to I0 kgs. Plasma was created by means of a neodyme laser /energy from I to I5 jouls, the pulse length 50 nsec/ acting on a Li target placed out-side of a boundary magnetic surface. Measurements of the density N and temperatures Te,Ti as functions of the laser energy and the magnetic field B_o were carried out. The Fig I shows the dependence of the trapped plasma desity and of the electron temperature on the laser energy. One can see that for energies Q below 4-5 jouls the density behaves as Q^2 and for $Q > 5$ jouls the dependence is close to linear one. Rather low values of the electron temperature can be explained in terms of adiabatic cooling due to the plasma bunch expansion. Q- dependence of the mean ion evergy measured

by various methods is presented in the Fig 2. The solid curve corresponds to time-of-flight measurements and shows the ion energy immediately after the capture. The dashed curve is obtained from probe and spectroscopic experiments and corresponds to the temperature of confined ions.

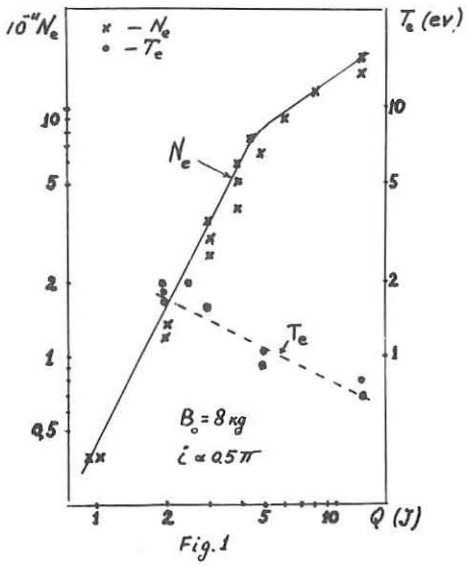

Fig. 1

It is interesting that a sharp change of the ion temperature dependence occures at $Q \simeq 4$ jouls. The mechanism of this phenomenon is not still clear, but one can suppose that the decrease of the ion temperature is due to an interaction /charge exchange/ between trapped ions of the plasma and neutral atoms the number of which increases sharply with the laser energy. These results are discussed in more details in one of the reports presented at this Conference.

Investigations were going on of low-frequency oscillations influence on a plasma decay in the L-I device /Lebedev Institute/ which is similar to TOR-I. The plasma parameters were $N \leqslant 10^{16}$ cm^{-3}, $T_i \sim 25$ ev, $T_e \sim 3$ ev. It was found out that the plasma decay rate depends on the distance from the axis. In central regions intervals of a relatively large decay time /about a millisecond/ take turns with intervals when the decay time is serveral times less. In peripherial regions the decrease of the plasma density is sometimes replaced by its increase. It is worth to note

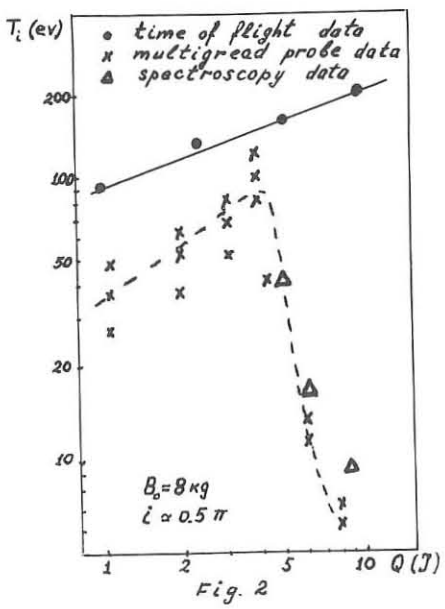

Fig. 2

that the fast decay is accompanied by a sharp increase of low-frequency oscillations /$\omega \sim 2.10^5$ sec^{-1} / which spread also over inner regions of the plasma. Characteristic oscillogramms of density behaviour are presented in the Fig.3 for radii r = 0,5 cm, I,I cm, I.7 cm and 2.5 cm / B_0 = 4,5 kgs $t = 2/3$/.

Appraently the process develops as follows. Since the plasma decay rate is smaller in the central region the density gradient increases with time. When it reaches certain threshold value oscillations which were localized in regions of maximal gradients increase sharply and spread over inner regions of the plasma. This decreases the density and its gradient in the central region and hence restores the value of the oscillation amplitude. Thenthe process repeats again.

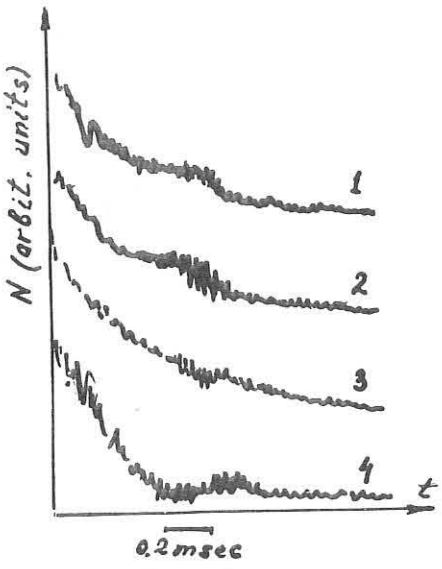

Fig. 3

Note that the process is the most legible at rational values of $t = \frac{i}{2\pi}$, e.g. at $t = \frac{1}{2}, \frac{2}{3}$.

An attempt was made to stabilize the obaserved oscillations by a probe placed at the point of the maximal density gradient to change the plasma potential. The results are presented in the Fig 4 where relative density fluctuations $\tilde{N}/N$ at r = 2 cm /solid curve/ and the plasma lifetime /dashed curve/ are plotted varsus the plasma potential at the axis. One can see that an optimal value of the potential exists which provides the minimal relative fluctuations and the

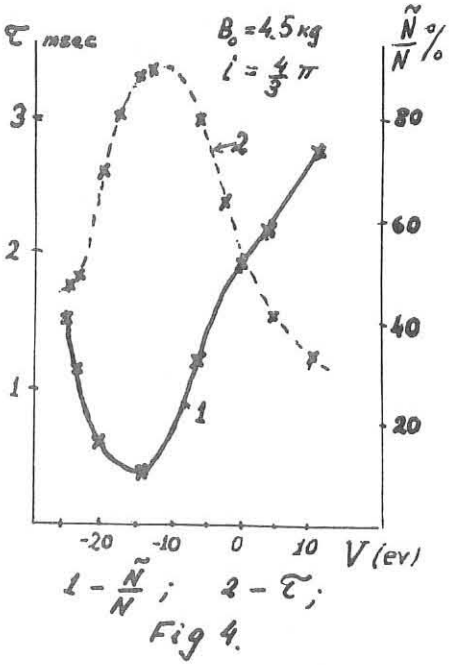

1 - $\frac{\tilde{N}}{N}$; 2 - τ;
Fig 4.

maximal life-time τ /the non-perturbed plasma potential was -25 ev/. Measurements showed that lower oscillation modes were damped mainly. Thus the stabilization leads to a decrease in the plasma decay rate in peripherial regions and to rarer drops of the density in the central region. This is illustrated by the oscillogramm of the Fig 5 showing density variations at I cm in a nonperturbed plasma /trace I/ and in the plasma with a stabilizing probe /trace 2/.

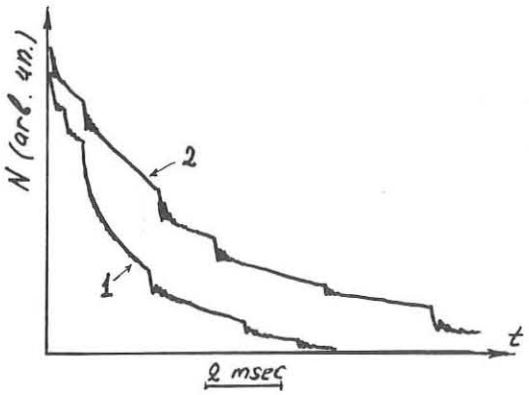

Fig 5

The results of these measurements will be also discussed elsewhere at this Conference.

Further investigations of confinement and heating on helium plasmas were carried out on the $\ell = 3$ stellarator /Kharkov/ for long /8-IC msec/ pulses of the heating current. Some preliminary data on local values of the density and the electron temperature were obtained by Thomson scattering. A ruby laser providing 4 jouls in 20 nsec was used for the experiments /magnetic field $B_o = 9{,}6$ kgs current amplitude $J_c = 4.5$ ka, $\tau \simeq$ I /. The results are presented in the Fig.6. One can see that the density distribution is asymmetric /its maximum being displaced upward/, but the electron temperature is almost uniform /$r_p = 6.8$ cm/.

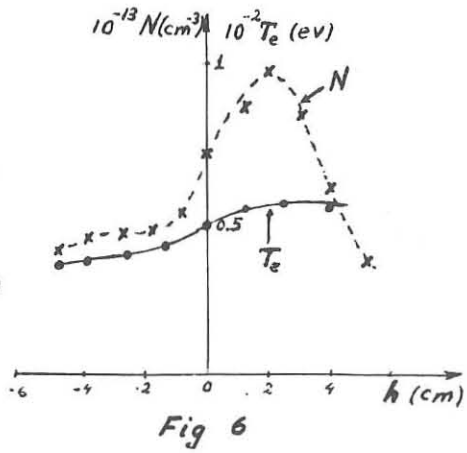

Fig 6

Another interesting peculiarity is a non-gaussian spectrum of the signal scattered in peripherial regions of the plasma column. This indicates that the electron

distribution function is non-maxwellian. The spectra of radiation scattered in the central region /trace I/ and at $r \approx 5$ cm /trace 2 / are shown in the Fig 7.

It would be of interest to measure the spectra for larger $\Delta\lambda$-s which would provide details of the electron distribution function in the central region as well as at the peripheria. Their possible non-maxwellian character would indicate kinetic plasma instabilities. Unfortunately, plasma impurities make these measurement still impossible. It is worth noting that measurements of microwave radiation from the plasma indicates the presence of intense modulated oscillations which frequency was by order of magnitude the electron Langmuire frequency ω_{Le}. The modulation frequency was close to the ion Langmuire frequency ω_{Li}.

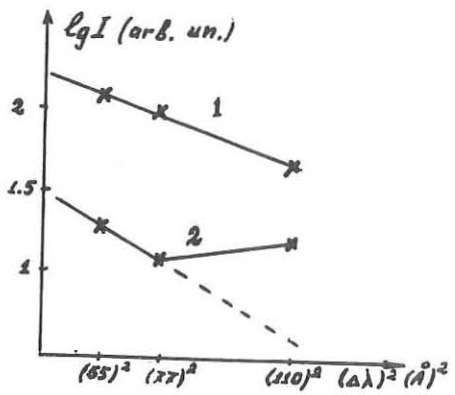

Fig. 7

The ion temperature was measured by a Doppler shift of singly ionized helium. The results are shown in the Fig.8 where the electron diamagnetic temperature T_e and the ion temperature T_i are plotted versus time Maximums of T_e and T_i are shifted in time and approximately correspond to the current maximum. The absolute value of T_i is about 10-20% of T_e. It has to be noted that the temperature of inner regions of the plasma column may be somewhat

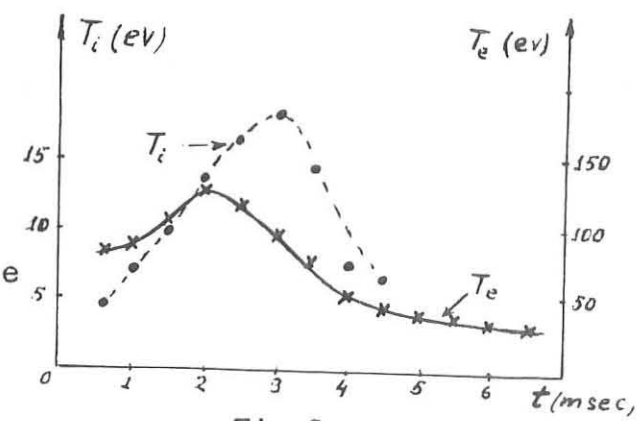

Fig. 8.

larger because He^+ ions are concetrated mainly in peripherial regions.

Now let us try to analyse briefly data on the life-time of plasmas created in various devices by various methods /laser plasma, gun plasma, UHF-plasma and current plasma/.

Interdependence of plasma and magnetic field parameters, difficulties of their independent variations and poor reproducibility of results make the analysis of life-time scaling with various parameters rather difficult.

Inspite of rather wide range of parameters of the installations at the Lebedev Institute /the magnetic field from 3 to I4 kgs , the angle of rotational transform ι from 0.04 to 0.7 the electron temperature from 0.2 to 2 ev, the ion temperature from 02 to 40 ev, the plasma density from 10^{5} to 10^{12} cm^{-3} / sufficiently reliable data on life-time scaling with main plasma and magnetic field parameters are still absent.

As for experiments on Uragan /Kharkov/, some results intricate that under certain conditions the plasma life-time is directly proportional to the angle of rotationd transform t and inversly proportional to T^{α} where $0.5 \leqslant \alpha \leqslant I$. However, the speread of the life-times under almost identical conditions /T_e, T_i , N, B_o ,t/ is too large /from I,7 msec to 7,9 msec/ and the temperature range is too small /$40 < T_e < 300$ ev/ to consider these results as final ones.

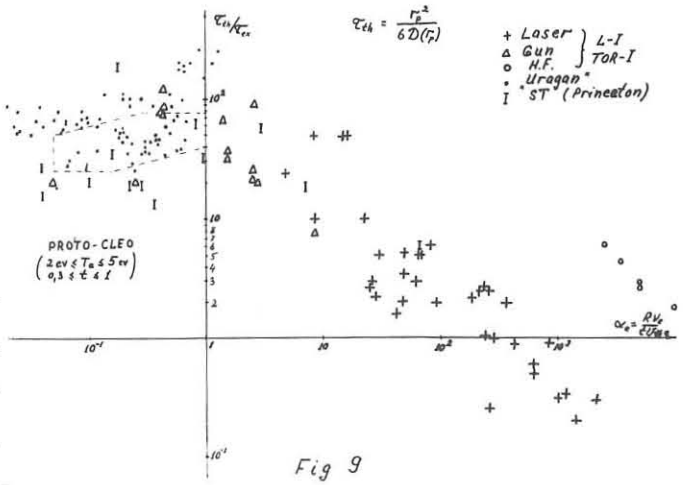

Fig 9

Moreover, a theoretical analysis of the obtained results is returded by the absence of some additional data which are essential for transport processes /a self consistent plasma potential, density and temperature gradients, κ - and ω -spectra of plasma oscillations etc./

However, an attempt was made to compare experimental data and predictions of the neoclassical

theory of transport phenomena. In the Fig 9 the ratio of the theoretical life-time τ_{th} to the experimental one τ_{ex} is plotted vs. $\alpha_e = \frac{r_p \nu_e}{\theta v_{th}} = \frac{R\nu_e}{\iota v_{th}}$ The physical meaning of α_e is the ratio of a length of the magnetic force line making one turn with respect to the small azimuth to an electron free path length. The values of τ_{th} were calculated as $\tau_{th} = r_p^2/6D(r_p)$ using measured plasma parameters. / r_p is the plasma column radius/. The diffusion coefficient D was taken from the neoclassical theory under assumption that the diffusion is determined by electrons and hence the plasma potential has an order of magnitude of the ion temperature.

It is easy to see that in the "plato" $/(\frac{r_p}{R})^{3/2} \ll \alpha_e \ll$ I / and intermediate $/\alpha_e \sim$ I/ regions the ratio τ_{th}/τ_{ex} by order of magnitude is $10^1 - 10^2$ .Only for large values of $\alpha_e > 10$ /when a hydrodynamic description of electrons is valid / the experimental values of τ_{ex} are close numerically to the theoretical ones.

It is interesting to note that the farther increase of α_e / $\alpha_e > 10^2$ / leads to experimental values τ_{ex} which are larger then theoretical ones. In all cases when $\tau_{th}/\tau_{ex} <$ I the ion parameter $\alpha_i = R\nu_i/\iota v_{th}$ is larger than unity, i.e. the ions can be described by hydrodynamics as well. Then estimations show that for $T_e \ll T_i$, the ion diffusion coefficient is smaller than the electron one and the plasma potential should change its sign and be positive. Some preliminary experiments with laser plasmas /$T_e \ll T_i$ / indicate that for $\alpha_e > 10^2$ the potential is octually positive. Nevertheless a rigorous comparison of τ_{th} and τ_{ex} does not seem possible now because complete data on the electric field distribution in the plasma are still absent. Rough estimates of the electric field show that the ion diffusion being taken into account the ratio τ_{th}/τ_{ex} is larger than unity in the region $\alpha_e > 10^2$ as well. Nevertheless from our point of view, it is too early to speak about a correspondence of experiments to the neoclassical /or any other/ theory of transport phenomena. As has been already mentioned we have not get sufficiently reliablt data on the life-time scaling with plasma and magnetic field parameters.

At the same time, inspite of the rather large spread

of experimental values of the life-time, it can not slip one's attention that the order of magnitude of the life-time is surprisingly insensitive to wide variations of certain parameters. This can be illustrated by the Figs IO, II, I2 where the normalized experimental life-time $\tau' = \frac{10\, T_e^{1/2}\, \tau_{ex}}{t B_c r_p^2}$ is plotted versus several parameters being varied in a wide range /T_e in ev, B_c in kgs, plasma radius r_p in cm, $t = \iota/2\pi$. The normalization was matched to get the smallest spread of the experimental points obtained both on various installations and successive experiments on a particular device. For a comparison in the same figures there are data from the tokamak ST /Princeton/ cited at the last year Madison Conference [I] and data from Proto-Cleo [2].

One can see from the Figs IO and II that within one order of magnitude the normalized life-time is constant within the very wide range of the density /from 10^9 cm^{-3} to $5\text{-}6\cdot 10^{12}$ cm^{-3}/ and of the electron temperature /within three orders of magnitude/. The Fig I2 is less impressive because the range of the angle of rotational transform is relatively small/$0.04 \leq t \leq 1.2$/ Nevertheless, no evident dependence of the normalized time on t can be found in this graph as well [3].

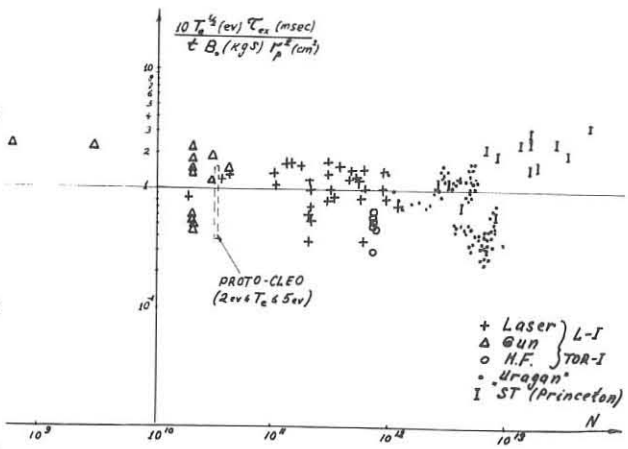

Fig. 10

The most doubtful point in the above normalization is the first power of the magnetic field. Unfortunately the range of employed magnetic fields is not sufficiently wide /3 kgs $\leq B_c \leq$ 44 kgs/ to expose a more definite scaling low.

So, if one assumes for a moment that the normalized life-time constancy mentioned above reflexes something but our wishes the conclusion should be made that due to some unknown processes the diffusion coefficient is proportional $D \sim T_e^{1/2}/tB_c$.

/of course, $\mathcal{D}$ may depend also on other parameters, which have not been analized here, e.g. on the ion temperature/. However we can not suggest a model providing this type of scaling with the plasma parameters.

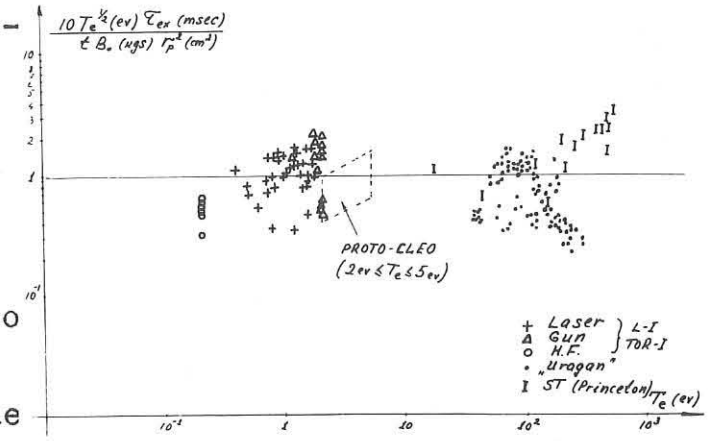

Fig. 11.

Thus the above analysis shows that in none regime a satisfactory agreement between the theory and experiments has been yet achieved. In the "plato region the disagreement is as large as two orders of magnitude In the hydrodynamic regime it is much less, but in both cases the problem of scaling laws remains open.

Although an origin of this disagreement is not still clear the oscillations excited in the plasma undoubtedly play essential /if not decisive/ role in the confinement process. Still unclear are the nature of these oscillations and the reason of their excitation.

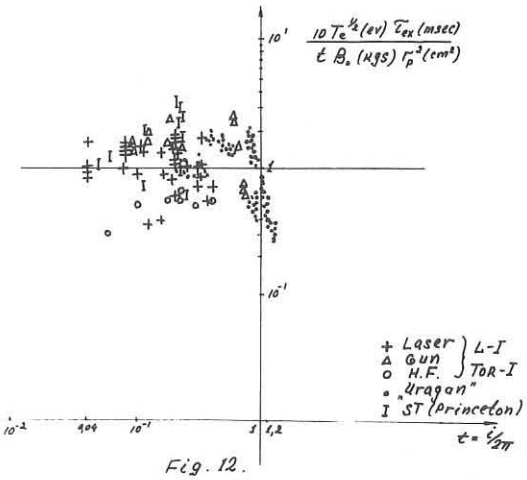

Fig. 12.

One can not exclude that the plasma potential and associated proper electric fields play larger role in the plasma confinement than it used to be thought. In particular, associated plasma flows along the magnefic force lines can be one of the reasons of the insufficient plasma confinement in magnetic traps. More attention is also to paid to what extent the coincidence of magnetic and equipotentical surfaces is essential for the plasma confinement.

To answer all these questions more careful and systematic measurements of possibly all plasma parameters seem to be necessary. In particular, radial and azimuthal distributions of the potential and plasma oscillation spectra are to be investigated. On one hand these measurements would make explicit experimental scaling laws; on the other hand they would permit a comparison with theoretical models.

The most experiments have been carried out under conditions when electrons are in the "plato" ragime and a stellarator as a trap does not differ essentially from a tokamak device. So more attention should be paid to the plasma confinement in regimes where specific stellarator effects may develop /e.g. in the " banana" and "superbanana" regimes/.

The author wishes to express his gratitude to all his colleagues who kindly presented materials for this report and took part in helpful discussions.

I D.Dimock et al. Fourth Conference on Controlled Nuclear Fusion paper CN-28/C-9 Madison, Wisconsin USA /I97I/.

2 R.A.E.Bolton et al. Phys. Fluids I4, 7/I97I/ /Fig II, p. I574/.

3 Proto-Cleo data are not brought here as we were not able to find out $\tau_{ex}(t)$.

NUMERICAL MODELS FOR PLASMA EVOLUTION IN TOKOMAK DEVICES

C. MERCIER, SOUBBARAMAYER

ASSOCIATION EURATOM-CEA SUR LA FUSION

Département de Physique du Plasma et de la Fusion Contrôlée
Centre d'Etudes Nucléaires
Boîte Postale n° 6 . **92 Fontenay-aux-Roses**(France)

I - INTRODUCTION : The performance of Tokomaks obtained first in USSR and later in USA have encouraged physicists to compare experimental results with the solutions of the equations of evolution in space and time of hot plasmas. These equations even in a very simplified form involve a system of non-linear partial differential equations connecting the density, ionic and electronic temperatures, currents and magnetic field in the plasma. To these mathematical difficulties one must add a very defective knowledge of the transport coefficients which govern the evolution of the plasma. So one must sometimes use phenomenological transport coefficients. The system of equations to be solved then becomes extremely complicated and can be solved only with the help of a computer and very perfected numerical codes which must give precise results even in regimes with large gradients. The code must be as simple as possible, enabling an easy change of the transport coefficients, the experimental conditions and being of quick interpretation. This last condition has been obtained in Fontenay-aux-Roses by visualizing the results on a scope.

II - HISTORICAL : The first numerical codes of this kind were presented to the Doubna conference (USSR) in September 1969 by Dnestrovskii et al.[1] and the Fontenay team[2]. These first studies immediately show that in order to get good orders of magnitude in the quasi-stationnary state of Russian Tokomaks, it was necessary to use anomalous transport coefficient mainly for the resistivity and the electron thermal diffusion coefficient ; confirming the more qualitative analysis done by Arsimovitch and the Kurchatov physicists. In the same way anomalous transport coefficients were necessary in order to explain the rapid disappearance of the skin effects during the transient phase. The Rome Conference[3,4] showed that this kind of research was developing and was becoming more accurate. To the Madison Conference, two new codes were presented by the Princeton and Oak-Ridge laboratories[5,6] ; the Princeton code took into account much more complicated formulae obtained by Rosenbluth et al.[7] in the banana regime. These formulae allow a first exploration of pinching effects of trapped electrons predicted by Ware[8] and of the "bootstrap" current.

At this same conference three attempts at the explaination of the sharp profile of the ST Tokomak were made.

a) Neutrals coming from the liner would cool down the periphery of the plasma increasing the thermal diffusion and peaking the plasma temperature at the center[5].

b) The pinching effect of trapped electrons[8].

c) The functional form of the transport coefficients[9].

Several works take into account the pseudo classical law introduced by Artsimovich [6] and Yoshikawa[11] for the electron thermal transport coefficient. The results are also very consistent with experimental data[5,12]. The effects of the neutrals have been introduced in the main codes [5,13]. These neutrals are either cold particles coming from the wall or a beam of hot neutrals injected to heat the plasma, as for example in the work of Dory et al. presented at the Kiev Conference (October 71) and of Girard presented at this Grenoble Conference.

Other kinds of heating can be studied with these numerical codes as for example the work of Brambilla for heating by TTMP done in CEN at Grenoble. To conclude this brief résumé one must note numerous extrapolation works showing the conditions of ignition depending on the hypotheses made on the form of the transport coefficients.

III - EQUATIONS OF THE MODEL : A fluid description may be adopted to simulate the evolution of the plasma in a Tokomak. A very simple model considers the plasma as a mixture of two fluids (electrons and ions) with electrical neutrality. The basic equations of the model include the mass continuity, the energy balance for electrons, the energy balance for ions[14], the Maxwell electromagnetic equations, the simplified Ohm's law and state equations for electrons and ions. This system of equations must be closed by specifying the dependence of transport coefficients and the expressions of particle and heat fluxes. The problem is completed by the data of proper initial and boundary conditions. Where do we now stand with the basic equations ? The particle and heat fluxes may be either given phenomenologically or derived from a microscopic treatment of the Vlasov equation[7]. All the codes now on use are one dimensional and the equations have the general form :

$$\frac{d\vec{G}}{dt} = M\vec{G} = \vec{F}$$

where $\vec{G}$ is a four component vector

$$G = \left| \begin{array}{l} n \\ T_e \\ T_i \\ B_\theta \text{ or } J \end{array} \right|$$

M, a matrix whose elements are non linear differential operators and $\vec{F}$ is a vector including terms characterizing sources or sinks of matter or energy. One simplified case of this set of equations has been given for example in[9] by neglecting the effect of the time evolution of the particle density on the energy balances. The influence of the neutral gases is an important problem. We treat this problem in the next section. The purpose is to compute the distribution of the neutrals in the plasma cross section and the sources or sinks which arise from these neutrals.

IV - NEUTRAL PARTICLES IN THE PLASMA AND THE CYLINDRICAL CODE OF FONTENAY.

When a neutral particle penetrates the plasma, it can either be ionized or proceed to a charge exchange with one ion of the plasma. Physically the process happens as if the ionization was a capture of the neutral and the charge exchange an inelastic diffusion of the neutral which continues its path with the velocity of the collided ion.

Let $q(\vec{r})$ be the number of neutrals proceeding to a collision (charge exchange) per unit time and unit volume. One can then easily establish that $q(\vec{r})$ satisfies the equation :

$$q(\vec{r}) = \int_o^{+\infty} \left\{ \Sigma_{ech}(v,\vec{r}) \int_v \frac{e^{-\tilde{\Sigma}_t R}}{4\pi R^2} \; m\,(T_i(\vec{r}'),\, v)\; q(\vec{r}')\, d\vec{r}' \right\} dv$$

$$+ f_s \int_o^{+\infty} \left(\Sigma_e(v,\vec{r}) m_s(v) \int_s \frac{e^{-(\tilde{\Sigma}_t R)_s}}{2\pi R^2_s} \; ds \right) dv$$

where Σ_{ech} and Σ_{ion} are the cross sections of charge exchange and ionization, taking into account the relative velocities of the particles

$$\Sigma_t(v,\vec{r}) = \Sigma_{ech} + \Sigma_{ion}$$

$$(\tilde{\Sigma}_t R)\, v, \vec{r}', \vec{r} = \int_o^R \Sigma_t\left(v, \vec{r} + \frac{\vec{r}' - r}{R}\, x\right) dx$$

f_s number of neutral particles entering the plasma per unit time and unit surface

$m(T,v)$ is the Maxwellian distribution of velocities. As we use a complete theory for the neutrals, that is the velocities of ions leaving the point $\vec{r}$ are not unique (for example the average velocity at that point), we will handle q and not the neutral density as basic function.

We also compute all the quantities which are the "source or well" terms in the basic equations of the evolution model. The code can also give the velocity spectrum of the neutrals leaving the plasma in a given direction.

Such a complete calculation takes a relatively long time on a computer : if desired, the computation may be simplified by replacing the Maxwellian distribution by a Dirac function $\delta(v-\bar{v})$ where $\bar{v}$ is the average velocity.The computations show that the differences between these two types of distributions are relatively small for the actual Tokomaks (of the order 10 %). But the precision for the computation of the velocity spectrum is much better. The results of our computations are very close to the calculations done by Cheglov[15] with a Montecarlo method. This code for the neutrals is coupled with the code for the evolution and allows us to study the effect of cold or hot neutrals on the behaviour of the discharge.

V - APPLICATIONS OF THE NUMERICAL MODEL

The resolution of these equations with very complex expressions for the transport coefficients can be achieved only by computational means. The results obtained during the transient period of the evolution or at the final stationary or quasi-stationary state depend strongly on the choice of the transport coefficients.

V.1 -STATIONARY STATES

We consider in this section the states actually stationary and also the states which are changing very slowly so that the observer may have the impression of a stationary state. For, in many regimes, one finds that during a period of time of the order of the discharge duration, the evolution of the plasma state is so slow that experimentally one can assume the equilibrium

state to be reached. However, if in these cases, one continues the computation, the profiles and the average values change in a relatively long time and the final state computed is often very far from the experimentally observed quasi-stationary state. We summarize in TABLE 1 the principal models utilized to explain the stationary states. In this table, we indicate the types of transport coefficients and the anormaly factor utilized in each model. Let us recall that D, K_e, K_i, α, η are respectively the particle diffusion the electron thermal conductivity, the ion thermal conductivity, the energy transfer coefficient from electrons to ions and the electrical resistivity. The signification of the symbols used in the TABLE is given below :

(N.C) Neoclassical transport coefficient [19,20,21]

(P.C) Pseudoclassical transport coefficient = $C_{Vee}\rho^2_I$ [6,11]

(P.S) P firsch-Schlüter thermal diffusion coefficient. [22,23]

$\gamma(\theta)$, γ_r Anomaly factors for the electrical resistivity. [3,16]

Z Multiplying factor representing an effective charge of ions.

D=0 means that we neglect the evolution of the particle density (simplified code).

The notation (F.P.) means "flat profile" and (P.P.) "peaked profile"

All these models explain equally well the experimental results. Though the functional forms used are quite different, their average values are approximately equal so that the overall quantities measured fit well with the computations. The distinctions between these functional forms are seen on the radial profiles computed and the time evolution.

V.2 -TRANSIENT STATES

V.2.a-Skin effect : During the period of increasing current, the elementary theories predict an important skin effect ; particularly, if we take all the transport coefficients neoclassical, we will find a persistent skin effect which was never observed in the actual experiments. We must then assume anomalous transport coefficients during the initial stage of the discharge. Many explanations are possible : the skin effect tends to decrease the shear and even up to the zero value and this may suppress an important stabilizing factor. The appearance of the tearing mode is also possible. The gradients of the current and the temperature having become

important, this may be a source of non M.H.D. instabilities. Whatever may be the physical reason, we can try to find the expressions of transport coefficients to simulate the experimental effects. The following results have been obtained :

The skin effect may be partially suppressed in the actual Tokomaks, by using an anomalous electrical resistivity of the type $\gamma(\theta)$ or a pseudo-classical heat conductivity K_e. But for the total elimination of the skin effect in the short period observed, one needs a resistivity or heat conductivity very anomalous. For example we have used[9] $K_e = 5000\ K_{PS}$ when the shear is less than some given value. However, Duchs et al.[17] have shown that, to suppress the skin effect in large Tokomaks with current intensity of Mega amperes rising linearily in 50 milliseconds, these anomaly coefficients are not sufficient (one needs a factor one hundred times greater); one may predict then that the skin effect will appear. But we can obtain the suppression of this skin effect by a moving limiter synchronized with the rising plasma current ; this solution was suggested by Kadomtsev and numerically studied by Duchs et al.

V.2.b-Variation of external conditions during the evolution.

The assumption of the heat conductivity dependent on the shear, which we use to suppress the skin effect during the rising of the current, can also explain the results of Mirnov's types[18]. In this case the reincreasing of the current after a slight decrease, impairs very strongly the confinement -time and the total energy of the plasma. This phenomenom seems to be due to the decreasing of the shear created by the reincreasing of the current, because in that case only the shear varies significantly, the temperature gradient remaining very normal.

V.3 -FUNCTIONAL FORM OF THE TRANSPORT COEFFICIENTS.

As we have just seen several forms have been suggested for K_e to explain the behaviour of Tokomak discharges. This coefficient is quite probably anomalous . Using the neoclassical form[19,20,21] one obtains a proper stationary state with multiplying factor of order 30. As the present Tokomaks are in the plateau regime we have $K_e \sim nT^{3/2}(\frac{r}{B_\theta})$. The temperature profile is found to be of parabolic type in good agreement with the results of T3. The pseudo-classical form can be written : [6,11].

$$K_{PC} = 5\,\frac{n\rho_{e\theta}^2}{\tau_e} \sim \frac{n^2}{\sqrt{T_e}}\,\frac{1}{B_\theta{}^2}$$

For the T3 experiment the values of K_{PC} and of 30 K_{NC} are roughly

the same, and this explains the similar results obtained. However, these two types of coefficients never give sharp temperature profiles as observed on S.T. (At least without a large amount of external neutrals ?). We had suggested at the Madison Conference the use of an expresssion of the type $\frac{n^2}{\sqrt{T_e}} \left(\frac{r}{B_\theta}\right)^2$ that is to say the Pfirsh and Schlüter form of K_e for large values of q[22,23]. We shall write it λK_{PS}. We then get either stationary profiles with permanent skin effects or profiles which become sharper and sharper about the center of the plasma. The sharp profile is due to the term $T_e^{-1/2} \left(\frac{r}{B_\theta}\right)^2$ in the transport coefficient. This term decreases strongly when T_e and the current density increase, leading to a reduction of thermal losses and a further increase of temperature and current density at that point. On the contrary, in the pseudo-classical case, the profile does not become sharp because $\frac{K_{PC}}{K_{PS}} \sim \frac{1}{r^2}$. This ratio goes to infinity in the vicinity of the center of the plasma and it is sufficient to prevent any thermal instability. So with the functional form K_{PS} the value of K_e decreases with time until it becomes smaller than neglected terms of K_e which can then stop this increase of temperature in the center of the plasma. This saturation might come neoclassical terms, but the simplest methos is to use the complete form of Pfirschand Schlüter

$$K_e = \lambda K_{Spitzer}(1 + 1{,}6\ q^2) \sim \frac{n^2}{\sqrt{T_e}} (1 + 1{,}6\ q^2)$$

with $q = \frac{r}{R} \frac{B_\phi}{B_\theta}$. The obtained profiles are different depending on the value of q_{edge}. The stationary sharpness decreases as q_{edge} decreases for the Spitzer term alone gives a very flat profile.

The numerical study of this law with $\lambda = 2000$ for hydrogen discharges gives a good agreement with experimental results but the computations show the very great importance of the initial conditions for all the transient states of the discharge.

If we employ an empirical law, taking into account that the plasma is most probably very turbulent at the beginning of the discharge and that the turbulent region progressively shrinks toward the boundary on a

few milliseconds, it is possible to obtain with the same law both peaked profiles of the S.T. and flat profiles obtained on T_3 in the experimental times. This remarkable result is due to the very great sensibility of the law in $\frac{1}{\sqrt{T_e}} (\frac{r}{B_\theta})^2$ with the various parameters of the discharge. Fig. 1 shows the electron temperature on the axis as a function of time for the following two cases a) S.T. $B_\phi = 27$ KG ; $I_{\phi max} \sim 35$ KA ; $\bar{n} \sim 2.10^{13}$

b) T3 $B_\phi = 17$ KG ; $I_{\phi max} \sim 60$ KA ; $\bar{n} \sim 10^{13}$

and Fig.2 shows the profiles obtained in these two cases compared with the experimental results.

V.4)-SCALING LAWS

One of the typical applications of the numerical model is to study the scaling laws in Tokomaks. As an illustration of such computations, we will present the study of the scaling law for the ionic temperature in Tokomaks and we will compare the results of our computations with the scaling laws given by Artsimovich [24]. The computations are carried out with the following assumptions for the transport coefficients :

Electronic heat conductivity $K_e = 30 \times K_{e\ \text{neoclassical}}$

Ionic heat conductivity $K_i = 1 \times K_{i\ \text{neoclassical}}$

Electrical resistivity $\eta = 2 \times \eta_{\text{classical}}$

We have plotted in Figure 3 the average ionic temperature versus the total current intensity for three values of the particle density. Logarithmic coordinates are used. The curve ($T_i \sim$ Log I) practically consists of two straight lines, with different slopes, joined by a Knee. The bigger slope corresponds to the "banana" regime and the lower slope corresponds to the "plateau" regime. The values of the slopes are respectively 2 and 2/3, which means that, for given B_z and n_o, the ionic temperatures vary as $T \propto I^2$ for banana regime and $T \propto I^{2/3}$ for plateau regime.
Moreover, the ionic temperature, in the two regimes, is decreasing for increasing particle density. These results are to be compared with the formulae of Artsimovich

$$(1) \begin{cases} T_i \propto (B_z n_o I R^2)^{1/3} \bar{A}_i^{-1/2} & \text{(plateau regime)} \\ T_i \propto I^2 \sqrt{\frac{R}{a}}\ \bar{A}_i^{-3/2} & \text{(banana regime)} \end{cases}$$

In the "plateau" regime, the slope 2/3 found in our computations is different from the slope 1/3 given by formula (1). In the "banana" regime, the law $T_i \propto I^2$ computed by our model is in agreement with the theoretical analysis, but our computations give a dependence of the ionic temperature on the particle density while the Artsimovich formula (1) does not show such a dependence.

The explanation of these differences is due to the basic assumption of Artsimovich's analysis

$$1.6 < \frac{T_e}{T_i} < 10.$$

This assumption shows that the ion energy balance equation is independent of the electron temperature.

We have plotted in Figure 4 the ratio T_e/T_i versus the current intensity I for different values of the particle density n_o. For increasing values of n_o, the condition

$$\frac{T_e}{T_i} > 1.6$$

is violated, since the energy transfer from electrons to ions by Coulomb collisions is proportional to the square of the particle density. So for higher values of n_o, in the formula of the "banana regime"

$$T_i = gI^2\sqrt{\frac{R}{a}}\ A_i^{-3/2}$$

the coefficient g is not a constant but a function of n_o. This coefficient is plotted in Figure 5. A dimensional analysis may be carried out when

$$T_e/T_i = 1 + h$$

(h being a small quantity ; this happens when n_o is high).
In this case, it is necessary to use the ion energy balance equation coupled with the electron energy equation. We find, for the "banana regime" when $\frac{T_e}{T_i} \simeq 1$,

$$T_i = \lambda \frac{I^2}{n_o a^2 A_i^{1/4} \varepsilon^{1/4}}$$

where λ is a constant depending on the distribution of current and density over the plasma cross section. We may conclude this discussion by stating that the scaling law for the ionic temperature in the "banana regime" is

$$\begin{cases} T_i = g\, I^2\sqrt{\frac{R}{a}}\ \bar{A}_i^{-3/2} & \text{for } \frac{T_e}{T_i} > 1.6 \quad (n_o \text{ small}) \\ T_i = \lambda \frac{I^2(\frac{R}{a})^{1/4}}{na^2 A_i^{1/4}} & \text{for } \frac{T_e}{T_i} \simeq 1 \quad (n_o \text{ high}) \end{cases}$$

(g and λ are constants).
Let us point out that the dependence of the ionic temperature on the atomic mass A_i is different in these two formulae : It is much less sensitive for

high values of the density n_o.

REFERENCES

[1] Y.N. DNESTROVSKII, D.P. KOSTOMAROV, N.L. PAVLOVA,Int. Symp. on closed Confin. System, Dubna (1969).

[2] H. LUC, C. MERCIER, SOUBBARAMAYER, Intern. Symp. on closed Confin. system, Dubna (1969).

[3] Y.N. DNESTROVSKII, D.P. KOSTOMAROV, N.L. PAVLOVA. Fourth European Conf. on Contro. Fusion and Plasma Physics, Rome, Italy (1970), p 17.

[4] C. MERCIER and SOUBBARAMAYER, Fourth European Conf. on Contr . Fusion and Plasma Physics, Rome, Italy (1970), p.16.

[5] D.F. DUCHS, H.P. FURTH and P.H. RUTHERFORD, 4th Internat. Conf. on Cont. Fusion, Madison, CN 28/C-4 (1971)

[6] BARNETT et al. 4th Internat. Conf. on Cont. Fusion, Madison,CN 28/C-1 (1971).

[7] M.N. ROSENBLUTH, R.D. HAZELTINE, F.L. HINTON, Physics of Fluids,15,n°1 (1972)116.

[8] A.A. WARE, Phys. Rev. Lett. 25 (1970) 916.

[9] C. MERCIER , SOUBBARAMAYER, J.P. BOUJOT, 4th Intern. Conf. on Cont. Fusion, Madison (1971), CN 28/C-7.

[10] L.A. ARTSIMOVICH,Zh . Eksp. Teor. Fiz. 13 (1971) 101,Sov. Phys.JETP Lett. 13 (1971) 70.

[11] S. YOSHIKAWA, Phys. Rev. Lett. 25 (1970) 353.

[12] M.M. WIDNER, R.A. DORY, J.T. HOGAN, Phys. Lett., 36, n°3 (1971) 217.

[13] Y.N. DNESTROVSKII, D.F. KOSTOMAROV, N.L. PAVLOVA, Atomnaya Energya 32, (1972) 301.

[14] S.I. BRAGINSKII, Transport processes in a plasma. Reviews of plasma Physics, Vol.1 , Consultants Bureau New-York (1965).

[15] L.F. ISAENKO, L.V. MAIOROV and D.A. CHEGLOV, Zh. E.T.F. Letters 12, (1970) p. 320.

[16] D. DIMOCK and E. MAZZUCATO, Phys.Rev. Letter 20 (1968) 713.

[17] D.F. DÜCHS, H.P. FURTH, P.H. RUTHERFORD, Nuclear Fusion, 12 n°3 (1972), 391.

[18] S.V. MIRNOV, Nuclear Fusion 9 n°1 (1969) 57.

[19] A.A. GALEEV, and R.Z. SAGDEEV, Zh. Eksp. Teor. Fiz. 53 (1967) 348 ; Sov. Phys. JETP 26 (1968) 233.

[20] L.M. KOVRIZHNYKH, Zh. Eksp. Teor. Fiz. 56 (1969) 877 ; Sov. Phys. JETP 29 (1969) 475.

[21] H.P. FURTH, M.N. ROSENBLUTH, P.H. RUTHERFORD and W. STODIECK, Phys. Fluids 13 (1970) 3020.

[22] D. PFIRSCH and A. SCHLÜTER, Max Planck Inst. Report N° MPI/PA/7/62.

[23] V.D. SHAFRANOV, Plasma Physic 8 (1966) 314.

[24] L.A. ARTSIMOVICH, Nuclear Fusion 12, n°2 (1972) 215.

TABLE I : TRANSPORT COEFFICIENTS IN SOME NUMERICAL MODELS.

Ref.	D	K_e	K_i	α	η	Observations
1,3	(NC)	$\gamma(\theta)$(NC)	(NC)	$\gamma(\theta)$	$\gamma(\theta)$	FP
13	(NC)	$\gamma_1\gamma(\theta)$(NC)	(NC)	1	$\gamma(\theta)$	γ_1=7 FP with neutrals
13	(NC)	$\gamma(\theta)$(NC)	$\gamma(\theta)$(NC)	$\gamma(\theta)$	$\gamma(\theta)$	FP with neutrals.
12	(PC)	(PC)	(NC)	1	γ_r	FP-C $=(\frac{10.8\times10^{13}}{n})^{3/2}$
5	(NC) or 0	Z(PC)	Z(NC)	1	Z	Z_i = 2-4 ; FP or PP with neutrals C = 5 The coefficients NC are very precise in the banana zone.
2,4	0	λ(NC)	(NC)	1	Z,$\gamma(\theta)$	$\lambda \# 30$; Z = 2-4 FP
9	0	λ(PS)	(NC)	1	Z	$\lambda \# 2000$; Z = 2-4 FP or PP according to the regimes. Now with neutrals.

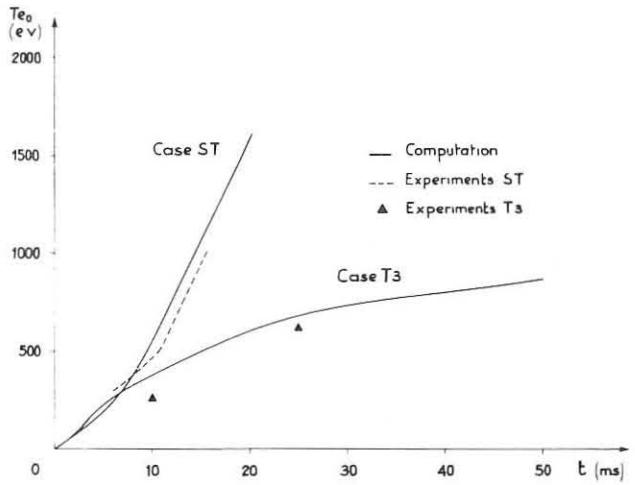

Time behaviour of the axial electron temperature

Fig. 1

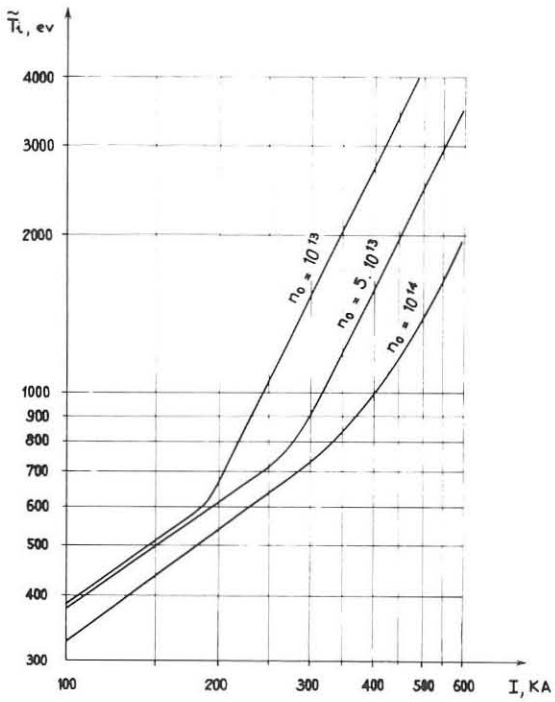

Ionic temperature versus total current intensity in the Tokomak of Fontenay (a = 20cm R = 98cm Bz = 60 KG)

Fig. 3

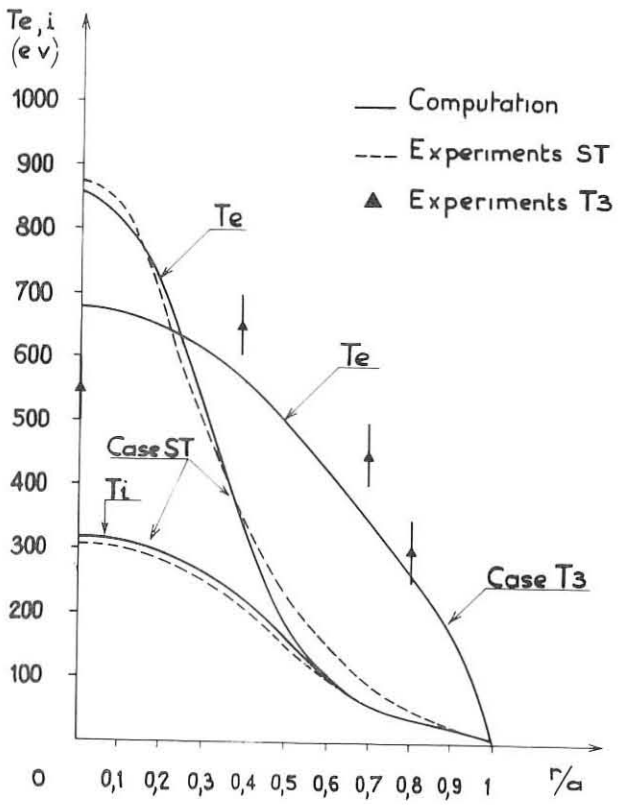

Fig. 2 Radial distribution of Te

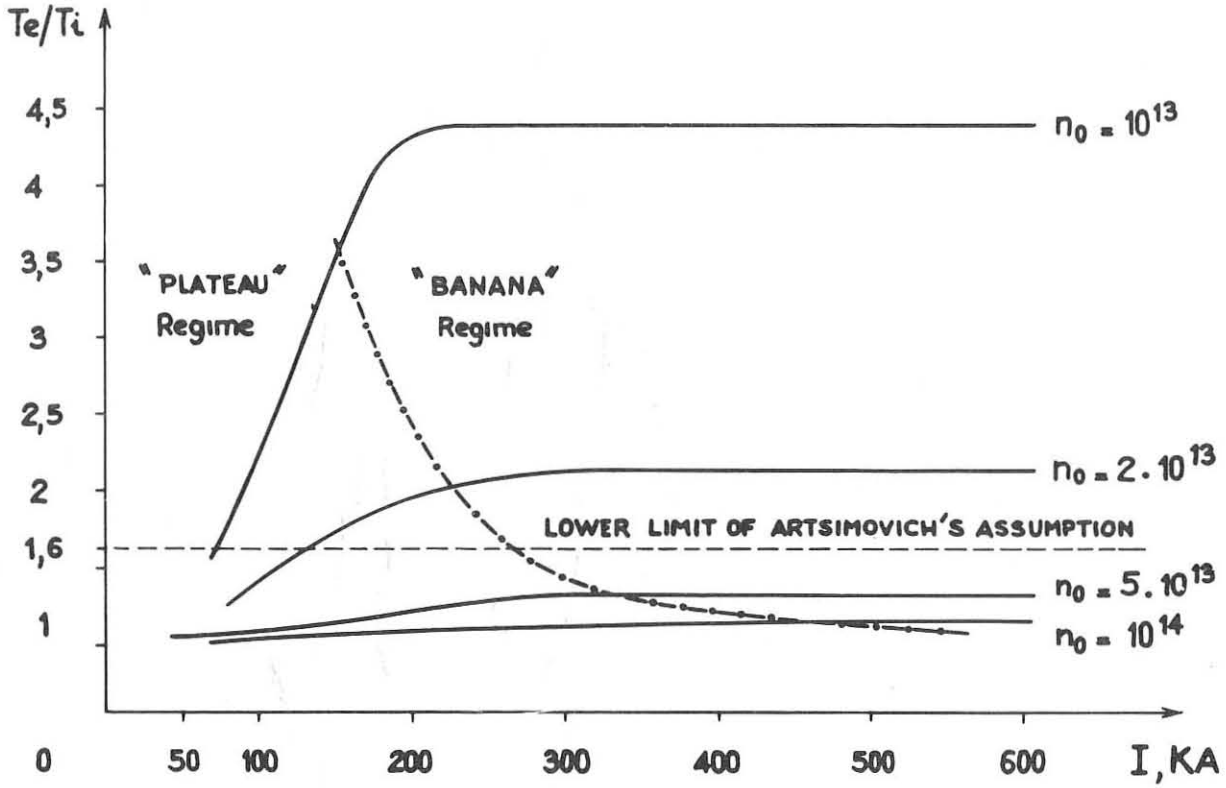

Fig. 4 Ratio Te/Ti versus the current intensity

—·—·— Separation limit of the regimes Plateau - Banana $(\nu = \nu_1)$

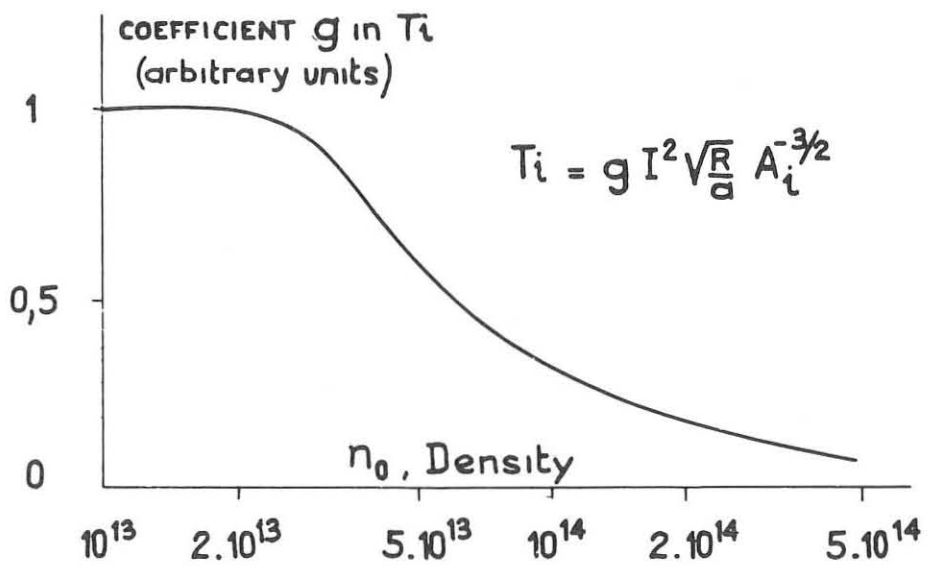

Fig. 5 Coefficient g in the formula for ionic temperature $Ti = g I^2 \sqrt{\frac{R}{a}} A_i^{-3/2}$

LASER CREATED PLASMAS AND CONTROLLED THERMONUCLEAR FUSION

by

J.L. BOBIN

Commissariat à l'Energie Atomique, Centre d'Etudes de Limeil

B.P. n° 27 - 94-VILLENEUVE-SAINT-GEORGES, FRANCE

Abstract : Up to date data about lasers and laser created plasma experiments are given. Possible mechanisms leading to neutron emission from such plasmas are discussed. Proposals for the use of laser created plasmas in controlled fusion systems are reviewed.

1. Introduction

Scientists have been thinking about the use of lasers in controlled thermonuclear fusion for nearly ten years. Indeed, three quantities should have high values in any kind of thermonuclear device : plasma lifetime density and temperature. It is expected that laser interaction with matter will heat significantly a fairly dense medium. Then, hopefully one would not even have to worry about the lifetime.

This is due to the fact that radiation at optical frequencies is easily concentrated by a lens or a mirror. Flux densities ϕ up to $10^{16} W/cm^2$ are thus obtained. If this energy is communicated to some motionless matter with a high efficiency, the subsequent energy density is somewhat greater than the corresponding instantaneous ϕ/c.

There exist several ways of using this basic idea in a fusion machine. Before they are reviewed, it is convenient to give an account of the laser state of the art and of the main data collected from interaction experiments.

2. High power laser data

So far, three laser materials have been used for delivering high powers : ruby, neodymium glass and gaseous CO_2. Due to its prohibitive cost ruby is not suitable for fusion research. The principle and operation of giant pulse Nd glass laser and TEA CO_2 lasers are extensively described in the litterature . So we shall restrict ourselves to the latest major improvements which allow experimentalists to get the laser performances

listed in the following table :

Table 1 : High power laser data

Operating mode	Ruby 694.3 nm		Nd Glass 1.06 µm		TEA.CO_2 10.6 µm	
Superradiant	-		1 kJ	1 µs	300 J	100 ns
Q switched	10 J	5 ns	1,3 kJ	15 ns	50 J	50 ns
Q switched + external shutter	1 J	1 ns	125 J	3 ns		
Mode locked		20 ps	50 J 500 J	2 ps 100 ps	4 J	2 ns

Nd glass

In order to increase the energy and power of such lasers one may set up several cascades in parallel (C.E.A. in Limeil - Lebedev Institute in Moscow) and at the same time improve the oscillator (NRL in Washington DC) and the efficiency of the last amplifying stage (NRL in Washington, L.R.L. in Livermore, University of Rochester). The main limitation to the energy delivered by a single cascade comes from the damage threshold. Hence the difficulty of pumping large diameter glass rods with the light of flash lamps. Due to the high absorption, only the outer part of the rod is efficiently used in laser action. The trick used to get rid of it, is the disc amplifier originally designed at Livermore : both optical pumping and extraction take place through the flat surface. Thus higher diameter beams can be amplified : typically 150 mm instead of 80 mm. Such a device is sketched on fig. 1.

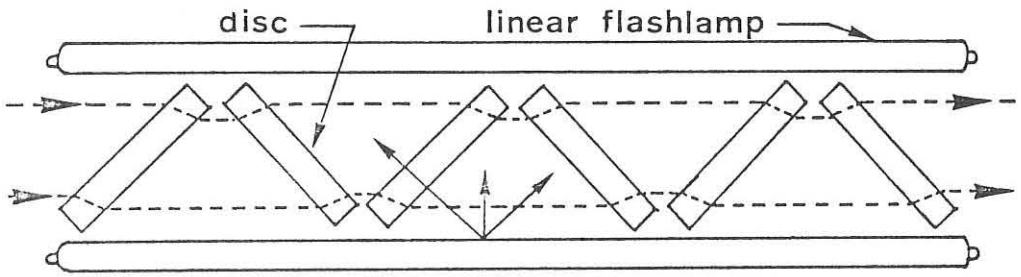

Fig. 1 : Principle of the disc amplifier

On the other hand, newly devised oscillators deliver stable pulses of controlable shape with a gaussian illumination distribution in the beam cross section.

Nd glass lasers of 10 kJ in the nanosecond or subnanosecond range are expected by 1975.

Transverse Electron pumping at Atmospheric pressure CO_2 laser

Such lasers look very attractive : their efficiency is comparatively high ($>$ 10 %). The internal breakdown threshold is low but since the active medium is gaseous, the damages are not serious. Furthermore pumping by electrons can be efficiently performed even in large diameter devices. Various geometries were successfully tested. The double discharge system originally devised at C.G.E. Marcousis, gives the higher power obtained so far : 3 GW from a superradiant 7 meters long laser set up at NRC Ottawa /1/. Another promising method under active research and development at Livermore and Los Alamos, uses 100 keV - 1 MeV electrons to preionize the active medium. Thus high presure gas (up to 20 atmospheres) or larger volumes can be pumped by the main discharge (fig. 2). The extracted power is then significantly increased /2/.

The TEA CO_2 laser is only 4 years old. Performances are rising rapidly and 10 kJ systems in the 100 nanosecond range migth be available within two years. Moreover since mode locking almost spontaneously occurs in diffraction limited oscillators, single pulse extraction by an acousto-optic modulator would allow amplification of a nanosecond pulse up to 200 GW.

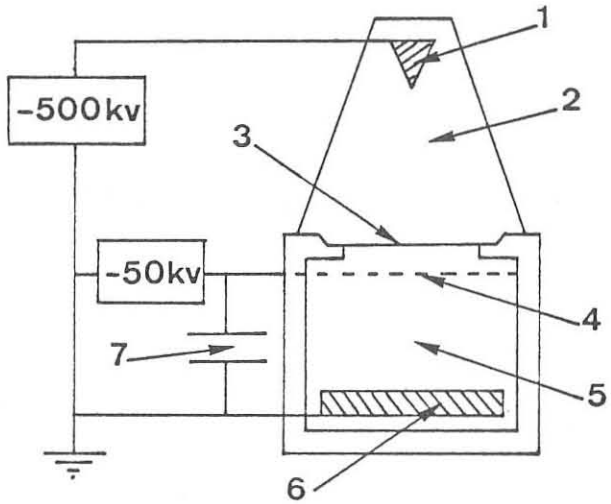

Fig. 2 : TEA CO_2 laser with electron beam preionization
1. field emission cathode
2. vacuum
3. thin Titanium window
4. grid
5. high pressure gas
6. anode
7. main capacitor bank

Some promising new comers

There is no basic physical reason why high power laser action should be restricted to neodymium glass and CO_2. Active researches are

carried on in order to get laser emission from new materials. Some recent results are worth mentioning. Giant pulses of 1.2 GW were obtained from molecular iodine pumped by chemical reactions. The wavelength is 1.315 μm /3/. On the other hand, the laser effect in the U.V. range was observed with various devices : in molecular hydrogen pumped by a travelling discharge /4/, stimulated emission was obtained at 160 nm and 120 nm. Delivered powers are still below 1 MW. Finally, electron beams pumping of high pressure xenon creates an excited state of the Xe_2 molecule. Stimulated emission at 150 nm might occur and was actually observed at Lebedev Institute in Moscow. The power is about 10 MW and the efficiency looks attractively high ($>$ 50 %).

3. Interaction of laser beams with deuteriated targets

When a laser beam impinges onto a cold solid state material, energy and momentum transfer from radiation to matter cause the latter to be heated and set into motion. If the target is located in vacuo a radiation wave of the flame type will appear. Its properties were extensively investigated both analytically and through computer experiments.

Only the main results of the theory will be stated and compared with experiments. In most experimental set-ups a single Nd glass laser beam is used. Light is concentrated by a lens onto a massive target : solid D_2 (Limeil, Rochester, Nagoya, Garching) or deuteriated polyethylene (Livermore, Moscow) or lithium deuteride (Sandia laboratories at Albuquerque, Moscow). All these lasers operate in the nanosecond or subnanosecond range or both by simply changing the oscillator. The biggest operating system has a different geometry : 9 cascades in parallel irradiating a spherical pellet. It was built at the Lebedev Institute, Moscow /5 /. Experiment with CO_2 lasers are still in a preliminary stage (Limeil, CREN in Montreal).

In many of the above quoted experiment neutrons were detected. However the numbers are quite low : 10^2 to 10^5 in the case of a single beam. The needed informations about the plasma density, temperatures and velocity are to be determined through different and more reliable diagnostics. The correspondence between the sought plasma parameters and various diagnostic methods is given on the following table.

Table 2 : Informations from diagnostics

	Plasma Velocity u	Electron density ne	Electron Temperature Te	Ion Temperature Ti	Non Linearities
Streak camera	x				
Interferometry	x	x			x
X ray emission			x		x
Reflected light	x		x		x
Light scattering	x			x	x
Mass spectrography			x	x	x
Neutrons				x	x

Collecting the results from different laboratories one may state that with fluxes about 10^{14} W/cm^2 electrons temperature around 1 keV were actually obtained. The ion temperature might be slightly above 500 eV. Furthermore, it is firmly established that the neutron emission from DD nuclear reactions is strongly correlated to a high reflectivity and also to unexpectedly high energy ions.

Now, theories predict two possible mechanisms for heating a target once the light energy is absorbed : 1) a heat wave due to the strong non linear thermal conductivity of free electrons ; 2) a propagating light driven flame. It can be shown that the former occurs for rapidly rising fluxes whereas the latter prevails in the case of a constant flux. So a first question arises : which mechanism is dominant in an actual interaction experiment ? Another question of importance deals with the absorption of laser light : does it occur only through linear processes or do non linear effects take place ?

The neutron yield and the plasma interferometry can bring elements to answer the first question. Assume the heat wave is the dominant heating process. The evaluation is simpler in the case of short pulses depositing instantaneously an energy W_A in the focal spot /6/.

Suppose the temperature is constant between the focal spot and the location r_p of the hemispherical wavefront. Then the heat equation is

$$r_p \frac{dr_p}{dt} = c\, T_e^{5/2} \tag{3.1}$$

the energy conservation equation is

$$T_e + T_i = \frac{W_A}{2\pi n r_p^3} \tag{3.2}$$

and the relaxation between ions and electrons is described by

$$\frac{dT_i}{dt} = b\, \frac{T_e - T_i}{T_e^{3/2}} \tag{3.3}$$

(b and c are constant determined from general properties of plasmas). If the above equations are solved for Ti one finds for this parameter a maximum value

$$T_{i_{max}} = a\, W_A^{1/7} \qquad \text{(a is a constant)} \tag{3.4}$$

The thermal wave is taken over by a rarefaction wave after a time

$$\tau = d\, W_A^{3/14} \tag{3.5}$$

at a position

$$r_p(\tau) = g\, W_A^{2/7} \qquad \text{(d and g are also constant)} \tag{3.6}$$

These two last equationsdefine the hot region of volume $\mathcal{V} \propto r_p^3$ in which thermonuclear reaction might occur. Their number is given by

$$\frac{dN_R}{dt} = \frac{n_i^2}{2} \langle \sigma v \rangle \mathcal{V} \tag{3.7}$$

where $\langle \sigma v \rangle$ is the thermonuclear reaction rate which in the range 0.5 - 1 keV is proportional to $T_i^{5.5}$

Hence in a time interval $\delta t \sim \tau$ a number of reactions proportional to

$$W_A^{6/7} \cdot W_A^{3/14} \cdot W_A^{5.5/7} = W_A^{13/7} \sim W_A^2 \tag{3.8}$$

On the contrary in laser driven flame there is a definite relationship between the plasma temperature and the incoming flux. For instance in the case of Nd laser light and deuterium one has /7 /

$$T_{keV} = 3.5\ 10^{-14}\ \phi_{cgs.}^{2/3} \qquad (3.9)$$

Hence the proportionality

$$T_i \propto \phi_A^{2/3} \qquad (\phi_A \text{ absorbed flux})$$

When such a regime is set up the hot plasma is not uniform. The cut off density at which most of the radiation energy is absorbed is located in a rather steep density gradient. Electron thermal conduction is a strong heating mechanism for an overdense region the thickness of which is /8/

$$L \propto \frac{T_i^2}{n_{i\ cutoff}} \qquad (3.10)$$

Since the number of thermonuclear reaction is proportional to n_i^2 it is expected that most neutrons come from the overdense region. Then (3.7) in the plane case reduces to

$$\frac{dN_R}{dt} \propto L \langle \sigma v(T_i) \rangle \qquad (3.11)$$

Hence

$$N_R \propto T_i^2 \cdot T_i^{5.5} = T_i^{7.5} \propto \phi_A^5 \propto W_A^5 \qquad (3.12)$$

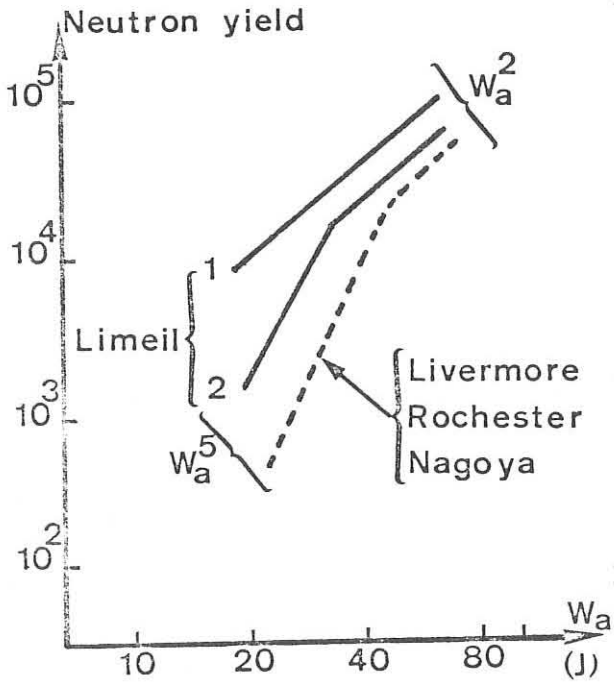

Fig. 3 : 1. focal spot 100 μm
2. focal spot 150 μm

Experimental results yield for the number of neutrons versus the absorbed laser energy the plot of fig. 3. These results were obtained with short (2 - 4 nsec) pulses with a steep leading edge (a factor 5 10^5 in 1.5 nsec at Limeil). It can be seen that if the neutrons were thermonuclear, they would be generated in a radiation driven flame at the lower fluxes, in a thermal wave at the higher fluxes associated with fast rising pulses. Figure 4 shows which regime is expected to be dominant.

The occurence of a thermal wave is indirectly confirmed by

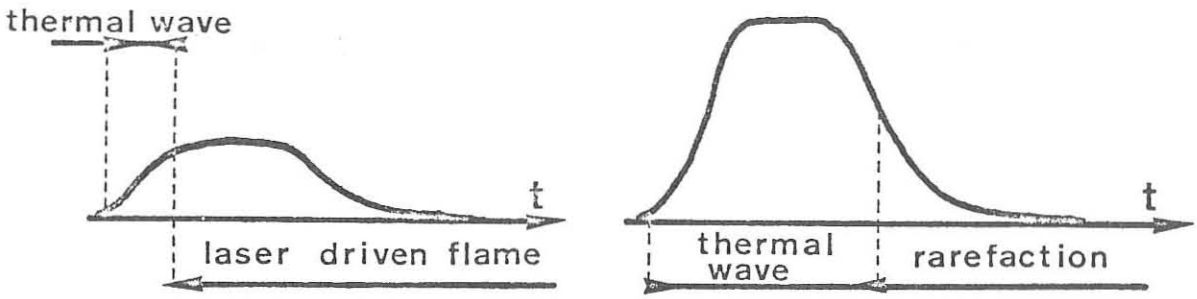

Fig. 4 : Possible heating mechanisms during the laser pulse

interferometric measurements of the electron density [9]. It was found that the density of the plasma expanding outside the target is well below the cut off. The cut off density is thus inside the target whereas it would be about 100 μm outside if a radiative flame had time to build up.

The origin of the observed neutrons is still unknown. The numbers are too small to perform any spectroscopy. The highest reported number is $2\ 10^6$ in the spherical experiment of the Lebedev Institute.

If the neutrons were not of thermonuclear origin, they would be due to some instability associated with non linear absorption of laser light by the plasma and this is the second crucial question. Many theoretical investigations were reported about these non linear effects : non linear free free absorption, anomalous heating, stimulated ion acoustic wave generation, stimulated Compton effect, harmonic generation ... Some have a definite threshold the predicted value of which is about 10^{14} W/cm^2 for 1.06 μm (Nd) light and scales as the laser frequency squared. Others have no such threshold but might influence the exchanges of energy when the flux is above that same value. Evidence of non linear effects was obtained at Limeil [10] by detecting second harmonic generation both in 90° and 0 180° directions with respect to the incident light. Also the detection of hard X rays inconsistent with thermal radiation at the expected electron temperature might be an evidence for non linear interaction. The following table 3 summarizes the connection between experimental observation with linear and non linear interaction of laser light with a plasma.

For any fusion device using lasers as a plasma heating process it is certain that higher fluxes will be needed. Then non linear effects are expected to become dominant. So they might be the essential topic in interaction physics for the coming years.

Table 3

	Linear	non linear
Expanding plasma	x	
High reflectivity	x	
Fluctuations of reflectivity		x
Satellites on the Stokes side		x
Harmonic generation		x
Soft X ray emission	x	
Hard X ray emission		x
Neutrons	x	x
Highly charged ions	x	
High energy ions		x

4. Approaches to the nuclear fusion problem

Basically, three ways are investigated : plasma injection, in which the laser created plasma is all but a source for an otherwise conventional confining device ; long wavelength heating and pellet explosion which both depend more tightly on interaction physics.

Long wavelength heating

This approach deals with magnetically confined plasmas. Fusion conditions require a temperature of about 10 keV. The needed magnetic field should be at least ($\beta = 1$)

$$B_{gauss} = 9.10^{-6}\sqrt{nT} = 9.10^{-6}\sqrt{10n} \qquad (4.1)$$

(n in cm^{-3}, T in keV)

Destructive methods have been able to yield magnetic field up to 25 megagauss whereas non destructive methods are limited to about 1 megagauss. Therefore, the density has to be less than 10^{18} cm^{-3}. Predictable technological improvements might allow one to confine a 10^{19} cm^{-3} plasma which is the cut-off density for CO_2 laser light.

Then one may imagine first a confined plasma column with density in the range 10^{16} - 10^{18} cm^{-3} produced by any kind of known process. Laser light propagating in the axial direction is absorbed. Subsequent "superheating" of the plasma occurs and conditions to get fusion were determined after detailed calculations /11/.

Assuming inverse free-free absorption, it can be shown that the energy to be transfered from radiation to the plasma ranges around 10^8 J/cm^2 and that the most favorable density is 0.1 the cut-off value. However, inverse bremsstralhung is not so good. The absorption length given by

$$\ell_{ab} = \frac{3.5\,10^7\, T_e^{7/2}}{B^4\, \lambda_L^2} \qquad (4.2)$$

is exceedingly long and an efficient system would require a plasma column about 1 km long to absorb 10μ laser radiation unless a multiple pass device is set up. Enhanced light absorption through non linear effects would markedly reinforce the interest of this scheme.

Now, it is well known that light absorption increases sharply at densities close to the cut-off : denote by ω_p the plasma frequency. Actually in (4.2) the right hand side should be multiplied by $(1-\omega_p^2/\omega_L^2)^{1/2}$ Moreover anomalous absorption is more likely to occur at cut-off. Hence the idea of using a plane one dimensional laser driven flame. The magnetic confinement helps in maintaining the geometry. Its value must be sufficiently high in order to contain the overdense region. Since this region is almost at constant pressure the needed field does not significantly exceed the one corresponding to conditions at cut-off. The energy yield in this scheme is about 2 10^8 J/cm^2 /12/. A preliminary experiment with a 350 J, 1μsec CO_2 laser and a magnetic field of 1 megagauss, looks feasible with present day technology. It would create a 1 keV plasma in the laser driven flame.

Pellet explosion

This proposal was made as early as 1963 /13/. It is the most consistent with the above stated property of laser light to be concentrated and yield high energy densities. Basically a small spherical speck strongly irradiated in the focal volume of one or several converging lenses is instantaneously heated to thermonuclear temperatures and is expected to react before it expands and cools down. Actually things are not so simple : the heating mechanism takes time and detailed calculations grounded on a

detailed analysis of the interaction physics are required. Starting from different assumptions the many theoreticians who studied this problem strongly disagree on the minimum energy needed and the size of the pellet (initially in the solid state). Results are in the range 10^8 - 10^{12} joules with a marked peak at 10^9.

An important parameter in the problem of fusion by pellet explosion is the initial density. As it is well known, for a given mass of fuel the number of thermonuclear reactions scales as n_i^2 whereas the deconfining time scales as $n_i^{-1/3}$. Obviously the higher the density, the larger is the number of nuclear reactions before the compressed medium blows apart.

It can be shown from simple minded ideas or from a more sophisticated analysis /14//15/ that the minimum energy to be communicated to the pellet is

$$W_{min} = k \left(\frac{n_s}{n} \right)^2 \qquad (4.3)$$

where n_s denote solid state density and k is a coefficient the value of which depends on the physical mechanisms investigated and on fusion criterions. For instance k would be 2 10^8 joules using the Lawson criterion and assuming an initially hot pellet. Since the Lawson criterion takes into account an overall efficiency of the energy cycle equal to 0.3, a more reasonable value for k might be 10^9 joules.

In order to match this requirement to present day laser state of the art or even to predictable technological advances, the compression ratio (with respect to solid state) should be at least 10^3. We know from the analysis of the laser driven deflagration that material pressures higher than 10^{13} baryes can be generated and were actually obtained in interaction experiments. Such pressures are still unsufficient to compress a solid pellet up to a very high density. However, detailed calculations were made by J. NUCKOLLS and his coworkers at Livermore /16/. They show that high energy subnanosecond pulses of Nd glass light would do the job. The energy range for breakeven (energy released by nuclear reactions equal to the laser beam energy) is 10^3 to 10^6 joules depending on compression. Finally it should be noted that the higher the laser frequency the easier high pressures are produced.

Conclusion

Requirements for lasers corresponding to both reviewed approaches : long wavelength heating and pellet explosion can be summarized on the following table. Up to date data concerning TEA CO_2 and Nd glass laser are also given for comparison.

Table 4 : Laser requirements for breakeven

	Heating of confined plasmas	TEA CO_2	Pellet Explosion	Nd
Efficiency	30 %	20 %	10 %	1 %
Energy	10^7 - 10^9 J	300 J	$n=n_s$ 10^9 J $n=10^3 n_s$ 10^3 J	10^3 J
Power	10^{11} - 10^{13} W	10^9 W	$\gg 10^{12}$ W	10^{10} - 10^{13} W
Wavelength	$>$ 10 μm	10 μm	100 - 200 nm	1.06 μm

Except for the case of pellet explosion after compression the energy gap is still quite large. In the latter approach the gap would rather exist for the powers. However, due either to the high temperatures, or the high pressure driven flows already available in experiments on laser interaction with matter, many advances can be expected in two domains : first, a better knowledge of the interaction physics under high fluxes, specially of non linear phenomena. Second, creation of plasmas, parameters of which are closer and closer to fusion requirements.

REFERENCES

/1/ M. RICHARDSON, 7th IQEC, Montreal, 1972
/2/ C.A. FENSTERMACHER et al., A.P.L., 1972, 20, p. 56
/3/ K. HOHLA, K.L. KOMPA, 7th IQEC, Montreal, 1972
/4/ R. HODGSON et al., R. WAYNANT et al., 7th IQEC, Montreal, 1972
/5/ N.G. BASOV et al., EPS conf. Quant. Elec. Hull, 1971
/6/ S.D. ZAKAROV et al., Kvantovaia Electronika, 1971, 2, p. 104
/7/ C. FAUQUIGNON, F. FLOUX, Phys. Fluids, 1970, 13, p. 386
/8/ J.L. BOBIN, Phys. Fluids, 1971, 14, p. 2341
/9/ F. FLOUX et al., 7th IQEC, Montreal, 1972
/10/ M. DECROISETTE et al., J. Phys., 1971, C2b, p. 119
/11/ J.M. DAWSON et al., Proceedings 4th I.A.E.A. conf. Madison, 1971, I, p. 673
/12/ J.L. BOBIN et al., Nuclear Fusion, 1972, 12, n° 4
/13/ N.G. BASOV, O.N. KROKIN, 3d IQEC, Paris 1963
/14/ J. NUCKOLLS and L. WOODS, annual meeting of A.A.A.S., december 1971
/15/ J.G. LINHART, Nuclear Fusion 1970, 10, p. 211
/16/ J. NUCKOLLS et al., 7th IQEC, Montreal 1972

RECENT PROGRESS IN RESEARCH ON PLASMA FOCUS

Ch.MAISONNIER, F. PECORELLA, J.P.RAGER, M. SAMUELLI
Associazione EURATOM - C.N.E.N. - FRASCATI

ABSTRACT.

For Dense Plasma Focus experiments, a model in which the plasma column is disrupted after maximum compression (first neutron burst) by m=0 instabilities, and later heated to higher temperatures by turbulent mechanisms (second neutron burst), is shown to check well with experimental observations. The scaling laws of Plasma Focus devices are deduced. They compare satisfactorily with the available experimental scaling laws. The main parameters of the Megajoule experiment to be built in Frascati within the framework of a joint European programme are indicated.

1. INTRODUCTION.

The detailed observations reported at the Madison Conference and later (ref.1,2,3,4,5) do not fit at all any of the simple models proposed previously (beam-target, moving boiler, Morozov flow) for the structure of the compressed phase of the Dense Plasma Focus (D.P.F.). Using a more sophisticated model (ref. 6), relying upon the interaction of ions accelerated non-axially by ExB fields during an assumed anomalous diffusion of the azimuthal magnetic field in the plasma column, it is possible to justify the results obtained from various time integrated neutron diagnostics making rather arbitrary assumptions. In the present work, a model based upon the turbulent heating of the plasma column after maximum compression is shown to describe conveniently the behaviour of D.P.F. devices working in the "high pressure" regime (ref.5), whereas ion acceleration mechanisms are likely to be of paramount importance in the "low pressure" regime (ref.5,7).

2. MODEL.

One of the striking observations is that most of the neutrons are emitted some time after the collapse on the axis. For the Frascati machine (fig.1) (a rather typical example of the high pressure regime), when working at 32 KV 77 Kj, the characteristics of the pinched plasma at the time of collapse are: radius $\simeq 2$ mm, temperature $\simeq 1,5$ KeV, density $\simeq 2.10^{19}$, life-time $\simeq 40$ nsec, whereas the main neutron emission comes later ($\simeq 60$ nsec) from a plasma which is more extended (radius $\simeq 8$ mm), hotter (6÷10 KeV), more tenuous ($n \simeq 10^{18}$), and of longer life-time ($\simeq 100$ nsec). The neutrons are mainly of thermonuclear origin ("moving boiler" who

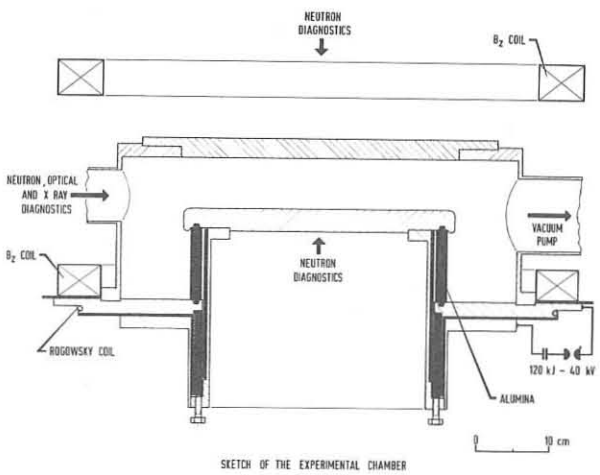

SKETCH OF THE EXPERIMENTAL CHAMBER

FIGURE 1

se axial velocity $\simeq 10^7$ cm/sec), the minority ($\simeq$ 20%) resulting from a beam-target interaction (beam of $\simeq$ 100 KeV). The values of the plasma parameters during the main compression (first, small, neutron and X-ray bursts) are in good agreement with the results of M.H.D. two-dimensional calculations (ref.8). The successive phases: absence of neutrons and X emission for $\simeq$ 50 nsec, second (and large) burst of neutrons and X, can be described by the following model: the dense plasma column at maximum compression (fig.2a) is disrupted by macroscopic m=0 instabilities (fig.2b), (ref. 2,4). The radial extension of the plasma increases, n goes down, and the magnetic field gets mixed up with the plasma. This is the "dark" pause (fig. 2c), (ref.1), during which the plasma column stores internally the magnetic energy which was present in the vicinity of the pinch; the resistivity is so low that this energy is not converted appreciably into thermal energy. At some radius of expansion, the conditions for onset of turbulent heating are satisfied

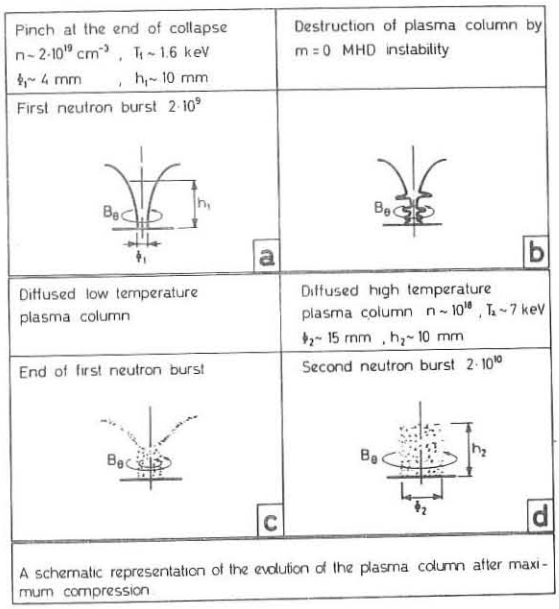

FIGURE 2

(macroscopic turbulence or some kind of microscopic instability such as the electron cyclotron drift instability), the magnetic energy stored in the plasma is transformed into thermal energy, and a second burst of neutrons and X-rays is obtained (fig.2d), (ref.1,4). Assuming that during the whole process the linear ion density N remains constant (or decreases), as well as the height H of the plasma column, the fact that the rate of neutron emission has increased (by about a factor of 4) from the first to the second burst implies that the temperature of the ions has increased noticeably. As just after collapse the only available energy is magnetic (the condensers are approximately discharged and kinetic energies are small at that time) ohmic heating should have occured at such a rate that turbulent heating is a necessity.

3. TEMPERATURE AFTER TURBULENT HEATING.

It is known (from M.H.D. calculations and from the relatively long life-time of the compressed state) that the Bennett relation holds at the instant of collapse:

$$I^2 = 4\,NkT \qquad (T_e \simeq T_i) \qquad (1)$$

There is evidence (ref.2,4 and paragraph 5 of this paper) that the current carrying column keeps contracting or at least does not expand immediately after collapse whereas the plasma radius r increases, and that the current intensity I remains roughly constant during the whole neutron emission. Between the first and the second neutron burst, the plasma column expands from r_1 to r_2, diffusing across the magnetic field, so that, when it reaches radius r_2, the magnetic energy per unit length

available inside the plasma is: $W_m = \frac{\mu_0}{4\pi} \cdot I^2 \cdot \text{Log} \frac{r_2}{r_1}$ (M.K.S.A.Units) (2)

Taking into account equation (1), and assuming that, due to turbulence, all this energy is abruptly transformed into thermal energy of 2N particles (we suppose $T_e = T_i$), the new temperature T_2 is related to the former T_1 by: $T_2 = T_1(1+4/3 \text{ Log } r_2/r_1)$ (3)

so that the ratio Q of the maximum rates of neutron emission during the second and first bursts is:

$$Q = \frac{\langle \sigma v \rangle_2}{\langle \sigma v \rangle_1} \cdot \left(\frac{n_2}{n_1}\right)^2 \cdot \left(\frac{r_2}{r_1}\right)^2 = \frac{\langle \sigma v \rangle_2}{\langle \sigma v \rangle_1} \cdot \left(\frac{r_1}{r_2}\right)^2 \quad , \text{ as } N = \pi r_1^2 n_1 = \pi r_2^2 n_2 \quad (4)$$

From (3) and (4) it results that, for a given T_1, Q is a function of r_2/r_1 only. Fig.3 shows how Q varies in function of T_1 and of the expansion ratio. The observed value $Q \simeq 4$ (ref.1) fits well with the temperature $T_1 = 1.5$-2 KeV and expansion ratio $r_2/r_1 \simeq 4$ (ref.2. paragraph 5) observed experimentally. In these conditions, eq.(3) gives $T_e \simeq 6$ KeV, which is consistent with what has been estimated (ref.1, 10 KeV) or directly measured (ref.2, 9 KeV).

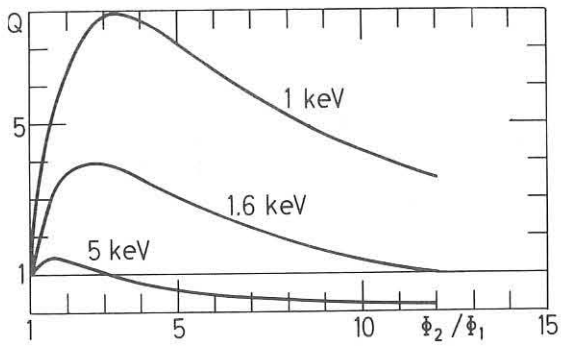

Multiplication factor Q of the rate of the neutron emission vs the radial expansion of the plasma column. FIGURE 3

4. CONDITIONS FOR TURBULENT HEATING

a) Macroscopic turbulence. Interferometric measurements (ref.2,4) show that, immediately after disruption of the plasma column by m=0 instabilities, the turbulence scale in the plasma is of the order of 2 mm. These large azimuthal vortices (ref. 9) will degenerate into smaller ones, which are not observable with the technics used up to now. Let us evaluate the time constant with which a toroidal vortex (radii A, a, thickness b, conductivity σ) dissipates its internal magnetic energy by ohmic heating:

$$\tau = L/R = \mu_0 \frac{\pi a^2}{2\pi A} \Big/ \frac{2\pi a}{2\pi A b \sigma} = \frac{\mu_0}{2} a b \sigma$$

Assuming that b is of the order of the skin-depth corresponding to the time τ (it can be checked that this is equivalent to assume $b = \frac{2}{\pi} a$, which seems reasonable), one has:

$$b \simeq \left[\frac{4\tau}{\pi \mu_0 \sigma}\right]^{1/2} \quad \text{so that} \quad \tau = \mu_0 a^2 \sigma / \pi$$

Taking for σ the classical expression (conductivity in presence of a strong magnetic field, at a temperature $T_{1/2} = 0.8$ KeV, as there should be some kind of equipartition between thermal and kinetic energy in strong turbulence), it comes:

$$\sigma \simeq \frac{4}{3} \cdot 10^7$$

and

$$\tau \simeq 5\, a^2 \qquad \text{(M.K.S.A. Units)}$$

The rise time of the second neutron burst being of the order of 20 ns, macroscopic turbulence can explain the rate of heating if the scale of turbulence goes down to: $2r \simeq 0{,}12$ mm, starting from about 2 mm some 60 nsec before (at the beginning of the dark pause). It is satisfactory to note that the Larmor radius of a 1 KeV deuteron in a 1 Megagauss field (or

der of magnitude of the azimuthal magnetic field) is 0,07 mm, that is to say of the same order of magnitude that the minimal scale of turbulence.
It seems then that macroscopic turbulence alone can explain both the existence of the dark pause and the fast plasma heating at the beginning of the second neutron burst.

b) Microscopic turbulence. As mentionned in paragraph 3, between the two neutron pulses the plasma radius r increases from r_1 to r_2 whereas the current diameter $2\alpha r$ decreases ($\alpha < 1$). Then, assuming that the plasma density is constant across r:

$$I = \alpha^2 . N . e . v_d \qquad (5)$$

where v_d is the drift velocity of the electrons.
Eliminating I between (1) and (5) gives:

$$\alpha^4 N = \frac{4}{3} \cdot \frac{m_e}{e^2} \cdot \left(\frac{v_{the}}{v_d}\right)^2$$

Numerically: $\alpha^4 N = 5.10^{12} . \left[v_{the}/v_d\right]^2$, (ions/cm)
where the thermal velocity of the electrons v_{the} remains roughly costant in time as no work is done against the magnetic pressure. The onset of microscopic turbulence occurs when v_d/v_{the} is larger than a given value; for instance, ion-acoustic instability would develop when $v_d/v_{the} \geqslant [m_e/m_i]^{1/2}$ (6)
which implies: $\alpha^4 N \leq 2.10^{16}$ (7)
and, as $N \simeq 2.10^{18}$, $\alpha \leqslant 1/3$
Then, when the radius of the plasma column reaches about 3 times the radius at maximum compression, ion-acoustic instabilities could set in. The growth rate, of the order of $\omega_{pi}[m_e/m_i]^{1/2}$, would be conveniently large (10^{10} per second) and the resistivity almost high enough, (thousand times Spitzer's) to justify the heating of 2N particles per cm height of the plasma column to a few KeV in less than 100 nsec.
It seems doubtful, however, that the condition $T_e \gg T_i$, necessary for the development of ion-acoustic instabilities, will ever be satisfied. It is well known anyway (ref.10) that turbulence is often observed even when $T_i \geqslant T_e$, and it seems that electronic cyclotron drift instabilities could be invoked in this case. To be noted that, for $\omega_{pi} \simeq \Omega_{ce}$ (electron cyclotron frequency), a condition which is certainly realized at some radius inside the plasma, this instability will require the same condition (6) and give the same growth rate as the ion-acoustic instability previously decribed.

Both macroscopic and microscopic turbulent heating seem then to find favorable conditions to develop. One could suspect that the powerful macroscopic effects, which are certainly present, are more likely to be responsible for the actual heating. Moreover, macroscopic heating can tap only the internal magnetic energy of the plasma, as calculated in paragraph 3, whereas microscopic heating has no such limitation. The agreement of Eq.(4) with experimental observations speaks then again in favor of macroscopic heating.

5) CONFRONTATION OF THE MODEL TO SOME EXPERIMENTAL OBSERVATIONS.

a) Energy absorbtion during turbulent heating. A careful time correlation between the various measurements is of paramount importance in interpreting the experimental results. Fig.(4) shows the correlation existing between the neutron signals and the values of the electrical parameters, inclu-

ding these of the ratio:

$$\left|\frac{\int_0^t U.dt}{I}\right| = L + \frac{\int_0^t R.I.dt}{I} \quad (8)$$

Up to a time t^* corresponding to the onset of turbulent heating, it is legitimate to assume that the contribution of the resistive effect is negligible so that:

$$L = \frac{\int_0^t U.dt}{I} \quad (9)$$

At time t^1, maximum of the first neutron burst, relation (9) is certainly holding, and one finds indeed a good agreement between the value of the internal inductance of the experimental chamber deduced from (9) (60 nH) and that calculated (50 nH) from the geometrical dimensions of the pinch (r= 2 mm, h=10 mm), taking due account of the additional inductance of the remaining of the current sheath and of the experimental chamber.

Fig. (4) shows that after the time t^* the quantity $\left|\int_0^t U.dt/I\right|$ is continously increasing up to a time t^{**} slightly posterior to t^2, maximum of the second neutron burst.

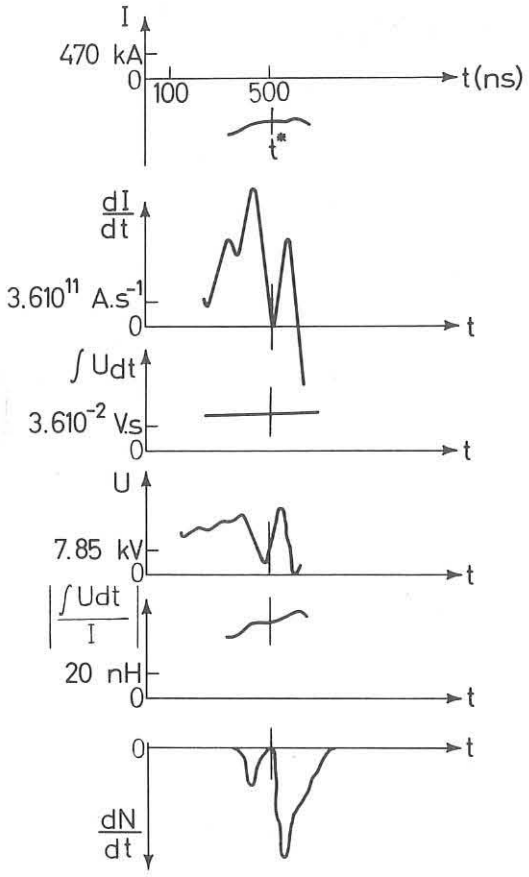

Time correlation between the electrical parameters and the PM neutron signal.
Inter-electrode gap : 7 cm
Initial conditions : V = 32 kV
p = 1.1 torr D_2

FIGURE 4

The experimental evidences (Ref.2,4) are that during this period the plasma column is expanding across the magnetic field lines (the inductance would then remain approximately constant) so that the increment of $\left|\int_0^t U.dt/I\right|$ must be interpreted in terms of a resistive effect (turbulent heating). The value of the energy absorbed in the process ($\int_{t^*}^{t^{**}} R.I^2.dt \simeq 5$ KJ) is in agreement with the energy required to heat 4.10^{18} particles up to a temperature of 5 - 7 KeV.

b) Expansion of the plasma column and neutron emission.

If the velocity of expansion of the density during the dark pause is assumed to be constant from shot to shot, the shorter is the time between the two neutron bursts, the higher will be the density during the second burst. As the magnetic energy which has been absorbed remains more or less a constant (logarithmic variation with the ratio of the final to the initial radius), the final temperature T_2 is roughly constant, and the second neutron burst should be more intense when τ is small. It is indeed observed experimentally (fig.5) that the total neutron output varies as τ^{-2} .

An examination of fig.3 shows that such a dependance had to be expected provided that the expansion ratio is appreciably larger than the value corresponding to the maximum of $\bar{Q}$.

c) Enhancement Q of the rate of neutron emission. Fig.6 shows that a typical value of $Q_{neutron}$ is 3,8 which is very close to the value given by the theory for an initial pinch temperature of the order of 1.5 KeV.
It is interesting to remark that the same ratio $Q_\gamma \simeq Q_n$ is observed for the rates of X-ray production when the X-rays are filtered by 4 mm of lead. In absence of lead shield, such a correlation between Q_γ and Q_n is not observed ($Q_\gamma \simeq 1$), which means that this excess of γ or X rays during the first burst is due to some electron beam accelerated at the time of collapse. It is then inferred that the X-rays shown in fig. 6 are produced by (n,γ) processes in the walls of the chamber ($\simeq$ 700 KeV).

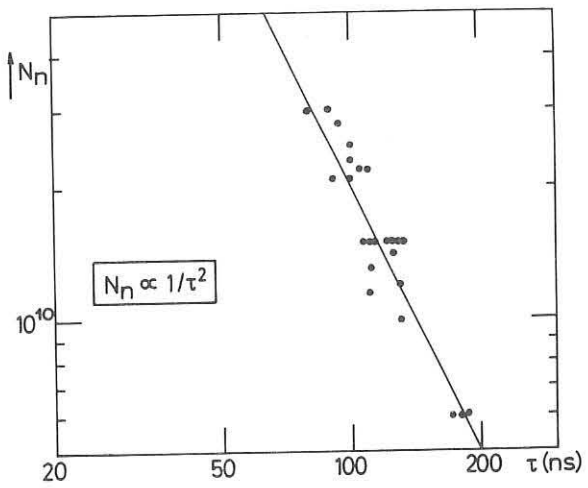

Total neutron yield vs. time delay between the two neutron bursts.

FIGURE 5

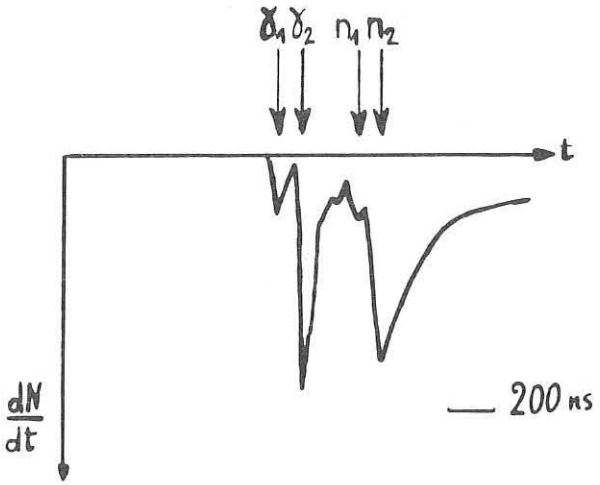

P.M. signals of γ rays and neutrons emitted from the DPF at a distance of 8.5 m. A 4 mm Pb shield is placed at 4 m between DPF and PM.
Neutron output 2.10^{10}; $Q_\gamma = 3.6$; $Q_n = 3.8$

FIGURE 6

6. INFLUENCE OF A BIAS MAGNETIC FIELD.

It is a well known feature of the plasma focus experiments that the application of a bias axial magnetic field has a net negative influence on the neutron production (Ref. 11,12).
An evaluation of the plasma parameters associated with the radial collapse of the current sheath shows that the axial field is trapped inside the sheath and therefore that its final value B_f can be deduced from the flux conservation law:

$$B_f = \left[\frac{r_{focus}}{r_{anode}}\right]^{-2} . B_c \simeq 10^4 . B_c$$

When the bias magnetic field reaches a value of the order of 100 Gauss, a sharp drop in total neutron yield is observed

(fig.7). This sharp fall is associated with the disappearance of the second neutron burst (fig.8) as well as with the

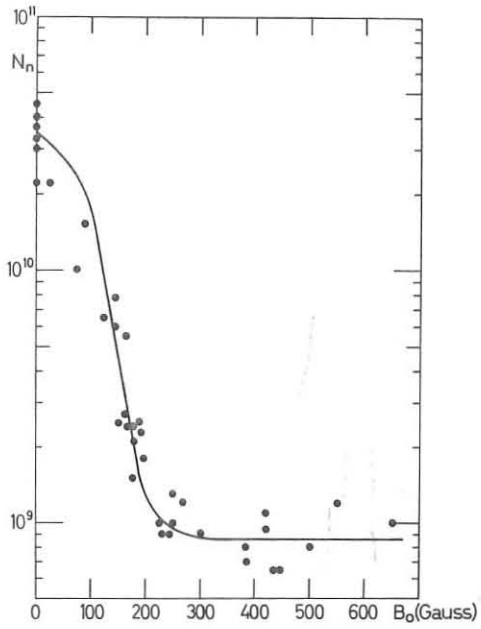

Neutron yield vs. the initial axial magnetic field

FIGURE 7

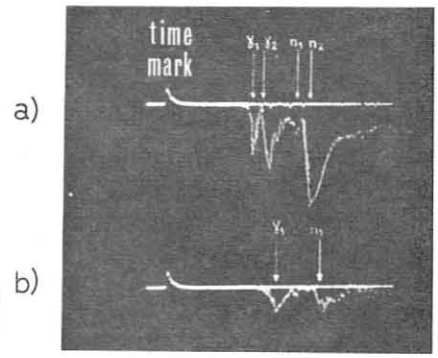

PM signals with and without the initial axial magnetic field
a) No magnetic field
b) 300 Gauss
Initial conditions : 32 kV, 1.1 Torr D_2

FIGURE 8

observation of a more stable and longer living pinch - like phase (fig.9). Increasing the field has no further inhibiting

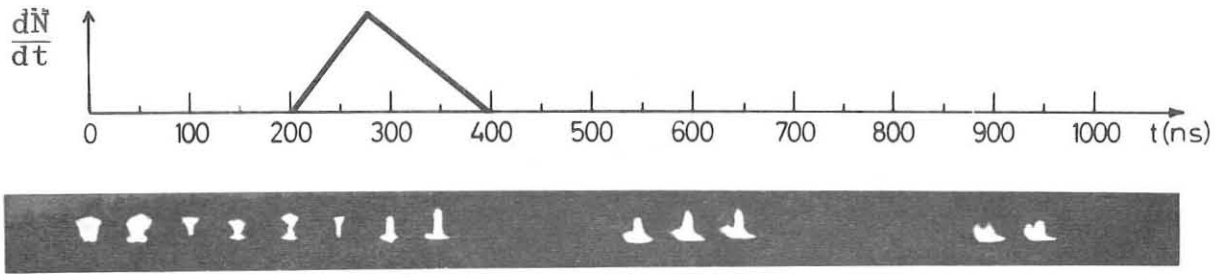

Time correlation between a typical neutron signal and framing pictures of the discharge. An initial axial magnetic field of 300 Gauss is applied.
(10 ns exposure time-visible light)

FIGURE 9

effect (it is observed that the first neutron burst, corresponding to the pinch-like structure, is almost unchanged thought a little expanded in time) up to a second critical value (900 Gauss) above which even the first neutron burst gradually disappears. These results can be interpreted as follows:
The stabilizing effect of the axial magnetic field becomes appreciable when B_z is comparable to the azimuthal field B_θ (typical value $\simeq$ 1 MG). This stabilization prevents the formation of the M.H.D. m=0 instabilities and hence the subsequent turbulent heating, so that the second neutron burst

disappears. For much higher B_θ fields (10^3 Gauss or more), the magnetic pressure associated with B_z is so large that the plasma sheath cannot collapse any more to a small radius and even the first neutron burst disappears.

7. INFLUENCE OF THE INTERELECTRODES SPACING.

The model under discussion takes only into account the radial distribution of both the plasma and the magnetic field. It was then interesting to check down to which axial height of the experimental chamber this purely radial dependence holds. For this purpose, a 2 cm electrodes spacing device has been realized and tested. Identical initial conditions were maintained with respect to the usual 7 cm spacing case: initial radius, filling pressure, and breakdown conditions, voltage, etc. The main result is that the total neutron yield is unchanged. A more detailed analysis, using as before the time correlation between electrical parameters and neutron signals (fig.10) shows that:

a) qualitatively, the mechanism for neutron production seems identical (two neutron bursts, the second one accounting for most of the emission), though occuring on a contracted time scale (dark pause twice shorter);

b) the time evolution of the inductance, as deduced from the electrical parameters, remains the same, though the absolute value of the inductance is smaller (37 instead of 60 nH). As a check, the usual kind of computation based upon the evaluation of the geometrical parameters has been performed, giving a reasonable 30 nH;

c) the final phase of the whole implosion occurs sooner for 2 cm that for 7 cm because of the smaller inductance and correlative higher current applying higher Laplace forces on the current sheath when it reaches the interelectrode region;

d) the same $1/\tau^2$ dependence of the total neutron yield with respect to the delay between two neutron bursts holds (fig.11).

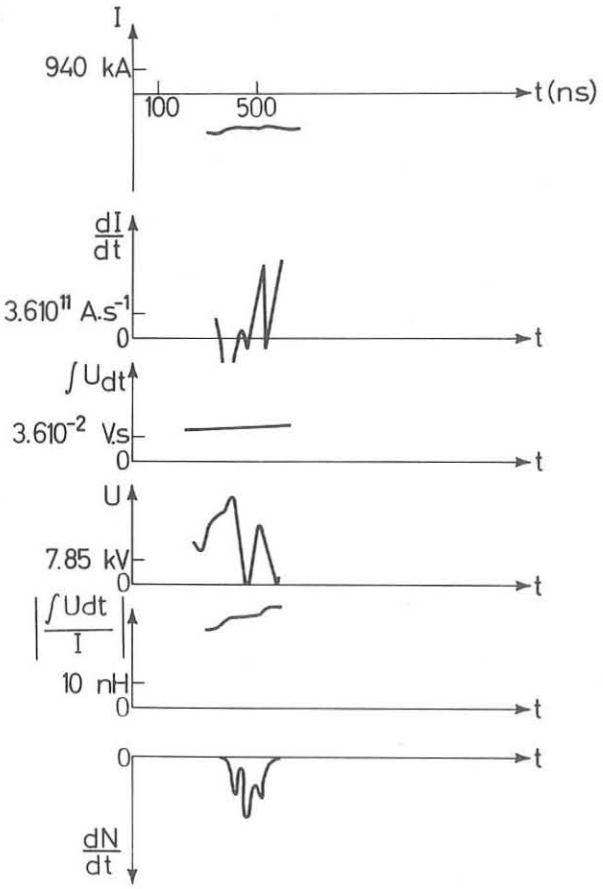

Time correlation between the electrical parameters and the PM neutron signal.
Inter-electrode gap : 2 cm
Initial conditions : V 32 kV
p = 1.1 torr D_2

FIGURE 10

From (fig.10) one can evaluate again the amount of energy absorbed in the turbulent heating of the plasma. It appears

that this quantity is almost equal for 7 and for 2 cm. Assuming an identical initial radius for both pinches, as the current is higher for shorter electrodes spacing it can be evaluated that the expansion needed in the 2 cm is about half that corresponding to the 7 cm case, in good agreement with the observation of the corresponding delay between the two neutron bursts.
It is likely that there is an optimum height between 2 and 7 cm for which the advantage of a smaller inductance is not yet balanced by the negative influence of the reduced height of the reactive region, which already shows up in the 2 cm device.

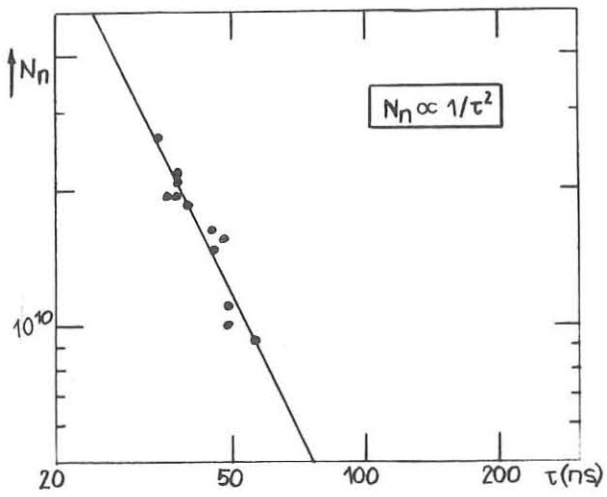

Total neutron yield vs. time delay between the two neutron bursts. Interelectrode distance 2 cm.

FIGURE 11

8. INFLUENCE OF THE POLARITY

It is known that inverting the polarity (i.e. having a negative central electrode) inhibits the production of neutrons in D.P.F. devices. A tentative interpretation put forward in the past was that in the inverted polarity configuration the high flux of cold electrons emitted by the central electrode to carry large current densities cools the focus below thermonuclear temperature. In the 2 cm device, the focus is as close from the anode as from the cathode and therefore one may think that there should be an equally low neutron emission for both polarities. Results reported in paragraph 7 are in contradiction with this interpretation: inverting the polarity has the same negative effect than in the 7 cm case. Therefore it should be thought that the inversion has a definite influence on the basic mechanism implied in the whole process.
Fig.12 shows the voltage and current traces for a 2 cm device and both polarities. It is seen that almost up to the collapse the respective evolutions are quite identical, and therefore that the inducatances up to that moment are identical too (same radius) But while in the normal case one observes just before collapse a neat increase of inductance (corresponding to the evidence of the continuation of the implosion of the sheath), in the reversed polarity case the contraction is stopped at a radius 2 or 3 times larger than the minimum radius for normal polarity. Similar evidence is derived from visible light framing pictures (see also Ref.13) This is also very well illustrated by the fact that the neutron yield is an order of magnitude smaller than that of the first phase of the normal focus (some 10^8 against 2.10^9).
We have yet no explanation for this polarity effect. It can

be remarked anyhow that the upward flux of ions, correlated to the geometrical shape of the sheath which is the same in both cases, has the same direction than the current in the normal case and an opposite direction in the reversed polarity case. One can then expect that in the second case the electrons will have to compensate for that reverse current and therefore that there will be a higher drift velocity between the two species. It is not clear whether this effect could play an important role in the final phase of the collapse.

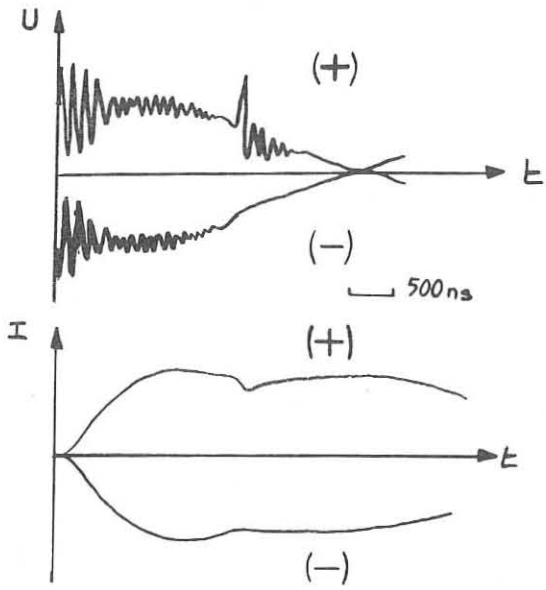

Voltage and current oscillograms for positive (+) and negative (-) central electrode polarity.

FIGURE 12

9. SCALING LAWS FOR OPTIMUM MACHINES.

Using the model previously described, it is interesting to derive the scaling laws of "optimum" D.P.F. devices. For the sake of conciseness, only machines of the Filippov type (no "run-down" phase) will be considered hereafter. A machine will be said to be optimum if:

a) the condenser bank is fully discharged at the time of maximum compression;

b) the temperature of the plasma at the instant of maximum neutron production is optimum (about 9 KeV for DD reactions, as shown later);

c) appropriate conditions for efficient breakdown and snow-ploughing are satisfied, whereas the damage to the electrodes is limited. Supposing one of these machines is known, how should one scale the various fundamental parameters (radius R_o and height H of the experimental chamber, filling density n_o, voltage of the bank U_o) in function of the energy W_o stored in the bank?

- Condition (a) has been established rigorously for a hollow Z-pinch (Ref.14) and writes (C being the capacity of the bank)

$$\frac{C W_c}{R_o^4 n_o} = C^{te} \qquad (10)$$

It can be shown to hold for a Plasma Focus of the Filippov type. A heuristic proof comes from the confrontation of two different evaluations of the acceleration of the imploding plasma layer:

$$\gamma = \frac{\text{magnetic pressure}}{\text{mass per unit area}} \propto \frac{I^2/R_c^2}{n_c R_o} \propto \frac{W_c}{L n_o R_o^3}$$

and $$\gamma = \frac{\text{distance}}{\text{time}^2} \propto \frac{R_o}{LC}$$ where L is the total inductance of the system.

- Provided the temperature T_2 at maximum neutron production is proportional to the temperature T_1 at maximum compression, condition (b) writes: $\frac{R_o^2}{HC} = C^{\pm}$ (11)

The heuristic proof (see ref.14 for demonstration in the case of a Z-pinch) is:

$$T_i \propto v_{implosion}^2 \propto \left[\frac{R_o}{time}\right]^2 \propto \frac{R_o^2}{LC} \propto \frac{R_o^2}{HC}$$

From Eq.3 and as r_2/r_1 equals a few units, T_2 is approximatively proportional to T_1 and equation (11) holds.

- Conditions c) should give two relationships to determine completely the solution. A rather obvious choice is:

$W_o/R_o^2 = C^{\pm}$ (12) $\qquad H = C^{\pm}$ (13)

Then, the energy and current densities on the cylindrical electrodes and insulator remain unchanged, and the Paschen conditions for breakdown are the same ($Hn_o = ct$).

- From equation (10), (11), (12) and (13) the following scaling laws are obtained:

$R_o \propto W_o^{1/2}$ $\qquad H = C^{\pm}$ $\qquad C \propto W_o$ $\qquad U = C^{\pm}$ $\qquad n_o = C^{\pm}$

- The neutron output is: $N_2 \propto \langle\sigma v\rangle . n_2^2 . r_2^2 . H . \Delta t_2$

where n_2 is the plasma density and Δt_2 the duration of the second burst of neutrons. As, following our model, the plasma is then radially unconfined: $\Delta t_2 \propto r_2 . T_2^{-1/2}$

On the other hand, if the snow-plough efficiency is the same in all machines; $n_2 r_2^2 \propto n_o R_o^2$

Taking into account (10) and (11), it comes: $N_2 \propto \frac{\langle\sigma v\rangle}{T_2^{2,5}} . \frac{W_o^2}{H.r_2}$ (14)

The optimum temperature for DD reactions is 9 KeV (maximum of $\langle\sigma v\rangle . T^{-2,5}$). Then, from our scaling laws: $N_2 \propto W_o^2/r_2$ (15)

It is difficult to evaluate how r_2 scales with W_o. Two plausible assumptions are:

(16) $\begin{cases} r_2 = C^{\pm} \longrightarrow \text{as the implosion velocity and } n_o \text{ are constant;} \\ r_2 \propto R_o \propto W_o^{1/2} \end{cases}$

One should then expect the neutron yield of optimum machines to vary as W_o^m, where $1.5 < m < 2$.

10. EXPERIMENTAL VERIFICATIONS.

The scaling laws published so far (ref.1,3) refer to a given experimental chamber. Keeping C constant and varying U and n_o (so that condition a is satisfied), T remains constant (eq.11,3), as well as r_2 (eq.16), and from eq.14, N_2 should vary as W_o^2, which is does. Keeping U constant, and varying C and n_o, N_2 should vary as W_o^2 only if T_2 is close to the optimum temperature of 9 KeV, for which $\langle\sigma v\rangle . T^{-2,5}$ has a flat maximum. In our device, it is believed that T_2 is not far from 9 KeV, and indeed $N_2 \propto W_o^{2.5}$. For "colder" plasmas, increasing C would be less advantageous, and could even be deleterious.

11. ONE MEGAJOULE DEVICE.

A joint programme on Plasma Focus research has been agreed upon recently by the Culham, Julich and Frascati laboratories. As a part of this programme, Frascati will built a large experimental facility (of the order of 1 MJ stored energy); the first experimental chamber to be installed will be of the Filippov type. Using the afore mentioned scaling laws, the megajoule experiment (Fig.13b) has been extrapolated from our present experiment (Fig.13a). The curves shown in Fig.13 are the result of 2 dimensional MHD calculations (Potter's code).

They confirm that the scaling laws conserve good matching between electrical discharge and dynamical collapse. The same calculations show that the temperature T_1 at maximum compression remains constant (within 5%), as expected.

REFERENCES

1) Ch.Maisonnier et al. Plasma Physics and Controlled Thermonuclear Research,Vol.1 p.511, 523,Madison (1971)

2) N.J.Peacock et al. Ibid p.537, Madison (1971)

3) N.V.Filippov et al.Ibid p.573, Madison (1971)

4) V.A.Gribkov et al.JETP Letters 15,329 (1972)

5) A.Bernard et al. Madison Vol.I p.553 (1971)

6) M.J.Bernstein, Phys.of Fluids,13,2858 (1970)

7) P.Cloth et al.Proc.of VI Symp.on Fusion Technology, Aachen p.525, (1970)

8) D.E. Potter, Phys.of Fluids 14,1911 (1971)

9) W.H.Bostick et al.Second Topical Conf.on Pulsed High Beta Plasma, Garching (1972) Paper E 3.

10) D.Forslund et al.Madison Vol.II, p.277 (1971)

11) M.J.Bernstein et al. Phys. of Fluids, 14,1010 (1971)

12) J.W.Mather et al. Phys. of Fluids, 12,2343 (1969)

13) J.P.Baconnet et al. IV Eur. Conf. on Controlled Fusion and Plasma Physics, Rome p.118 (1970)

14) M.Bineau et al. "Gas Discharges and Electricity Supply Industry", p.517, Butterworths Pub. (1962).

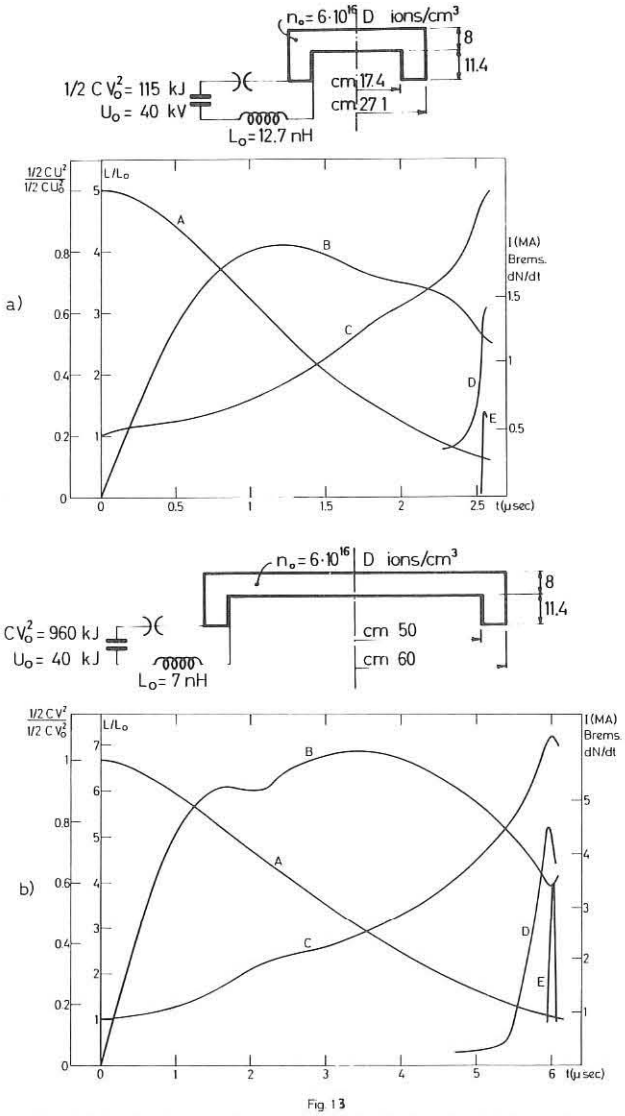

Fig. 13

Computed characteristic curves relative to a) the existing 115 kJ experiment, b) the projected 960 kJ experiment.
Where
A is the energy in the condenser bank, B is the current, C is the total inductance of the circuit, D is the total Bremsstrahlung power (arbitrary units), E is the neutron emission per unit time (arbitrary units).

FIGURE 13

THE EUROPEAN COMMUNITY ACTIVITIES IN THE FIELD OF CONTROLLED THERMONUCLEAR FUSION

by

D. PALUMBO

COMMISSION OF THE EUROPEAN COMMUNITIES
200 rue de la Loi
1040 Brussels

INTRODUCTION

The subjects of my talk today are the motives, development, structure and content of the EAEC (Euratom) programme in the field of plasma physics and controlled thermonuclear fusion.

In my capacity of responsable in Brussels, of this branch of activities of the Commission of the Communities, I have been asked by the organizers of this Conference to tell you about our work.

As you know, the Community at present consists of six States Belgium, France, Italy, Luxembourg, The Netherlands and West Germany, which will probably be joined by four new members, Denmark, Ireland, Norway and the United Kingdom.

The Euratom Commission's action in the field that concerns us is aimed at fostering the activities of the Member States in a coordinated manner, with a view to achieving results that will be used in common. Thus within the Community Fusion has given rise to more thorough going international collaboration than in the rest of the world, through an original form of assistance by Euratom which in itself is an experiment worthy to notice.

During the past week we have had a wide, full survey of the research in progress and the results obtained in the European laboratories, I shall therefore confine myself to three points which, although they

do not strictly deal with science, may be of some interest to you:

(1) Why the European Community is interested in fusion;

(2) the means by which it takes action in this field;

(3) the programme planned for the near future.

I. Why the European Community is interested in fusion

It is generally recognized that within the foreseeable future the demand for energy will keep on rising, and that for various reasons we shall have to resort to nuclear power sources-fission, which is already on the market, and fusion, which it is hoped to employ later on.

It is also recognized that even if U^{235} cannot itself provide a longterm solution, the advent of the breeder reactors could supply power for a very long time, even more cheaply than the sources available today.

If all goes well, we may hope that fusion will start to back up the breeders towards the end of this century. According to the conclusions of the IAEA Review Panel in June 1970, it may offer a number of attractive features:

(a) the fuel is abundant and widespread.
If, to begin with, only the D-T reactions can be used, the quantity of Li available at a low price is sufficient for some two thousand years. The amount contained in the sea is practically unlimited. As with the breeders, the incidence of the fuel cost on the kWh cost is very small, the cost per kWh being practically unaffected by the cost of Li.

(b) The end products of the reactions are not radioactive.
Whilst it is true that large quantities of tritium will have to produced (1 kg a day, equivalent to 10^7 curies a day for a 5 GW thermal reactor), this tritium will have to be consumed each day; and if there is a surplus, which appears to be easily obtainable, it will have to be stockpiled to start up another reactor. For once, therefore, the interests

of the energy producers will match those of the environmentalists in quality, even if the latter demand stringent performance levels quantitywise; and these, it appears, can be achieved without too much difficulty. So much for the volatile radioactive substances.

(c) The activation of the structural materials by the neutron fluxes, bigger and of higher energy than in the breeders, will certainly be very intense. It will depend very much on the materials finally chosen, but in any case there is no recycling problem and there remains only a problem of elimination which should not be harder than it is with fission.

(d) The amounts of fuel present in a reactor and its auxiliaries are small, and by the very nature of the reactor operation the risk of nuclear accidents is practically nil.

(e) It is predicted that the fuel cycle cost will be very low, and this is a potential economic advantage over fission.

(f) Lastly, and particularly as regards the D-T reactor, the fact that 80 % of the energy is deposited directly in the blanket means that high thermodynamic efficiency can be attained and might make chemical applications such as hydrogen production possible.

The advantages anticipated are of interest to all. They are especially attractive to Western Europe for a number of reasons.

The population density is higher in our part of the world than elsewhere and the resultant safety problems are more critical.

Secondly we, to a far greater extent than the major industrialised regions, are largely dependent on foreign sources for our energy requirements.

Today, the primary energy consumption in the Community is equivalent to 8.10^{12} kWh a year, 8 % of this in electric power, and 66 % of the primary energy it is produced from imported fuels.

According to studies by the Commission of the European Communities on the trend of the energy demand up to 1985, at a mean estimate, consuption will rise to the equivalent of 16.10^{12} kWh total energy per year, including $1,7.10^{12}$ kWh in electric energy, 33 % of the electrical energy will be of nuclear origin, but this does not answer the supply problem, since the availability of low-cost uranium in the Community is limited.

For the end of the century, the long-term trend suggests that the enlarged Community will require about $2,8.10^{13}$ kWh of total energy, including 6.10^{12} kWh of electric energy.

In line with the conclusions drawn by the IAEA Review Panel, let us assume that all the advantages of fusion result in a direct or indirect saving of 0.5 mill in the fusion kWh cost as against the other sources available at the same time. This, on the Community scale, would mean a saving of 3.10^{9} u.c. a year. This might come about in any case, even if the Community made no effort to contribute to the development of fusion research. We have to remember, however, that at the time when fusion can be expected to arrive on the market, it will be necessary to build plants capable of supplying about 20 GW(e) a year; this means a market totalling several thousand million dollars/y. The European industry will not be able to meet these requirements unless it has prepared for the job by sharing in the construction of large-scale confinement experiments, of test units, and finally of prototypes, moving step by step from the stage of collaboration with the laboratories to the point where it takes over their work.

Hence we need to develop research and development in the Community in order to give industry these opportunities, even if the cost of arriving at a prototype should amount to several thousand million dollars. At the moment it is impossible to give a closer estimate based on a more knowledgeable cost/profit analysis. All the initial data are still uncertain, including the date at which fusion might enter the energy market. One has to know this date in order to determine the value in present-worth terms of the potential profit.

In spite of all the uncertainties, however, the above considerations suggest that the risk involved in undertaking a fusion R 8 D effort is a reasonable one, provided that it is spread over a sufficiently large unit.

There are some minimum costs independed of the size of the unit while the potential benefit is roughly proportional to this size.

The Community as a whole possesses the critical size, but it is by no means certain that the same can be said of each of its members.

II. Structure and scope of the activity

Historical introduction

Even though these considerations were not so obvious in 1957 when the Euratom Treaty was signed, joint action in the field of controlled thermonuclear fusion figured in Euratom's first five-year programme (1958-62).

Two favourable circumstances had helped us. The 1958 Geneva Conference, in making public the results and current programmes in the UK, the USSR and the USA, confirmed the great number and difficulty of the problems to be overcome. Secondly, the activity developed in the Member States was still in the early stages as regards the experimental phase, whilst important theory work had already been achieved, particularly in West Germany.

Euratom's action started with a contract with the CEA, France, in 1959. At the outset it was not clear whether in the future Euratom was going to develop its own activities or have the work done through contracts of association with the member countries' laboratories. The turning point came when it entered into a contract with the IPP at Garching.

Thus the Commission adopted as its policy the conclusion of a series of contracts of association with all Member States institutions actively engaged in the field to any significant degree.

By the end of the first five-year plan (1958-62) the following associations were in operation:

(a) CEA (1959) laboratories at Fontenay-aux-Roses and Saclay (nowadays Fontenay-aux-Roses and Grenoble);

(b) CNEN (1960) Frascati and now also with CNR: Milan and Padua;

(c) IPP (1961) Garching near Munich;

(d) FOM (1962) Jutphaas (Utrecht), Amsterdam and later Eindhoven;

(e) KFA (1962) Jülich.

An additional contract was subsequently entered into, with the Belgian Government in 1968 (laboratories of the "Ecole Royale Militaire" and the theoretical department of the ULB).

On the basis of the existing national programme, the Commission sought to achieve a coordinated programme which would avoid useless duplication, while at the same time encouraging the exchange of information and a certain redistribution of work. From the very beginning the following approximate breakdown, appeared feasible:

- CEA (Fontenay-aux-Roses and Saclay): low beta open-ended configuration and plasma electromagnetic waves interaction;
- mainly Jülich and Garching: high beta open-ended configuration (theta pinch);
- mainly Garching, with some Jutphaas participation: closed configuration;
- Frascati: very high density plasmas.

Obviously the above plan allowed for a certain amount of reasonable and sometimes necessary overlapping.

General plasma physics as well basic as applied theory was also a major preoccupation in all the laboratories.

The Commission participated in the different associations, to the rate of about one-third of the total budget and by means of an international staff, recruited by the Commission, equivalent to about one-eight of the total professional staff. At present 64 scientists out of an approximate total of 500.

The year 1963 marked the setting-up of the Liaison-Group composed of the scientific heads of the Community's associate institutes. The main aim of this consultative group is to discuss and give its views on the programmes as well as on problems of common interest. The Liaison Group is assisted by Advisory Groups responsible for the following lines of activity:

(a) Tokamak, low beta Stellarator;

(b) Screw Pinch high beta Stellarator;

(c) Open configuration;

(d) Heating and injection;

(e) Very high density;

(f) Fusion reactor technology.

For some time now experts from Culham have been regular members of all the Advisory Groups.

During the first two five-year programmes (1958-62 and 1963-67) the Commission spent a total of 45,4 million units of account on fusion. The main effect of this was to promote the expansion of these activities in Europe and to assure their continuation, even during periods of difficulty. An effective basis has been laid for the exchange of information and a certain degree of coherence has been maintained with regard to the programme as a whole.

The present situation

In the light of scientific and technical developments, the third five-year programme (1971-1975) has been prepared on the basis of the programmes put forward by the laboratories and in collaboration with the Liaison Group. The third five-year programme is to pave the way for closer forms of collaboration which, if all goes well, will become necessary in the future.

On 21 June 1971, after long discussions, the five-year Programme was finally adopted by the Council of Ministers. The financial provisions are based on a total expenditure estimated at 185 million u.a. The Commission contribution, fixed provisionally at 46,5 million, breaks down as follows:

(a) 38,2 million in the form of general aid to the budgets of the existing associations over five years at a level of approximately 24 %;

(b) 0,3 million to finance the exchange of national personnel between the associate laboratories;

(c) 8 million for financing at approximately 44 % the equipment for supporting projects of major interest for fusion launched during the first three years of the programme. witting the following area:

- Tokamak, low beta Stellarator
- Screw pinch, high beta Stellarator
- Heating and Injection
- Very high density.

A further approprietion for these projects may be approved by the Council of Ministers for the last two years of the plan.

Point (b) and (c) are typical of the third five-year programme.

A real responsibility to decide which projects are to be given priority rests with the Liaison Group even if officially this body holds a consultative status only. The Liaison Group submits its

recommendations to the Commission following an examination of the laboratories' proposals by the competent Advisory Groups.

In reaching its decision of 21 June 1971, the Council of Ministers took into account the considerations above mentioned. It decides that "the programme represents an element for long-term collaboration covering the entire range of Member State activities in the field of fusion and plasma physics. This programme tends to reach, in due time, to the common achievement and commercial use".

Moreover, in the case of priority projects the Council of Ministers has decides that "in return for financing at the preferential rate all associates will enjoy the option of participating in the experiments carried out with the help of this equipment".

To this group we think will soon be added the Culham and Risö Laboratories, with which the common programme is under discussion.

This tightening of the bonds in the Community doesn't mean at all a closure to the outside.

In the past Euratom has encouraged larger-scale collaboration and will continue to do so. Here I would draw attention to the role played by the Commission and its staff in the agreement between FOM and MIT on ALCATOR.

III. Current programme and prospects

The scientific programme which all these projects go to make up is centred on research into closed configuration in a large range of geometrical and physical parameters, as well as research into methods of heating and injection with particular emphasis on their application in closed configurations.

A certain amount of research is proposed in the field of

inertial confinement, while work will continue on a modest scale in the field of open-ended configurations.

Low β closed configurations

a) Tokamak. Since 1968-69, at least three laboratories have shown interest in this relatively new field, even though the machines currently under construction or on the drawing-board differ conderably from the initial proposals.

- Pulsator (Garching) : R = 70 cm, a = 11 cm, Bo = 28 kG
  I = 0,1 MA (q = 3). The application of moderate Stellarator fields is planned in the initial phase. The machine's interest lies in studying the initial phase and afterwards the "limiter" problem. The machine is in the process of being assembled and is expected to come into service by the end of 1972.

- TFR (Fontenay-aux-Roses) : R = 98 cm, a = 20 cm, Bo = 60 kG
  I = 0,4 MA (q = 3). The main aims are to extend the scaling laws, to study the effects of injection heating of neutral particles and to make a careful study, using a special diagnostic methods, of the configuration of the poloidal magnetic field and therefore of the current profile. The equipment is now being assembled and is expected to come into operation (early in 1973). Elaborate theoretical studies have preceded and will be carried out in parallel with the exploitation of the device.

- Tokamak Frascati : R = 82 cm, a = 22 cm, Bo = 100 kG,
  I = 1 MA (q = 3).

The purpose of this ambitious project is clearly to test these configuration at high magnetic field approaching the region which is probably important as regards thermonuclear applications. The dimensions have been chosen in order to proceed parallel with the ALCATOR project, with which there are close links. The design has been completed and the machine could be in operation by 1974.

b) Stellarator. Following the results obtained with low temperature plasma in the "Wendelstein" Stellarators at Garching and in view of the desirability of comparing the Stellarator and Tokamak principles at higher temperature when the physics might differ greatly, a large Stellarator, Wendelstein VII, is to be built : R = 200 cm, A = 30 cm, B = 35 kG, $\ell = 2$ and $\ell = 4$. Firstly, the plasma will be created by induction and OH, additional heating is planned by neutral injection and RF (see Heating and Injection). Commissioning is planned for 1974-75.

To this list will be added, with the Culham laboratory coming into the Community sphere, the CLEO machine, which already works as a TOKAMAK and will be operated as a $\ell = 3$ Stellarator. Injections of neutrals will supplement ohmic heating.

The Levitron Stator II, in operation at Fontenay-aux-Roses, the superconducting Levitron in Culham, and the levitated quadrupole, Wendelstein VI, under construction at Garching, also deserve mention.

High β closed configurations. Activity in this field is along three lines :

a) Screw pinch. This concerns concepts initially developed in Jutphaas, basically similar to those used in the Tokamak project, but which differ as regards magnetic field generation, methods of heating (shock waves and compression) and parametric ranges. Three experiments are under construction.

- SPICA : FOM Jutphaas. R = 60 cm, a_w = 20 cm, bank power = 1 MJ, I = 0.8 MA.
  The main objective are the study of the influence of current in the low presure plasma surrounding the compressed plasma in the Tokamak ($q > 1$) and ultra Tokamak ($q < 1$) system.
  Awaiting construction : 1973.

- COMPACT TORUS : Jülich. R = 25 cm, a_w = 9,5 cm, I=0.030 MA
  The main object concerns the study of Tokamak type of configurations with high beta and of the behaviour of a machine

without limiter.

- SCREW PINCH : Padua. R = 40 cm, a_w = 6 cm.
  The main objectives are the study of initial ionization and of the heating processes. The machine is under construction.

  H B T X : Culham. In Culham high beta toroidal experiment R = 1 m, a = 6 cm, 2 M J,is already operating as screw pinch stabilized Z pinch or "reversed field pinch". The emphasis is on the latter configuration for which the toroidal field changes its sign going from the magnetic axis to the wall.

b) Non-circular Cross sections : Experiments aiming at the study of the influence, in axisymmetric configurations, of cross-sections shapes which are considerably (TENQ) or grossly (BELT PINCH) non-circular.

They are an upward extension, towards energy levels of 1 MJ, of experiments already in progress at Jülich and Garching.

- TENQ : R_{ext} = 75 cm, Rint = 23 cm, h = 130 cm (Jülich)
- BELT PINCH : R_{ext} = 75 cm, Rint = 30 cm, h = 250 cm (Garching)

c) High-beta Stellarators. The ISAR T1 machine went into service at Garching a few months ago. It is of the circular Stellarator type. R = 135 cm, a_w = 11 cm, supplied from the 2.6 MJ bank.

The main field (Bo_{max} = approx. 37 kG) and the ℓ = 1 fields are generated by independentcoils; heating is, of course, by means of shock waves and compression. The main aims are the study of equilibrium and stability.

A proposal for a linear in its first version machine with ℓ = 1 is under preparation at Jülich.

In this section, mention should also be made of the continuation of very careful studies on shock waves which have already produced major results at Jülich and Garching.

Open configurations

Interest in this line of research has waned rapidly in the Community, for reasons which are well known. Collisional end losses, however imperfect calculations of them may be, would appear to show that thermonuclear applications of this type of configuration are difficult, and leave no margin to allow for additional losses due to the instabilities foreseeable in essentially non-isotropic plasma.

Studies on the feasibility of improving end confinement by means of electromagnetic fields in the region of the electron or ion cyclotron frequencies have shown the difficulty inherent in practical application of this principle. Using the CIRCE experiment at Grenoble, however, which was commissioned recently, experimental researches are continuing in this fields.

No work is in progress on the direct conversion of the energy of the escaping particles, nor on their re-injection. Activity at Fontenay-aux-Roses is confined to the operation of two machines, DECA and BET. It is not impossible that new experimental or theoretical results will bring about a revival of interest in the future, but no new action is planned at present.

Heating and Injection

Great attention has been directed to the possibility of adapting the use of RF to low-beta toroidal configurations.

A joint Brussels-Garching-Grenoble project has been set up aiming at heating, chiefly through TTMP, in Tokamak-Stellarator configurations. Two machines, PETULA (TTMP-Tokamak) and WEGA (RF - Stellarator) are to be built at Grenoble, in

cooperation with Garching. The power supply for the magnetic field and the RF generator will be common; this will mean an appreciable saving.

In addition, the ERM (Brussels) is continuing studies on the interactions between electromagnetic waves and a finite plasma; studies are underway on a small scale on the TTMP at Garching and other methods are under investigation at Fontenay-aux-Roses.

An IPP/CEA project has been put in hand at Fontenay-aux-Roses for the future development of the injection of neutrals.

The injection of neutrals is also planned using conventional sources, on the Tokamak at Fontenay-aux-Roses and Wendelstein VII at Garching. An important contribution is expected from the Culham laboratory, already very active in this important field. Turbulent heating is being studied at Jülich and Jutphaas and the use of electron beams at Amsterdam.

In addition, laser heating is being considered at various laboratories.

Very high density

The "plasma focus" is being studies under a joint Frascati-Jülich-Culham project. The chief task at Frascati is the extension of the scaling laws to energies corresponding to a capacitor bank in the MJ range; Jülich's main task is the improvement of the repetition rate, while Culham is concentrating principally on diagnostics and theory.

The general aim is to study plasma focus as a neutron source rather than its application to thermonuclear energy generation, which now seems a doubtful starter.

Laser action on solid targets, both for the production of very dense and hot plasma and for filling magnetic configurations, is being studied at Garching.

Fusion reactor technology

In this difficult field exploratory work will be initiated, notably on "systems studies". The only true experimental activity underway concerns surface physics and the interaction between the plasma and the wall, for which a Department is in operation at Garching.

At a general level this fields of activity is the object of discussion inside the Liaison Group.

To summarize : In the low β field there is already large-scale activity Tokamak covering a wide range of magnetic fields, plasma currents, and geometrical dimensions, and with pulse duration longer than the expected confinement time. The operation of W. VII should provide a very useful comparison between Stellarator and Tokamak.

In the case of the medium and high beta configuration, I feel that the exploration of several avenues by means of small or medium-scale machines constitutes the most appropriate course of action.

Certain of these approaches will probably converge on the Tokamak or Stellarator lines at intermediate beta values. Ideas concerning the later stage in the high beta range have not yet crystallized.

As regards the open configurations, there is a considerable unbalance in relation to the U.S.A. and possibly the U.S.S.R.

The same applies to laser-produced plasma, at least as far as the association laboratories are concerned. A satisfactory Community collaboration is developing as regards heating and injection, with a level of activity perhaps unevenly balanced between RF and NI. This situation will be improved by the Culham contribution.

The field of fusion reactor technology is at present in an

exploratory phase. The emphasis which should be placed upon it will depend to a considerable extent, on the possibility of making reasonable forecast on the future of fusion.

Looking further ahead, a common project for a possible JOINT EUROPEAN TORUS is considered as a collective effort by all the associated laboratories. The project would have as its assential purpose nuclear heating and it would possibly contribute an answer to the problem of scientific feasibility of a fusion reactor. A great many problems regarding fusion reactor technology such as the possible production of the magnetic field by superconducting coils, the divertor, and refuelling, would be envisaged during the design and the construction of this machine, or should be considered as a part of its working programme.

A Joint European working group is already working on defining the range of parameters and alternative technical conceptual solutions. We hope that a proposal can be ready in 1975. In the meantime we have to examine the political and financial feasibility aspects and prepare adequate structures for this common enterprise.

As regards the more distant future, it is more difficult to make forecast. The pace will depend on both : the physical and technical results obtained and also on the assessment of needs and the outlook as seen by the political authorities. However, this argument should be taken into consideration in due time ; let us suppose that economic benefits G units per year (G is supposed constant in time) can be expected. The present mathematical expectation for the total benefits is $\sim \frac{PG}{r} e^{-rT}$

T being the expect delay, r the rate of interest, P the probability of reaching the target. Of course I should be very hesitant today about suggesting any numerical value between 0 and 1 for P. On the other hand, the actual value of the required total cost is not necessarily highly dependent on T expect for the major risk connected with a strong acceleration of the activity.

But we than seen, with a fairly high degree probability, that T is in itself an important economical target, even more than this naive picture indicates.

The problem is to know if and when a significant increase in the effort can produce a significant reduction in the remaining T. It would be a pity to delay a benefit for mankind beyond the technical threshold if it were to be found that physics and technology will finally achieve a positive value for G.

*

* *

RESEARCH AND PROSPECTS ON CONTROLLED THERMONUCLEAR FUSION IN THE U.S.A.

by

Roy W. Gould
U.S. Atomic Energy Commission
Washington, D.C. 20545

The near-term objective of the U.S. Controlled Thermonuclear Research Program is to further develop understanding of the plasma state, especially in those magnetic confinement configurations and heating methods which may be suitable for development into fusion reactors. Experiments now in progress or being fabricated (see Table 1) are preparatory for moving ahead toward larger experiments capable of producing plasmas which meet the Lawson criterion, thus demonstrating fusion scientific feasibility. It is believed that, with favorable results from the existing or planned experiments and with increased level of effort, this may be possible within about ten years.

Three main lines of effort are being emphasized in magnetic confinement. These are magnetic mirror open systems, pulsed high-beta pinch systems, and near steady-state toroidal systems. In addition, a program of laser initiated fusion is being carried out, aimed at studying inertial confinement of higly compressed fusion pellets. Basic research in plasma phenomena and supporting theoretical studies, as well as plasma technology developments, are carried out. Over the past two years exploratory studies of reactor concepts and associated technological questions have been initiated, which now amount to about five percent of the program budget.

Magnetic Mirror Research. In the magnetic mirror open systems area, three major experiments are underway : 2X-II and Baseball II at Lawrence Livermore Laboratory and IMP at Oak Ridge National Laboratory.

The research objective of the 2X-II is to continue correlations between theory and the observed loss processes of high temperature ($\sim$ 6 keV), high density ($\sim 10^{13}$ cm^{-3}) plasma formed by adiabatic compression. Plans for FY 1973 include a study of the effects of adding neutral beam injection to the 2X-II plasma. The objectives of the Baseball II is to achieve a high

temperature plasma by neutral injection in which the ion distribution is randomized by collisions. Experimental studies are in progress. No major program modifications are anticipated in FY 1973. The objective of the IMP is to study the buildup of plasma by neutral injection combined with trapping on a "target" plasma formed by electron cyclotron resonance heating. Research to date has been concerned with studying the properties of the target plasma.Plans for the next year are to study the injection and trapping with ~ 100 ma neutral beams at 20 keV.

A theory which seems to account for the enhanced losses (a factor of 2 to 15) previously reported in the 2X-II magnetic mirror device has recently been advanced by Baldwin and Callen. The origin of the extra loss is an amplification by the Rosenbluth-Post convective loss-cone instability of individual particle fluctuation level. The theory predicts that the enhancement of particle scattering is small for large n/B^2 so should not be of major consequence in a reactor regime.

High-Beta Research. The principal activity in this area involves the Scyllac Facility at the Los Alamos Scientific Laboratory. The research objective of Scyllac is to study the high-beta toroidal equilibrium in a high-beta stellarator-like configuration, and to test the idea of feedback stabilization. The plasma is produced and heated by implosion followed by magnetic compression. Experiments in a 5-meter toroidal sector and a 5-meter linear section with magnetic mirrors are underway and should be completed in order to make begin conversion to a full torus in the first half of 1973.

The toroidal Z-pinch, also at Los Alamos, has achieved a reversed field equilibrium with $\beta_\theta = .4$, in which the temperature is inferred to be several kilovolts. At the Oak Ridge National Laboratory, a high-beta bumpy torus (EBT) is under construction and should be completed during 1973. The EBT will utilize a series of 24 connected magnetic mirrors with high-beta annular relativistic-electron plasmas sustained and heated by microwaves as in the ELMO device. It is expected that the high-beta relativistic electron plasma will stabilize the less energetic toroidally confined plasma.

Experiments on a sector comprising one-third of the 4.8 meter diameter Scyllac torus have been performed during the past year. The toroidal force and the outward plasma drift are compensated by a combination of

$\ell = 1$ helical fields and $\ell = 0$ bumpy fields. Toroidal equilibrium has been observed followed by a sideward motion (m = 1) of the plasma column. This motion is nearly the same all along the torus, independent of the $\ell = 0$ periodicity. Plasma containment times are as large as 11 microseconds, comparable to the times for plasma end loss. The sideward motions, which occur predominantly in the horizontal plane of the torus, suggest either an imbalance between the $\ell = 1, 0$ and toroidal forces at later times or a long wavelength m = 1 instability. Measurements of the applied magnetic fields show that the product of $\ell = 1$ and $\ell = 0$ fields for plasma equilibrium agrees with sharp-boundary MHD theory. A toroidal compression coil with $\ell = 1$ and $\ell = 0$ grooves is under fabrication. An $\ell = 0$ MHD feedback experiment to control the m = 1 sideward motion is underway on Scylla IV-3 and is planned for the Scyllac toroidal sector as well as on the complete Scyllac torus.

Experiments have also been performed on the Scyllac 5-meter linear theta-pinch with and without strong magnetic mirrors. Operation without mirror fields produced a 2-3 keV plasma column which lasted about 15 microseconds. The plasma showed considerable "wobble". When mirror field with a mirror ratio of 2-3 are applied at the same time as the main field, the plasma column shows evidence of an m = 1 instability.

Consideration of a pulsed high-beta fusion reactor based on the theta-pinch configuration indicate that it may be desirable to employ wall stabilization of the plasma column with a smaller degree of magnetic compression, preceded by a separate implosion heating phase.

Low-Beta Toroidal Research.

This area, which encompasses tokamaks and internal current devices, receives the greatest emphasis in the U.S. program. The internal current devices are employed, generally, for supporting studies in toroidal confinement physics, whereas the tokamak devices are seen as leading to reactors. The Princeton ST has been the principal operating tokamak during the past year, with the ORMAK, Doublet, and ATC just beginning to yield results. A new large tokamak (plasma minor diameter 90 centimeters or 3 times that of the ST) the PLT, is under fabrication and is expected to be completed in 1975.

Studies of plasma transport rates in the D.C. octupole at Gulf General Atomic, in which a toroidal field has been added, have shown the

transition from classical to neoclassical diffusion as the mean free path increases so as to become comparable with the machine size. Diffusion rates have been found to agree with theoretical predictions over a wide range of density and temperature. In the short mean free path regime, the experimental results agree with the Pfirsch-Schluter theory and in long mean free path regime with the Galeev-Sagdeev theory. In both regimes, the diffusion rates were found to vary inversely as the square of the magnetic field.

Particle containment times in excess of 1 second have been observed in the Princeton FM-1, which is a single levitated superconducting ring device with a magnetic configuration similar to that of the Spherator. For temperatures less than 1 to 2 electron volts and for densities from 2.5×10^{10} cm^{-3} to 2×10^{11} cm^{-3} the confinement time has been found to increase with temperature ($\sim T_e^m$ with $m \sim 3/4$) and decrease with increasing density. The classical confinement time is exceeded by about a factor of 5. At higher temperature where the plasma is sustained by continuous application of as much as several hundred watts of non-resonant microwave power the confinement time appears to be independent of density and to decrease with temperature. The confinement time is about $300\,\tau_{Bohm}$ and the cause of the latter behavior, though possibly connected with the method of plasma production or magnetic field asymmetries, is not known.

The past year has been a productive period for the ST tokamak at Princeton. As reported earlier, electron and ion temperatures of 2000 eV and 600 eV, respectively, have been obtained. Efforts are now concentrated on trying to obtain a detailed understanding of the tokamak discharge which, not unexpectedly, is turning out to be rather complicated. The density range for "good" operation is somewhat limited. As density is reduced, a runaway distribution of energetic electrons is achieved and when the density is increased, disruptive instabilities are encountered. The density of neutral particles, including impurity atoms, seems to play a major role in the particle and energy balance.

Nevertheless, some very important trends have emerged. When impurities are taken into account, the Spitzer formula seems to account for the observed resistivity. Plasma energy content increases as the square of the plasma current($\beta_\theta \sim .5$) Particle and energy confinement time are approximately equal and increase with temperature and magnetic field in accord with the pseudo-classical theory (not Bohm). Measurements of radial

profiles are still not sufficiently detailed so as to permit a determination of local values of the transport coefficients and hence to compare with theory. The recently developed thallium ion beam probe has already given space and time resolved density and potential measurements and should soon be able to give the plasma current distribution. Meanwhile from Thompson scattering measurements of electron temperature profiles, the expected skin effect has been inferred, at early time in the discharge. However the skin disappears more rapidly than expected.

The Ormak, Doublet II, and Adiabatic Toroidal Compressor (ATC) were brought into operation and only after extensive discharge cleaning could significant electron temperatures be reached. While definitive results are yet to be obtained, early results from each of these devices are encouraging. The Ormak, which as a plasma minor radius of 23 cm has operated stably for 100 msec at a plasma current of 140 kiloAmpere. The Doublet II, a non-circular cross-section tokamak, or plasma current multipole has operated at 500 kiloAmpere plasma current. Possibly the most important feature of the initial operation of ATC is that stable operation at about 50 kiloAmpere plasma current is obtained at $q = 3$ with the equilibrium field being supplied by the vertical (shaping) field with no copper shell. Furthermore the plasma column can be positioned in major radius by varying the vertical field strength. The plasma remains stable upon compression and the plasma current and temperature rise as expected.

These and other results have encouraged the design of a new larger tokamak, the Princeton Large Torus. The PLT is the largest device consistent with the existing generator capacity and will have $B \simeq 49$ KGauss, $I = 1.6$ megaAmpere, major and minor vacuum vessel radius of 130 cm and 50 cm respectively. Since no copper shell will be provided in PLT initially, the ATC results are especially significant. While there are potential problem areas, such as a pronounced skin effect preventing the establishement of a proper current profile, it is necessary to confront the important questions such as the radial transport and scaling of confinement times in larger tokamaks. Construction of PLT has begun and it is estimated to require 3 1/2 years to complete at a cost of 13 million of dollars. Since Ohmic heating of tokamaks cannot be relied on to reach ignition temperatures, provision is made in PLT for later addition of one or more possibly supplementary heating methods: neutral beam injection,ion cyclotron resonance,lower hybrid resonance.Heating experiments on existing devices (e.g. neutral beam injection on Ormak) are expected to determine which of the supplementary methods are employed on PLT.

Laser Initiated Thermonuclear Fusion Interest in this approach has increased significantly. Until recently, most discussions centered on the use of laser energy to simply heat a liquid target of fusion fuel to ignition temperature . Simple arguments suggest that the laser energy required for a scientific breakeven experiment (thermonuclear energy = laser light) might be a few megajoules, but the laser energy required for a reactor with net energy gain would be impractically high.

During the past year,the notion that the laser could be used to drive a spherical implosion, thus reaching possibly 10^4 times liquid density and reducing the laser energy requirement by many orders of magnitude,was revealed. In essence, a series of spherically converging shock waves are driven by ablation of material from outer layer of the pellet. The pressure thus generated exceeds the light pressure by the order of c/v_s. The pulse shape of the incident laser must be chosen so as to produce a series of weak shocks of successively increasing pressure which converge simultaneously at the origin.

By ablating about 3/4 of the mass, computer calculations by the Livermore group show that compressions of 10^4 times liquid density can be achieved with some 5-10% of the laser energy having been delivered to the remaining mass.According to these calculations it may be possible to reach the condition: (thermonuclear energy = laser light energy) with less than 1 kilojoule and an overall net energy gain (assuming laser efficiency of 10% and thermal conversion efficiency of 40%) with between 0.1 and 1.0 megajoule. No experiments have yet been performed to demonstrate that such large compressions can be achieved and a large part of the U.S. effort is going into development of energetic short pulse lasers, of the Neodymium-glass and CO_2 types. By 1973 AEC Laboratories project 1000 joule outputs, which should provide a means for performing critical physics experiments to determine whether the physics of laser fusion is favorable.

Fusion Reactor Studies.While Lawson criterion plasmas may not be reached for another decade, there is sufficient optimism that these plasma conditions can be reached by one or more of the approaches now being persued to begin examining more seriously the technological questions of fusion reactors. Furthermore early research on these questions could materially shorten the time to the ultimate application of fusion reactors. Also because of the increased public interest in the United States in all methods of energy generation,there is greater demand for assessments of potential environmental and economic impact

of new methods. Such assessments for fusion, will be, by necessity, incomplete.

Fusion reactor studies in the U.S. are largely exploratory and designed to identify as clearly as possible the nature of the technological problems, their severity and potential solutions. Presently about 2 million of dollars annually or 5% of the budget for fusion research, is spent on approximately 25 individual studies of varying size. These studies capitalize in existing expertise in AEC laboratories and include :calculations of neutron economy in blankets, cost estimates for large superconducting magnets, methods of recovery and processing of tritium, thermal and electrical stress of materials, magnetic energy storage systems, radiation effects in fusion reactor materials, fuel injection, and general design, system, economic ,and environmental studies. It is generally felt that these studies should not only be increased but that serious efforts be started over the next decade to solve the technical problems which are so identified, so as to lead into a fusion reactor development program in the 1980's.

Table I

MAJOR U.S. CTR DEVICES

MAGNETIC MIRRORS		
IMP	ORNL	Neutral injection
Baseball II	LLL	Neutral injection
2X-II	LLL	Magnetic compression
HIGH BETA		
Scyllac - Linear	LASL	θ-pinch with mirrors
Scyllac - Sector	LASL	θ-pinch toroidal sector
ZT-1	LASL	Toroidal Z-Pinch
EBT	ORNL	Bumpy Torus
TOKAMAKS		
ST	PPPL	Small bore
ORMAK	ORNL	Intermediate bore
PLT	PPPL	Large bore
Doublet	GGA	Noncircular cross-section
ATC	PPPL	Magnetic compression
Alcator	MIT	High field
TT	Texas	Turbulent heating
INTERNAL CURRENT DEVICES		
FM-1	PPPL	Superconducting ring
Superconducting Levitron	LLL	Superconducting ring
D.C. Octupole	GGA	Supported rings
Octupole	Wisconsin	Levitated rings
Astron	LLL	Relativistic beam

RESEARCH and PROSPECTS on CONTROLLED THERMONUCLEAR FUSION in USSR.

L.A. Artsimovich.
Kurchatov Institute of Atomic Energy, Moscow (USSR)

The problem of controlled thermonuclear fusion is so complicated that up to now it is limited within a pure physical sphere and is still very far from practical applications. Today , the basic problem continues to be a laboratory development of methods for obtaining a high temperature plasma with the parameters required for the thermonuclear reactions. Required conditions are not yet fully achieved in any experimental device, but nevertheless we are gradually approaching their fulfilment by proceeding to this objective along several different ways.

In the course of many years ,the predominant idea in developing the problem of controlled thermonuclear fusion was the concept of a magnetic confinement of a high temperature plasma (sometimes the term "magnetic confinement" is used). This concept resulted in a number of lines of research that may be refered to as traditional and involved the major studies in this field.

In the USSR, the most intensive work developed along two lines :

. The studies of plasma in closed (toroidal) magnetic systems ;

. The investigation of the properties of a high temperature plasma in open magnetic systems with "magnetic mirrors".

In addition to it, rather recently a new line of development in the thermonuclear programme has emerged : the heating of a substance to super high temperatures by a laser pulse of a very high power and so short in duration that heat insulation in the heating phase loses its importance.

Let us discuss the results of the studies in separate sections of the general programme. Let us begin with the closed magnetic systems. One of such systems is the "Tokomak" device. In devices of this type, a high temperature plasma exists at quasistationary conditions. The current generated by an induction method flows along the plasma ring. The magnetic field of the current plays the main role in providing a magnetic heat insulation of the plasma. The plasma is heated by Joule heat

produced by the current.

Now several devices of the Tokomak type are being operated in the I.V. Kurchatov Atomic Energy Institute. The largest of these devices is T-4 (the modified model of T-3 that has a large diameter of the toroidal chamber of 1.8 m and the diameter of a plasma cross-section equals 38 cm with a longitudinal magnetic field of up to 50 kiloersted).

Similar but somewhat differing results are being obtained with different Tokomak devices. We will present a short summary of these results here.

The measurements of thermal energy of a plasma made by various independent methods in the T-3 device have shown that for the steady thermal conditions, the ratio of the average value of the gas kinetic pressure to the pressure of a poloidal magnetic field of the current at the boundary of the plasma $\beta_\theta = 8\pi p/B_\theta^2$ (a) is equal to 0.4 ± 0.1 for not too small concentration. The electron temperature is usually higher than ion temperature. The maximum value of T_e at the axis of the plasma in the T-3 device reaches 2 keV when $n_e = 2.10^{13}$ cm^{-3}.

The profile of temperature distribution across the plasma is well approximated by the function $T_e = T_e(o)\,(1-r^4/a^4)^2$. The characteristic feature of this distribution is a flat top indicating that the heat conductivity reaches very high values near the axis of the plasma (where $B_\theta = 0$).

The results of experimental measurements of ion temperature are well approximated by the following function :

$$T_i = 6.10^{-7}\ \sqrt[3]{IB_z R^2 n_e}\ \frac{I}{A}\ \text{ev}$$

where n_e is the averaged electron concentration and A the atomic weight.

This relation is in a good agreement with the predictions by the neoclassical theory of Galeev-Sagdeev for ion heat conduction. However, it is too early to say that quantitative conclusions of the neoclassical theory are experimentally definitively confirmed at this point. In particular, there is no confidence that in transition from the plateau region, for which the above formula has been derived, into a "banana" (collisionless) region, we shall obtain the reduction of ion heat conduction in this region predicted by the neoclassical theory. In any case, the preliminary experiments that have been carried out do not indicate

any hint about the dependence of the ion heat conduction on the rate of ion-ion collisions. The maximum T_i value measured experimentally at the T-3 device was equal to 600 ev for deuterium (in this case a considerable neutron radiation is observed for 20-30 msec).

The mechanism of the processes, defining the heat losses from the plasma, has not yet finally established. The electron component of the plasma looses energy at a much faster rate than it is predicted by neoclassical theory. The energy confinement time τ_e was 3-10 msec for the T-3 device. There is an empirical relation $\tau_e \sim a^2 \sigma_e$, where σ_e is an electric conductivity of a plasma averaged over the cross-section. In other words, there is an anomalous electron heat conduction and its value raises linearly with the electron collision frequency.

Recently a high frequency heating of a plasma by electron cyclotron resonance was used and provided to be effective at small TM-3 device. This permitted to make the plasma parameters in Tokomak independent one from another and in particular to confirm that the plasma lifetime is increasing with raising electron temperature. The mechanism of an anomalous electron heat conduction is not yet clear. It is possible that it be associated with a trapped electron instability. An interesting effect of increasing plasma resistance when high frequency waves are superimposed was found in these experiments. It should be mentioned that under usual experimental conditions the electrical resistance in Tokamak devices always exceeds by several times the value predicted by the theory. The reason for this abnormal behaviour is not yet established. The increase in resistance may be caused partly by the presence of heavy impurities. In addition to it, one should expect that, due to the low plasma concentration, the flow of current will be accompanied by excitation of oscillations in the plasma that will lead to an intensive slowing down of the electrons... But it cannot be excluded, that the additional resistance is caused by a simple exchange of momentum between electrons and high frequency waves.

The stabilization of hydromagnetic instabilities in tokamaks achieved first of all by means of a strong longitudinal field (i.e. the Kruskal-Shafranov criterion $q = \frac{B_z a}{B_\theta R} > 1$ is satisfied, where B_z is a

azimuthal field, a is the small plasma radius, R is the large radius). But the definite role is played by the copper wall and in order to determine this role the T-6 device has been constructed with the copper wall located much closer to the plasma surface. The experiments with this device indicate that the plasma actually becames more stable microscopically, permitting to achieve the values of q = 1. Alongside with this, it was found that the longitudinal field is very homogeneous. In this case, the acceleration processes are easily occured when the basic plasma remains cold ($T_e \simeq 10$ ev) and the current is carried by a small group of electrons. Fortunately , these conditions are easily eliminated by a preionization of the plasma or by a small bumping (2 + 3%) of the magnetic field. Perhaps, the formation of accelerated particles is associated with the development of the so called "disruptive instability" which sometimes is observed in tokamaks.
A rather interesting effect of considerable concentration of heavy impurities near the axis of the plasma was observed recently. This effect is purely classical, it was predicted theoretically longtime ago.

Though experiments on tokamaks have been carried out for many years, it is not possible as yet to say that the optimal geometry of the plasma has been found. It is not excluded that for improving the main physical parameters it may be desirable to change the shape of the plasma cross-section.

The other version of closed systems is being realized in stellarators. The longitudinal plasma current is not necessary for plasma equilibrium in stellarators. Therefore the plasma in this system may be produced not only by induction discharge, but also by plasma guns or by high frequency gas ionization.

The different methods of production of high temperature plasma in stellarators are being developed in the Physical-Technical Institute (Kharkov) and in the Lebedev Physical Institute. Many devices of stellarator type have been built. The largest of them, "Uragan",was built in Kharkov. The length of the plasma ring of the device is equal to 10 m, and the maximum strength of the magnetic field is 10 kgauss.

It was shown experimentally that the plasma decay rate decreases when the angle of the rotational transform increase s.The time of plasma energy confinement increases with the electron temperature. For the "Uragan" device it reaches 0.5 msec at $n = 2.10^{13}$. The T_e value measured by scattering of the laser light is 100-400 ev. It should be noted, that the extrapolation of the "Uragan" data to the size and the values of magnetic fields of the large Tokomak device, show that the energy and particle lifetimes are closed to those for T-3 device. The dependence of plasma diffusion in "Uragan" on the collision frequency is similar to that predicted by the neoclassical theory, but is 10 times higher in its absolute value.

The second traditional branch of thermonuclear programme is adiabatic or mirror traps. After Ioffe experiments in 1961 ,the adiabatic traps are usually designed in accordance with the "minimum B principle". However, other methods are being studied for suppression of flute instability, for example, feedback control.

It should be noted that ,in addition to the flute instability ,more subtil the so-called "loss-cone instabilities" have been predicted theoretically. They should develop in mirror traps due to nonequilibrium distribution of ions in the velocity space. The studies of the role of these instabilities and the possibility of their stabilization are the major objective of studies in adiabatic traps. The genral results of the studies is that loss cone instabilities are less dangerous than it may seem from the theoretical point of view. Namely the following results have been obtained.

The experiments on plasma confinement with an initial concentration of 2.10^{12} and the ion temperature of 200-300 ev were made by Ioffe and collaborators on minimum B device (PR-6 with six rods). The plasma studies with such a relatively low temperature is of interest, since it most fully scales the plasma state with the thermonuclear parameters. Due to relatively low temperature ,the dominant role in plasma processes is played by Coulomb collisions between the particles.

The measurement of the decay time of such a plasma indicates that the initial desintegration phase, of the order of 0.2-0.3 msec, is quiescent i.e. without instabilities. The life time in this initial phase is

in agreement with the results of classical theory for a stable plasma (in such calculations only Coulomb collisions are taken into account). Particularly, it is shown experimentally, that confinement time grows while the ion energy increases, which is in agreement with classical theory. But later instability develops which is probably a drift loss cone one, and the rate of plasma decay goes up. The development of the instability is accompanied by heating of electrons and by the increase of plasma potential, which in its turn disrupts the ion function distribution. The instability becames non-linear at very low level and, after that, the amplitude is controlled by the plasma potential.

Different methods of filling the traps with a dense, high temperature plasma were developed. One of the most natural ways is the injection of an intensive flux of fast neutral atoms which, while in the trap, may somehow be ionized. Several fast neutral injectors were designed and built for Ogra 1 and Ogra II devices. The latest one, with equivalent current up to 0.5A and energy of 20 keV was installed on LIN-5 facility (plasma volume 5ℓ). The experiments on stabilization of different types of plasma instabilities by means of electric feedback systems were continued. It was shown that in the simpliest version with one electrode feedback loop, the employment of feedback system permits to increase plasma density from 10^8 to 10^9 cm^{-3}.

After some modification of "Ogra II", experiments were carried out to investigate the possibility of creating an high temperature dense plasma by means of the so-called "turbulent heating". This was achieved in the following way : a special injector produces a stream of cold plasma which is distributed along the axis of the system. Between the plasma injector and the opposite electrode, a high voltage pulse is applied for several microseconds. Due to instabilities, an intensive turbulent heating of electrons and ions takes place. Measurements of plasma parameters, performed directly after the heating phase,have shown that,at concentrations of $n = 1.10^{13}$, the ion energy spread is very large and that their mean energy is 1 + 1.5 keV.

The confinement time of a such plasma at H = 12 kgauss is 0.4 msec, which is only twice lower than the classical value. It is worthwhile to point out that in this facility no means were provided to stabilize flute

instability (there is no B minima) and that the value of the additional plasma leakage (compared to classical) is in good agreement with that predicted by Kadomtsev's formula for turbulent plasma in a trap without minimum B. Another interesting fact is that the loss cone instability, which according to theory should inevitably occur in the plasma with available parameters, gives no evidence of its presence. Possibly, in this case, it also reaches non-linear regime at a very low level. Adiabatic magnetic traps continue to be an important element of scientific programme for controlled thermonuclear fusion.

Besides these two major approaches, the investigations were more moderately pursued in other probable directions. Particularly, the work on the so-called plasma focus-cumulation in Z-discharge of complex geometry, on Z, θ and combined pinches, on electrostatic confinement of plasma was continued.

For a number of years,much attention was paid to the analysis of plasma interactions with RF electromagnetic fields. Such processes are of interest from two points of view. Firstly, RF fields may suppress various instabilities of a plasma confined in a magnetic field. Secondly, application of RF fields heats the plasma and such fields can be used for heating the ion component in closed systems, such as "Tokamak". One should distinguish two major versions :

a. resonance heating with external source of RF-voltage,
b. stochastic heating by fluctuating RF-fields, which occur during the decay of plasma oscillations (turbulent heating).

Experiments on plasma stabilization by RF fields (so-called dynamic stabilization) was investigated for several years at Sukhumi Physical-Technical Institute, at Kurchatov Atomic Energy Institute and at Leningrad Institute of Electron-Physical Apparatus. In these experiments, the object of stabilization was a plasma pinch with a strong longitudinal current. In a number of experiments, it was shown that major instabilities and particularly Kruskal-Shafranov instability can be suppressed by additional RF currents in the pinch.

In Atomic Energy Institute and in Leningrad Physical-Technical Institute a number of methods of plasma resonance heating by RF-fields are

being investigated; the methods are based on electron-cyclotron resonance and on the so-called "hybrid"resonance. Besides that, plasma heating in toroidal systems by means of magnetic-sound resonance is being studied at Kurchatov Institute of Atomic Energy.

The turbulent heating of plasma by current was used for heating of the ion component in the "Ogra II" mirror trap . In Kharkov Physical-Technical Institute, by means of this method, the ion component of the plasma was heated up to a temperature of 2 kev, the density being 10^{15} cm^{-3}.

Due to the rapid development of new fields and of new methods in experimental physics, new practical approaches becomes possible. We mean first of all heating by laser. This method was proposed by Basov and Krokhin in 1962. Laser beam is focused on a very small deuterium target. At the initial phase of the process, a super dense plasma is produced, and its temperature rises very rapidly. Due to a very high thermoconduc - tivity of hot plasma and due to shock waves, the energy rapidly penetra-tes inside the target and heats it.

The experiments on laser heating were performed in Physical Institute of the Academy of Sciences of USSR. Recently, a new installation has been built which gives spherically symmetrical irradiation of a target (nine beams are used) and provides total energy up to 1300 j per beam in a regime of 30 nsec pulse. At energy of 240 j and pulse time of 6 nsec, neutron yield was 10^6 neutrons per pulse.

An interesting possibility of super strong compression of hydrogen target up to 10^4 times using programmed spherical laser pulse was recently reported by Teller. He stated that beam energy of 10^5 j is quite sufficient for ignition of thermonuclear reactions. Calculations which were carried in USSR support this conclusion and show that super strong compression is one of the possible ways of achieving controlled fusion by means of laser. At present, investigations of laser heating processes are very widely spread and in the nearest years they can grow into one of the most important directions of the thermonuclear fusion programme. Prospects of this direction depends primilarly on the progress of increasing the effi-ciency of laser sources. Power efficiency of pulsed lasers is still very

low. Moreover, one should note that the experiments on laser heating are in their initial stage so far. They still have not furnished us with sufficiently complete information required for checking-up and correcting the theoretical conclusions about the process of laser heating.

Recently, a new method of superfast pulsed heating of matter up to thermonuclear temperatures by relativistic electron beams came into being. In this method the efficiency of initial power source - pulsed electron injector - is of order of several ten percent. That is why this method of heating will gain good chance for further development. However, one should overcome difficulties connected with focusing of electron beams at currents of 10^6 A. Powerful relativistic beams may be also applied for fast injection of energy into plasma. Experiments on such method of heating are underway in Novosibirsk, where a bumped field is suggested for longitudinal confinement of plasma (in transverse direction, the plasma should be confined by the walls).

In the last years, a theory of physical phenomena in high temperature plasma continued to be developed in USSR. A theory of plasma equilibrium and stability in toroidal systems of complex geometry was developed (in particular systems of Tokamak type with not-round cross section of plasma ring were studied) and neoclassical theory of transfer processes, theory of propagation and transformation of waves in non-homogeneous plasma were studied as well. Major attention was devoted to different types of non-linear collective phenomena in a plasma and a number of interesting results were obtained.

Considering the general outline of scientific research in the field of thermonuclear fusion, one can say that in the last several years we progressed in a number of traditional directions and besides that, some new fruitful ideas came into being, which open approaches for solving the problem.

At present, the state of investigation of the problem is on a sufficiently high level. After overcoming distructive instabilities, physicists have learnt how to obtain quiet plasma but with not very high density.

The next stage, which probably will take from 5 to 10 years, should be completed by achieving the Lawson criterion. Then it will be necessary to overcome the technological difficulties of designing thermonuclear power facilities. These are the rates of advancing along traditional paths. These rates are not so high to inspire great satisfaction, but still not so low to justify pessimism. Advancing is a continual process, although it is not so fast, as we would like it to be.

SUPPLEMENTARY PAPERS

3

Tokamak Apparatus (JFT-2) in JAERI

by

S. Itoh, M. Ohta, N. Fujisawa, T. Takeda, M. Maeno, A. Funahashi, K. Inoue, S. Kunieda, S. Matsuda, T. Tazima, N. Suzuki, T. Ohga, T. Matoba, S. Kasai, T. Sugawara*, K. Toi and S. Mori

JAPAN ATOMIC ENERGY RESEARCH INSTITUTE

Tokai, Ibaraki-ken, Japan

Preliminary experiments of the JFT-2 have been carried out by using the magnetic probes and the visible monochrometer. Displacement of the plasma column have been measured by the horizontal and vertical sets of the magnetic probes. The CII line from the plasma has been observed and compared with the temporal evolution of the other signals. The ordinary fixed limiters of 327 mm and 500 mm were used to define the plasma boundary. Because a single condenser bank was used to drive the primary current of the transformer, the plasma current duration time was as short as about 15 msec. Hydrogen of 10^{-3}~10^{-4} Torr was filled and preionized by ECRH microwave. Though the 2 mm microwave interferometer is being adjusted, the electron density was estimated to be more than 10^{13} cm^{-3} by the reflection of ECRH microwave.

After about 1000 discharges the loop voltage was reduced considerably and the initially unobserved negative voltage spikes were observed (Fig. 1). The temperature was estimated to be about 20 eV for Z=1. Figure 2 shows that the intensity of CII line increased when the negative spikes were observed. Displacement of the plasma column has been measured under the presence of only the DC vertical field. The plasma was produced initially near the inner edge of the limiter and then the column expanded outwards, and shrank inwards simultaneously with the negative spikes (Fig. 3). Figure 4 shows the comparison between the experimental values and the theoretical ones of the horizontal position of the plasma column. The result of the measurement by the vertical set of the magnetic coils shows that the plasma column is displaced upwards by about 1 cm, which is blamed to the fact that the distribution of the current between the two returning windings of the toroidal coil was not adjusted properly. Figure 5 shows the vertical fields generated by the shell and the current transformer in the presence of the current ring in the shell center, and suggests the importance of the effects of the shell gaps and the iron core.

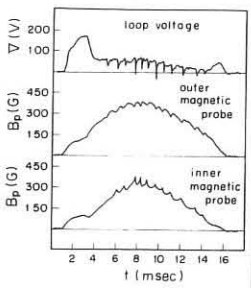

Fig. 1. The loop voltage and the magnetic probe signals. P_p=2x10^{-4} Torr, B_t=10 kG, B_p=40 G, B_p=100 G corresponds to I_p=15 ka.

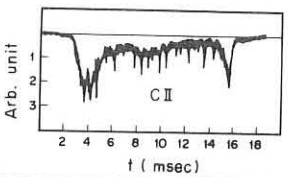

Fig. 2. The CII line.

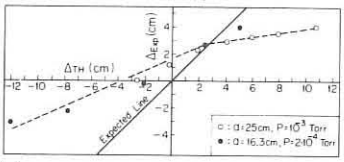

Fig. 4. The comparison of the displacement of the plasma column.

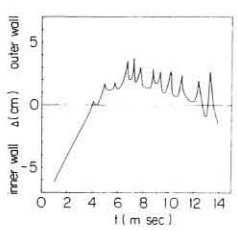

Fig. 3. The time behaviour of the horizontal position of the plasma column.

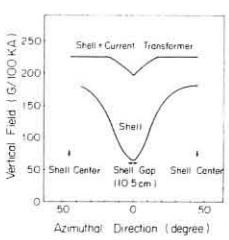

Fig. 5. The vertical fields generated by the shell and the current transformer in the presence of the center current ring.

* On loan from Tokyo Shibaura Electric Co. Ltd., Kawasaki, Japan.

24

NUMERICAL STUDIES OF MHD EQUILIBRIUM AND STABILITY IN TOKAMAKS WITH NON CIRCULAR CROSS-SECTION

P.Grelot, J.Weisse

ASSOCIATION EURATOM - CEA
Département de Physique du Plasma et de la Fusion Contrôlée
Service IGn - Centre d'Etudes Nucléaires
Cédex 85 - 38 GRENOBLE Gare (France)

TRIANGULAR DEFORMATION OF ELLIPTICAL SHELLS

(1) Shell given by $(\gamma/\sqrt{a^3b^3})\cdot\rho^3\cos 3(\theta-\theta_1)+\rho^2(A+B\cos 2(\theta-\theta_0))-1=0$
On the first figure (polar coordinates) we plot J as a function of θ_1, for $\theta_0=\frac{\pi}{2},\frac{\pi}{3},\frac{\pi}{6}$, 0. γ is kept constant and equal to 0.1.
For each value of θ_0 one can find an optimal value of θ_1, so that J is maximum. Nevertheless these maximum values are almost equal for $\beta^*=1$. We may add that the maximum value of J increases when increasing γ
On the second figure the dotted curves show the stability regions in two limiting cases ($\theta_0=0$; $\theta_0=\frac{\pi}{2}$) for the maximum value of γ in each case. (The shell must be a closed curve).
Again at $\beta^*=1$ the results for J and β are almost the same.

(2) Shell given by $\rho=\rho_E(1+\alpha\cos 3\theta)$
It is obvious on the second figure that for $\alpha=0.3$ this kind of deformation gives higher values for J and β when β^* is less or equal to 1.
The detailed study of Mercier criterion is now necessary away from the magnetic axis.

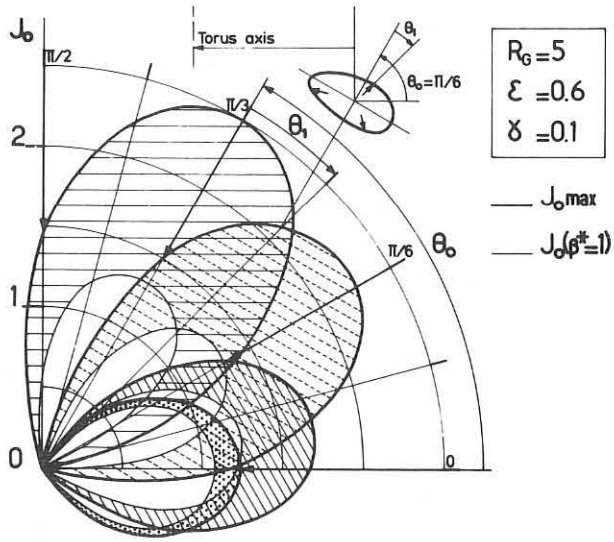

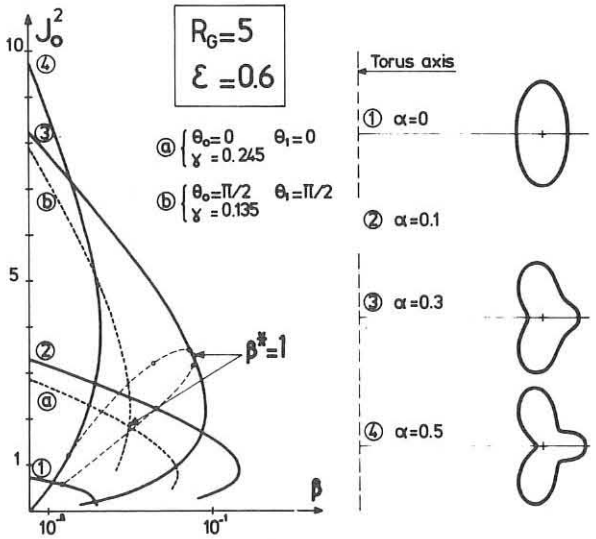

29

TEARING INSTABILITY DUE TO THERMAL EFFECTS

by

P.H. Rebut and A. Samain

ASSOCIATION EURATOM-CEA SUR LA FUSION

Département de Physique du Plasma et de la Fusion Contrôlée
Centre d'Etudes Nucléaires
Boite Postale n° 6 . **92 Fontenay-aux-Roses** (France)

We study the non linear instability of the tearing perturbation B_1 specified above, when $\Delta = (L_s \tilde{\psi}/B_0)^{1/2}$ has a finite value, by considering a neighbouring (or slowly growing) equilibrium state of the plasma. We assume that $\chi_\parallel = \infty$. Then T and η are constant along the lines of force , i.e. $T = T(\psi)$ and $\eta = \eta(\psi)$ where $\psi = u^2 + \sin^2 v$, $u^2 = B_0 x^2 / 4 L_s \tilde{\varphi}$ and $v = Ky/2$ (The axis of the magnetic islands and the separatrix correspond to $\psi = 0$ and $\psi = 1$, respectively) . To simplify, we assume that there is no zero order temperature and density gradients. We find a solution which is consistent with the dynamical equations and the generalized Ohm Law by taking $I = I(\psi)$, $n = n(\psi)$, $\eta I = E_0$ and $nT = n_0 T_0$. We assume that the perturbations $n - n_0$, $T - T_0$, $I - I_0$, $\eta - \eta_0$ are small. Then the heat equation for electrons in the plane x, y may be linearized with respect, to these variables. We thus obtain:

$$(6)\quad (I - I_0)/I_0 = \frac{3}{2}\theta(\psi), \quad (T - T_0)/T_0 = (n - n_0)/n_0 = \theta(\psi)$$

where $\theta(\psi)$ satisfies the differential equation:

$$(7)\quad \frac{d}{d\psi}\left(S \frac{d\theta}{d\psi}\right) + A \frac{dS}{d\psi}\theta = 0$$

Here $S(\psi) = \oint (\psi - \sin^2 v)^{1/2} dv$, $A = 2Z\Delta^2/\Delta_{cr}^2$, $\Delta_{cr}^2 = \chi_\perp T_0 / \eta_0 I_0^2$ and $Z = 3/2 + (\lambda - \mu) P_0 / \eta_0 I_0^2$. We assume that $0 < Z \sim 1$. Then (7) admits a solution $\theta_R(\psi)$ which is regular at $\psi = 0$, $(\theta_R(0, A) = 1)$ and which is finite for large ψ in the bulk of plasma .

We may take $\theta(\psi) = \Lambda \theta_R(\psi)$, where Λ is a constant, to describe the desired neighbouring equilibrium. The perturbations $I - I_0$, as given by (6) mainly consists of an y modulated contribution $\tilde{I}(x) \cos Ky$, .. plus a contribution $I_0'(x)$,... which is uniform along $0y$. It may be shown that the function $\tilde{I}(x)$ is localized near $x = 0$ in a range $\sim \Delta$. This function must satisfy the first part of the condition (1) , which actually determines the constant Λ as $\Lambda = -(\Delta/L)(cB_0/4\pi I_0 L_s)\, g(A)$.

where $g(A) = \frac{\pi}{3}\left(\int_{-\infty}^{+\infty} d\psi\ \theta_R(\psi, A) \oint (\psi - \sin^2 v)^{-1/2} \cos 2v\, dv \right)^{-1}$

On the other hand, the functions $I_0'(x)/I_0$, T_0'/T_0 behave as $\sim \cos(x\, 2^{1/2}/\Delta_{cr})$ far from the magnetic islands. In principle, the instability mechanism could act for very small values of Δ . However we must have $\Lambda \ll 1$ for the above linearization to be admissible . For $\Delta/\Delta_{cr} \ll 1$ this constraint reads

$$1 \gg (\Delta_{cr}/L)(cB_0/4\pi I_0 L_s)$$

If the zero order pressure gradient $\partial p_0/\partial x$ is not zero, we find a self consistent neighbouring equilibrium taking $T = T(\psi)$, $I = I(\psi)$, $\eta = \eta(\psi)$ and $\eta I = \eta_0 I_0$. However a x dependent pressure $p(x)$ must be introduced. The ions must have a uniform velocity V in the direction $0y$. The electrons must move along the surfaces ψ = cste. In particular they do not contribute in the current I_y along $0y$ in the plane $x = 0$, where $B_1 y = 0$ In that plane we may write $I_y = ne\, V$; $I_y = (c/B_0)(\partial p/\partial x)_{x=0}$ (8)
By averaging the y component of the generalized Ohm Law in the plane $x = 0$ we obtain

$$\overline{v_x} = \frac{c}{B_0}\left(\overline{\frac{v_z}{c} B_{1x}} - \eta I_y \right)$$

where v_x is the x particle velocity , v_z is the ion velocity along $0z$ and the bars means averaging in the y direction . The velocity v_z results from the equilibrium between the Laplace force $-I_0 B_{1x}/c$ and the viscosity force $\nu \partial^2 v_z/\partial x^2 \sim \nu v_z/\Delta^2$ Therefore we have $\overline{v_z B_{1x}} \sim -\Delta^2 B_{1x}^2 I_y/\nu c$ and the diffusion velocity $\overline{v_x}$ at $x = 0$ is equal to $-(1+\alpha)(\eta_0 c^2/B_0^2)(\partial p/\partial x)_{x=0}$ with $\alpha \sim B_{1x}^3 L_s/\nu \eta_0 c^2 K B_0$
This velocity must be equal to the x particle velocity $-\eta_0 c^2/B_0^2\, \partial p_0/\partial x$ in the bulke of plasma . Therefore we have $(\partial p/\partial x)_{x=0} = (\partial p_0/\partial x)(1+\alpha)^{-1}$ as a consequence of the presence of the magnetic islands. The y velocity of the magnetic perturbation relative to the ions in the bulke of plasma is equal to $-V$ and may be deduced from (8).

38

NUMERICAL STUDIES OF DIFFUSION IN TOKAMAK CONFINEMENT

by P.M. Keeping, R.C. Grimm and J. Killeen
U.K.A.E.A., Research Group, Culham Laboratory, Abingdon, Berkshire, U.K.

The most significant feature of our latest computations is the appearance of skin effects in constant current models, i.e. peaks in the T_e and $j_\parallel$ profiles near the wall. This is much more pronounced when the plateau regime is introduced. In figure 3 we compare the evolution of the electron temperature profile as shown in figure 1 with that from an identical run, but using smoothed banana-plateau coefficients and Connor and Hastie's form for the conductivity.

In contrast to this moderate skin effect we display in figures 6 and 7 the initial and final T_e and $j_\parallel$ profiles, for the various coefficients, for runs over 150 ms of an ST model (R = 109cms, a = 14 cms, B_0 = 44Kg, I = 42KA), with initial profiles based on experimental observations[8]. A slight peaking in the pure banana cases becomes extreme with the smoothed banana-plateau coefficients and the axial T_e and $j_\parallel$ values drops even lower. (The peaking is reduced by increasing the pedestals but it is still the dominant feature of the final profiles.) In figures 5, 6 and 7 the later profiles shown are close to their final steady states. In the sm. b-p runs, for the case with the most severe skin effect, the plateau zone extends outwards over 80% of the radius while for the case shown in figure 3 it occupies only the inner 26%.

As figures 3 and 4 indicate we do not find skins in larger tokamaks (with smaller aspect ratios), where the plateau regime is less important. This is further confirmed by the results shown in figures 8 and 9 for a run with smoothed b-p coefficients and Connor-Hastie conductivity (note $\varepsilon_{max} = 1/3 > 0.26$). Here R = 195, a = 65cms, B_e = 45Kg, I = 1600KA, and the initial n, T_e and T_i profiles were parabolic with 10% pedestals and maxima at 10^{14}/cc, 2500eV and 2500eV. After 300 ms a steady state has not been reached, because the axial Ware density peak has not yet begun to diffuse outwards.

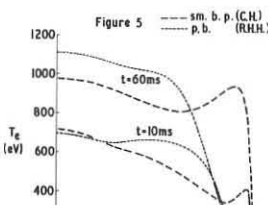

(8) Dimock et al., Ibid.(3), Vol.1, p.451.

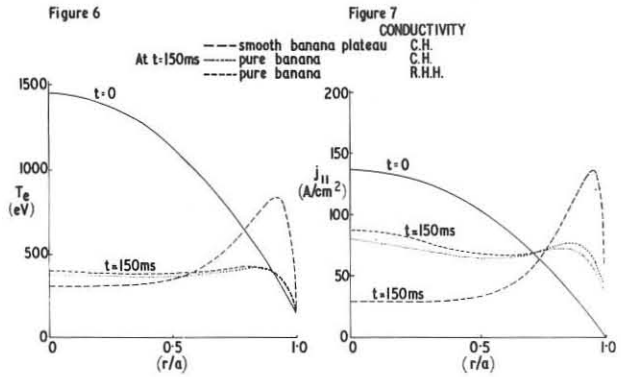

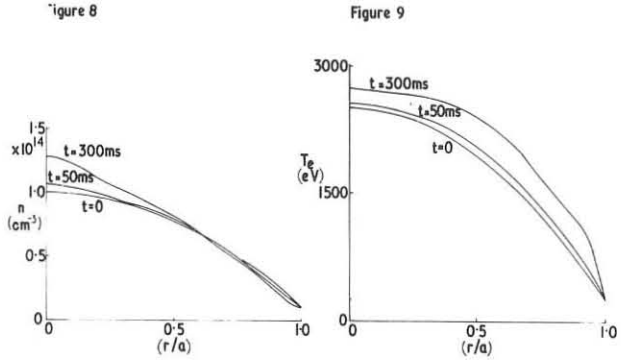

40

TOKAMAK TWO-FLUID CODE: EFFECTS OF NEUTRAL BEAM HEATING, RADIATION LOSS, AND CHARGE EXCHANGE*

J. T. Hogan and R. A. Dory

Oak Ridge National Laboratory
Oak Ridge, Tennessee, USA

The neo-classical version of our code has been used to compare results with those described in Ref. 1, Fig. 18. We choose ST parameters: a = 14 cm, R = 109 cm, B(toroidal) = 30 kGauss, total current I = 40 kAmperes, constant in time. The initial and boundary values are:

Initial values	Boundary values
$T_e(r) = 200\ (1 - .8r^2/a^2)$ eV	$T_e = 40$ eV
$T_i(r) = 20$ eV	$T_i = 20$ eV
$J(r) = 130\ (1 - r^2/a^2)$	B(poloidal) = 571 Gauss
$N(r) = 10^{13}\ (1 - .8r^2/a^2)$	$N = 2\ 10^{12}$ cm^{-3}

We use transport coefficients recently derived for the banana-plateau regime and so, although the general features of the solutions are in agreement, there are the expected differences in detail. We show in Figure 1 the electron temperature profiles at t = 10 and 30 Msec. The characteristic particle and current density profiles are shown in Fig. 2.

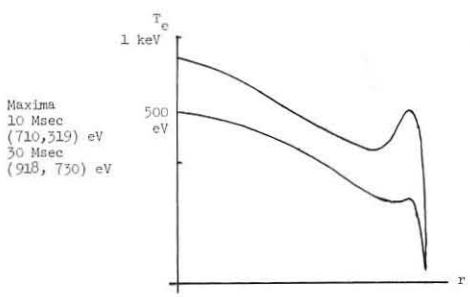

Fig. 1. Electron Temperature Profiles

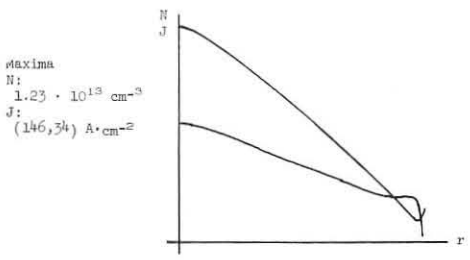

Fig. 2. N and J Profiles at 10 Msec

*Research sponsored by the United States Atomic Energy Commission under contract with the Union Carbide Corporation.

1. D. F. Düchs, et al., 4th Intl. Conf. on Cont. Fusion, Madison (1971).

43

NUMERICAL RESULTS ON THE INFLUENCE OF AN AXIAL ANTIPARALLEL BIAS MAGNETIC FIELD ON THE ENERGY TRANSFER IN AN HIGH BETA DIFFUSE PINCH

BY

G.F.Nalesso, S.Ortolani

CENTRO DI STUDIO SUI GAS IONIZZATI - C.N.R. - UNIVERSITA' DI PADOVA
Istituto di Elettrotecnica, 6/a via Gradenigo - PADOVA - ITALY

In the main paper we discussed the positive effect of an axial antiparallel bias magnetic field on the plasma energy transfer. We pointed out that this positive effect was strongly related to the assumption of an anomalous description for the plasma resistivity. Moreover we mentioned that the result depends also on the compression rate.

When we wrote the main paper this dependence was not completely analyzed. By the kindly collaboration of the Culham Laboratory the one-dimensional MHD code is now available also in Padova. We have then obtained new results concerning the dependence of the heating effect, due to an increased antiparallel bias field, on the compression rate. Fig. 4 shows the percentage final energy variation, corresponding to an increase in the magnitude of the antiparallel bias field from 2 up to 4 kG, plotted against the product $\dot{B}_z \hat{B}_z$.

The results shown in the figure refers to a simple theta-pinch configuration.

We find that in order to obtain a positive effect in the plasma energy transfer, by increasing the magnitude of the axial antiparallel bias field, we must take into account the relative amplitude of the confining field and its rise time.

In particular we get that approaching low compression regime the positive effect vanishes becoming even strongly negative. Moreover we tried to distinguish the weight of $\dot{B}_z$ and $\hat{B}_z$ and we found that the critical parameter is $\dot{B}_z$.

The result is clearly shown in fig. 5 where the percentage variation of the final plasma energy corresponding to an increase in the antiparallel bias field from 2 up to 4 kG, is plotted against $\dot{B}_z$. All the results discussed are obtained assuming in the computation 10% of initial ionization level. The evolution of the ionization phase obviously affects the energy transfer. In particular the partial ionization in the theta-pinch configuration is expected to have a cooling effect dependent on the initial rate of rise of magnetic field (4). Our mind is to analyze at first the weight of this parameter.

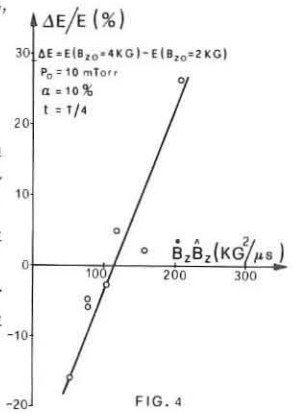

FIG. 4

The authors wish to thank D.Hasby of the Culham Laboratory, F.Bombi of this Institute and G.Favarin for the support given to have the MHD code available in Padova.

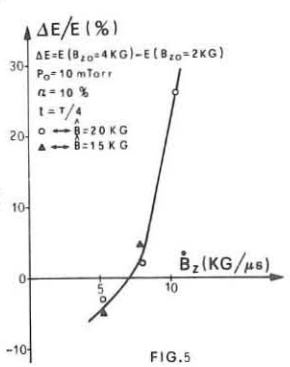

FIG.5

References:

[4] A.A. Newton - Paper A4 - "2nd topical Conference on pulsed high-beta plasmas" Garching - July 1972.

45

RESULTS FROM THE TOROIDAL Z-PINCH EXPERIMENT ZT-1

L. C. Burkhardt, J. N. DiMarco, P. R. Forman, A. Haberstich, H. J. Karr, J. A. Phillips

Los Alamos Scientific Laboratory*, Los Alamos, New Mexico, U.S.A.

Abstract: Magnetic field programming has produced reversal of the B_z field outside the pinch, with the zero in the field ~ 0.5 cm from the wall. MHD stability analysis of the magnetic field profiles shows a reduction in the growth rate and range of unstable wavenumbers with B_z reversal.

Programming of the magnetic field is accomplished by rapidly reversing the external I_θ approximately 1 μsec after the start of the main pinch current I_z. The radial distribution of the magnetic fields and the pitch are shown in Fig. 1, with and without B_z reversal. The plasma conductivity is sufficiently high so that the initial positive flux is trapped and compressed, increasing the B_z on axis and moving the B_θ field inward. With the magnitude of field reversal achieved so far, pressure balance prevents the zero in B_z from moving further than a few millimeters from the wall. An MHD stability analysis of the measured magnetic fields is presented in Fig. 2. The shaded areas represent the unstable modes calculated for a specified wavenumber from the diffuse pinch theory of Freidberg.[1] The amplitude of these modes is normalized to their growth rate. Horizontal lines indicate wavenumbers for which no unstable modes are found. Reversal of B_z removes the pitch minimum and reduces the range of unstable wavenumbers as well as the growth rates. The smoothed magnetic field profiles used in computing the results presented in Fig. 2(b) imply a residual pressure at the wall. Removal of the wall pressure by a slight alteration of the B_θ profile increases the band of unstable wavenumbers. From these data and streak photography some improvement in stability is noted, but reverse field profiles that are stable for all wavenumbers are not yet achieved.

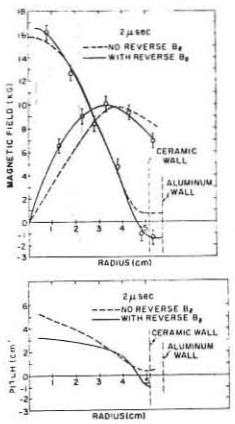

Fig. 1

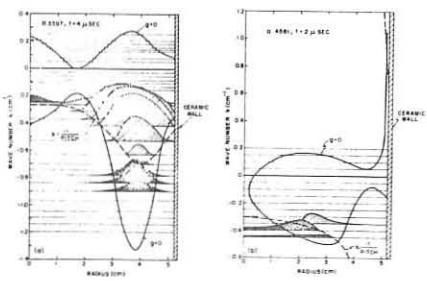

Fig. 2

* Work performed under the auspices of the United States Atomic Energy Commission.

1 J. P. Freidberg, Phys. Fluids, 13, 1812 (1970).

47

Shock Heating of Plasmas to Thermonuclear Temperature in a Megavolt Theta-Pinch

by

M.Keilhacker, M.Kornherr, G.Maret, H.Niedermeyer, and K.-H.Steuer

Max-Planck-Institut für Plasmaphysik, Euratom Association, Garching, Germany

In Paper No. 47 presented in the Proceedings of the 5th European Conference on Controlled Fusion and Plasma Physics (Vol. I) we have reported the first results of the Garching High Voltage Theta Pinch experiment. Meanwhile the measurements were expanded systematically to lower densities and charging voltages. Furthermore, density and electron temperature on the axis have been measured by laser light scattering.

Experimental results

During the strong neutron emission the electron density of the compressed plasma is about $2 \cdot 10^{13} cm^{-3}$ and is roughly constant (initial density $1{,}3 \cdot 10^{12} cm^{-3}$). Assuming constant line density one can calculate a plasma radius of 5 cm in good agreement with the magnetic field profile measurements (Fig. 3 of Paper No. 47). Shortly after the compression the electron temperature measured by laser light scattering with a multichannel arrangement is about 500 eV. In the following 300 nsec the electron temperature decreases to about 50eV and seems to be kept down by energy losses to the background neutral gas and by axial heat conduction. Simultaneously an increase of density due to ionization collisions is observed.

Neutron and magnetic probe measurements were performed down to initial densities of $3 \cdot 10^{10} cm^{-3}$ and charging voltages to 150 kV. These measurements show that strong piston heating holds for the whole parameter range investigated so far.

Scaling law for anomalous sheath broadening

Assuming the magnetic field diffuses into the plasma due to ohmic resistivity the sheath thickness Δ is given by the skin depth formula

$$\Delta = c/\omega_{pe}\,(\nu t)^{1/2}$$

The effective collision frequency ν is assumed to be proportional to ω_{pi} and the compression time to be described by the snow plough. For compression to one half the initial radius one finds that

$$\frac{\Delta}{R} \sim (R^2 \pi \dot{B})^{-1/4} \quad (R^2 \pi n_o)^{-1/8}$$

Fig. 5 shows this relationship with the parameter range investigated so far. The weak dependence of the sheath thickness from the initial density is verified by the measurements.

The lower bound of the diffuse sheath region results from the fact that the instability responsible for the effective collisions must grow to large amplitudes in a time short compared to the compression time.

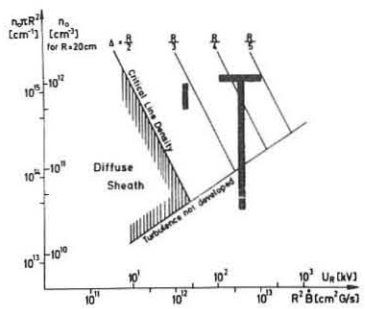

Fig. 5

48

EXPERIMENTAL INVESTIGATION OF COLLECTIVE PROCESSES IN A THETA-PINCH

T.A. El-Khalafawy, M.A. Bourham, A.Z. El-Behay, L.G. El-Hak, A.A. Gabr, V.V. Demchenko@ and A.M. Ternopol@
Atomic Energy Authority, Cairo, Egypt

In the main paper [1] investigation of turbulent processes in a theta-pinch are reported. From the results of experimental data obtained by means of microwave probes (MWP) introduced into the plasma and a horn placed outside of the discharge chamber, the unstable oscillations (UO) were proved to develop in the plasma. Since ref. [1] points out to an electrostatic nature of UO, a question arises: how is it possible that MWP (sections of rectangular waveguides) detect electrostatic UO?. The answer is ready if we take into account that, according to [2], the plasma density distribution is strongly inhomogeneous. To verify this statement made in [2] on the basis of magnetic probe measurements, we performed additional MW measurements. The amplitude distribution of the MW signal along the chamber radius is plotted in Fig. 1. One sees clearly the inhomogeneity of this distribution with maximum in the region of current sheath. In an inhomogeneous plasma, as known [3], the longitudinal oscillations can be transformed into transverse ones, the bulk of the transformation takes place in the regions of hybrid resonance, where a component $\varepsilon_{ij} \approx 0$. It was demonstrated in [4] that longitudinal oscillations in the region of the upper hybrid resonance

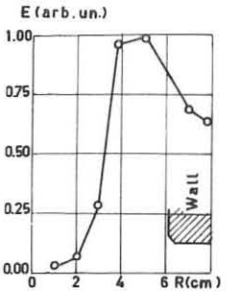

Fig. 1 Dependence of MW signal vs discharge radius.

$\omega_h = (\omega_{pe}^2 + \omega_{ce}^2)^{1/2}$ (ω_{pe}, ω_{ce} are the plasma and cyclotron frequencies, respectively) can be transformed into EMW with a frequency $\omega_{em} \sim 2\omega_h$. In our case $\omega_{em} \sim 6 \cdot 10^{11} sec^{-1}$, which agrees well with the experimental value $\omega_{rad} \sim 2 \cdot 10^{11} sec^{-1}$. Another argument in the favour of the above transformation is the direction of polarization of MW radiation. Following from Fig. 2, the MW signal amplitude attains a maximum when its E-plane coincides with the direction of UO electric field. The MW radiation is thus polarized in such a way that the wave electric vector is perpendicular to B_z. This result agrees with the theoretical prediction [4].

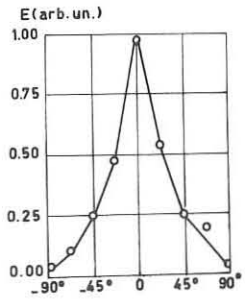

Fig. 2 Dependence of MW signal vs angle between E plane of MWP and direction of E_0.

It is naturally attractive to detect the region of transformation, because the hybrid resonance may occur both in the plasma itself and at the plasma-MWP interface. Though it has been indirectly proved that the transformation occurs at the plasma MWP interface (the probe signal was about ten times bigger than the horn signal), more scrupulous measurements are required to make the final conclusion.

REFERENCES

[1] T.A. El-Khalafawy et al., Vth Europ. Conf. on Contr. Fus. and Plasma Phys., Grenoble, 1972.
[2] T.A. El-Khalafawy et al., Phys. Lett., 39, 1972 (to be published).
[3] Tsytovich, V.N., Nonlinear Effects in Plasma, Plenum Publ. Corp., N.Y., 1970.
[4] Demchenko, V.V. et al., Izv. VUZ, Radiofizka, 15, 1971, issue VIII.

@ On leave from the Atomic Energy State Committee, USSR.

52

Mode Coupling in Dynamic Stabilization of MHD Modes (Part II)

by
G.Becker
Max-Planck-Institut für Plasmaphysik, Euratom Association, Garching bei München, Germany

In the first part of this paper (Conf.Proc.,Vol.I,p.52) it has been shown that the existing linearized theory of dynamic stabilization of MHD modes is not applicable in the case $\omega_s \gg \omega_i$. This result is proved in more detail in /5/. Since $\omega_s \gg \omega_i$ was assumed in the normal mode analyses and is experimentally true as well, presently there exists no theory of dynamic stabilization of MHD modes that can be compared with experiment. The fairly intuitive model calculation presented in the first part of this paper cannot of course replace an exact non-linearized MHD analysis of the whole problem of dynamic stabilization that takes into account mode coupling terms. Therefore theoretical predictions concerning for example the optimization of the $\tilde{B}_z$-stabilization of the m = 1 mode on a linear or toroidal screw pinch should only be based on a non-linearized MHD analysis.

Apart from the small loss of HF power compared with other dynamic stabilization methods /1/ the $\tilde{B}_z$-method has the advantage that many MHD modes with growth rates $\omega_m \ll \omega_s$ can be dynamically stabilized at a time. This is true because all these modes can be coupled at the same time to the enforced m = 0 oscillations. It is necessary to dynamically stabilize with the smallest possible relative field amplitude in order to reduce the HF power loss in the outer circuit. This can be accomplished in two steps:

1) Optimize the relation between the relative plasma amplitude (m = 0 oscillation) and relative field amplitude
2) Maximize the coupling between the driving m = 0 mode and the unstable mode.

The relative field amplitude necessary to generate a certain relative plasma amplitude may be reduced by working in resonance with the natural frequency (ω_0) of the m = 0 oscillation /6/.

In this case the HF energy circulated in the system is a minimum because the HF circuit feeds energy into the cylindrical oscillations in all phases and thus only has to feed back the power lost by m = 0 damping processes. Therefore such a system with an indirect dynamic stabilization may be especially economic when the damping of the driving mode (m = 0) is small. For this type of dynamic stabilization it is important how the damping coefficient of the driving mode scales with the parameters of a fusion plasma. As for the strength of mode coupling this can only be optimized on the basis of a non-linearized theory of dynamic stabilization.

References (continued)

/5/ G.Becker, to be published in Plasma Physics
/6/ O.Gruber, Z.Physik, 251, 333 (1972)

53

Dynamic Stabilization Experiments on a Screw Pinch with Standing Wave Magnetic Fields (Part II)

G.Becker, O.Gruber, H.Herold
Max-Planck-Institut für Plasmaphysik, Euratom Association
Garching bei München, Germany

Experiments: The dynamic stabilization experiments described in the first part of the proceedings are extended to values of $\varepsilon = \left(\frac{\tilde{B}_z}{B_{z0}}\right)_{max}$ up to 0.26 in a shorter θ pinch coil. Also the distortion δ_o of the plasma normalized to the plasma radius in a bulge of the standing wave field has been measured. The parameters of the two experiments are shown in table 1. Typical

Table 1

Screw Pinch	Exp.1	Exp.2	Standing Wave Magnetic Field	Exp.1	Exp.2
θ coil length (cm)	175	111	number of loops	10	6
tube diameter (cm)	8	8	wavelength λ_B (cm)	29	29
B_{z0} (kG)	18	18	frequency ω_s (s^{-1})	6.6	5.5
$\tau_{/4}$ (μs)	4	4.3	Q	35	35
$\tau_{crowbar}$ (μs)	30	30	ε	0.12	0.26

growth rates of the m = 1 test instability with the reduced pinch length were $\omega_i \gtrsim 4\cdot10^5\ s^{-1}$ at $\lambda \lesssim 310$ cm. In addition the filling pressure was varied between 40 and 80 mTorr D_2. Again there was not observed any stabilizing effect due to the standing wave. A further increase of ε was not meaningful because the wall breakdown limit with strong damping of the HF currents [1,3] has already been reached at $\varepsilon \approx 0.25$.

The amplitude δ_o of the enforced m = 0, h ≠ 0 oscillations was measured by photometric evaluation of streak pictures taken in integral light close to the position of a loop. For the evaluation of $n_e(r)$ in successive compression and expansion phases of an individual discharge only continuum emission with a coefficient $\sim \frac{n_e^2}{\sqrt{T_e}}$ was assumed. The electron temperature was considered to be constant over the plasma cross section and also constant in time. The radial density profiles for the compression (a) and expansion (b) phases are well described by Gaussians (Fig.5). These measurements yield $\delta_o \approx 0.8\ \varepsilon$ at a frequency $\omega_s \approx 0.15\ \omega_k$ ($\omega_k \approx \frac{B_{z0}}{\sqrt{\rho_\ell}}$; ρ_ℓ line density). This is well in agreement with previous experiments [1,3] with homogeneous $\tilde{B}_z$ where $\delta_o \approx \varepsilon$ at $\omega_s \approx 0.2\ \omega_k$ was obtained by holographic interferometry for the same ε values.

Comparison with theory: The assumptions of the theory [2] were experimentally realized. According to this theory $\delta_{o(1)} > 0.074$ and $\delta_{o(2)} > 0.11$ are necessary for dynamic stabilization in experiment 1 and 2. Experimentally $\delta_{o(1)} = 0.11$ and $\delta_{o(2)} = 0.21$ were achieved. One can conclude that the dynamic potential due to the standing wave magnetic field is at least a factor of 4 smaller than theoretically derived. Probably the theoretical model is too much idealized since it takes sharp boundary, linearized MHD equations and neglects mode coupling (c.paper 52 of this conference). This mode coupling effect was found in the dynamic stabilization of the m = 1 mode by $\tilde{B}_z$ enforced m = 0, h = 0 oscillations of the plasma column [1,3] and it should exist for the m = 0, h ≠ 0 oscillations, too. In this case ε and δ_o have to be averaged along z giving $\bar{\varepsilon} \approx \varepsilon/2$ for the measured ε(z) respectively $\bar{\delta}_o \approx \delta_o/2$. These values are too small to fulfill a stabilizing condition corresponding to $\tilde{B}_z$ experiments [3]:

$$\bar{\varepsilon} > C\omega_i/\omega_s \text{ with } C = 2.5 \text{ for } \bar{\delta}_o \approx 0.8\ \bar{\varepsilon}.$$

Therefore the mode coupling effect should not be observed here.

Conclusion: The experiments show that the stabilizing effect of the standing wave scheme on the helical m = 1 instability is fairly weak compared with that expected from linearized MHD theory. Generally, if only mode coupling effects are considered, all inhomogeneous $\tilde{B}_z$ configurations need a field amplitude in the region of the bulges that is larger than in the homogeneous $\tilde{B}_z$ case since a certain averaged dynamical force per unit length has to be applied. Therefore the mentioned breakdown limit becomes more critical for inhomogeneous $\tilde{B}_z$.

References:

[1], [2] see part I
[3] O.Gruber, Z.Physik, 251, 333 (1972)

Fig.5

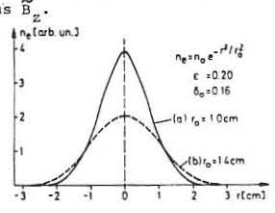

55

A TOROIDAL HIGH-BETA PLASMA IN A PERIODIC CAULKED-CUSP FIELD

by

T Uchida, K Sato, R Akiyama, N Noda, A Mohri,
N Inoue* and H Yoshimura**

* Present Address: Faculty of Engineering, University of Tokyo
** Permanent Address: College of Science & Engineering, Nihon University

This additional paper represents the summary of the experimental results obtained so far for the confinement of a theta-pinch plasma in the CCT field. Accordingly, this summary includes contents reported at the Madison Conference, 1971 J-1 and at the Garching Conference on Pulsed High-Beta Plasma, 1972, F7.

(i) Plasma Production. Sufficiently higher temperature (~ 10^{16}/cc) plasmas are obtained in spite of the insertion of rings. The axial homogenuity of plasma that might result from the induced ring current is hindered fairly well by the pinch phenomena of the contracting shock heated plasma layer.

(ii) Axial Motion. Just after the maximum contraction, an axial movement of the plasma towards the ring-plane and back to the midplane is seen when a negative bias field is applied. However, such axial motion disappears by 4 μs when the field reaches the maximum. When a positive bias field is applied, such an axial motion is not observed but the maximum Doppler temperature is estimated to be 10 eV and the produced plasma should have a low-beta value. This is due to the relatively lower rate of change of the magnetic field: 5 x 10^9 G/sec.

(iii) Equilibrium. As far as our experiments show, the existence of a magnetic field minimum at the midplane is necessary and sufficient to establish the equilibrium state of a toroidal cylindrical high-beta plasma.

(iv) Instability. A resistive ballooning mode instability might be probable to occur in the unfavourable curvature region of the magnetic lines of force on the outside of each ring conductor. In our case of 24 rings used, the growth time is estimated to be 40 μs for m = 1 mode.

(v) Plasma Pressure Decay. The decay time constant of the beta-ratio is deduced to be 6 μs, which is around equal to that of the ion temperature. After investigating for several loss mechanisms to be taken into account, the most likely cause of the pressure decay is the expansion of plasma pinched near the minor axis into the confining region of the CCT field. Namely, the value of 6 μs estimated as the pressure decay time is not for the high-beta plasma filling up the whole confining region of the CCT field, but for the high-beta cylindrical plasma produced near the minor axis of the CCT field.

(vi) Confinement. The particle confinement time estimated to be 20 μs may be limited by the plasma contacting on the inside of the ring, owing to the approach of the stagnation point to the ring. This approach is caused by the difference between the decay time of the coil current and that of the induced ring current, which originates in a proximity effect between both currents. When the higher conductivity metal is used for the ring, the contacting should occur at the later time.

61

THE EXPANSION OF A LASER PRODUCED PLASMA

P.T. Rumsby and J. Beaulieu
(UKAEA Research Group, Culham Laboratory, Abingdon, Berks., U.K.)

Abstract. The density of expanding laser produced plasma has been observed to fall as $n \propto R^{-3}$. Temperature measurements at large distances show a decay $T_e \propto R^{-1}$ as proposed theoretically.

I. Experiment

The experimental arrangement is as described in the main Conference Proceedings.

II. Results

The density decay of the expanding plasma shell has been examined out to a distance of one metre using charge collector probes. The decay of the density peak remains constant with $n_e \propto 1/R^3$ showing conclusively that particle recombination has negligible effect on the density decay rate.

Earlier we reported preliminary microwave absorption temperature measurements. This technique has now been improved and we have been able to measure collision frequencies and derived temperatures with reasonable accuracy. Fig.1 shows experimentally measured values of the collision frequency in the expanding shell. Points marked with circles and the dashed line correspond to the peak shell density. For $R < 60$ mm the peak density is greater than $n_{critical}$ for 4 mm u-waves (6×10^{13} cm^{-3}) so that the points marked with squares correspond to a density of 3×10^{13} cm^{-3} in the leading-edge of the shell.

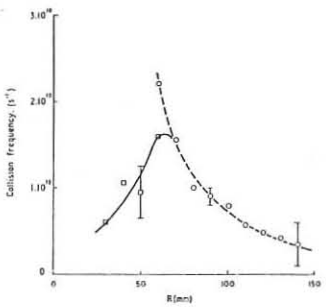

Fig.1

The plasma is highly collisional.

Fig.2 shows the dependence of the calculated electron temperature on expansion distance. The calculation is now straightforward as in the region in which we have made measurements n_{Debye} is roughly constant around 10 and not 2 as reported earlier. The two points plotted at 60 mm, corresponding to the shell peak and the leading-edge, agree closely suggesting a constant temperature within the shell. The temperature decay has a near 1/R dependence.

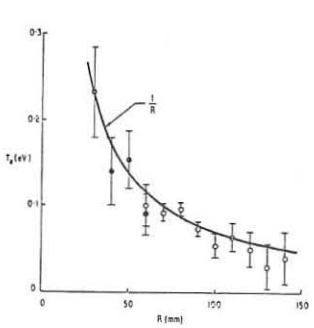

Fig.2

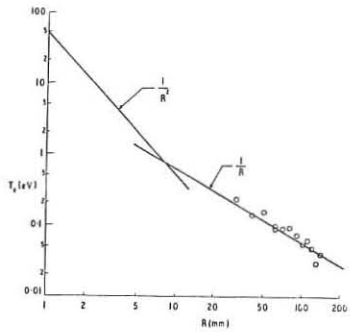

Fig.3

This result confirms theoretical predictions about the effect of particle recombination on the temperature decay. In such models initially $T \propto 1/R^3$ until recombination becomes important when a gradual transition to $T \propto 1/R$ occurs. Note that for $T \propto 1/R^3$ all collision frequencies remain constant with radius while for $T \propto 1/R$ they decrease as $1/R^{\frac{3}{2}}$.

Assuming an initial temperature of 50 eV in our laser produced plasma shell we find that our data fits such a model, as shown in Fig.3.

62

Absorption of Picosecond Light Pulses by Solid Targets

by

A.J. Andrews, T.A. Hall and T.P. Hughes

In fig. 3 results are shown for the reflectivity of boron, bismuth and lithium fluoride targets. In this figure the reflectivity is plotted as a function of incident energy rather than incident power. More careful measurements on these quantities indicate that the threshold power may be a factor of 5 less than that shown in fig. 2. This would bring the results into the same range as those quoted by Caruso (2).

The threshold values for the three conducting materials are not significantly different from each other, whereas for lithium fluoride no change in reflectivity is observed within the range of observations.

The lack of variation in threshold between the three conductors supports the hypothesis that ion motion can play no part in the absorption mechanism.

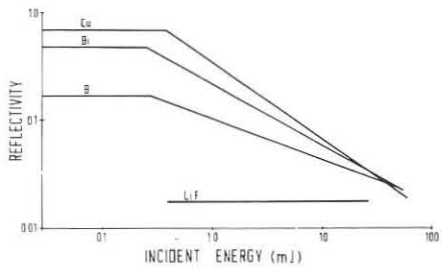

Figure 3 Reflectivity of various target materials as a function of incident energy.

65

NEW EXPERIMENTAL RESULTS ON THE PLASMA FOCUS

by

A. BERNARD, A. COUDEVILLE, J. DURANTET, A. JOLAS, J. LAUNSPACH
J. de MASCUREAU and J.P. WATTEAU

Commissariat à l'Energie Atomique, Centre d'Etudes de Limeil
B.P. n° 27 - 04 - VILLENEUVE-SAINT-GEORGES

We report the latest results on neutron measurements and holographic interferometry.

The neutron energy spectra taken at 117 meters confirm previous reports. The width of the spectrum after time of flight is measured with better accuracy and it is found that in some discharges at 7 Torr the width squares with a deuteron temperature lower than 1.5 keV. Thus all measurements fit with a thermal origin of the neutrons for these discharges.

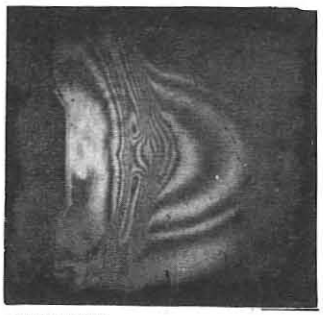

The density measurements have been made on a 27 kJ device with a 5 cm diameter hemispherical inner electrode and a 10 cm diameter outer electrode made of parallel bars. The machine can be operated at different filling pressures (1.5 - 10 Torr). The laser (2.5 nsec half-width) and the experimental arrangement are described in reference 1. Fig. 1 shows a typical interferogram obtained at 3 Torr D_2 filling pressure. It was recorded at peak neutron emission, 50 nsec after the beginning of the pulse. The axial shock wave created after the radial compression can be seen clearly. By Abel inversion the electron density can be measured as a function of space. Isodensity curves for the plasma of fig. 1 are drawn just below. They indicate a rather low density plasma ($\sim 5.10^{17}$ cm^{-3}) of extended volume (many cubic centimeters). For this régime the neutron pulse starts after the disruption of the filament which then does not contribute to the neutron yield. At 3 Torr the machine is reproducible so that it is possible to know the plasma development. The density on axis has been drawn for different times (Fig.2). At t = 0 one observes a broken filament and also a plasma located along the center electrode with density larger than 4.10^{18} cm^{-3}. From the three profiles one can estimate the plasma axial velocity to be about 3.10^5 cm.s^{-1}.

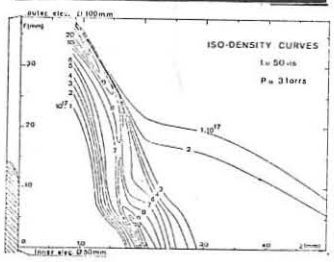

Fig. 1

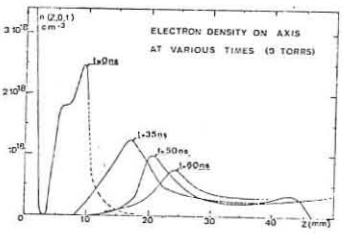

Fig. 2

The study of the plasma at higher filling pressures is not made yet so that no complete comparison can be done with the functionning of the 100 kJ device. However the first results indicate that the lifetime and the density of the filament increase with the initial D_2 pressure.

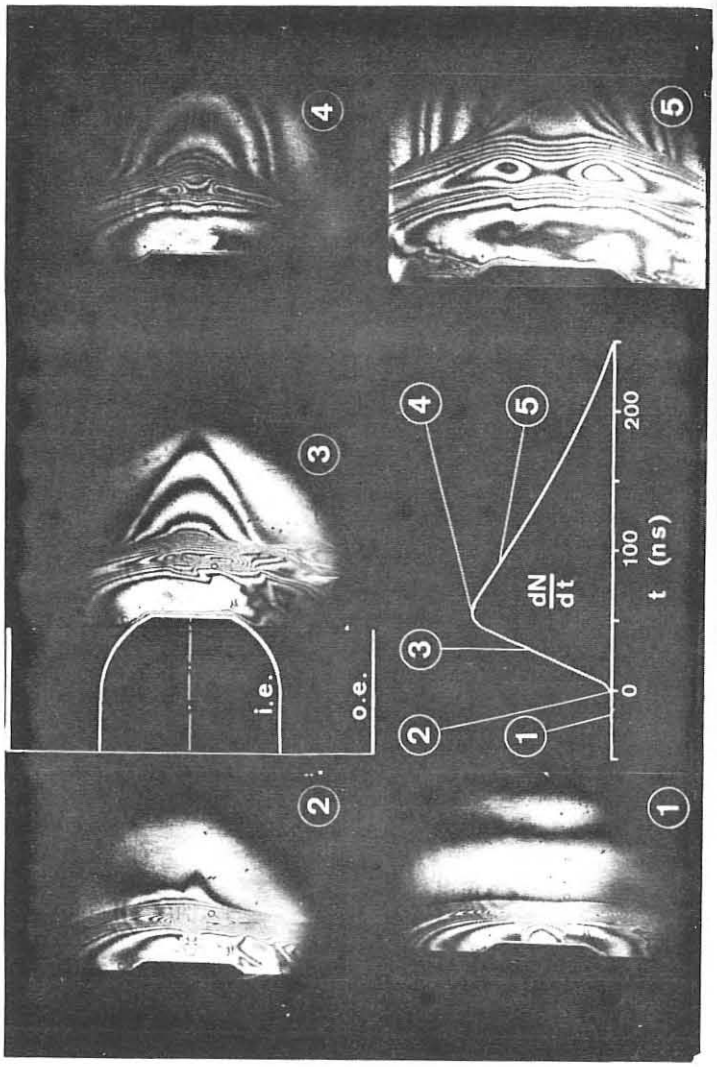

/1/ A. BERNARD, A. JOLAS, J. LAUNSPACH, J.P. WATTEAU.- Etude d'une décharge linéaire non-cylindrique par interférométrie holographique (A paraître)

70

Intensity Anisotropy and Fine Structure in the X-Ray Images of the Dense Plasma Focus (II)

W. H. Bostick, V. Nardi, W.J. Prior and F. Rodriguez-Trelles
Stevens Institute of Technology, Hoboken, N.J., U.S.A.

Abst. The intensity anisotropy of localized x-ray sources is numerically estimated from several films all obtained under similar conditions.

A quantative estimate of the anisotropy of the x-ray intensity emission has been carried out from the images (pinhole camera photographs) of many localized x-ray sources (elongated spots usually with a cylindrical or a concave spool shape) in the plasma far (at a distance > 1.5cm) from the hollow anode wall. Each localized source has sharp boundaries and frequently appears as the core of a more diffuse source which radiates softer photons with a lower intensity I for unit of volume. The major dimension or spot length, ℓ (on film), defines the source axis ∿ parallel to the electrode axis or z-axis; a diameter d orthogonal to ℓ is also defined for each spot by boundaries which are particularly sharp in this direction. The purpose is to assess possible fluctuations in the x-ray anisotropy as given by the ratio I_{80^o}/I_{0^o} where I_{80^o} = X-ray intensity in the direction at 80^o with respect to the source axis; I_{0^o} = intensity along source axis. Films at different angular positions are located on a circle with the center p at 8mm above the center of the anode-end-section on the electrode axis. We have analized only the localized sources which can be clearly identified on both 0^o and 80^o films and are located at an axial distance < 1cm from point p, within a distance R' <Max R' = 2mm (the radius of the axial plasma column at maximum compression) from the electrode axis where sources appear most frequently. Quantitative estimates of the anisotropy require some numerical elaboration of microdensitometer readings because of the different dimensions of each spot (typically $\ell \sim 0.5$ - 1mm; $d \sim 0.1$ - 0.3mm on film) in 0^o and 80^o directions and because of the space integration performed by photographs.

The value of the x-ray intensity $\bar{I}_{0^o}(erg/cm^2)$ at a specific position (x,y) on the 0^o film [film orthogonal to z-axis; unprimed x,y,z,ℓ,d,R etc. on film are the images of x';y';z';ℓ';d';R' etc. in the plasma; $r_i(x,y)$=distance of point (x,y) from the point of peak intensity Max $\bar{I}_{0^o i}$ on spot labelled by i] results from all the emitting plasma regions with the same distance $r'_i(x',y')$ from the source axis [(x,y) is the image of all points (x',y',z') with z' varying inside the length ℓ' of a source in the plasma, if $d'/L' < \ell'/L' < P'/L' << 1$; object-pinhole distance L' - 76mm; pinhole-film distance L - 40mm] i.e. $\bar{I}_{0^o}(x,y) - \int_{\ell'_i} I_{0^o}(x,y,z')dz'$. In the same way $\bar{I}_{80^o}(y,z) = \int_{d'_i} I_{80^o}(x',y,z)dx'$ on the 80^o film. In all steps of our numerical elaboration we have treated $\bar{I}_{80^o}$ as if it was $\bar{I}_{90^o}$ (80^o films are more conveniently handled than 90^o films) with an ultimate error which is much smaller than the other errors listed below. By assuming (a) cylindrical symmetry for each source and (b) a dependence on z' described by the same factor $a(z')$ for both intensities $I_{80^o}(r',z') = a(z')\hat{I}_{80^o}(r')$, $I_{0^o}(r',z') = a(z')\hat{I}_{0^o}(r')$ then these local values can be obtained by unfolding the convolution equation which relates them to the microdensitometer readings $\bar{I}_{80^o}, \bar{I}_{0^o}$. Instead of disentangling the local values I by this procedure we have estimated the anisotropy of a localized source i (say) by calculating the ratio $A(y_i) = \bar{\bar{I}}_{80^o i}/\bar{\bar{I}}_{0^o i}$ where $\bar{\bar{I}}_{80^o i}(y) = \int_{\ell_i} \bar{I}_{80^o}(y,z)dz$, $\bar{\bar{I}}_{0^o i}(y) = \int_{d_i} \bar{I}_{0^o}(x,y)dx$. The implication is that a strict relation exists between intensities of source (I) and on film ($\bar{I}$) i.e. that $\bar{\bar{I}}_{80^o i}/\bar{\bar{I}}_{0^o i} = \int \hat{I}_{80^o i}dx'/\int \hat{I}_{0^o i}dx'$ is satisfied for y',y close to the axis of source, spot, i.e. for $y' \simeq y'_i$, $y \simeq y_i$. The z (x) integral for a specific spot i on a 80^o (0^o) film is then carried out on the line y=const=y_i (on both films) which goes through the peak value of $\bar{I}$ on each scanning step. The numerical results for 10 different spots are reported in Table I: ε is derived by the maximum fluctuation in the integrals due to the uncertainty Δy_i in these peak positions on each scanning step (essentially a silver-grain effect on the film). An additional error of 8% (maximum) in the values of $A(y_i)$ is introduced by the fluctuations of source distances from p. The ratio $\bar{\bar{I}}_{80^o}/\bar{\bar{I}}_{0^o}$ of the total intensities $\bar{\bar{I}} = \int \bar{I} dy$ at 80^o and 0^o from a few spots is reported in the last column. The fact that $\bar{\bar{I}}_{80^o}/\bar{\bar{I}}_{0^o} > \bar{\bar{I}}_{80^o}/\bar{\bar{I}}_{0^o}$ indicates that the anisotropy can be a function of position inside a localized source and is larger near the axis of the source. We notice that the intensity anisotropy of each source is evident even before elaborating the densitometer data: $Max\bar{I}_{80^o i}/Max\bar{I}_{0^o i}$ is varying between 1.10 and 1.75 (in spite of $\ell_i > d_i$) for all films from the D_2+0.5% Ar discharges that we have examined. For pure D_2 discharges the anisotropy (smaller than for D_2+0.5%Ar) becomes clear only after considering the spot parameters ℓ,d. The electron beam picture discussed by previous work[1] is supported by these results. Reciprocity failure of X-ray film (Kodak RPR54) response is considered negligible[2]. We have considered data[3] on film response (exposure factor) vs X-ray energy $\simeq$2.30keV.

film&spot label	$A(y_i)$	ε	$\bar{\bar{I}}_{80^o}/\bar{\bar{I}}_{0^o}$
8Torr D_2 + 0.5 % Ar			
# 2-71a	3.89	15	-
# 2-71b	3.05	17	-
# 2-71c	7.30	26	-
# 2-77a	3.09	25	-
# 2-77b	3.57	14	-
# 2-79a	3.37	9	2.28
# 2-79b	3.49	5	2.61
# 2-79c	3.40	13	2.92
8 Torr D_2			
# 2-87c	2.21	13	-
# 2-87b	2.31	12	-

Table I. Anisotropy $A(y_i)$ and % error ε of $A(y_i)$. Each film was exposed to single 15kV discharge, 0.050 mm thick Be window covering films. Pinhole diameter 0.075 mm.

Work supported by A.F.O.S.R. and (V.N.) by I.Avogadro Tec. (C.P.10757, Rome).

References:
(1). Bostick, Nardi, Prior, Rodriguez-Trelles: II Topic. Conf. Pulsed High-Beta Plasmas, 1972.
(2). Birks, Whitlock, Vierling, Nagel, Corbics: J. Optical Soc. of Amer. 60, 649, (1970).
(3). Dozier, Gilfrich, Birks: App. Optics, 6, 2136 (1967) & private com. (unpublished) 1972.

71

OBSERVATION OF ION LANDAU DAMPING OF THE DRIFT WAVE IN A SHEARED MAGNETIC FIELD

T. Dodo,* Y. Nishida,+ T. Kuroda, and G. Horikoshi++
Institute of Plasma Physics, Nagoya University, Nagoya, Japan

Abstract: The drift wave stabilization by the magnetic shear is discussed by taking into account the effect of ion Landau damping. It is shown that near stabilization the ion Landau damping is more effective than that expected theoretically.

The critical values for the drift wave stabilization by the magnetic shear, which are determined experimentally, are a little smaller than that obtained theoretically as mentioned in the main paper. In the theoretical work,[1] it has been assumed a priori that the ion Landau damping is completely effective, i.e., $\omega/k_{\parallel}^{eff}v_i < 1$, when the wave is stabilized by the megnetic shear, where $k_{\parallel}^{eff}$ is the parallel wave number effected by the shear and is given by $k_{\perp}x/L_s$. In the present experiment, however, $\omega/k_{\parallel}^{eff}v_i$ is larger than one, as will be shown later, and the ion Landau damping effect is weaker than that expected theoretically. So, the ion damping effect must be taken into account carefully.

The growth rate γ of the drift wave instability is given by

$$\frac{\gamma}{\omega^*} = \frac{2\sqrt{\pi}}{k_z v_e}\frac{\beta(1-\beta)}{(2-\beta)^3}\omega^* - \frac{4\sqrt{\pi}}{k_z v_i}\frac{\beta^2}{(2-\beta)^3}e^{-z^2}\omega^*, \qquad (1)$$

where $\beta = I_o e^{-b}$, $b = k^2 T_i/M\omega_{ci}^2$, $z = \omega/k_z v_i$, $k_z = k_{\parallel o} + k_{\parallel}^{eff}$, $k_{\parallel o}$ is the parallel wave number without the shear, ω^* is the drift angular frequency, and v_i and v_e are the ion and electron thermal velocity, respectively. The wave growth term contributed by the resonance electrons, the first term in the right hand side of Eq.(2), is about $(1.37-0.97) \times 10^{-7}\omega^*$ under our present experimental conditions with the shear field. The ion damping term, the second term in the right hand side, is calculated as follows: When T_i is 2.0 eV, the wave damps away at about $\delta_{crit} \sim 0.025$, and there $\omega/k_{\parallel}^{eff}v_i$ is about 3.1 and the ion damping term is $0.48 \times 10^{-5}\omega^*$ at the critical point. Here, we take x to be the wave spreading width and $x \sim 1.0$ cm. When T_i is 1.0 eV, $\delta_{crit} \sim 0.08$ and $\omega/k_{\parallel}^{eff}v_i \sim 1.7$. So, the ion damping term is $1.4 \times 10^{-5}\omega^*$. These values of $\omega/k_{\parallel}^{eff}v_i$ are still larger than one, but the growth term by electrons is smaller than the damping term by ions. The ambiguity of the critical value δ_{crit} in the experiment does not largely change the values of ion damping rate. Thus, the wave is stabilized by the ion Landau damping effect. If the magnetic shear is absent, the growth term is always larger than the damping term.

In conclusion, it is shown that near stabilization the ion Landau damping is effective even though the resonant ions are a few.

Reference

* Permanent address, Central Research Laboratory, Hitachi Ltd.

\+ Permanent address, Department of Electronics, Tohoku Univ.

++ Present address, National Laboratory for High Energy Physics.

1 N.A.Krall and M.N.Rosenbluth, Phys. of Fluids, 8, 1488 (1965).

78

Plasma Confinement Experiment in Heliotron D (continued)

A.Iiyoshi, S.Morimoto, S.Konoshima, S.Yoshioka, M.Sato,
I.Otake and K.Uo
(Plasma Physics Laboratory, Faculty of Engineering,
Kyoto University, Gokasho, Uji, Japan)

Joule heating experiment:

An eight turn air core coil is mounted along the discharge chamber. A typical set of pictures of plasma current, loop voltage and probe signal are shown in Fig.1. When the plasma current reaches a certain critical value, the observed current and probe signals show violent fluctuations. The critical current might be due to kink instability[1],[2]. The relation between the rotational transform angle produced by helical windings at the radius of the plasma boundary, ι_0, and that due to the critical plasma current, ι_{ohc}, is shown in Fig.2. Assuming constant current distribution in the plasma, the latter is given by $\iota_{ohc}=\frac{\mu_0 R I_c}{2\pi r_p^2 B_0}$. The figure seems to show that the macroscopically stable plasma would be maintained until $\iota_{ohc} \simeq 1$. In Fig.3 the density profile is shown for α=0 (without toroidal field coil). Although we have not any limiter, the plasma is well separated from the helical conductor. This suggests that it might be useful to employ fields in the separatrix region as a divertor[3].

RF heating experiment:

Heating methods due to ion cyclotron wave (I.C.W) and fast wave (F.W) are applied to the plasma in Heliotron D. The waves are generated by a two section reverse turn induction coil (Stix coil) whose fundamental wave length is 84 cm. A helium plasma is produced by joule heating to maximum density 5×10^{13} cm^{-3}. RF current with frequency range of 1 MHz to 3 MHz is pulsed during 300 μs into the induction coil. Fig.4 and 5 show the equivalent load resistance measured as a function of density for I.C.W at $\omega/\Omega_i \simeq 0.91$ and for F.W at $\omega/\Omega_i \simeq 4.7$, respectively. Vertical arrows on these figures indicate the densities predicted theoretically for the coupling resonance and for cut off. The experimental peaks agree reasonably well with the predicted density. I.C.W shows better coupling resonance at 3rd harmonics wave length. It is interesting that the 3rd harmonics wavelength of λ = 28 cm is almost exactly same value as one half of helical coil pitch length. As the net power coupled to the plasma is only a few joule in these experiments, we have not seen appreciably heating yet. However, the results of high coupling efficiency up to several tens percent encourage us to further study.

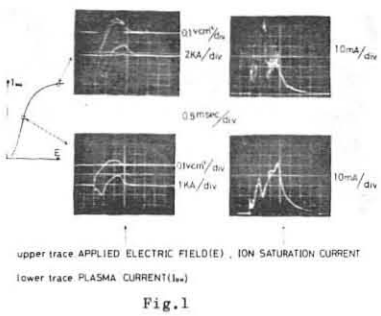

Fig.1

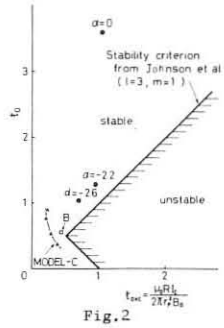

Fig.2

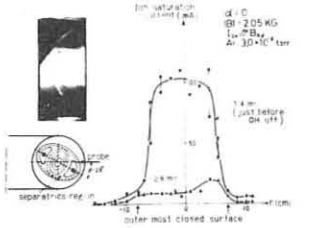

Fig.3

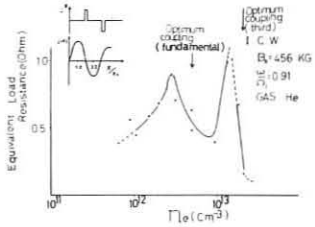

Fig.4

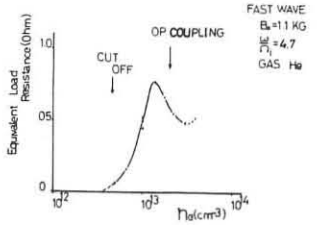

Fig.5

References:
(1) M.Kruskal et al Proc. Roy. Soc. A233 (1954) 348
(2) L.Johnson et al Physics Fluids 1 (1958) 281
(3) C.Gourdon et al Nuclear Fusion 11 (1971) 161

94

CONFINEMENT AND FLUCTUATION STUDIES IN THE JAERI HEXAPOLE

by

S.Tamura, H.Yamato*, T.Nagashima, H.Ohtsuka,
S.Arizono, T.Shiina, M.Yoshikawa, and S.Mori
JAPAN ATOMIC ENERGY RESEARCH INSTITUTE, Tokai, Ibaraki-ken, Japan

We describe here properties of the fluctuations observed in the JAERI hexapole and identications of these instabilities.

Mode B Maxima of the fluctuation lebel along a magnetic field line are found to be located at maxima of unfavorable curvature or at maxima of the hexapole field (Fig.1). The oscillations at P and Q are 180 degrees out of phase, while in phase at Q and R. A possible instability which is localized in the unfavorable curvature is a drift ballooning instability (1). In the hexapole geometry, however, drift wave cannot be localized in a bad curvature, since the maximum of $\kappa + b$ corresponds to a minimum of the magnetic field. ($\kappa = 2\,\partial \ln B/\partial \ln n$, $b = k_\perp^2 T_e/M\Omega_i^2$). Another possibility is a mode discussed by Rutherford et al. (2) as "electron drift trapped particle instability" and also by Coppi et al. (3). Observations made so far are consistent with this mode, but more detailed comparison, for example comparison of observed amplitude distribution with theoretical prediction, is required to confirm the identity.

Mode A and C After careful correction of E x B drift, the frequency of mode A and mode C is found to be close to drift frequency ($0.7\,\omega_{*} - 0.9\,\omega_{*}$) and propagations of both modes are in the direction of electron diamagnetic drift. Various observations of this mode seem to support that this nonlocalized mode is a drift universal instability. One problem to be explained is disappearance of the mode under application of small toroidal field. This difficulty can be eliminated if the mode C is assumed to be the same type of instability with different mode number. It is also found that the mode C itself is devided into several modes with different mode numbers n, as the toroidal field is increased up to about 90 G (Fig.2). The mode numbers along the poloidal field and along the toroidal field are given by n and m respectively. The mode transition can be understood physically from the relation between parallel wave number k_{11} and toroidal field intensity (Fig.3) under an assumption that the drift wave is more unstable for smaller k_{11}.

REFERENCES
1. P.H.Rutherford and E.A.Frieman, Phys. Fluids 11, 569 (1968)
2. P. Rutherford et al., Plasma Physics and Controlled Thermonuclear Fusion, Vol. 1, p. 367, (IAEA Vienna 1969).
3. B. Coppi et al., Phys. Rev. Letters 21, 1055 (1968).

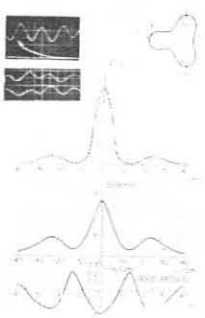

Fig. 1

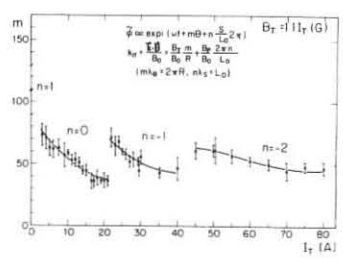

Fig. 2

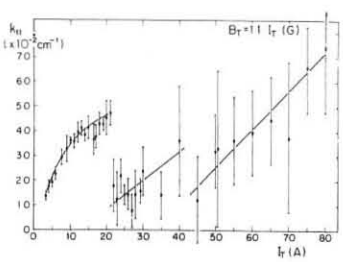

Fig. 3

* On leave from The Research and Development Center, Tokyo Shibaura Electric Co., Ltd., Kawasaki, Japan.

99

NON ADIABATIC MOTION OF A CHARGED PARTICLE IN A SPATIALLY AND SINUSOIDALLY MODULATED MAGNETIC FIELD

by

D. A. Dunnett and G. A. Jones

Department of Applied Mathematics,
University of Liverpool, England.

The question of whether an invariant exists throughout the phase plane may be restated as whether it is possible to generate an invariant which predicts behaviour sufficiently complicated to explain the numerical results. We shall examine this point using the methods of reference (1).

The Hamiltonian for the problem may be transformed using action angle variables to

$$H = p + \tfrac{1}{2}p_z^2 + \epsilon(P + A \sin 2Q)g(z) + \tfrac{1}{2}\epsilon^2(P + C + A \sin 2Q)g^2(z).$$

Following (1) we generate an invariant by writing $\left[J, H\right] = 0$, where $\left[\ \right]$ is the Poisson bracket, and expanding J in powers of ϵ as

$$J = J_0 + \epsilon J_1 + \epsilon^2 J_2 + - - - - - - - .$$

It is easily seen that J_0 is any arbitrary function of P, p, pQ-z and J_1 may be obtained from the relation

$$\left[J_1, H_0\right] = - \left[J_0, H_1\right].$$

In fact, changing variables to α, β where $\alpha = pQ - z$, $\beta = z$ and $p = \gamma$ J_1 is obtained by an integration over β. In a similar manner $\left[J_2, H_0\right] = - \left[J_0, H_2\right] - \left[J_1, H_1\right]$ gives J_2 in terms of J_1 and similarly for $J_3 - - - - J_n$. The J_i are, of course, of increasing complexity but we may note that J_1 contains terms proportional to $\frac{1}{\lambda - n\pi}$ and $\frac{1}{\lambda + n\pi}$ resulting from the interaction of the field perturbation term g(z) with the gyromotion term (A sin 2Q).

This predicts a resonance at $p = \pm \frac{\lambda}{n}$ as would be expected and corresponds to the centre of the main quasi-circular closed orbit curves presented.

However J_2 also contains terms proportional to $\frac{1}{\lambda \pm 2n\pi}$ which are due to the interaction of J_1 and H_1. These are the terms which cause the secondary quasi-circular closed curves at $\xi \sim .75$.

If the calculation is continued in this way further harmonic terms are generated, for example J_3 will contain terms proportional to $\frac{1}{\lambda \pm 3n\pi}$ and $\frac{1}{2\lambda \pm 3n\pi}$. The first of these terms corresponds to another quasi-circular curve above $\xi \sim .75$ (seen on the $\epsilon = .0637$ curves), while the second may be shown to correspond to an island chain containing two islands.

Clearly we may continue in this way and generate terms which predict increasingly complicated behaviour of the type observed in the numerical solutions. Of course as the terms become more complicated their effect is diminished by multiplication by increasing powers of ϵ and for small enough ϵ it seems that high harmonic effects do not contribute appreciably to the invariant curves. The curves drawn for the two different values of ϵ (.0318 and .0637) demonstrate this point.

This is remarkably similar to the "overlapping of resonance" ideas discussed by Lichtenberg (2). However it is not clear that this overlapping of the resonance effects will destroy the invariants in a given case. Possibly for large enough ϵ the terms of the invariant which contribute appreciably to the curves are sufficiently complicated to give the appearance of quasi ergodic behaviour when a particle orbit is plotted. Our results suggest that this is the case for $\epsilon = .0637$ at least.

105

TOKOMAK PLASMA HEATING BY FAST NEUTRAL INJECTION

J.P.Girard, M.Khelladi, D.Marty

ASSOCIATION EURATOM-CEA SUR LA FUSION
Département de Physique du Plasma et de la Fusion Contrôlée
Centre d'Etudes Nucléaires
Boîte Postale n° 6 . **92 Fontenay-aux-Roses** (France)

In order to know roughly the ignition domain of our large Tokomak, a simple energy balance code has been developed. Two inequalities have been introduced in it : *the first one* is the equilibrium limitation ($\beta_\theta \leq \frac{R}{a}$), *the second one* is the balance between the ohmic and α particle heating and the losses due to ion conduction, bremstrahlung and synchrotron radiation [1].

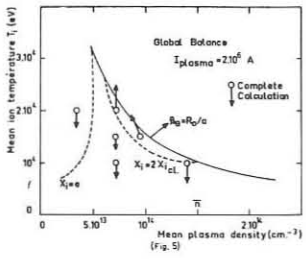

(Fig. 5)

The obtained diagramm is shown on Fig.5 where the upper limit is given by the equilibrium, the lower by ion conduction and the left one by synchrotron radiation. The points with arrows give the results of complete calculations obtained with the neutral heating code. The injection is stopped when the wished temperature is obtained. The ignition is achieved for densities of 7 - 9 10^{13}cm^{-3} and temperature of 20 keV with injection at 100 keV of 20 A (D_0) during 7 sec. We observe that the domain is rather narrow, nevertheless it can be increased significantly if a lower q factor (1.8) is feasible.

Application to a Tokomak Reactor [2] :

With the global model we have first checked the possibility of ignition by only ohmic heating with the minimum q value (1.5). We can see (Fig.6) that the resistivity has to be 4 times anomalous providing that the anomaly is not due to impurities. If this were the case, the ignition should not be obtained due to enhanced radiation losses. So additionnal heating seems necessary at all densities. We calculate completely the ignition by neutral

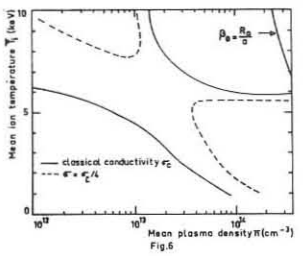

Fig.6

injection at low density (3.10^{13}cm^{-3}) and this is possible with a rather modest neutrals energy (100 keV) and current of 260 A, that is a deposited power of 1.5 10^{-2}W/cm^3 (Fig.7). Having obtained the ignition at low density and supposing that refuelling is feasible, we find to obtain a density of 2.10^{14}cm^{-3} and temperature of 10 keV that the fuel injection rate has to be 10^{23} p/sec during 3 sec. If the α particles are not all trapped in the machine [3] we observe that ignition temperature is increased from 8 keV to 10 keV (Fig.7) and the temperature profiles are more peaked than precedently.

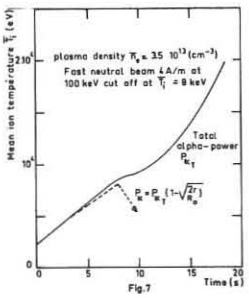

Fig.7

If the ion conduction ("banana regime") is increased by a factor up to 100 times, the ignition at low density by injection of neutrals of usual energy (100 keV) and unusual current (300 A) is always obtained. It is only in the case when the ion heat conduction follows the "plateau regime", even at low collision frequency that ignition should be obtained at high density. We obtain a minimum density of 10^{14}cm^{-3} and temperature of 7 keV. The heating by neutrals injection then need a beam of D_0 of high energy (1 MeV).

References.-

[1] Rosenbluth : Nuclear Fusion 10, 3, 1970.

[2] Lubbel and all : Madison Conference, CN.28/K.10, 1971.

[3] Anderson-Furth : Nuclear Fusion 12, 2, 1972.

120

ANOMALOUS MICROWAVE ABSORPTION NEAR THE PLASMA FREQUENCY

H. Dreicer, R. F. Ellis, and J. C. Ingraham

Los Alamos Scientific Laboratory*, Los Alamos, New Mexico, U.S.A.

Abstract: Additional data is presented for the experiment of Ref. [1].

A detailed mapping of the threshold for anomalous absorption onset in a microwave resonator as a function of electric field and plasma density is given in Fig. 1. The horizontal axis is the square of the ratio of plasma to microwave frequency, ω_{po}^2/ω^2, and has been determined absolutely from the microwave resonator frequency shift plus a detailed knowledge of the plasma density and electric field distributions within the resonator. The vertical axis is the ratio of the electron AC drift speed to the electron thermal velocity. The threshold data are determined using the AM method[1]. Theoretical threshold curves for the decay and AC two-stream parametric instabilities[1],[3] are shown. The agreement between infinite plasma theory and experiment is reasonable.

The microwave resonator allows quantitative measurement of the anomalous absorption. If in addition, the plasma volume in the resonator which contributes to anomalous absorption is known, the effective anomalous collision rate, ν_{eff}, of the electrons can be computed. An estimate for this plasma volume is obtained by measuring the radial profile of the hot electron

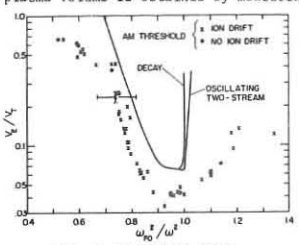

Fig. 1 Threshold data

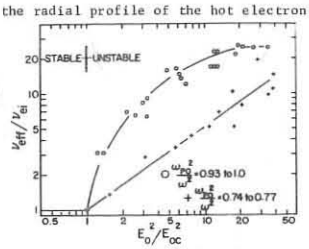

Fig. 2 ν_{eff}/ν_{ei} vs. E_o^2/E_{oc}^2

pulse[1], which is produced as a result of the anomalous absorption. This pulse profile, measured outside of the resonator, is assumed to correspond to the radial profile of anomalous absorption region in the resonator, and the length of the region is assumed equal to the resonator length. The data in Fig. 2 are thus obtained. The horizontal axis is the square of the ratio of the electric field in the resonator to the electric field at threshold, E_o^2/E_{oc}^2. The vertical axis is the ratio of ν_{eff} to the electron-ion collision rate, ν_{ei}. It is interesting to note that the dependence of ν_{eff}/ν_{ei} on E_o^2/E_{oc}^2 depends strongly on whether the plasma density corresponds to the threshold minimum, $0.93 \leq \omega_{po}^2/\omega^2 \leq 1.0$, (see Fig. 1) or not, e.g. $0.74 \leq \omega_{po}^2/\omega^2 \leq 0.77$. Theoretical calculations[2] predict $\nu_{eff}/\nu_{ei} \simeq E_o^2/E_{oc}^2$ for $E_o \geq E_{oc}$. This dependence would be a straight line of slope unity in Fig. 2 lying between the two data curves.

*Work performed under the auspices of the United States Atomic Energy Commission.

1 H. Dreicer, R. F. Ellis, and J. C. Ingraham, Paper 120, "Anomalous Microwave Absorption Near the Plasma Frequency", Proceedings of the Fifth European Conference on Controlled Fusion and Plasma Physics, Grenoble, France, August 21-25, 1972.

2 P. K. Kaw, E. Valeo, and J. M. Dawson, Phys.Rev.Letters 25, 430, (1970); D. F. Dubois, and M. V. Goldman, Phys.Rev.Letters 28, 218 (1972); E. Valeo, C. Oberman, and F. W. Perkins, Phys. Rev. Letters 28, 340 (1972); W. L. Kruer, and J. M. Dawson, Phys. of Fluids 15, 446 (1972).

3 We are indebted to J. P. Freidberg and B. M. Marder at Los Alamos for the use of their computer code.

123

THE PLEIADE ACCELERATOR EXPERIMENT

by

R.Geller, W.R.Hess+, M.Hesse, B.Jacquot, C.Jacquot

ASSOCIATION EURATOM-CEA
Département de Physique du Plasma et de la Fusion Contrôlée
Service IGn - Centre d'Etudes Nucléaires
Cédex 85 - 38 GRENOBLE Gare (France)

In order to increase the density of the ionic current it is necessary to have :

1/ a higher density of cold plasma in the preionization zône (limited by the cut-off of the R.F. wave and triggering of instabilities).

2/ the sharpest gradient of pressure in the resonance zone where the fluid must be collisionless.

Therefore we utilize a single injector where the hydrogene gas is introduced in a capillary tube of (NiB) ϕ = 5 mm sliding in a quartz tube ϕ = 20 mm The position of the NiB tube is determined in order to obtain the best ionic density current. With this single injector we obtain 100 mA of ions with an energy between 1,5 KeV and 3 KeV. (ni $W_{//i} \simeq 10^{13}$ eV/cm^3) an an ionic density current of 60 mA/cm^2.

The product of current density and particle energy beeing roughly constant, we can increase the total current by increasing the plasma cross section S, provided that the incident R.F. power is also increased. As a matter of fact, we know that the total available power in the ionic beam is proportionnal to the R.F. power. But if we want also to maintain the optima injection conditions, and enhance the efficiency by loading more the cavity then we must multiply the number N of injectors (cross-section s) to have S = ns with s $\ll \lambda^2_{RF}$.

This simple scaling law indicates that we can expect with 3 injectors 3 times more particle current with a little less particle energy.

Example : 300 mA of ions (S = 4 cm^2) with $\sim$ 1,5 KeV energy and $\sim$ 2,5 KW of R.F. power.

The following corrections should be made on page 123, line 16 should read : 10 GHz - line 3 should read 57 mA.

126

ABSORPTION OF THE MICROWAVE ENERGY IN A MAGNETOACTIVE PLASMA

J. Musil, F. Žáček

Institute of Plasma Physics, Czechoslovak Academy of Sciences, Nademlýnská 600, Prague, Czechoslovakia

Because the efficiency of the collision absorption strongly decreases with the increasing electron temperature of the plasma it is very important to find out if the absorption of a microwave energy described in main conference paper is caused by collision or if is collisionless one. The character of the absorption was determined on the basis of the analysis of the measured dependence of the reflection coefficient R on the plasma density $n = \omega_0^2/\omega^2$. We have measured the reflection coefficient R of the RHCP wave at $\omega_c/\omega \simeq 1{,}1$. RHCP wave was incident on the system: quarter wavelength dielectric plate ($\varepsilon = 2{,}55$) - plasma. The dielectric plate, which was placed tightly in front of the flat very thin bottom of the discharge tube, made possible more efficient transfer of the microwave energy into a plasma at higher densities $n \geq 1$.

The measured dependence $R^2 = f(v)$ for argon at a pressure 4.10^{-3}torr was then compared with the theoretical dependence calculated from the formula

$$R = \frac{\sqrt{1-(\lambda_0/\lambda_c)^2}\cdot\sqrt{\varepsilon_p-(\lambda_0/\lambda_c)^2} - \sqrt{\varepsilon-(\lambda_0/\lambda_c)^2}}{\sqrt{1-(\lambda_0/\lambda_c)^2}\cdot\sqrt{\varepsilon_p-(\lambda_0/\lambda_c)^2} + \sqrt{\varepsilon-(\lambda_0/\lambda_c)^2}} \qquad (1)$$

where

$$\varepsilon_p \equiv n^2 = 1 - \frac{n(1-Y)}{(1-Y)^2+Z^2} - i\,\frac{nZ}{(1-Y)^2+Z^2} \qquad (2)$$

$Y = \omega_c/\omega$; $Z = \nu^*/\omega$; ν^* is the effective collision frequency which determines what part of the incident microwave energy is absorbed in the plasma; λ_0 is the free-space wavelength of the incident wave, λ_c is the critical wavelength in the circular waveguide. The formula (1) satisfies the energetic balance condition $R^2+T^2+A^2 = 1$, where T^2, A^2 denotes the transmitted and absorbed power. The calculation shows that the agreement of the measured dependence $R^2 = f(v)$ with the calculated one can be obtained only in the case when ν^* increases with the plasma density in such a way as it is shown in Fig. 1. The magnitude of the effective collision frequency ν^* is about two orders of the magnitude greater than is the collision frequency of electron with ions and neutral particles, i.e. $\nu^* \gg \nu_{ei}+\nu_{en}$. This analysis clearly shows that the absorption of the microwave energy cannot be caused by classical collisions but it is caused by some essentially more efficient collisionless absorption mechanism. The absorption probably arises in consequence of waves transformation - in regions of waves resonances at oblique propagation - into short wavelength plasma waves which are very effectively absorbed in an inhomogeneous plasma.

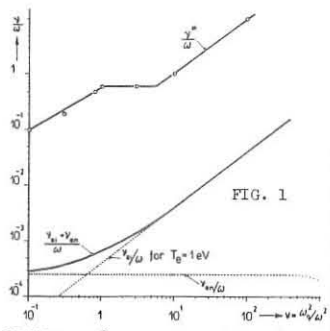

FIG. 1

This result is very important. It shows that this mechanism of the microwave energy absorption could be suitable for heating of a dense and hot magnetoactive plasma.

In many practical cases (toroidal devices) is advantageous to generate and heat a plasma by means of a microwave gun. Therefore we had measured also the dependence of the density of the plasma, created directly by the gun, on the magnetic field ω_{ce}/ω. Experiment was carried out with two cylindrical guns, see Fig. 1 in main paper. The gun I was fed from the generator (f = 2,35 GHz) the power of which is to be absorbed in a plasma. The gun II produced the independent plasma at $\omega_{ce}/\omega \gg 1$. Results, given in Fig. 2, are very promising. It is worthwhile to note that at great incident powers the absorption strongly increases in vicinity of $\omega_{ce}/\omega = 0{,}5$.

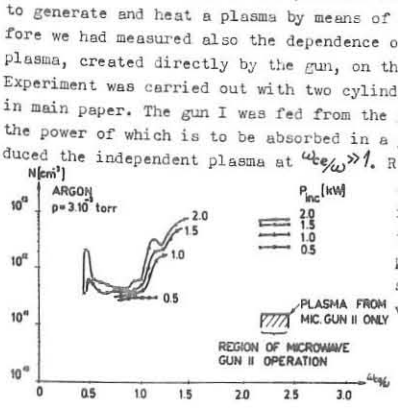

FIG. 2

132

EXPERIMENTAL RESULTS ON THE DAMPING OF A FINITE AMPLITUDE ELECTRON WAVE

R.N. Franklin, S.M. Hamberger, G.J. Smith

(UKAEA Research Group, Culham Laboratory, Abingdon, Berksmire, United Kingdom)

Wave propagation over more damping lengths ($k_i x \leq 8$) than shown in Fig.2 is shown in Fig.4; this was achieved by increasing k_i and keeping $x \leq 50$ cm (as earlier). It shows clearly that there is some initial amplitude such that the wave propagates, at distances for which $k_i x \geq 5$ with a constant amplitude. From our data we estimate the value of the parameter $q = \gamma_L/\gamma_B$ at which this occurs to be $q = 0.72 \pm 0.07$, in good agreement with $q = 0.77$, the value predicted by Sugihara and Kamimura. We believe that this is the first laboratory observation of a stable BGK equilibrium.

When the resonant electrons are prevented from becoming trapped a large wave exhibits linear Landau damping. This is shown in Fig.5: (i) shows the amplitude variation of a very small amplitude wave ($e\varphi_0/kT_e \simeq 2\times10^{-3}$) which Landau damps; (ii) shows a larger wave ($e\varphi_0/kT_e \simeq 10^{-2}$) whose damping clearly departs from exponential at $x \geq 15$ cm, and (iii) shows the same wave as (ii) but in the presence of a second perturbing wave (ω_1, k_1), of amplitude similar to that of ω_0 but at a frequency well removed from ω_0, whose effect is to prevent electrons becoming trapped in the potential wells of ω_0.

Supplementary references relevant to non-linear wave theory

I.B. Bernstein, J.M. Greene and M.D. Kruskal, Phys. Rev., 108, 546 (1957).
G. Knorr, Z. Naturforsch, 16a, 1320 (1961); 18a, 1304 (1963).
T.M. O'Neil, Phys. Fluids, 8, 2255 (1965).
L.M. Altshul and V.I. Karpman, Zh. Eksp. Teor. Fiz., 49, 515 (1965). [Sov. Phys. JETP, 22, 361 (1966)].
S.P. Gary, Phys. Fluids, 10, 570 (1967).
T.P. Armstrong, Phys. Fluids, 10, 1269 (1967).
J.M. Dawson and R. Shanny, Phys. Fluids, 11, 1506 (1968).
T. Imamura, R. Sugihara and T. Tanuiti, J. Phys. Soc. Japan, 27, 1623 (1969).
T. Tanuiti, J. Phys. Soc. Japan, 27, 1634 (1969).
V.L. Bailey and J. Denavit, Phys. Fluids, 13, 451 (1970).
A. Lee and G. Schmidt, Phys. Fluids, 13, 2546 (1970).
E. Ott and C.T. Dum, Phys. Fluids, 14, 959 (1971).
J. Denavit and W.L. Kruer, Phys. Fluids, 14, 1782 (1971).
J. Nöthrenberg, Z. Angew. Math. Phys., 22, 1057 (1971).
G.J. Morales and T.M. O'Neil, Phys. Rev. Lett., 28, 417 (1972).
R. Sugihara and T. Kamimura, J. Phys. Soc. Japan, 33, no.1 (1972).
I.H. Oei and D.G. Swanson, to be published in Phys. Fluids.

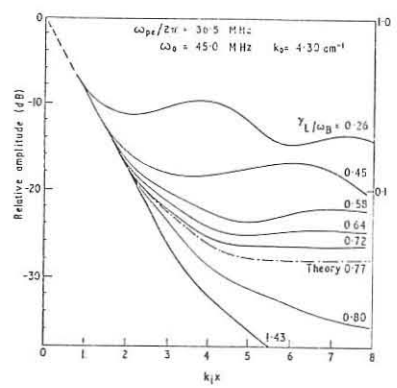

Fig.4 Experimental data and theoretical curve [from Sugihara and Kamimura] for $q = 0.77$ showing relative spatial amplitude variations for different initial amplitudes, $k_i = 0.17$ cm^{-1}.

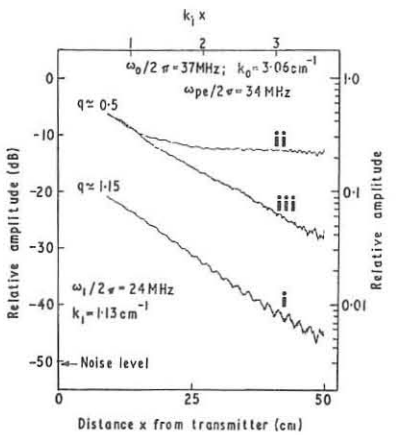

Fig.5 Spatial amplitude variation of (i) wave (ω_0, k_0) with $\varepsilon\varphi_0 = 0.1$ mV; (ii) wave (ω_0, k_0) with $\varepsilon\varphi_0 = 2.2$ mV; (iii) same wave as (ii) but in presence of (ω_1, k_1) launched at $x = 67$ cm with initial amplitude $\simeq 1$ mV.

133

RESONANT INTERACTION OF TWO ELECTRON WAVES WITH AN ION WAVE

by

R.N. Franklin,* S.M. Hamberger and G.J. Smith

(UKAEA Research Group, Culham Laboratory, Abingdon, Berks., U.K.)

Measurements of the spatial variation of the mixing product have been made. In order to carry out such measurements with the plasma unperturbed by the antenna detecting the ion wave, it is necessary for the antenna to be of small area and the signal is consequently small. Care has to be taken to ensure that mixing is occurring in the plasma rather than in the detection circuit or in the sheaths surrounding the probes. The distortion of this latter effect has been removed in the dashed portions of Fig.4. It is expected from theory[5] that the spatial variation of φ_s will be of the form

$$\frac{e\varphi_s}{kT_e} \simeq \frac{e\varphi_1}{kT_e} \cdot \frac{e\varphi_2}{kT_e} \cdot \frac{3}{2} \frac{K_1^2 K_2^2 K_s X}{\left[1+\sqrt{\left(T_i/T_e\right)}\right]^{\frac{1}{2}}}$$

where wave numbers and lengths are normalized to

$$k_D \equiv \left(\frac{n_e^2}{2\varepsilon_o kT_e}\right)^{\frac{1}{2}}$$

and the assumption has been made that the damping of all the waves is small, i.e. $K_1 X$, $K_s X \ll 1$.

Figure 4 shows the spatial variations of φ_1, φ_2 and φ_s for particular frequencies corresponding to resonant mixing. Direct pick-up leads to the interference shown in the ion wave signal. Note that the scale for φ_1, φ_2 and $\varphi_1\varphi_2$ is logarithmic; that for φ_s is linear.

Figure 5 shows, for different frequencies, a comparison between measured values of the interaction strength M defined by $\varphi_s(K_1,K_2,X) = \varphi_1\varphi_2 M_{s12}(K_1,K_2)[\exp-(K_1-K_2)X - \exp-K_sX]$ and theoretical prediction[5]. The fall-off at higher frequencies is due to increased Landau damping.

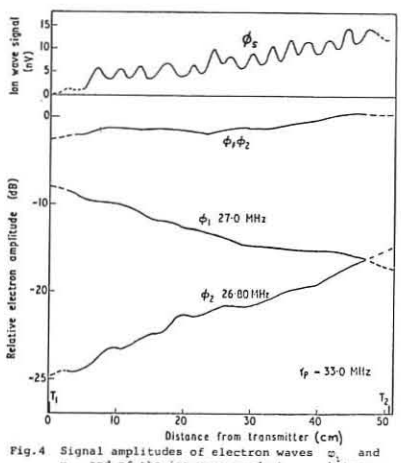

Fig.4 Signal amplitudes of electron waves φ_1 and φ_2 and of the ion wave product φ_s between transmitters T_1 and T_2

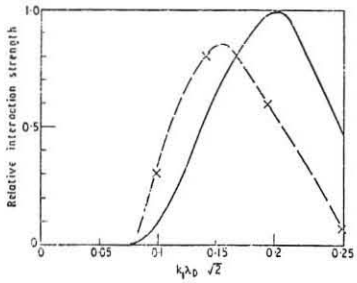

Fig.5 Comparison between theory ——— and experimental measurement ------ of the resonant interaction strength as the wavenmbers are varied.

NONLINEAR PLASMA OSCILLATIONS IN TERMS OF VAN KAMPEN MODES

by

Robert W.B. Best

FOM-Instituut voor Plasmafysica, Association Euratom-FOM

Rijnhuizen, Jutphaas, Nederland

4. Initial value problem. We take new amplitude functions in terms of phase velocities instead of frequencies and we further restrict $\underline{A}_2$, in addition to the symmetry condition (6), as follows:

$$\underline{A}_1(k,\omega) = |k|^{-1}\,\tilde{\underline{A}}_1(k,w),$$
$$\underline{A}_2(k,k',\omega,\omega') = |kk'|^{-1}\,\tilde{\underline{A}}_2(k,k',w")\;\delta\,(w-w'), \qquad (17)$$

in which

$$w = \omega/k,\; w' = \omega'/k',\; w" = \omega"/k". \qquad (18)$$

In these new variables the potential (3) reads

$$-V = \iint \tilde{\underline{A}}_1 e^{ik(x-wt)}dkdw + \iiint \tilde{\underline{A}}_2 e^{ik"(x-w"t)}dkdk'dw", \qquad (19)$$

and the corresponding distribution function (15):

$$f = F(v) - \frac{\varepsilon_o}{e}\iint k^2\tilde{\underline{A}}_1\,K\,e^{ik(x-wt)}dkdw$$
$$- \frac{\varepsilon_o}{e}\iiint k"^2\tilde{\underline{A}}_2 K" e^{ik"(x-w"t)}dkdk'dw"$$
$$+ \frac{\varepsilon_o}{2m}\iiint\tilde{\underline{A}}_1\tilde{\underline{A}}_1'\left\{\frac{k"}{kk'}\frac{P}{(w-w')^2}\left[k^3K+k'^3K'-k"^3K"+3kk'k"\delta(v-w")\right]\right.$$
$$\left. + \frac{P}{w-w'}\frac{\partial}{\partial v}\left(k^2K-k'^2K'\right)\right\} e^{ik"(x-w"t)}dkdk'dwdw' , \qquad (20)$$

in which K is given by (16) with ω/k replaced by w, and $\tilde{\underline{A}}_1' = \tilde{\underline{A}}_1(k',w')$. Writing the initial condition as

$$f(x,v,o) = F(v) + \int \underline{g}_1(k,v)e^{ikx}dk , \qquad (21)$$

Eq. (20) for t = 0 reduces to the set of Eqs.

$$\int k^2\tilde{\underline{A}}_1 K dw = -\frac{e}{\varepsilon_o}\underline{g}_1 \;,\; \int k"^2\tilde{\underline{A}}_2 K"dw" = \frac{e}{2m}\iint\tilde{\underline{A}}_1\tilde{\underline{A}}_1'\{\ldots\}dwdw' , \qquad (22)$$

in which $\tilde{\underline{A}}_1$ and $\tilde{\underline{A}}_2$ occur in the same way in the l.h.s. The curly brackets in (22) contain the same expression as in (20).

The solution of (22) involves the introduction of functions $\phi^{\pm}(v)$ associated with any function $\phi(v)$ defined by

$$\phi^{\pm}(v) = \frac{1}{2}\left[\phi(v) \pm \frac{i}{\pi}\int\frac{P}{v-u}\,\phi(u)\,du\right] .$$

It can be shown that ($^{\pm}$ operates always on the v-variable)

$$K^{\pm} = \underline{\tilde{\varepsilon}}_{\pm}(k,v)\,\delta^{\pm}(v-w) = \pm\frac{i}{2\pi}\frac{\underline{\tilde{\varepsilon}}_{\pm}}{v_{\pm}-w} \qquad (23)$$

in which $v_{\pm} = v \pm i0$ (cf. $k_{\pm}$ in Eq. 10) and

$$\underline{\tilde{\varepsilon}}_{\pm} = 1 \mp 2\pi i\frac{e^2}{\varepsilon_o mk^2}\frac{d}{dv}F^{\pm}(v) = 1 + \frac{e^2}{\varepsilon_o mk^2}\int\frac{1}{v_{\pm}-u}\frac{d}{du}F(u)du. \qquad (24)$$

We find that

$$k^2\tilde{\underline{A}}_1^{\pm}(k,v)\,\underline{\tilde{\varepsilon}}_{\pm}(k,v) = -(e/\varepsilon_o)\underline{g}_1^{\pm}(k,v) \qquad (25)$$

and

$$k"^2\tilde{\underline{A}}_2^{\pm}\underline{\tilde{\varepsilon}}_{\pm}" = \pm\frac{ie}{4\pi m}\iint\tilde{\underline{A}}_1\tilde{\underline{A}}_1'\left\{\frac{k"}{kk'}\frac{P}{(w-w')^2}\left[\frac{k^3\underline{\tilde{\varepsilon}}_{\pm}}{v_{\pm}-w} + \frac{k'^3\underline{\tilde{\varepsilon}}_{\pm}'}{v_{\pm}-w'}\right.\right.$$
$$\left.\left. - \frac{k"^3\underline{\tilde{\varepsilon}}_{\pm}" - 3kk'k"}{v_{\pm}-w"}\right] + \frac{P}{w-w'}\frac{\partial}{\partial v}\left[\frac{k^2\underline{\tilde{\varepsilon}}_{\pm}}{v_{\pm}-w} - \frac{k'^2\underline{\tilde{\varepsilon}}_{\pm}'}{v_{\pm}-w'}\right]\right\}dwdw' , \qquad (26)$$

in which $\underline{\tilde{\varepsilon}}_{\pm}'$ and $\underline{\tilde{\varepsilon}}_{\pm}"$ signify $\underline{\tilde{\varepsilon}}_{\pm}(k',v)$ and $\underline{\tilde{\varepsilon}}_{\pm}(k",v)$, respectively.

Further work will deal with the connection of (26) with known results, e.g. Eq. (A 16) of the reference.

The author acknowledges helpful discussions with Prof. H. Bremmer and Dr. M.P.H. Weenink.

This work was performed under the association agreement of Euratom and FOM with financial support from ZWO and Euratom.

Reference

C.T. Dum, R.N. Sudan, Phys. Fluids 14 (1971) 414.

138

CLASSIFICATION AND STABILITY OF THE B.G.K. STATIONARY STATES FOR A DOUBLE WATER-BAG MODEL

U.Finzi[+], J.Holec[++], J.P.Doremus[++]
[+]ASSOCIATION EURATOM-CEA
Département de Physique du Plasma et de la Fusion Contrôlée
Service TGn - Centre d'Etudes Nucléaires
Cédex 85 - 38 GRENOBLE Gare (France)

[++]Groupe de Physique Théorique et Plasma
Université Nancy I (54) NANCY (France)

A new set of parameters which simplifies the representation of results in the case of aperiodic solutions has been introduced in recent calculations. Instead of assuming the potential ϕ to be zero at neutrality, one sets $\phi = 0$ and $d\phi/dx = 0$ at $x = 0$. The parameter characterizing nonuniformity is now $\gamma = n_1/n_2(0)$. For $\gamma > 1$ the potential ϕ has thus its maxima at $\phi = 0$. The rate β between the total energies of the particles on the inner and outer contour is now always $0 \leq \beta \leq 1$. The definition of α is kept unchanged. For each value of $\gamma > 1$ all the points of the square $(0 \leq \alpha \leq 1,\ 0 \leq \beta \leq 1)$ represent a physically meaningfull equilibrium.
In regions 1 and 2 of Fig. (4) one has oscillating solutions without and with trapping of the inner contour respectively. In the remaining part of the (α,β) square, solutions are aperiodic. The problem of their stability has been completely solved. An example of the results is given in Fig. (3) which concerns the case $\gamma = 1.5, \beta = 0.5$. The bars cover the values of α for which a given symmetric (n S) or antisymmetric (n AS) mode of rank n is unstable. The mechanism of the instabilities is the same as in ref. /5/. The values of ω^2 corresponding to instability are always complex (no absolute instability). These instabilities are due to a resonance between two eigenmodes of the same rank of the inner and of the outer contour. Near the boundary between regions 2 and 3 a series of secondary instabilities can appear, due to resonances between eigenmodes of different rank.
In Fig. 4 the boundary of the unstable region is partially shown ; each tail corresponds to a single unstable mode. On the left of the curve $\tau_1 = \tau_2$ all the solutions are stable.
On the right of the deshed curve one has :

$$\int_0^{\lambda} (\bar{\phi}_e - \phi_e)\, n_e\, d\alpha > 0 , \qquad \phi_e = \phi - \tfrac{1}{2}\gamma x^2, \quad \bar{\phi}_i = \frac{1}{\lambda}\int_0^{\lambda} \phi_i\, d\alpha$$

This is, according to Minardi, a sufficient condition for instability. Agreement of the eigenmode analysis results with both criteria ($\tau_1 = \tau_2$ and Minardi) has been obtained for all the values of α, β, γ examined.

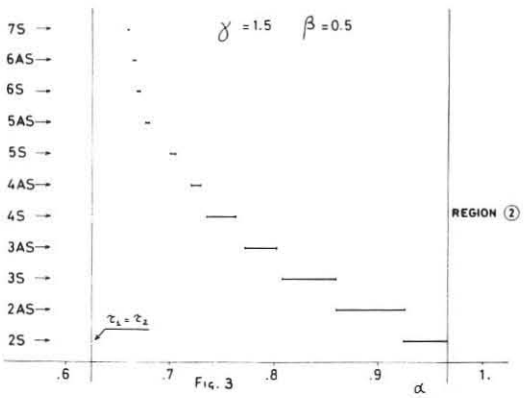

Fig. 3

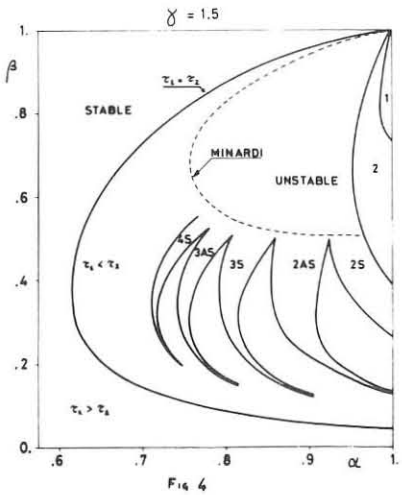

Fig. 4

146

MICROWAVE RADIATION FROM A TURBULENTLY HEATED TOROIDAL PLASMA

S.M. Hamberger, L.E. Sharp, J. Jancarik, H. Kyama

Detailed studies of radiation emitted both radially and tangentially to B_φ have been made for H_2 plasma, $n \sim 1\text{-}2 \times 10^{13}$ cm^{-3}, $E_\varphi \sim 70\text{-}350$ V cm^{-1}. Under these conditions the Buneman instability is excited during the current rise ($v_d > 2 \times 10^8$ cms^{-1}). Fig.4 shows the time variation of (i) ion fluctuation energy (ii) electron temperature, (iii) total microwave emission ($\lambda_0 \leq 4$ cm), (iv) radial density fluctuations with $|k| \approx 30$ cm^{-1}, $\omega \leq \omega_{pi}$ (from scattering of 2 mm microwaves). This shows that most radiation and electron heating occurs <u>following</u> the collapse of the strong Buneman oscillation, and coincides with the appearance of ion-sound fluctuations $_\perp B_\varphi$. Fluctuations $_\parallel B_\varphi$ at this $|k|$ were much weaker (NB the most unstable modes would have $|k| \geq 100$ cm^{-1}). This suggests that the original modes generated $_\parallel B_\varphi$ decay into longer wavelengths propagating across the field.

Fig.5 plots broad-band power received tangentially and radially vs. E_φ, together with v_d and σ. It shows emission increases roughly with input power.

Fig.6 shows radiation spectra measured tangentially for two values of B_φ : they exhibit distinct peaks at ω_{ce} and harmonics. No clear correlation with ω_{ce} are observed, however, for the radial spectra (Fig.7).

The general shape of the continuum spectra roughly follows a power law $I(\omega) \propto \omega^{-\alpha}$ where $\alpha \approx 2\text{-}4$ and is insensitive to n, E_φ, B_φ over our parameter range. Comparison with (a) the black-body limit at $T \sim 10^4$ eV, (b) classical bremsstrahlung, (c) bremsstrahlung based on the measured effective collision frequency ($\nu_e \approx 7 \times 10^8$ s^{-1}) shows that the measured level is generally much more intense than any of those estimated for incoherent radiation.

The peak emitted power from the whole column is ~ 40 kW, corresponding to a total energy loss $< 10^{-2}$ J, cf. $\sim 10\text{-}100$ J in the plasma.

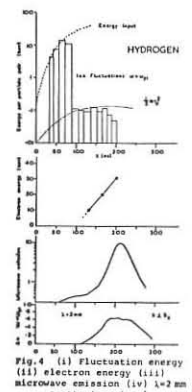

Fig.4 (i) Fluctuation energy (ii) electron energy (iii) microwave emission (iv) λ=2 mm scattering signal

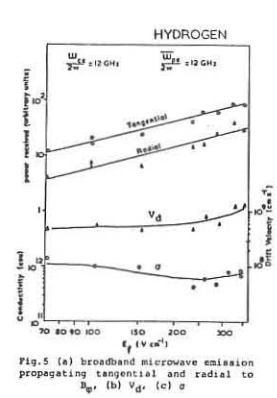

Fig.5 (a) broadband microwave emission propagating tangential and radial to B_φ, (b) V_d, (c) σ

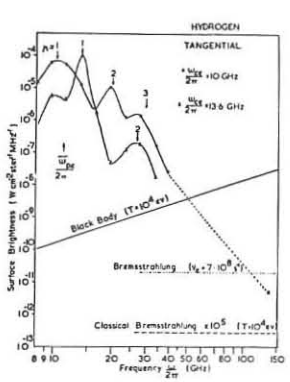

Fig.6 microwave emission propagating tangential to B_φ

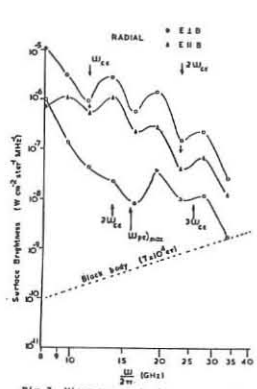

Fig.7 Microwave emission propagating radial to B_φ with polarization $E \perp B_\varphi$ and $E \parallel B_\varphi$

155

LINEAR AND NON-LINEAR PROPERTIES OF CONVECTIVE AND ABSOLUTE INSTABILITIES IN A BEAM-PLASMA SYSTEM

by

D. Bollinger, D. Boyd, W. Carr, J. Manickam, H. Liu, M. Seidl
Stevens Institute of Technology, Hoboken, New Jersey 07030 U.S.A.

Abstract: Recent results show that the saturation of the convective instability is due to the trapping of the beam particles.

Fig I illustrates the spatial growth of a convective wave. At saturation three harmonics of the fundamental appear. After saturation, trapped particle induced bounces in the amplitudes of the fundamental and harmonics are seen. Both the growth rates of the harmonics and the phase relation of the bounce oscillations are in agreement with ref(1). Fig II shows the measured wavelength change after particle trapping. Above the wavelength diagram, the growth rate of the fundamental is plotted. A sketch from ref(1) is included for comparison. The measured changes are larger than predicted. A small energy analyser which can move along the plasma column has been used to measure the beam velocity distribution as a function of axial position. Fig III shows the measured distribution at the positions marked on the R.F. plot. The original beam energy is 350 volts and the phase velocity in the linear growth region corresponds to an energy of 335 volts. The trapped electrons are easily seen at positions (5) and (6). By taking the spatial equivalent of equating the bounce frequency to the growth rate to get the saturation amplitude of the wave, one would expect $P_{SAT} \propto \gamma^4$. Our measurements indicate the exponent to be 3.5 ± 0.5.

Ref(1) T.M. O'Neil et al. Physics of Fluids 14, 1204. (1971).

Fig. 1

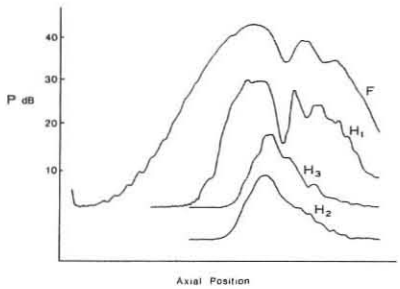

Fig. 2

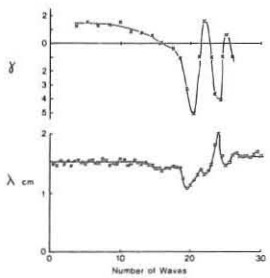

Fig. 3

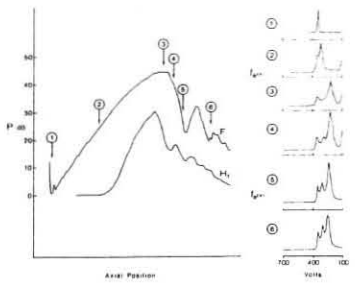

AUTHOR INDEX[+]

Akiyama R.	(55)	236
Andrews A.J.	(62)	237
Arizono S.	(94)	240
Artsimovitch L.A.		221
Beaulieu J.	(61)	237
Becker G.	(52)	235
	(53)	236
Bernard A.	(65)	238
Best R.W.B.	(137)	244
Biskamp D.		93
Bobin J.L.		171
Bodin H.A.B.		47
Bollinger D.	(155)	246
Bolton R.A.E.		135
Bostick W.H.	(70)	239
Bourham M.A.	(48)	235
Boyd D.	(155)	246
Burkhardt L.C.	(45)	234
Burnett S.C.		35
Carr W.	(155)	246
Cattanei G.		135
Chodura R.		93
Coensgen F.H.		71
Coudeville A.	(65)	238
Crow J.E.		47
Cummins W.F.		71
De Mascureau J.	(65)	238
Demchenko V.V.	(48)	235
Di Marco J.N.	(45)	234
Dodo T.	(71)	239
Doremus J.P.	(138)	245
Dory R.A.	(40)	233
Dreicer H.	(120)	242
Dunnett D.A.	(99)	241
Durantet J.	(65)	238
El-Behay A.Z.	(48)	235
El-Hak L.G.	(48)	235
El-Khalafawy T.A.	(48)	235
Ellis R.F.	(120)	242
Ellis W.R.		35
Finzi U.	(138)	245
Forman P.R.	(45)	234
Franklin R.N.	(132)	243
	(133)	244
Fujisawa N.	(3)	231
Funahashi A.	(3)	231
Gabr A.A.	(48)	235
Geller R.	(123)	242
Girard J.P.	(105)	241
Gould R.W.		213
Gowers C.W.		47
Grelot P.	(24)	231
Gribble R.F.		35
Grimm R.C.	(38)	232
Gruber O.	(53)	236

[+] *Numbers in brackets refer to the page of the first volume.*

Haberstich A.	(45)	234
Hall T.A.	(62)	237
Hamberger S.M.	(132)	243
	(133)	244
	(146)	245
Hammer C.F.		35
Harder C.R.		35
Harris H.W.		35
Herold H.	(53)	236
Hess W.R.	(123)	242
Hesse M.	(123)	242
Hintz E.		119
Hogan J.T.	(40)	233
Holec J.	(138)	245
Horikoshi G.	(71)	239
Hugues T.P.	(62)	237
Iiyoshi A.	(78)	240
Ingraham J.C.	(120)	242
Inoue K.	(3)	231
Inoue N.	(55)	236
Itoh S.	(3)	231
Jacquot B.	(123)	242
Jacquot C.	(123)	242
Jahoda F.C.		35
Jancarik J.	(146)	245
Jolas A.	(65)	238
Jones G.A.	(99)	241
Karr H.J.	(45)	234
Kasai S.	(3)	231
Keeping P.M.	(38)	232
Keilhacker M.	(47)	234
Khelladi M.	(105)	241
Killeen J.	(38)	232
Konoshima S.	(78)	240
Kornherr M.	(47)	234
Kovrizhnikh L.M.		147
Kunieda S.	(3)	231
Kuroda T.	(71)	239
Launspach J.	(65)	238
Lees D.J.		135
Liu H.	(155)	246
Maeno M.	(3)	231
Maisonnier Ch.		183
Manickam J.	(155)	246
Maret G.	(47)	234
Marty D.	(105)	241
Matoba T.	(3)	231
Matsuda S.	(3)	231
Mercier C.		157
Millar W.		135
Mohri A.	(55)	236
Molvik A.W.		71
Mori S.	(3)	231
	(94)	240
Morimoto S.	(78)	240
Musil J.	(126)	243

Nagashima T. (94) 240
Nalesso G.F. 47
(43) 233
Nardi V. (70) 239
Newton A.A. 47
Nexsen W.E. 71
Niedermeyer H. (47) 234
Nishida Y. (71) 239
Noda N. (55) 236

Ohga T. (3) 231
Ohkawa T. 25
Ohta M. (3) 231
Ohtsuka H. (94) 240
Ortolani S. (43) 233
Otake I. (78) 240

Palumbo D. 195
Pecorella F. 183
Phillips J.A. (45) 234
Plinate P.L. 135
Prater R. 25
Prior W.J. (70) 239

Quinn W.E. 35

Rager J.P. 183
Rebut P.H. (29) 232
Ribe F.L. 35
Robinson D.C. 47
Rodriguez-Trelles F. (70) 239
Rumsby P.T. (61) 237

Sagdeev R.Z. 105
Samain A. (29) 232
Samuelli M. 183
Sato K. (55) 236
Sato M. (78) 240
Sawyer G.A. 35
Seidl M. (155) 246
Sharp L.E. (146) 245
Shiina T. (94) 240
Siemon R.E. 35
Simonen T.C. 71
Smith G.J. (132) 243
(133) 244
Soubbaramayer 157
Steuer K.H. (47) 234
Stodieck W. 1
Strelkov V.S. 13
Sugawara T. (3) 231
Suzuki N. (3) 231

Takeda T. (3) 231
Tamano T. 25
Taylor J.B. 83
Tamura S. (94) 240
Tazima T. (3) 231
Ternopol A.M. (48) 235
Thomas K.S. 35
Toi K. (3) 231

Uchida T. (55) 236
Uo K. (78) 240

Verhage A.J.L. 47

Watteau J.P. (65) 238
Weisse J. (24) 231
Wilhelm R. 59

Yamato H. (94) 240
Yoshikawa M. (94) 240
Yoshimura H. (55) 236
Yoshioka S. (78) 240

Zacek F. (126) 243
Zwicker H. 59

GRATIANOPOLIS.

GRATIANOPOLIS, inter Galliæ Narbonenſis vrbes antiquiſsima, & Allobrogum populis nulla non ætate adſcripta, non ſemper id nominis habuit: quippe olim Accuſio, vel Accuſiorum colonia, vocata, Caballoniorum in Prouincia colonia fuit. Nam & ita Ptolemæo in Geographia dicitur, idemque ei permanſit nomen vſque ad Diocletiani & Maximini tempora. Quamobrem Cularona exinde vocata fuerit, nullam rationem accepi. Poſt autem imperante Gratiano, cùm ampliore murorum circuitu eius pomœria nonnihil prolata eſſent, à Gratiano eius rei auctore, Romanis primùm Grationopolis, Gallis deinde, corrupto vocabulo, Grenoble, appellata fuit. Itaque non ipſe Gratianus (vt aliqui falſo exiſtimant) hanc vrbem condidit, ſed quam reſtauratam ampliaſſet, nomen ab ſeſe habere voluit, Gallicæ quidem gentis, apud quam Ambiani Romanorum Imperator factus eſſet, ſtudioſus: poſt autem Anno Chriſti CCC.LXXXVII. Lugduni à Maximino tyranno cæſus. Cæterum, ante Gratianum Maximianus à Diocletiano in Galliam miſſus, vt ſubortos illic tumulus componeret, hanc vrbem ita communierat, vt Romanorum veluti propugnaculum quoddam aduerſus Gallorum vim eſſet: portas autem exſtruxerat duas ex lapide quadrato inſignes, opere ſcalptorio per quàm ſubtili, coagmentatione tam ſolida, vt ne hodie quidem illarum pulchritudinem, vlla in parte, vetuſtatis iniuria læſam appareat. Harum altera, quod ad viam ſpectaret, quæ Romam ducit, appellabatur Romana louia: altera, per quam milites in Prouinciam graſſatum prodibant, Viennenſis Herculanæ nomen habebat. Hæc Maximiano, qui ſibi pari cum Hercule felicitate blandiens, Hercules dici vellet, illa Diocletiano, qui rebus geſtis parem ſe Ioui crederet, dicata. Id hodieque ſcalptæ illæ inſcriptiones docent, quas non Viennæ, (vt ſomniauit Pomponius Lætus) ſed Gratianopoli videas: alteram quidem in porta, quæ ad meridem pertinet, & Romana dicitur:

DD. NN. IMPP. CAES. GAIVS AVREL. VALERIVS DIOCLETIANVS PP. IN VICTVS,
Auguſt. & Imp. Cæſ. M. Aurel. Valerius Maximianus, pius, felix, inuictus, Auguſt. muris Cularonenſibus, cum uterioribus ædificijs prouidentia ſua inſtitutis atque perfectis, portam Romanam louiam vocari iuſſerunt.

Alteram verò in porta, qua Viennam itur, quæque ad ſeptentriones vergit:

DD. NN. IMPP. CAES. GAIVS AVREL. VALERIVS DIOCLETIANVS PP. INVICTVS,
Auguſt. & Imp. Caſar, Marc. Aurel. Valerius, Maximianus, pius, felix, inuictus, Auguſt. muris Cularonenſibus, cum interioribus ædificijs prouidentia ſua inſtitutis atq; perfectis, portam Viennenſem Herculeã vocari iuſſerunt.

Sed nulla Maximiani tanti momenti Cularonæ fuit ſubſtructio, quin ei vrbi Gratianus, ampliori ab ſe factæ, veteri abolito nomine, ſuum dare voluerit. Cumque is orthodoxæ religionis Princeps, Gallis etiam charus eſſet, facile in ea vrbe nominis ac virtutis æternam memoriam aſſequutus eſt. Antiqua eius forma longior eſt, quàm rotundior, in angulum deſinens acutum, ac tantummodo oualis. Planiciem occupat, quæ paulatim à montium radicibus ad Orientem extenſa, ita pingue habet ſolum, vt nulla omninò regio fertilitate ipſam vincat. Sed neque tantùm ab hac parte regio fructuoſa eſt. Quocunque enim oculos vertas, amœnitas, deliciæ, & rerum omnium copia ſeſe offert. Iſara, ex altis Alpium iugis ab Oriente lapſus, hanc perluit, qui magno impetu per Centrones & Viconcios (Tarentaſios hodie, & Moriennos vocant) delatus, irrigata Delphinatium regione, in Rhodanum ſe, intra Tinum, & Valentiam confundit, quo loco Fabius olim Maximus Allobrogas memorabili prælio ſuperauit. Ad Septentrionem in Iſara pons ſtratus, omnium, quos vſquam videas, pulcherrimus, ad ſuburbia, quæ D. Laurentij dicuntur pertinens. Nec longè ſodinæ lapideæ, ex quibus lapides ad omnem ciuitatis vſum eruuntur. Ad meridiem præterlabens Dracus, torrens ira moroſus, & vehemens, vt non raro limoſis inundationibus vicinos agros deformet, nec vllo aggere coerceri poſsit, non longè à ciuitate in Rhodanum excipitur. Qui ab hoc torrente longius abſunt agri, latiſsimis extenduntur campis, omni fructuum genere onuſtis, & aſpectui perpetuo quodam virore, fontiumque, ac riuorum ſcaturigine, mirum in modum blandientibus. Franciſcus, eius nominis Rex Gallorum primus, Gratiani ſequutus exemplum, conſtituerat hanc ciuitatem maiore murorum ambitu concludere, & iam fundamenta, quæ hodie quoque videre licet, iacta erant, ſed pendet opus interruptum, nullam ciuibus inuenientibus rationem, qua tanti momenti rem cœptam abſoluant. Gratianopolis ſedem habet Epiſcopalem, Viennenſi Archiepiſcopo ſubditam. Habet & Curiam iudicialem primariam, ad explicandas maioris momenti cauſas, quæ apud inferiores iudices decidi non poſſunt: in qua viri ſemper ſunt ſcientia præſtantiſsimi, tum iuſtitia & vitæ integritate ſummi, & qui patriæ iura conſeruent, & libertatem tueantur. Denique, ad cætera huius ciuitatis ornamenta accedit, rationum ærari cognitio.